Report No. FAA-RD-72-22

INERTIALLY AUGMENTED AUTOMATIC LANDING SYSTEM:

Autopilot Performance With Imperfect ILS Beams

R.J.Bleeg

H.F.Tisdale R.M. Vircks

The Boeing Company

Box 3707

Seattle, Washington 98124

transpo 72

U.S. International Transportation Exposition
Dulles International Airport
Washington, D.C.
May 27-June 4, 1972

APRIL 1972

FINAL REPORT

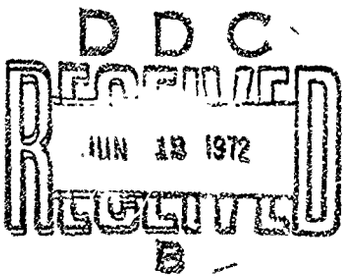

Prepared for

DEPARTMENT OF TRANSPORTATION

FEDERAL AVIATION ADMINISTRATION

Systems Research & Development Service

Washington, D.C. 20591

The contents of this report reflect the views of the Boeing Flight Controls Technology organization which is responsible for the facts and the accuracy of the data presented herein. The contents do not necessarily reflect the official views or policy of the Department of Transportation. This report does not constitute a standard, specification or regulation.

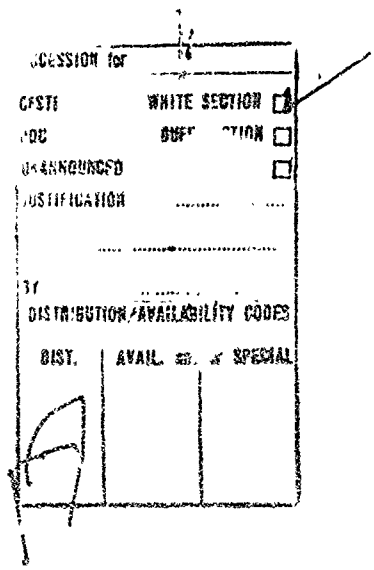

TECHNICAL REPORT STANDARD TITLE PAGE

1. Report No.	2. Government Accession No.	3. Recipient's Catalog No.
FAA-RD-72-22		

4. Title and Subtitle	5. Report Date
INERTIALLY AUGMENTED AUTOMATIC LANDING SYSTEM: Autopilot Performance with Imperfect ILS Beams	April, 1972
	6. Performing Organization Code: Flight Controls Technology
7. Author(s): R.J.Bleeg, H.F.Tisdale, R.M.Vircks	8. Performing Organization Report No.: D6-40560
9. Performing Organization Name and Address: The Boeing Company, Box 3707, Seattle, Wa. 98124	10. Work Unit No.: 073-320-023
	11. Contract or Grant No.: DOT-FA71WA-2629
12. Sponsoring Agency Name and Address: Federal Aviation Administration, Systems Research & Development Service, 800 Independence Ave. S.W., Washington, D.C. 20590	13. Type of Report and Period Covered: Final Report, July 1, 1971 - April 1, 1972
	14. Sponsoring Agency Code: FAA/RD-322

15. Supplementary Notes

16. Abstract This report considers the capability of three autopilots, with varying dependency on inertial navigation inputs, to perform the automatic landing task in the presence of ILS beam anomalies. Three sets of pitch and roll axis control laws for a commercial jet transport were analyzed and flight tested to determine their comparative advantages and limitations. Conventional autopilots with only minor or no reliance on inertial inputs are sensitive to ILS beam imperfections. It is shown that complementary filtering of ILS position information with INS-derived acceleration and velocity results in a very marked attenuation of airplane response to beam bends, noise, and overflight interference. A set of equations is derived by which the acceptability of system performance during an automatic approach can be assessed. The capability of the three autopilots to provide acceptable performance on Category I and II ILS beams is investigated.

The three sets of autopilot control laws were analyzed on an analog computer and also test flown on a Boeing 727 airplane. The mechanization of control computations on board the aircraft was such as to permit the selection of any of the three control laws on successive approaches on the same flight. In this way it is possible to compare the performance of the autopilots under nearly identical circumstances of aircraft characteristic, ILS beam quality, environmental disturbances and sensors characteristics. Beam disturbances were artificially inserted into the autopilots both on the analog computer and in flight.

17. Key Words	18. Distribution Statement
Instrument Landing System (ILS) Automatic Landing System Inertial Damping Inertial Smoothing	Availability is unlimited. Document may be released to the National Technical Information Service, Springfield, Virginia 22151, for sale to the public.

19. Security Classif. (of this report)	20. Security Classif. (of this page)	21. No. of Pages	22. Price
Unclassified	Unclassified	228	3.00 P.C. .95 MF

Form DOT F 1700.7 (8-69)

CONTENTS

ILLUSTRATIONS

ILLUSTRATIONS (Continued)

ILLUSTRATIONS (Continued)

TABLES

ABBREVIATIONS AND SYMBOLS

P	Probability Density
γ	Flight Path Angle
S	Laplace Operator
α	Angle of Attack
h_R	Radio Altitude
ψ	Course Error
ϕ	Roll Attitude
$\dot{\phi}$	Roll Rate
η	Localizer Beam Error
η_{DIST}	Beam Transients
$\Delta\psi_G$	Ground Heading Error
ψ_{TA}	True Track Angle
ψ_{TS}	Selected Magnetic Track
ψ_{RW}	Runway Magnetic Heading
ψ_{CHE}	Course Heading Error
ϕ_C	Roll Command
$\dot{\phi}_C$	Roll Rate Command
$\phi_{C_{BA}}$	Roll Command - Beam Acquisition Mode
δ_{ac}	Aileron Command
$\phi_{C\,SYNCH}$	Synchronization Roll Command
$\phi_{C_{TS}}$	Track Select Roll Command
$\Delta\psi_{TS}$	Track Select Error
$\Delta\psi_G$	Ground Heading Error
$\hat{\dot{\eta}} = \frac{S\eta}{(\tau_{\eta_1}S + 1)(\tau_{\eta_2}S + 1)}$	Derived Beam Rate

ABBREVJATIONS AND SYMBOLS (Continued)

$\bar{\eta}$	Average Localizer Beam Error
θ	Pitch Attitude
$\dot{\theta}$	Pitch Rate
β	Glide Slope Beam Error
$\ddot{h}$	Vertical Acceleration
θ_C	Pitch Command
$\dot{\theta}_C$	Pitch Rate Command
δ_{ec}	Elevator Command
$\dot{h}$	Altitude Rate
V_G	Ground Speed
T/D BIAS	Touchdown Bias
T/D	Touchdown
τ_{ϕ_C}	Roll Command Time Constant
τ_{ϕ_L}	Lagged Roll Time Constant
τ_η	Localizer Beam Error Time Constant
$\tau_{\eta_{COMP}}$	Complementary Filter Time Constant
$\tau_{\eta_{BA}}$	Localizer Beam Error Time Constant -- Beam Acquisition Mode
τ_{η_1}	Derived Beam Rate Time Constant 1
τ_{η_2}	Derived Beam Rate Time Constant 2
$\tau_{\psi_{TS}}$	Track Angle Error Time Constant -- Track Select Mode
τ_{ψ_G}	Ground Heading Time Constant
τ_{WO}	Washout Time Constant

ABBREVIATIONS AND SYMBOLS (Continued)

$\tau_{1_{\dot{\theta}}}$	First band pass break point on $\dot{\theta}$ filter
$\tau_{2_{\Delta h}}$	Second band pass break point on $\dot{\theta}$ filter in alt hold only
$\tau_{2_{\dot{\theta}}}$	Second band pass break point on $\dot{\theta}$ filter in G/S
τ_{β}	Time constant of vertical path filter
$\tau_{\ddot{h}}$	Acceleration wash-out time constant
$\tau_{\dot{h}_F}$	Time constant of $\dot{h}$ comp filter
$\tau_{\ddot{h}_{B_2}}$	Second lag on $\ddot{h}$ shaping network for inner loop damping
$\tau_{\ddot{h}_{B_3}}$	Lead time constant on $\ddot{h}$ shaping network for inner loop damping
τ_{C_1}	Initialization time constant (inverted) for complementary filter
τ_{C_2}	Normal time constant (inverted) for complementary filter
$K_{\dot{\phi}}$	Roll Rate Gain
K_{ϕ}	Roll Attitude Gain
K_{ϕ_L}	Lagged Roll Gain
$K_{\delta a_{SYNC}}$	Aileron Command Synchronization Gain
K_{OUT}	Synchronizer Discharge Gain
$K_{\psi_{TS}}$	Track Angle Error Gain -- Track Select Mode
$K_{\psi_{G_{COMP}}}$	Ground Heading Gain for Complementary Filter
K_{ψ}	Heading Gain
K_{ψ_G}	Ground Heading Gain

ABBREVIATIONS AND SYMBOLS (Continued)

$K_{\psi_{G_{BA}}}$	Ground Heading Gain -- Beam Acquisition Mode
K_{η}	Localizer Beam Gain
$K_{\eta_{BA}}$	Localizer Beam Gain -- Beam Acquistion Mode
K_{i}	Beam Integral Gain
$K_{\dot{\eta}}$	Localizer Beam Rate Gain
K_{SYNC}	Roll Command Synchronization Gain
$K_{\psi\,SYNC}$	Heading Hold Synchronizer Gain
K_{θ}	δe to θ in G/S mode
$K_{\dot{\theta}}$	δe to $\dot{\theta}$ in G/S
K_{β}	θ to beam error gain
K_{I}	θ to $\int$ beam gain, Sys.
K_{h}	θ to $\int \ddot{h}$ (damping)
$K_{\Delta h}$	θ_C to Δh
$K_{\Delta\dot{h}}$	τ_{C_2} x $\frac{\text{G/S angle}}{1500\ \text{ft}}$
$K_{\ddot{h}}$	θ to $\int \ddot{h}$, G/S capture,
$K_{hA_{FD}}$	θ to $\int$ (fly down - $\dot{h}$)
$K_{I_{\Delta h}}$	θ_C to $\int \Delta h$
$K_{\theta_{\Delta h}}$	δ_e to θ in alt hold
$K_{\dot{\theta}_{\Delta h}}$	δ_e to $\dot{\theta}$ in alt hold
$K_{\dot{h}\,FLARE}$	θ to $\hat{\dot{h}}$ (flare)

ABBREVIATIONS AND SYMBOLS (Continued)

$K_{\dot{h}\int_{FLARE}}$	θ to $\int \dot{\hat{h}}$ (flare)	
$K_{h\int_{FLARE}}$	θ to $\int h$ (flare)	
$K_{h_{FLARE}}$	θ to $\bar{h}$ (flare)	
$K_{F\ SYNCH}$	θ to $\int$ (flare composite)	
K_{VG}	$\dot{h}_c$ to Vg	
K_{SYNCH}	δec	synchronization gain, prior to capture
K_{TRIM}	δe	pre-engage synch
$\ddot{h}_T$	Acceleration at the tail	
CG	Center of Gravity	
$\ddot{h}_{CG}$	Acceleration upward at center of gravity	
$\ddot{h}_N$	Induced pitching moment	
ua	Microamps	
σ	Standard Deviation	
μ	Mean Deviation	
β_{DIST}	Glide Slope Beam Disturbance Amplitude	
h_{DIST}	Sinusoidal Forcing Function for Bode plots	
$\delta\omega$	Wheel	
β_{NOISE}	Sinusoidal Forcing Function for Bode Plots	
Y_{DIST}	Sinusoidal Forcing Function for Bode Plots	

ABBREVIATIONS AND SYMBOLS (Continued)

J	Roll Axis Footprint Criterion Threshold Value ~ Ft.
Y	Roll Axis Maneuver Criterion Threshold Value ~ Ft.
y	Lateral displacement from runway centerline ~ Ft.
h	Altitude ~ Ft.
R	Pilot Reaction time in roll axis Footprint Criterion
A	Cross track acceleration roll axis Footprint Criterion
M.E.	Pitch or Roll Axis Maneuver Equation Value ~ Ft.
M.E.A.	Pitch or Roll Axis Maneuver Equation Average Value ~ Ft.
M.C.	Pitch or Roll Axis Maneuver Criterion Exceedance
F.C.	Pitch or Roll Axis Footprint

NOTE: Subscript A = System "A"
Subscript B = System "B"
Subscript C = System "C"

SECTION 1

INTRODUCTION

Commercial jet transports have, for more than 10 years, been equipped with autopilots capable of tracking ILS beams. Progressively over this period of time, improvements in performance and reliability have been achieved as better ILS beams, airborne sensors and control laws became available. And yet, anomalies of the ILS beams such as noise, bends, centering error, overflight interference, and failure shutdown remain dominant factors in the formulation of automatic approach coupler control laws. The principal objectives in the continuing development of new controls laws are to attenuate the adverse effects of atmospheric disturbances, and to increase the tracking accuracy to the average beam center. The resultant control laws always include some performance compromise in allowance for beam imperfections. The reasons for these compromises and their impact on performance are discussed in this report.

Since the introduction of inertial navigation systems on commercial jet transports, much theoretical analysis (Ref. 5,6) has been devoted to consideration of the potential of using INS outputs to enhance autopilot approach coupler performance. Several similar control laws have been independently derived. The Boeing research which led up to the subject program has been paralleled by other Government and industry efforts, with generally similar results. During the current program, two different inertially aided autopilots were analyzed and successfully test flown.

The general objective of this program was to analyze and demonstrate the performance capabilities of three autoland control laws which have varying degree of dependency on inertial navigation system inputs. Thus, a perspective on the relative merit of the autopilots is gained. All three control laws had been developed by The Boeing Company prior to the award of the contract.

The specific objectives of this program were to:

1. Identify the advantages of inertial smoothing
2. Define the limitations of inertial smoothing
3. Determine criteria which will permit exploitation of the advantages of inertially smoothed systems

The advantages of inertial smoothing were determined by a performance comparison between a conventional autopilot that requires no inertial system inputs; a contemporary autopilot that employs inertial inputs for path damping; and the inertially smoothed autopilot which uses

Ref. 5. Todd M., Complementary Filter Scheme for Premixing INS and ILS Information, Service Technology Corp., Report 580, October, 1970.

Ref. 6. Design, Development and Flight Evaluation of Inertially Augmented Automatic Landing Systems, Lear Siegler, Inc., Interim Report ADR-754, April, 1971.

inertial inputs for both path damping and beam filtering. The conventional autopilot control law, used in this study, is nearly identical to a control law which has been in commercial service for several years. This autopilot is certified for Cat II operation and is configured for automatic flare to touchdown. Thus, the conventional autopilot control law is quite representative of early versions of autoland autopilots. The contemporary autopilot control law, referred to as the inertially damped system, is similar to recently certified autopilots both in the degree of dependency on inertial system inputs and performance capability. Thus, it is representative of the best autoland autopilots presently in service.

The inertially smoothed autopilot control law, used in this study, is the inertially damped autopilot with a first order complementary filter added. Thus, the performance differences between the inertially damped and the inertially smoothed control law are solely attributable to the complementary filtering of an inertially derived rate signal with the ILS beam signal. In summary, the three autopilot control laws were specifically chosen to illustrate the progressive performance improvement attainable through the use of inertial feedback terms.

The second program objective: to define the limitations of inertial smoothing, was pursued through analysis of the sensitivity of the control law to inertial navigation system errors. It follows that when the dependence on inertial system input is high, that the propagation of inertial system errors will also be high. Thus, there is a point of diminishing returns. This point of diminishing returns is identified for a first order complementary filter method of inertially smoothing. The inertial navigator used is a commercial type with a one nautical mile per hour circular error probability (CEP). There is no discussion of the relative merit of first and second order complementary filtering. That subject has been analyzed and information is available in the literature (Ref. 7).

The third program objective: to determine criteria which will permit exploitation of the advantages of inertially smoothed systems, was accomplished through two stages of analysis. In the first stage, criteria were developed which define the required levels of automatic approach system performance for Cat II and Cat III operation. These criteria were used throughout the program as the "yardstick" for measurement of absolute performance. The criteria define both the touchdown and approach tracking requirements. In the second stage, having defined these performance criteria, and also having analyzed the three autopilots performance capabilities in presence of ILS beam anomalies, it was then possible to determine approximately what type and magnitude of ILS beam anomalies are tolerable and yet result in acceptable system performance. The product of the third program objective is a set of automatic approach system performance criteria and, secondly,

Ref. 7. Todd M., Second Order Complementary Filter for Premixing INS and ILS Information, Service Technology Corp., Report STC-DOT-TSC-43-71-755, May, 1971.

a matrix set of tentative conclusions relating the FAA Cat I and Cat II beam inspection criteria to the resultant system performance with conventional, inertially damped and inertially smoothed autopilots.

This final report was generated in partial satisfaction of the terms of Contract DOT-FA71WA-2629 between the FAA and The Boeing Company. Essentially, the program was divided into three parts: an analog computer simulation of the autopilots to analyze performance and develop the performance criteria, a flight test equipment preparation culminating with six flights, and a simulation and flight test data reduction effort.

2.0 AUTOLAND CONTROL LAWS

The three types of autoland control laws used in this study exhibited varying degrees of dependence on the inertial navigation system (INS) as shown below:

- o System A - Independent of INS
- o System B - Derives damping signals and, hence, basic stability from INS
- o System C - Derives basic stability plus short term position data from INS

Until recently, approach control laws have been developed under annoying constraints imposed by the lack of high quality feedback sources. Consequently, performance achieved was mediocre by present day standards. ILS couplers developed under such constraints provided rather loose beam tracking, poor wind performance, and a high level of control activity.

Now the INS has alleviated many of the design problems by providing high quality attitude information, stabilized acceleration signals, and highly accurate ground speed. With the availability of these high quality signals, the practical restriction on higher gains was relieved, and this cleared the way for achieving near-optimal-tuning of the system; i.e., tighter tracking and better performance in the presence of atmospheric upsets. The inertially damped coupler thus has the potential to provide a substantial improvement over the conventional coupler.

The designer's goal of routinely achieving accurate automatic landings was still hampered by an acute problem, that of anomalous behavior of the ILS beams. For perfectly transmitted azimuth and elevation references, the INS-damped autopilot, properly designed, would meet the designer's goals. However, three distinct anomalies stand between the real ILS beams and a perfect space reference:

1) Multipath distortion (bends caused by signal reflections)
2) Localizer interference caused by overflying aircraft
3) Susceptibility of ILS beams to ground equipment failures

Reduction of system dispersion and activity, caused by ILS beam anomalies, to an acceptable level cannot be achieved simply through heavy filtering of the localizer and glide slope beam deviations. Excessive filtering of the beam through straight-forward techniques gives rise to system destabilization. That is, the larger the filter time constant, the greater the phase shift, and the stability of the guidance system is very sensitive to phase lag. However, the INS velocity and acceleration signals provide an excellent means to derive an inertial estimate of aircraft trajectory and, hence, complement the ILS radio information. As a result, considerably larger time constants can be introduced into the beam filter as long as the high frequency signal attenuation is compensated by inertial information. Thus, both the ILS beam deviation and the inertial signal may be summed into the same filter (with proper gains), and the output of the filter will estimate

quite accurately, and virtually noise-free, the average ILS beam center. This technique is commonly referred to as "complementary filtering"[1], and provides "inertial smoothing" of the ILS beams.

2.1 Conventional

The conventional autoland control law is referred to as System A in this report. System A makes relatively little use of inertial information. This system is non-inertial in the sense of not requiring an inertial navigator to provide signals. The inertial signals used by System A are usually the sensor outputs of a vertical gyro, rate gyros, and body mounted accelerometers.

The configuration and gains of System A were selected to be typical of systems designed before the sophisticated INS was available. System A is not an exact duplication of classical autoland systems in service, but was designed to have similar response to ILS distortion. System A, as simulated and flight tested, is representative of conventional autoland control laws in the sensitive region of the ILS anomaly response spectrum.

2.1.1 System A Lateral Control Law

The System A lateral control law is shown in the simplified block diagram of Figure 2.1.1. The roll attitude command is formed by a combination of proportional plus integral localizer deviation together with derived beam rate, lagged roll and course heading error. The ILS localizer is used as the lateral deviation sensor by all autoland systems to which this report is applicable. Integral control is used by System A as well as Systems B and C to prevent steady state standoffs from the localizer beam. The last three signals approximate lateral velocity which is needed for airplane path damping.

A wide variety of sensors and signal processing has been used to estimate lateral velocity. Some systems have used only heading for damping. Others have used only beam rate, or a combination of beam rate and lagged roll. System A uses all three in a blend similar to that used by some conventional systems. System A exhibits the characteristics of each damping signal by employing the three most commonly used by conventional autoland systems.

Derived beam rate contains the lateral velocity information necessary for damping. The time constants in the rate taker and the gain $K\dot{\eta}$ could be adjusted to achieve excellent performance if it were not for the presence of noise on the localizer. The rate taker magnifies the high frequency noise. This leads to excess activity and path dispersion because the response is quickened through the addition of the derivative of the disturbance.

Realistic localizer noise considerations lowered the derived rate break frequency a factor of three, and $K\dot{\eta}$ by an order of magnitude, compared to the desirable values obtained without considering noise.

[1] See Appendix A

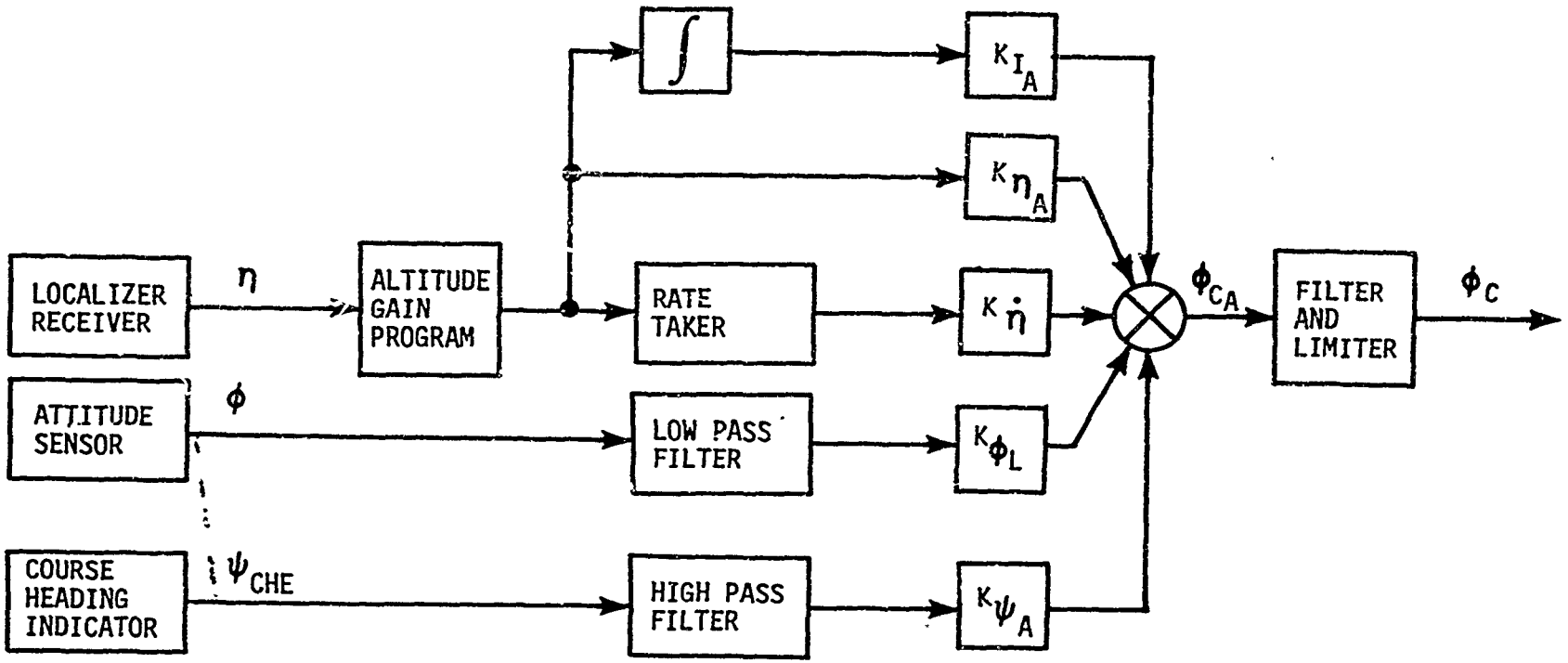

Figure 2.1.1
SYSTEM "A" LATERAL CONTROL LAW

The beam rate gains and time constants for System A are typical of conventional autoland systems in service. A more detailed discussion of derived beam rate and the other damping terms appear in Appendix B and the first two sections of Appendix A.

The lagged roll term is a lateral velocity approximation ignoring sideforce. The simplified aircraft model in Appendix B ignores side force to show that heading is the integral of roll attitude. A lag is used instead of an integrator so that steady state stand off from the localizer beam cannot occur. Dynamic sideforces become significant at the dutch roll frequency causing the approximation to break down and limit the value of K_{ϕ_L}. In addition, lagged roll is not as effective as it might be for damping low frequency modes because bank angle is lagged rather than integrated. Lagged roll is effective in combating wind upsets only to the extent that bank angle represents the derivative of lateral velocity.

The course heading error is a lateral velocity approximation ignoring drift. Since sideslip cannot be completely eliminated, the airplane drifts during maneuvers. The approximation errors during maneuvers increase the phase shift at the dutch roll frequency. The resulting decrease in gain margin restricts K_{ψ_A} to a value less than the equivalent gain for true lateral velocity.

The use of course heading error increases lateral deviations resulting from cross wind shear. The heading path, in its attempt to maintain heading, inhibits aircraft weathercocking to prolong the action of sideforce. A low frequency windshear response mode arises from the time required by the path integrator to command the heading which produces the proper crab angle. These effects increase the wind shear induced deviation by a factor of five when course heading error is included for damping.

Figure 2.1.2 shows this increase in wind shear induced lateral displacement resulting from the incorporation of heading into the System A control law. The upper lateral displacement trace shows 4 feet of deviation by a modified System A control law retaining the same beam rate and lagged roll paths but not using course heading error. Simply including the heading signal, to get the unmodified System A control law with its improved damping, changes the response to the one shown by the lower lateral displacement trace which peaks at 21.5 feet of deviation.

The complete detail block diagram showing all gains, time constants and switches for System A is shown in Figure 2.1.3. The reader will note that the system is not completely independent of the INS. The roll attitude feedback is obtained from the INS rather than the conventional vertical gyro, in order to reduce mechanization complexity and instrumentation requirements.

It will be noted that Systems A, B, and C all use the same roll and roll rate gains, aileron authority, and roll and roll rate command limiters. Thus, all performance differences can be attributed to the lateral control law alone because the same aircraft and inner loops were used for all three systems.

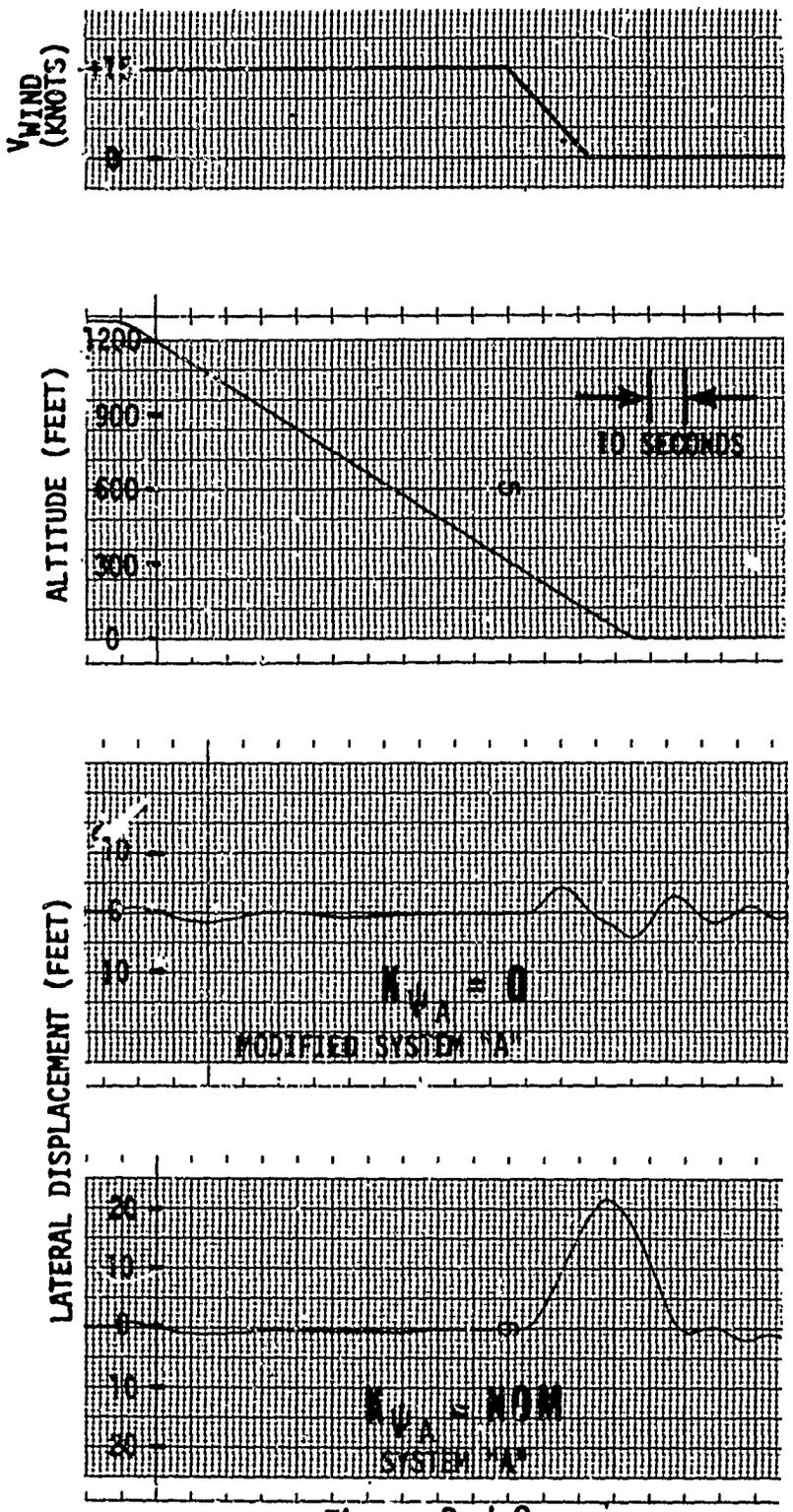

Figure 2.1.2
THE EFFECT OF HEADING ON CROSSWIND SHEAR RESPONSE

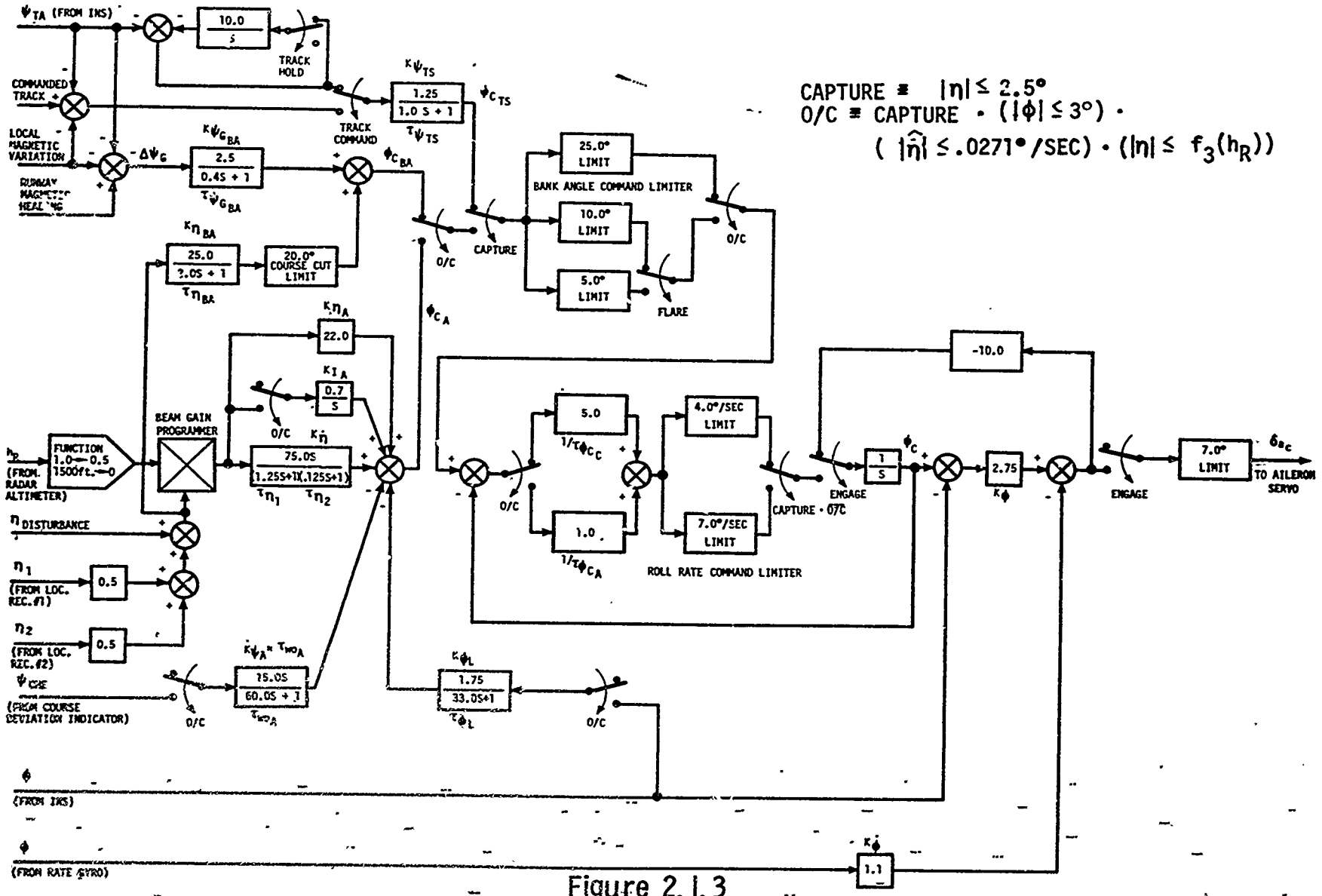

Figure 2.1.3

SYSTEM "A" LATERAL BLOCK DIAGRAM

All approaches were flown with the speed brake handle slightly out of the zero detent to eliminate spoiler deadzone. This increased rolling moment gradient and authority which decreased path deviation in turbulence. This allowed better separation between beam disturbance responses and atmospheric disturbance responses during flight testing.

The cruise and capture modes are identical for Systems A, B, and C. Two simple lateral cruise modes, Track Hold and Track Command, were provided for use prior to localizer capture. All three modes employed true track angle with a resolution of 0.044 degrees which the G.E. flight control computer received digitally five times per second from the INS binary bus. The local magnetic variation, an internal constant in the flight control computer, was included to enable the pilot to select on the G.E. mode panel the track command and runway heading with standard magnetic reference.

Only two localizer modes were used so that system complexity was minimized. Lateral autoland systems typically use three modes, switching to the final mode only after the aircraft is accurately tracking the localizer. The System A control law assumed the guidance task at On Course, the completion of the capture maneuver. Autopilot tracking was good prior to the insertion of simulated localizer anomalies at low altitude.

2.1.2 System A Longitudinal Control Law

The System A longitudinal control law is shown in the simplified block diagram of Figure 2.1.4. This control law is typical of control laws which were mechanized to achieve early Category II certification and are presently in widespread use.

The basic feature of this control law, in contrast to systems B and C, is the pitch attitude feedback for minor loop stabilization. Pitch attitude command, the output of the guidance computer in the early autopilots, was compared with airplane pitch attitude from a vertical gyro, and the difference between these signals was used to modulate the elevator control actuator. This same principle was employed in designing the early longitudinal autoland systems. It will be shown in Section 2.2.2 that pitch attitude feedback is detrimental to the achievement of good wind performance and, hence, is replaced with signals derived from vertical acceleration.

The bandpass filter on the pitch rate feedback signal in Figure 2.1.4 exists for the purposes of 1) filtering high frequency body bending modes and general sensor noise, and 2) washing out the steady state component of the pitch rate gyro output during sustained turns. For autoland, the filter is essentially a low pass device.

During glide slope control, the pitch attitude command is comprised of a signal that is proportional to glide slope beam error and the output of the path integrator. This integrator performs two distinct functions, 1) it nulls the beam error, and 2) it integrates the washed-out accelerometer signal to produce an estimate of change in descent rate.

Beam error, which is derived from the glide slope receiver output, provides the estimate of vertical deviation. This signal is limited to 0.2 degrees in all three systems so that the evaluation of system

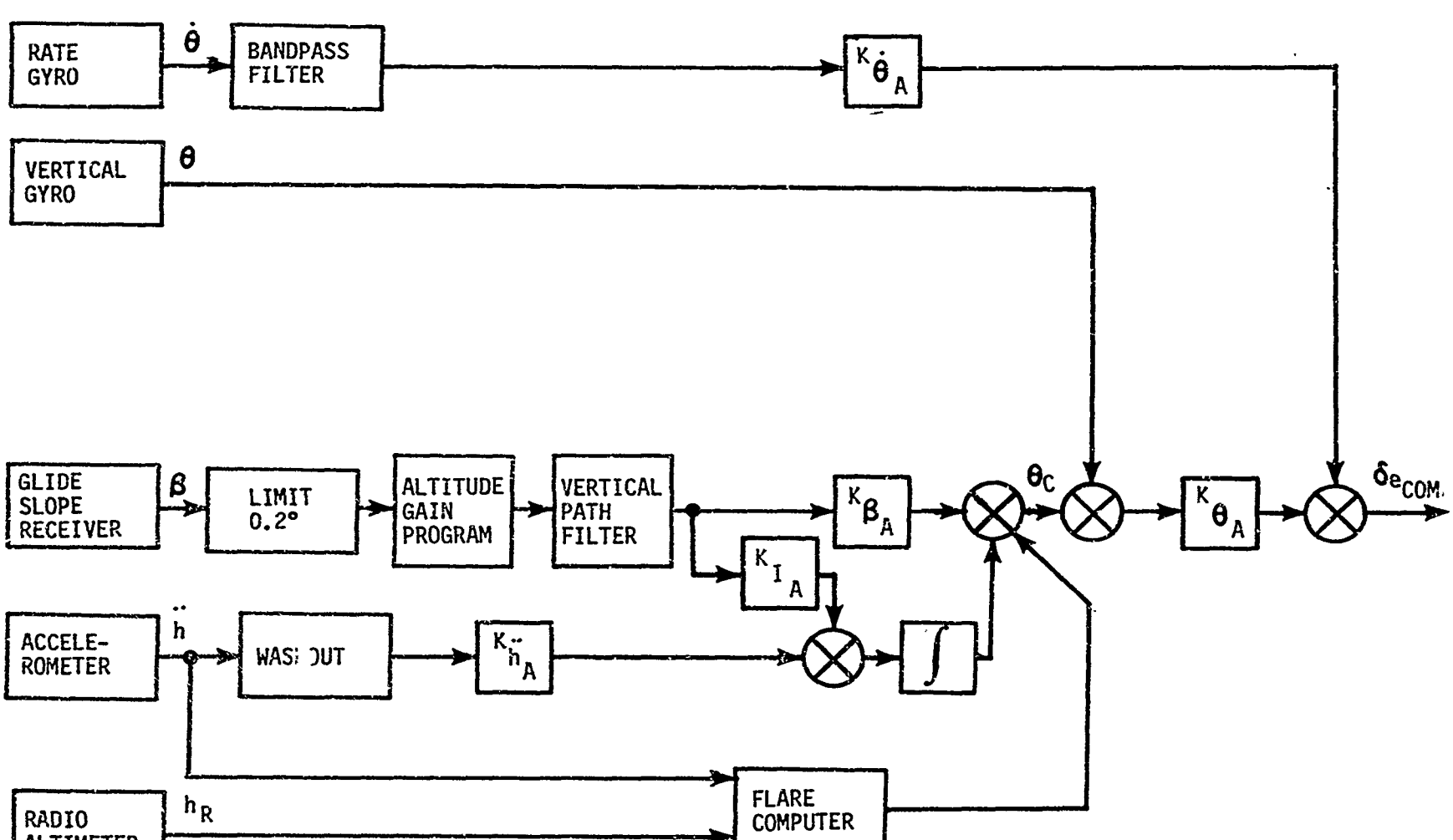

Figure 2.1.4
SYSTEM "A" LONGITUDINAL CONTROL LAW

performance in the presence of glide slope beam disturbances would be based on control law criteria only. However, the 0.2 deg limiter was frequently saturated during flight test due to wind disturbance and beam tracking was consequently degraded. In practice, autopilots typical of System A do not employ a beam limiter to reduce the effect of anomalous beam behaviour. An analysis of the effect of this limiter is presented in Section 4.

The vertical path filter through which the glide slope signal is passed provides only minor filtering of ILS beam disturbances, as the break frequency is rather high. However, without another good quality source from which to estimate vertical position, the break frequency cannot be reduced without degradation in stability.

At flare altitude, the pitch command control is switched to the flare computer, which prior to this time, was continuously synchronized in such a manner that the change in pitch command at the instant of switching is zero. Also at flare, the gain programmer applies a zero gain to the glide slope feedback, the accelerometer signal is switched out of the path integrator and the integrator assumes a hold condition.

Figure 2.1.5 contains the complete block diagram including gains, time constants, and switches for System A. Mechanization of the A System in the digital computer was accomplished using this block diagram to describe the transfer functions.

As pointed out in Section 2.1.1, the A system, as actually mechanized in the autopilot computer, was not independent of the INS. Attitude feedback as well as vertical acceleration were obtained from the inertial navigation system simply as a matter of convenience. Performance using a vertical gyro pitch attitude signal would have been substantially unchanged.

2.2 Inertially Damped

The inertially damped autoland control law is referred to as System B in this report. System B relies on extensive use of inertial information to provide a high quality damping signal. The configuration and gains of System B were selected to be typical of systems designed to utilize INS outputs for damping.

System B is not an exact duplication of inertially damped autoland systems in service, but was designed to have similar response to ILS distortion.

2.2.1 System B Lateral Control Law

The System B lateral control law is shown in the simplified block diagram of Figure 2.2.1. The roll attitude command is formed by proportional plus integral localizer deviation with washed out* track angle deviation for damping.

*A washout device is a high-pass transfer function used to eliminate an unwanted steady state signal standoff.

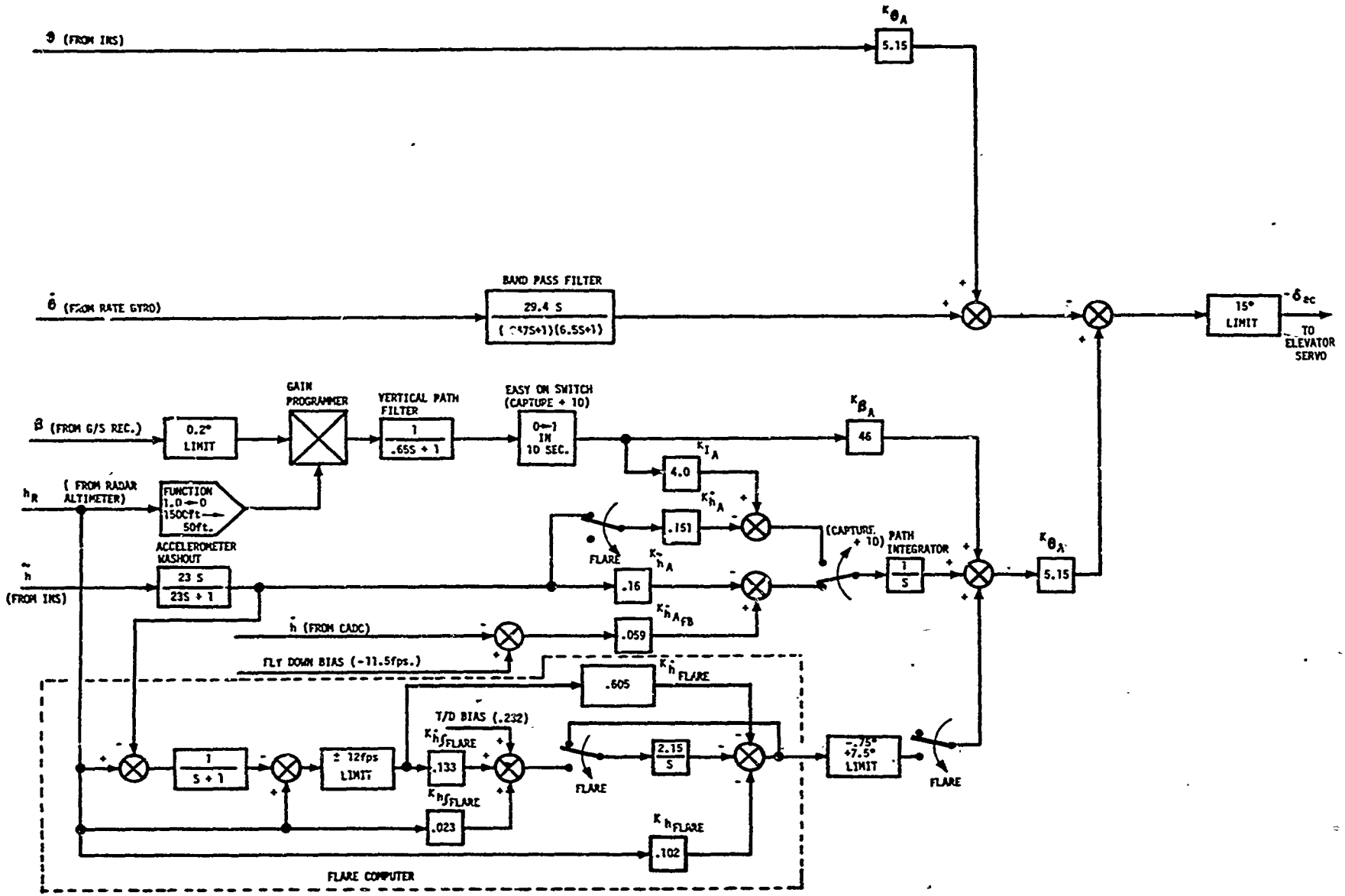

Figure 2.1.5

SYSTEM "A" LONGITUDINAL BLOCK DIAGRAM

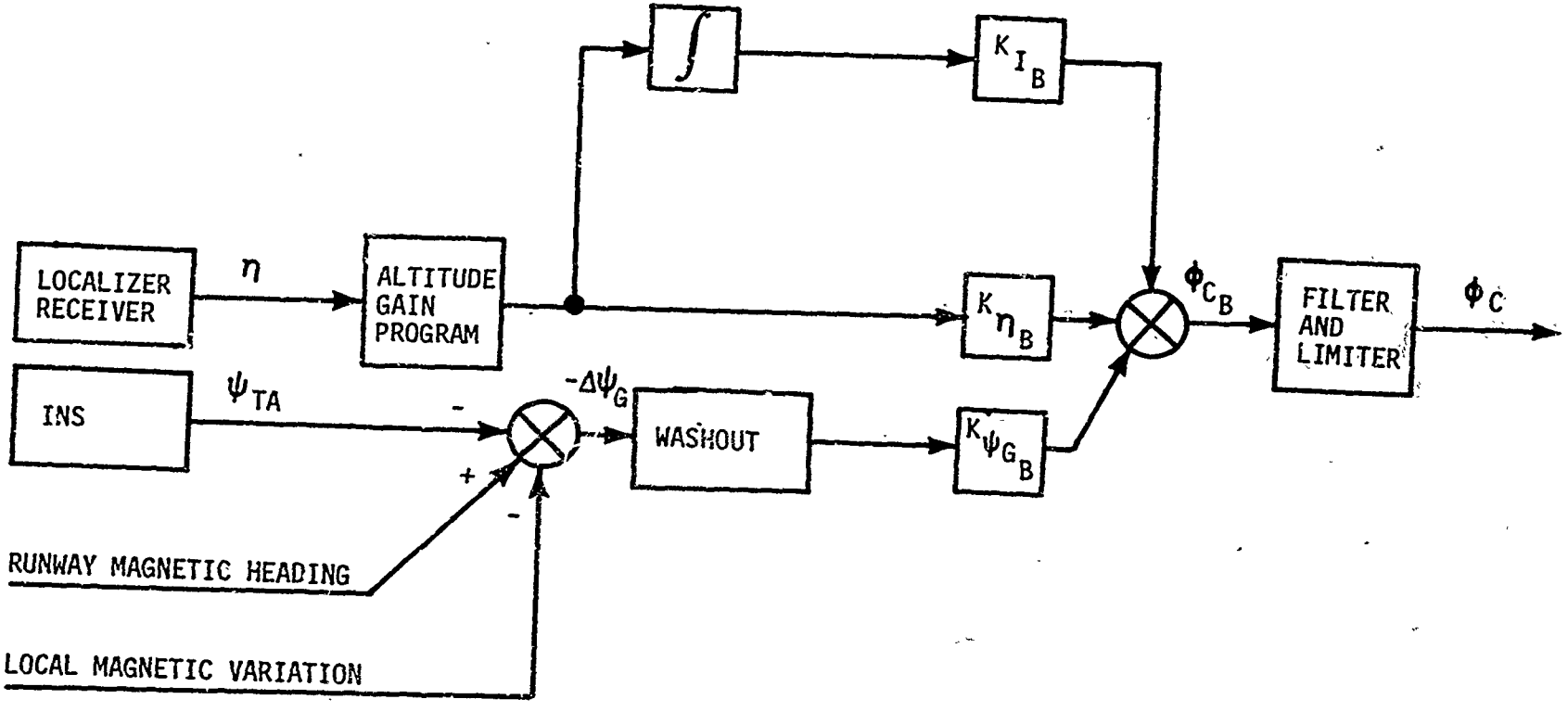

Figure 2.2.1
SYSTEM "B" LATERAL CONTROL LAW

The INS track angle does not have approximations as did the damping signals used in conventional autoland systems. The track angle deviation is the angle between the extended runway centerline and the velocity vector of the airplane with respect to the ground. The only barrier to achieving the desired high damping gains is the magnitude of INS drift errors since track angle signal does not have dynamic approximation errors other than digital sample data effects.

The washout is placed on the track angle deviation signal to remove the low frequency errors. A drawback of this error cancellation technique is the loss of low frequency damping capability. The third section of Appendix A treats the use of the INS as the velocity signal source for damping.

The complete detail block diagram showing all gains, time constants and switches for System B is shown in Figure 2.2.2. Comments applicable to the inner loops, cruise modes, capture mode and mode switching appear in Section 2.1.1.

2.2.2 System B Longitudinal Control Law

Figure 2.2.3 describes the basic longitudinal control law for the B system. The absence of pitch attitude is apparent and, hence, the basic difference between systems A and B is established.

Two paths of vertical acceleration feedback are to be noted in Figure 2.2.3. One path is shaped according to basic stability considerations and is fed back in place of pitch attitude for minor loop damping. The other feedback path of vertical acceleration is introduced into the derived altitude rate network to complement, and hence smooth, the altitude rate from the air data computer.

The excellent wind resistance exhibited by the B (and C) system is directly attributable to the vertical acceleration feedback to damp the inner loop. Although pitch attitude feedback offers an excellent means to provide phugoid mode damping, this classic means of stabilization actually degrades glide slope tracking performance. To illustrate, refer to Figure 2.2.4.

The hypothetical updraft Ug produces an uneven distribution of instantaneous upward acceleration along the body as shown. Acceleration at the tail, $\ddot{h}_T$, is greatest because the nose down pitching moment induced by the gust is added to the vertical acceleration aft of the CG. At the CG, the upward acceleration $\ddot{h}_{CG}$ is independent of the induced pitching moment, while $\ddot{h}_N$, the resultant acceleration at the nose, is smallest because the acceleration and the pitching moment are subtractive. This distribution gives rise to an inherent tendency of a statically stable airplane to return to its trimmed angle of attack. However, the pitch attitude signal opposes the downward pitching moment and commands the elevator to produce a nose-up moment. This increases the amount of deviation from the beam.

In the acceleration damped system (B and C), an instantaneous, nose-down elevator command is generated by the accelerometer. Thus, the

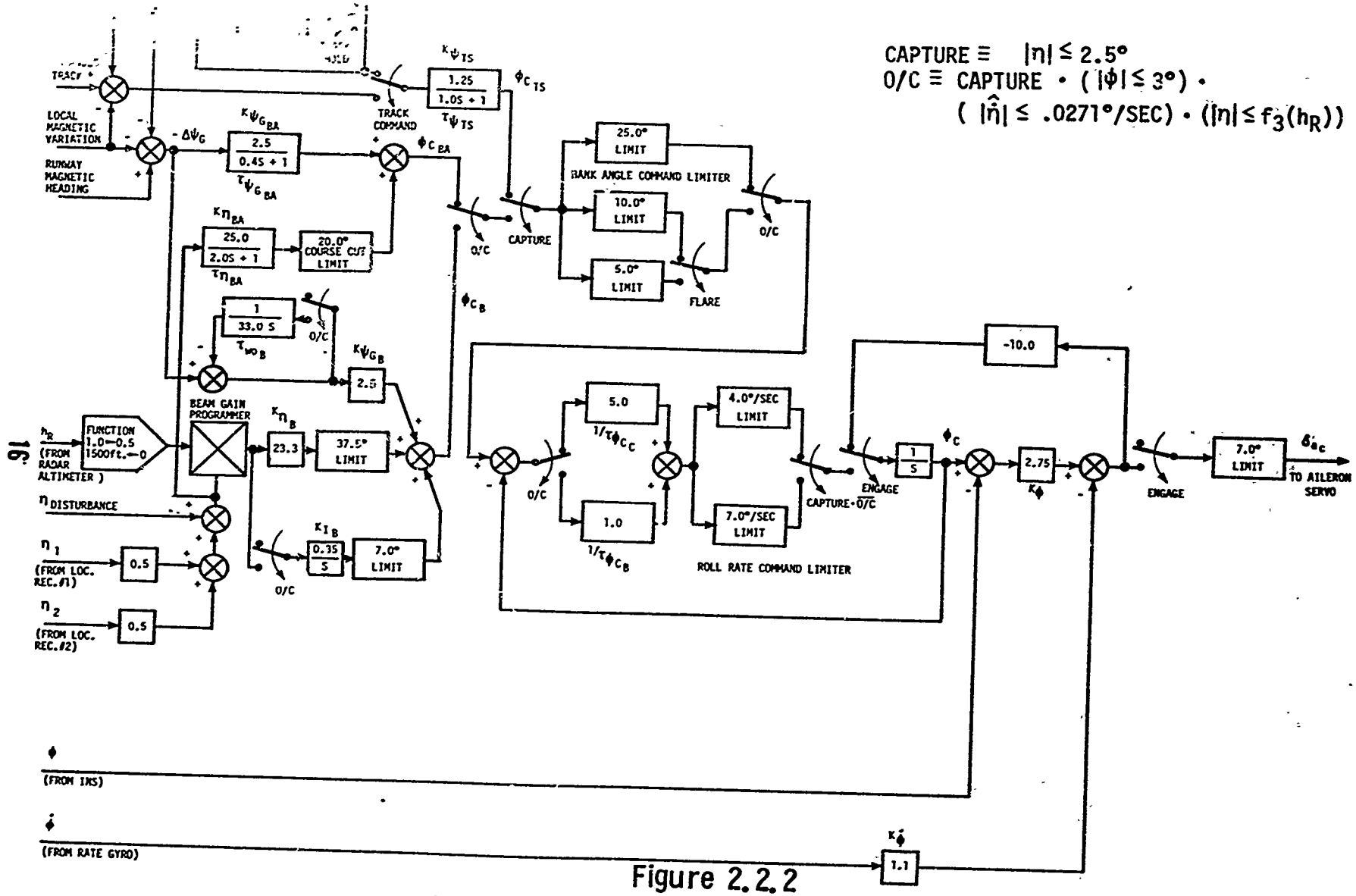

Figure 2.2.2
SYSTEM "B" LATERAL BLOCK DIAGRAM

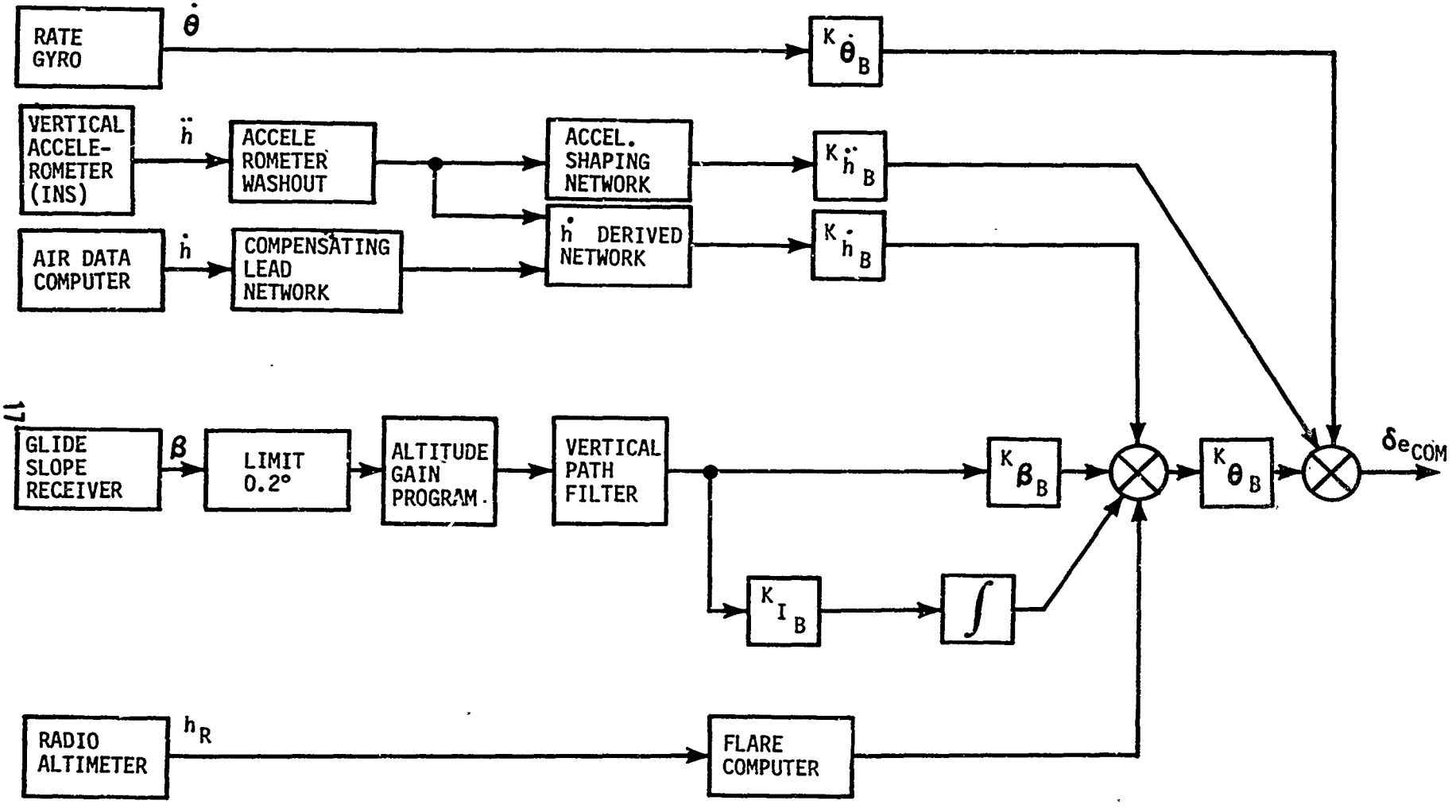

Figure 2.2.3
SYSTEM "B" LONGITUDINAL CONTROL LAW

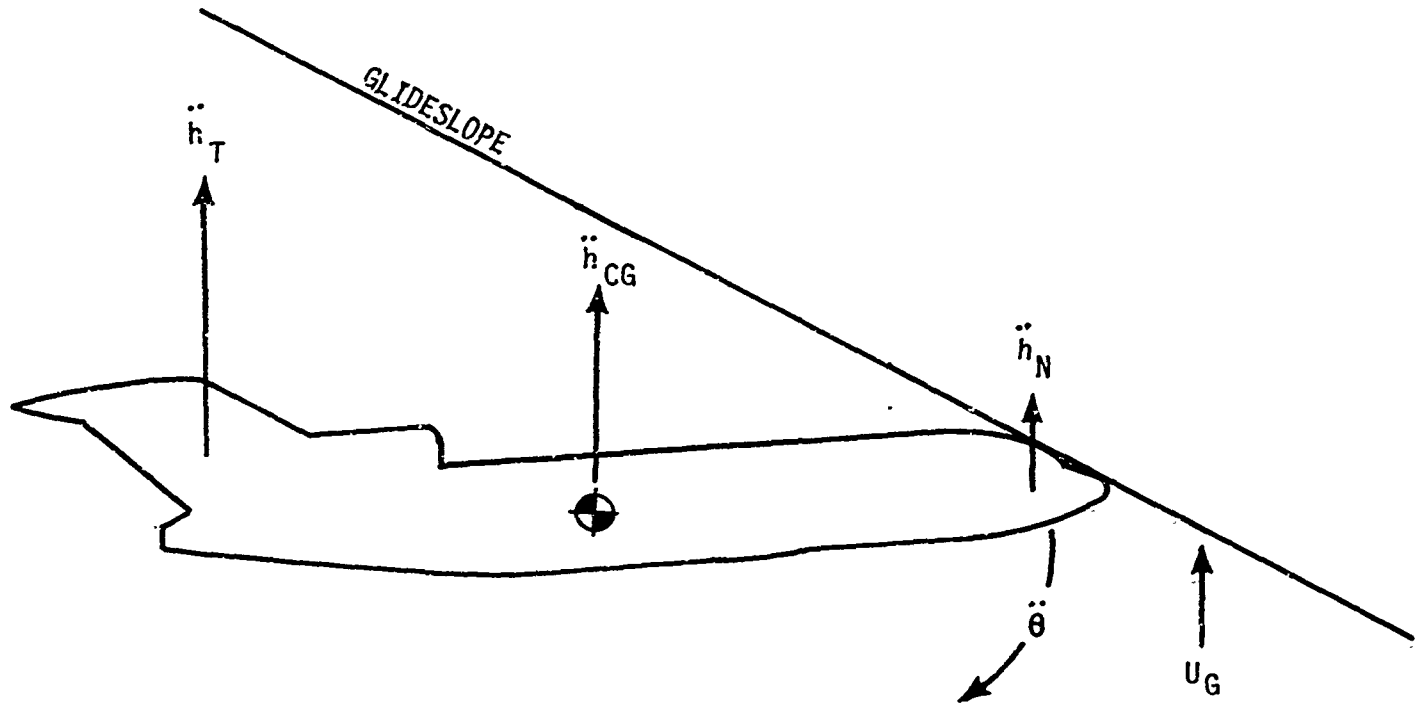

Figure 2.2.4
DISTRIBUTION ALONG BODY
OF RESULTANT ACCELERATIONS INDUCED
BY VERTICAL WIND GUST

inherent tendency of the airplane to pitch down is supplemented rather than opposed by the action of the elevator. Consequently path deviation is minimized.

Referring again to Figure 2.2.3, it is to be noted that the B system employs the same vertical path filter as did the A system. As a result, the response of systems A and B against beam disturbances is approximately equal.

The detailed block diagram of the B system in Figure 2.2.5 points out three other distinct differences between Systems A and B. First, the glide slope capture in the B system employs pre-capture synchronization which results in a pre-loading of the path integrator. Consequently when glide slope capture occurs, the elevator command does not "step" to a new value and the nose-over maneuver of the airplane is smooth. No bias is necessary to achieve a "fly-down" maneuver, as in the A system. Further, no additional switching is necessary in the B system after glide slope capture is achieved - including FLARE. This is the second fundamental difference in control law between systems A and B.

The flare maneuver is achieved by programming the beam error to zero, and utilizing radio altitude to command a diminishing altitude rate. In Figure 2.2.5, it can be seen that the altitude rate command during G/S control is nothing more than a constant gain on the beam and beam integral path. That is, whenever radio altitude is greater than 50 ft., the limiter on the flare command is saturated at 50 volts. This constant value is then multiplied by the beam error (plus integral).

The third difference in systems A and B is the high quality altitude rate feedback in the B system which is obtained by mixing the washed-out vertical acceleration from the INS with a compensated altitude rate signal from the air data computer. This process is the same form of smoothing as used by the C system on the glide slope beam.

2.3 Inertially Smoothed

The inertially smoothed autoland control law is referred to as System C in this report. System C not only relies on extensive use of inertial information to provide a high quality damping signal, but also derives short term position information from the INS to smooth the estimate of ILS deviation. The configuration and gains of System C were selected to represent a practical implementation of the concept that could easily be mechanized with present day equipment.

2.3.1 System C Lateral Control Law

The System C lateral control law is shown in the simplified block diagram of Figure 2.3.1. The roll attitude command is formed by a combination of complementary filtered localizer deviation plus integrated beam error together with INS track angle deviation for damping.

The inertially smoothed System C replaces the proportional localizer deviation signal path with a first order complementary filter position estimator. The complementary filter removes high frequency localizer deviation information and derives short term position from INS

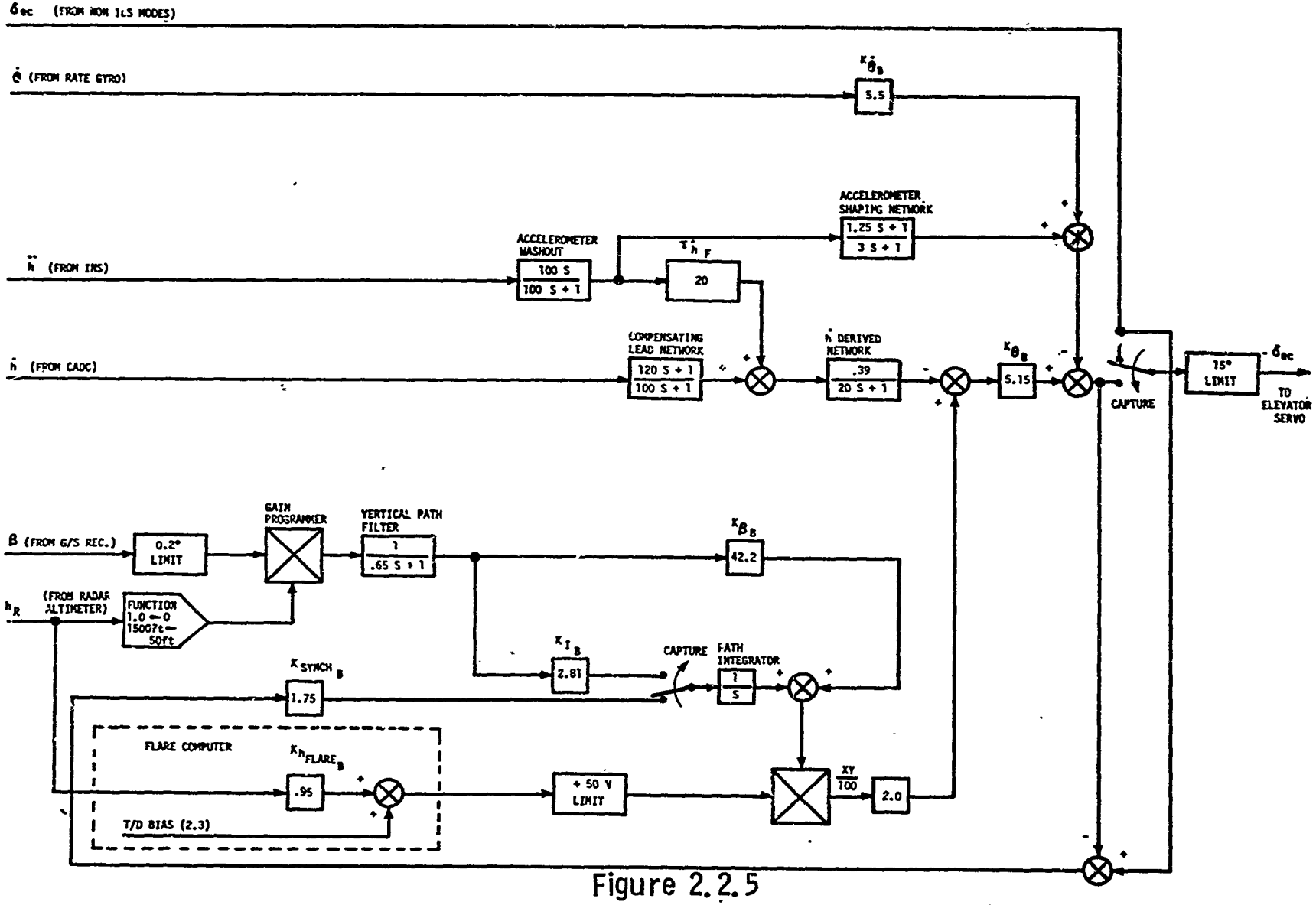

Figure 2.2.5

SYSTEM "B" LONGITUDINAL BLOCK DIAGRAM

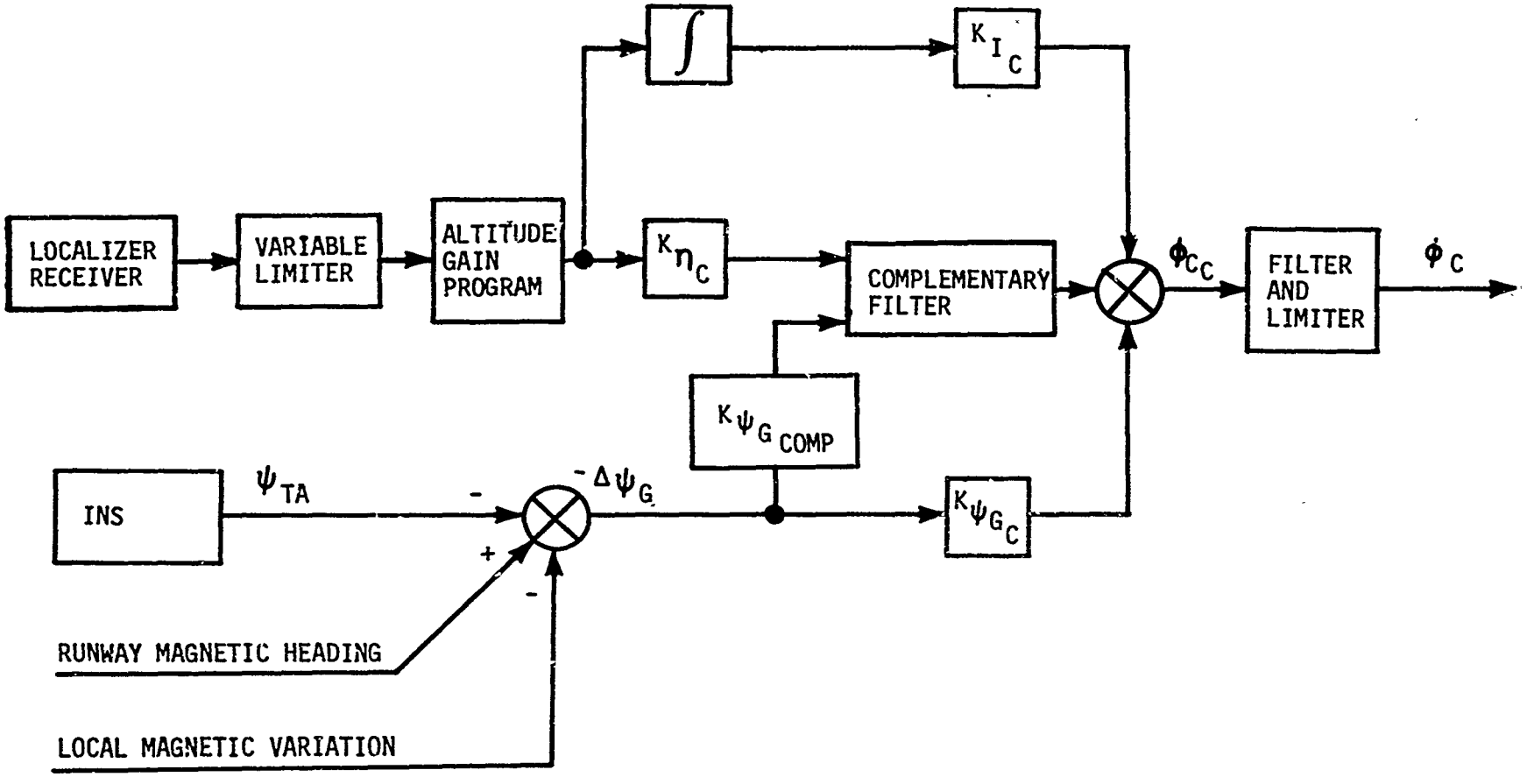

Figure 2.3.1
SYSTEM "C" LATERAL CONTROL LAW

track angle deviation to exactly replace the loss. The output of the complementary filter is true position with no dynamic modification together with low passed ILS and INS errors. A more detailed discussion of the complementary filter is given in Appendix A.

The input to the path integrator is localizer deviation. This prevents bias errors at the complementary filter output from causing steady state stand offs from the localizer beam.

The washout on track angle deviation (reference System B) was omitted to improve low frequency damping since the path integrator also prevents standoff resulting from bias errors in the track angle deviation signal.

The complete detail block diagram showing all gains, time constants and switches for System C is shown in Figure 2.3.2. Comments applicable to the inner loops, cruise modes and capture mode appear in Section 2.1.1.

System C uses the path integrator for mode synchronization prior to On Course*. Thus, when the System C control law assumes the guidance task at On Course, there is no transient in the roll attitude command.

The complementary filter output is initialized by allowing the filter to run with a relatively short time constant and without track angle deviation during capture. At On Course the complementary filter time constant is increased and track angle deviation is included as an input. As a consequence of this initialization and mode switching, System C smoothly and rapidly converged to the extended runway centerline to produce consistently small lateral displacements at low altitude and touchdown.

2.3.2 System C Longitudinal Control Law

The simplified block diagram in Figure 2.3.3 illustrates the basic mechanization of the C system. It will be noted that the B system and the C system are identical in every detail with one exception - the vertical path filter in system B is replaced by the complementary filter in system C. This complementary filter, as shown in the figure requires two additional inputs to complement the beam error. V_g (ground speed) from the INS is necessary to compute a valid descent rate command. Derived altitude rate is also required to develop an altitude rate error. It is this rate error which is used to complement the beam error from the gain programmer.

Figure 2.3.4 shows the complete block diagram for the C system. This diagram shows very clearly the mechanization of the complementary filter. Two switches and two time constants are included within the filter to provide for a glide slope capture that is similar to the B

*On Course (O/C) is a submode of the roll axis approach mode. The logic state exists subsequent to the first time the conditions given at the top of Figure 2.3.2 are satisfied.

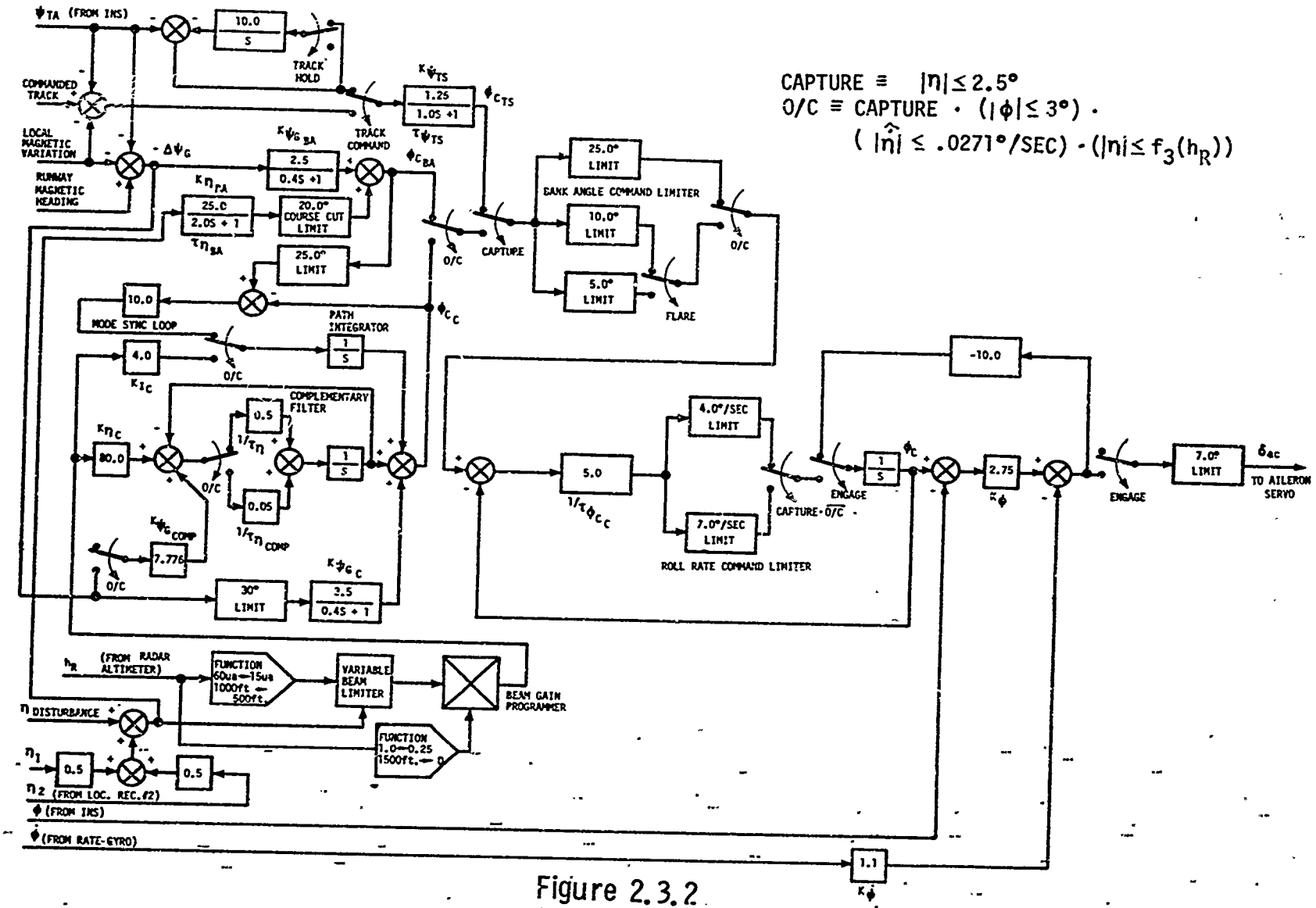

Figure 2.3.2
SYSTEM "C" LATERAL BLOCK DIAGRAM

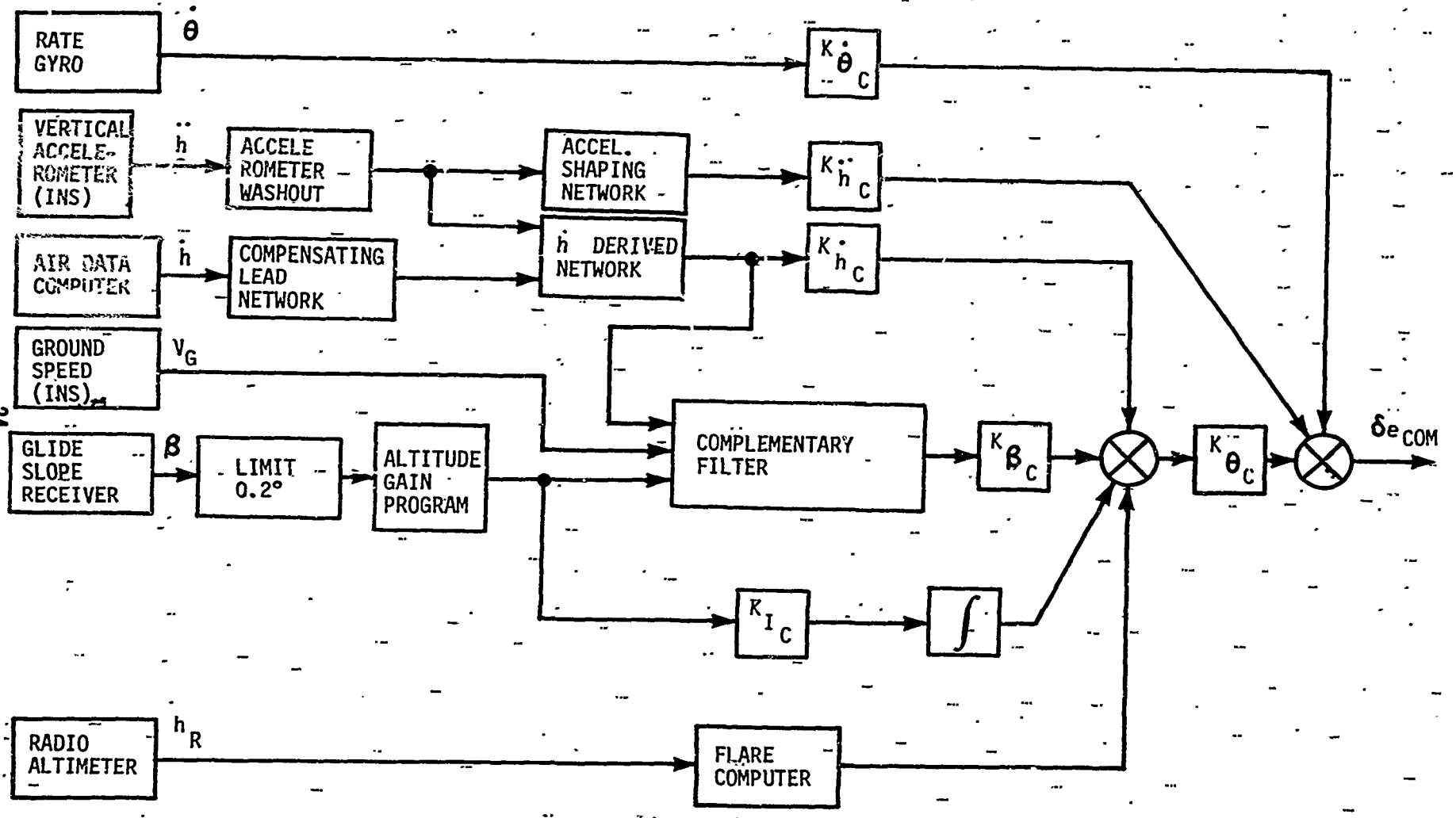

Figure 2.3.3

SYSTEM "C" LONGITUDINAL CONTROL LAW

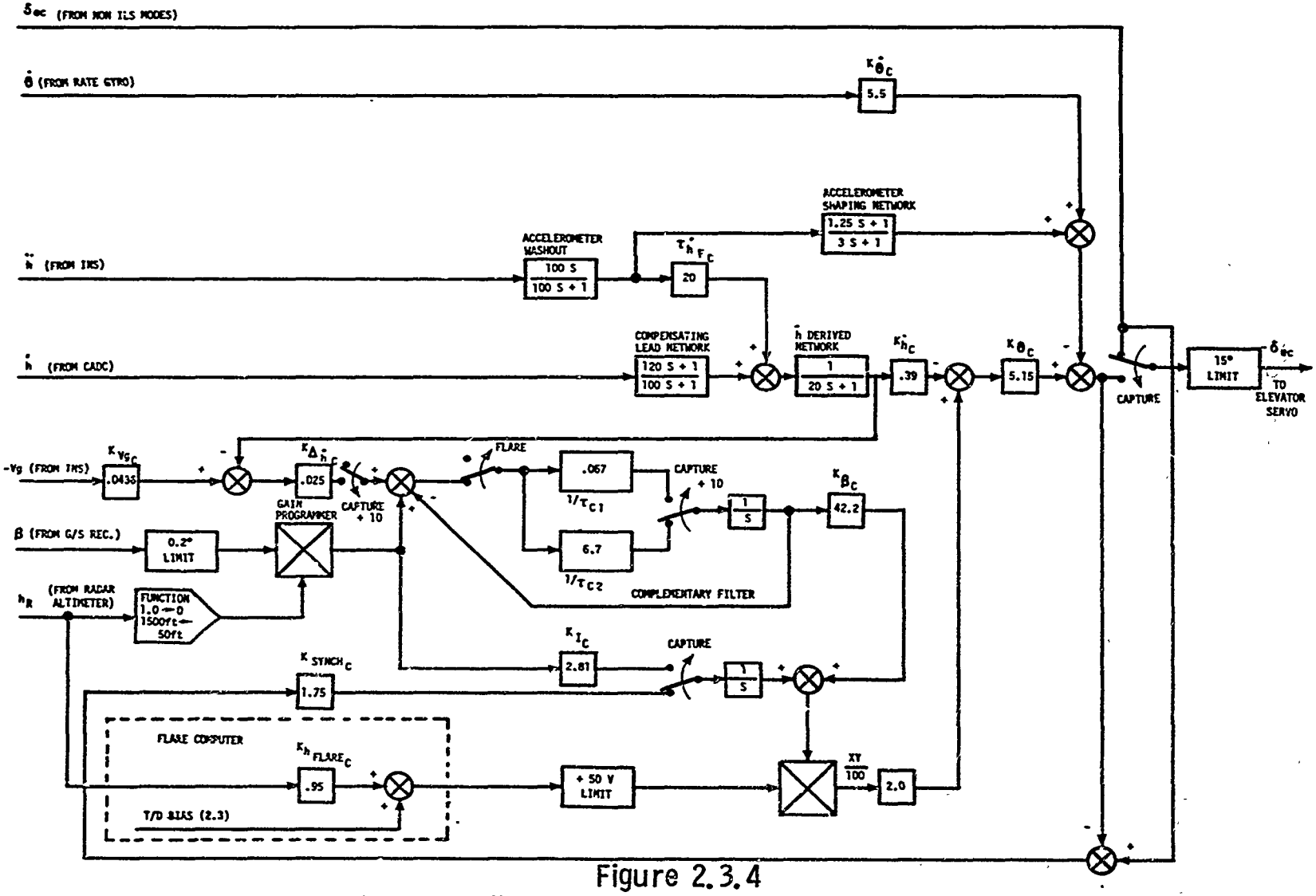

Figure 2.3.4

SYSTEM "C" LONGITUDINAL BLOCK DIAGRAM

system. However, 10 seconds after capture, the time constant is switched from .15 to 15 seconds and the altitude rate error is introduced to the filter. At this point, the system begins to wash out all initial condition errors, and steady state is achieved only after the beam error from the gain programmer is nulled to zero by the path integrator.

At FLARE*, the complementary filter is essentially placed in HOLD; otherwise, the mechanics of FLARE are the same as in the B system.

*FLARE is a submode of the pitch axis approach mode. The submode exists when sensed radio altitude is less than 50 feet.

3.0 AUTOLAND PERFORMANCE CRITERIA

The intention in developing a refined set of criteria for acceptable autoland is twofold: firstly, performance criteria are the principle basis upon which different autopilot control laws can be compared and, secondly, on an absolute basis the criteria will aid in the determination of the performance level of the automatic approach system.

The autoland performance criteria are considered to be the same for both Category II and III operations. This stems from the fact that in both cases the airplane trajectory is to be controlled in such a manner that the airplane is safely landed on the runway without subjecting the occupants to unnecessary or unpleasant maneuvers. The quality of approach performance is determined by the success in meeting this objective and is independent of visibility.

The lowering of visibility reduces the pilot's ability to detect poor approaches and take corrective action. Hence, the probability that the system makes a good approach must increase so that system safety is maintained at a constant level. For this study, the required probability of a successful approach was chosen to be 95% for Cat II and 99.9999% for Cat III. That is to say that for Cat II, it is acceptable for one in twenty approaches to result in a go-around for reasons other than failure to acquire visual reference. For Cat III, the airplane must not, more often than once in a million approaches, execute an unacceptable landing.

The failure to achieve a successful approach and landing could be the result of equipment malfunction or inadequate performance, but for this study it was assumed that all the failures are attributable to poor performance of a normally operating system. Abnormal performance due to equipment malfunction must be detected through redundancy or independent monitoring. Failure detection is considered a problem independent of the requirement to provide satisfactory normal performance, and is beyond the scope of this report.

Presently, two performance criteria are outlined in AC 20-57A and AC 120-29 to specify a "window" at 100 feet altitude and the autopilot beam tracking accuracy. The two criteria are related as one establishes a target dimension (the "window") and the other, an autopilot maneuver specification (beam tracking accuracy). In this section two new, but similar, criteria are derived. The first is referred to as the "footprint" criterion and is an extension of the existing "window". The second is referred to as the "maneuver" criterion and is a refinement of the existing tracking specification.

The footprint criterion specifies the target, at low altitude, which the airplane must hit with the specified Cat II or Cat III probability. The footprint is a two dimensional constraint on displacement and displacement rate from the desired line of flight. In contrast, the "window" concept has only a displacement dimension and thus does not fully take into account the correction in flight path that may be required very shortly after disconnect. Specifically, the footprint criteria for both lateral and longitudinal axes are designed such that successful passage through the footprint will assure that a minimum of subsequent correction to flight path need be made during flare and

rollout. In the case of the lateral axis, path corrections up to an acceleration of one foot per second squared are considered acceptable subsequent to entry within the footprint. This level of corrective acceleration is considered reasonable both for flight path corrections after decision height for Cat II and rollout corrections after touchdown for Cat III. Therefore, the footprint is applied for all altitudes between zero and 100 feet and independent of the category of approach being made. The footprint, like the window, is defined by the location of two ideal planes within which the localizer and glide slope would lie if they were perfect. Therefore, the footprint is referenced to the runway and not to measured glide slope and localizer beam deviations.

The maneuver criterion is an extension of the present autopilot performance specification. The maneuver criterion is designed to be representative of a typical pilot's assessment technique when monitoring the performance of an autopilot during a coupled approach in VFR conditions. The VFR stipulation implies that the pilot is capable, through visual reference, of determining flight path deviation and rate with respect to the ideal flight path which is extended runway centerline and the published glide slope angle and aim point. In contrast, the present autopilot and flight director performance specifications call for localizer tracking to within 25 ua of beam center with no sustained oscillation. Thus, beam misalignment in conjunction with a 25 ua tracking error may result in airplane displacement off the runway edge (equivalent to 28 ua) and yet the autopilot performance would be classified as satisfactory. Clearly a pilot is concerned with overall system accuracy and would consider such performance unacceptable. Therefore, the new maneuver criterion is referenced, just as the footprint, to the runway location and not to the measured beam. It is expected that the vast majority of coupled approaches to touchdown will be made, at least initially, under VFR conditions to allow pilots to gain confidence in the operation of the system and to gather data on its performance. A pilot may reasonably expect that a good autopilot will filter out nearly all of the "incorrect" beam information. This further justifies taking the view that the maneuver criterion, just as the footprint, be measured with respect to the runway and not to the beams. The pitch maneuver criterion is applied between one thousand feet altitude and flare altitude (50 feet for the 727). The roll axis maneuver criterion is applied between one thousand feet altitude and touchdown.

3.1 Roll Axis Footprint Criterion

The roll axis footprint criterion which is used in this report requires the satisfaction of all four inequalities which follow:

$$J \geq |y| \tag{3.1.1}$$

$$-J \leq R\dot{y} + y - \frac{\dot{y}^2}{2A} \text{ for } \dot{y} \leq 0 \text{ and } 0 \leq h \leq 100 \tag{3.1.2}$$

$$J \geq R\dot{y} + y + \frac{\dot{y}^2}{2A} \text{ for } \dot{y} \geq 0 \text{ and } 0 \leq h \leq 100 \tag{3.1.3}$$

$$|\dot{y}| \leq (10 - R)\,A \tag{3.1.4}$$

The symbols in these inequalities are defined in the Table of Abbreviations and Symbols.

The following parameters for the footprint criterion were used:

$R = 1.0$ seconds

$A = 1.125$ feet/second^2

$J = 60$ feet

The roll axis footprint criterion is plotted in Figure 3.1.1.

The roll axis footprint criterion defines the lateral limits of the runway between which touchdown must occur in order to be safe and acceptable on a routine basis. FAA Advisory Circular 20-57A defines these limits by specifying that the outboard landing gear shall be no closer than five feet from the lateral limits of a 150 foot runway. This defines a one dimensional "restricted zone" which the aircraft landing gear may not penetrate for an acceptable landing as shown in Figure 3.1.2.

This one dimensional (lateral deviation only) restricted zone defining the region outside the footprint is an insufficient constraint for acceptable touchdown. If the lateral velocity is not zero at touchdown, that velocity must be arrested through an acceptable maneuver before penetrating the restricted zone further down the runway. Not only is this a dynamic property of physical systems, but the pilot does, in fact, recognize this property and his estimate of the success in avoiding the restricted zone after touchdown is factored into his rating of the acceptability of the landing. The pilot has some reasonable idea of the performance of his aircraft, both the response during the maneuver to arrest the lateral velocity and the time required to establish that maneuver.

Since we know that the acceptable lateral acceleration for the maneuver is small compared to the forward velocity, the radius of the turn will be large. Thus, it is a reasonable approximation to use the equations for constantly accelerated motion from an initial condition at $t = t_o$. That is:

$$y = y_o + R\,\dot{y}_o + \dot{y}_o\,t + 1/2\,a\,t^2 \qquad (3.1.5)$$

Now the criterion is that the min-max of y not be in the restricted zone. The min-max of y occurs when $\dot{y}$ equals zero. The equation for $\dot{y}$ is:

$$\dot{y} = \dot{y}_o + a\,t = 0 \qquad (3.1.6)$$

Solving for the time of the min-max as a function of $\dot{y}_o$ yields:

$$t = \frac{\dot{y}_o}{a} \qquad (3.1.7)$$

Figure 3.1.1
ROLL AXIS FOOTPRINT CRITERION

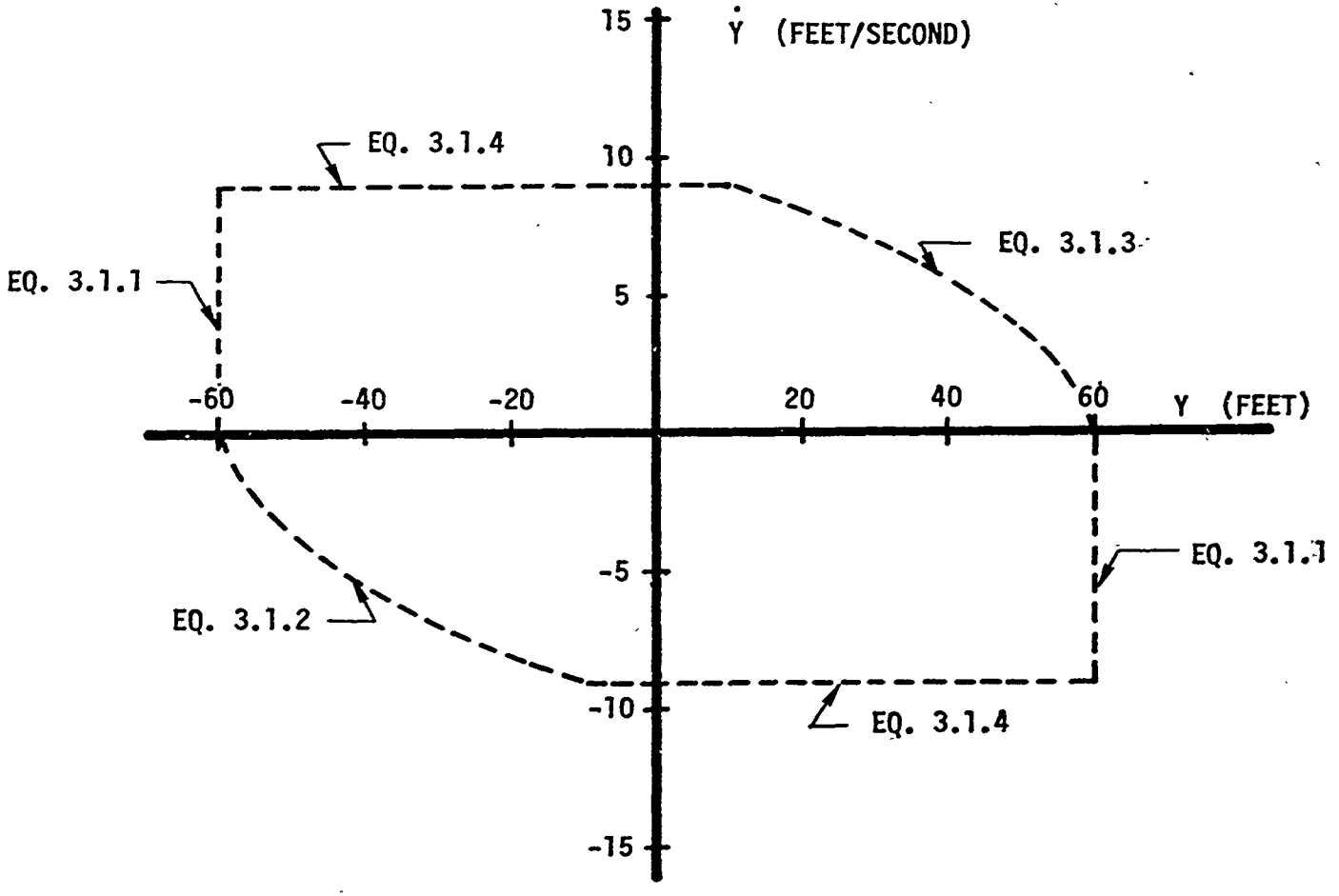

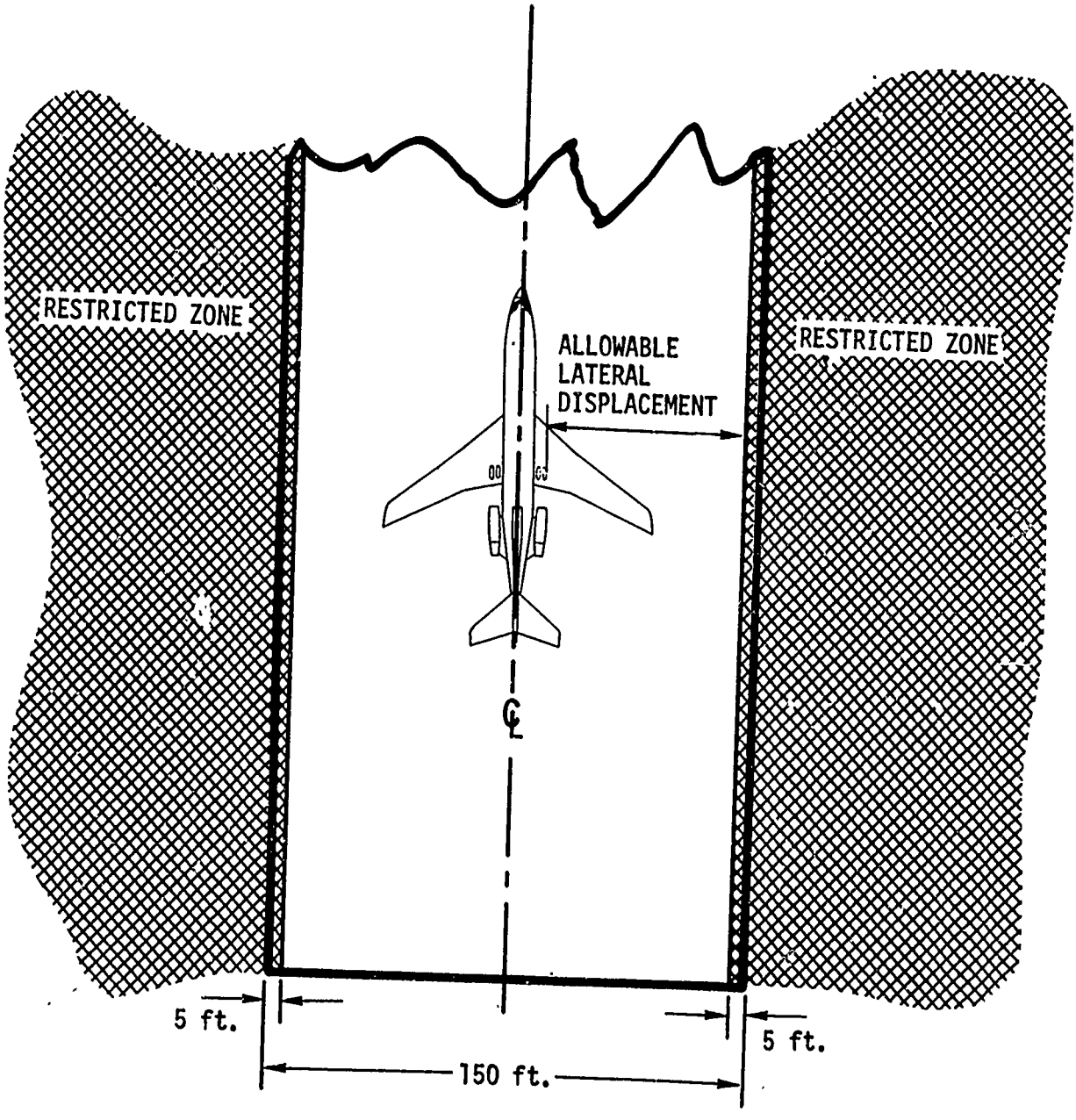

Figure 3.1.2
LATERAL DISPLACEMENT LIMITS

Substituting equation (3.1.7) into equation (3.1.5) yields:

$$y = y_o + R\dot{y}_o - \frac{\dot{y}_o^2}{2a} \qquad (3.1.8)$$

For the case of $\dot{y}_o \leq 0$, (a) must equal + A and the min-max may not lie in the left restricted zone.

$$-J \leq y_o + R\dot{y}_o - \frac{\dot{y}_o^2}{2A} \quad \text{for } \dot{y}_o \leq 0 \qquad (3.1.9)$$

And for the case of $\dot{y}_o \geq 0$, (a) must equal - A and the right restricted zone must be avoided.

$$J \geq y_o + R\dot{y}_o + \frac{\dot{y}_o^2}{2A} \quad \text{for } \dot{y}_o \geq 0 \qquad (3.1.10)$$

Equations (3.1.9) and (3.1.10) yield a constraint in the $y - \dot{y}$ plane which evaluates the ability of the aircraft to remain within the lateral bounds of the restricted zone when a corrective maneuver is applied. When the restricted zone constraint itself, equation (3.1.1), is added a closed footprint criterion in the $y - \dot{y}$ plane is formed.

This criterion does not only apply at the instant of touchdown. It is clear that the pilot is assessing the situation in a manner similar to this at altitudes up to decision height and acquisition of visual reference. Thus, in this report the footprint criterion is considered applicable between the 100 foot altitude and touchdown. The lateral position and velocity in the constraint equations are always with respect to the extended runway centerline.

The extension of the applicability of the footprint criterion to 100 feet suggests the additional constraint that, if the corrective maneuver is initiated at an altitude of 100 feet, the cross runway velocity be reduced to zero at or before touchdown. In this way, the need to continue the maneuver through flare and touchdown which increases the landing risk, is eliminated. Considering the time to go and the response time of the pilot and aircraft, the constraint may be derived from equation (3.1.6) by solving for $\dot{y}_o$. This yields the final constraint equation for the roll axis footprint criterion:

$$|\dot{y}| \leq (10 - R)\, A \qquad (3.1.11)$$

Here the ten seconds represent a conservative estimate of the time from 100 feet to touchdown which tends to emphasize reducing lateral velocity to zero before touchdown.

Now having derived the full set of four constraint equations for the footprint criterion, it is necessary to evaluate the parameters J, A, and R in order to use the criterion. Referring to Figure 3.1.2, it is clear that the allowable lateral displacement to reach the restricted zone is given by:

$$J = \frac{\text{restricted zone width}}{2} - \frac{\text{landing gear width}}{2} \qquad (3.1.12)$$

This requires that the landing gear of the aircraft with the given size be over the allowable portion of runway width and not in the restricted zone.

For the 727 aircraft on a 150 feet wide runway, this becomes:

$$Y = 70 - 10 = 60 \text{ feet} \qquad (3.1.13)$$

In the determination of the parameter, A, it must be remembered that the footprint criterion is not expressing safety considerations alone, but rather restricts aircraft positions and corrective maneuvers to those which are acceptable on a routine basis. In commercial passenger service, the pilot wants the corrective maneuver to be minimal at altitudes below 100 feet. A maneuver equivalent to two degrees of bank angle was considered suitably minimal without being excessively restrictive. For coordinated maneuvers, the bank angle and cross runway acceleration are related by

$$a = g \tan \phi \qquad (3.1.14)$$

Using this relationship leads to

$$A = 1.125 \text{ ft/sec}^2 \qquad (3.1.15)$$

A reasonable value for R, the reaction time of the pilot combined with the time required to establish the 2 degree bank maneuver, at low altitude is

$$R = 1 \text{ second} \qquad (3.1.16)$$

Now the constraint equations and parameter values have been derived to plot the roll axis footprint criterion of Figure 3.1.1. This restricts the lateral position, velocity, and corrective maneuvers from decision height through touchdown to those acceptable day in day out during commercial passenger service. The footprint is conservative in that the corrective maneuver is restricted to be very gentle. This footprint is more restrictive and realistic than the one dimensional footprint of AC20-57A because lateral velocity is taken into account. The flight test experience of 65 automatic landings and simulation of many hundred automatic landings has demonstrated that this refined footprint criterion is representative and not excessively restrictive.

3.2 Roll Axis Maneuver Criterion

The roll axis maneuver criterion which is used in this report requires the satisfaction of the inequality

$$Y \geq |y + K_1 \psi_G + K_2 \phi| \qquad (3.2.1)$$

for altitudes between localizer approach on course and touchdown. The symbols in this inequality are defined in the table of abbreviations and symbols.

The following parameter values for the maneuver criterion were used:

$K_1 = 17$ ft/degree for $0 < h < 100$ Ft.

$K_1 = 17 + \frac{(h-100)}{65}$ ft/degree for $h \geq 100$ Ft.

$K_2 = 5$ ft/degree

$Y = \frac{h - 100}{5.3} + 60$ ft for $h \geq 100$ Ft.

$Y = 60$ ft for $0 < h < 100$ Ft

In addition, a criterion on nuisance wheel activity should be imposed in the form of the allowable power spectral density of wheel motions resulting from localizer anomalies. However, this specification was not developed during this study. This report does not use a criterion on nuisance wheel activity.

The roll axis maneuver criterion with the proper parameter values should provide a separation between acceptable and unacceptable autoland which shows similarity to pilot evaluations. Defining the largest routinely acceptable maneuver is a more difficult task than sizing the footprint. The footprint size was determined by requiring that the aircraft land on the runway and not run off the edge. That led to firmly fixed numbers. The basis of the maneuver criterion is pilot confidence and passenger comfort which are much more difficult to describe quantitatively in terms of aircraft motions. In spite of this difficulty, the maneuver criterion developed and used for this report is a reasonable model for pilot opinion. This criterion is practical and useful even though it does not reflect the variability among pilots or aircraft.

A maneuver criterion is essential because although the aircraft landed in the target footprint, the manner in which it got there may have been unacceptable. The maneuvers above 100 feet may not have been the kind to be tolerated every day in commercial passenger service. Or at some point during the approach, the pilot may have become extremely doubtful that the autoland system would get the aircraft into the target footprint.

The autoland performance criteria of AC 120-29 are one dimensional (displacement only), contain large discontinuities, and apply to deviations from beam center. With most autolands likely to occur in VFR conditions the extended runway centerline should be the reference rather than the beam center as discussed earlier. In addition, the pilot tightens his tolerance on system performance in a nearly continuous manner rather than in a stepwise fashion. Further, the pilot evaluates performance using attitude and cross runway velocity as well as displacement.

Early attempts to refine and extend the performance criteria of AC 120-29 placed constraints on additional state variables one at a time. As these criteria were evaluated, it was found necessary to vary the allowable deviation of each state variable as a function of the other state variables. This interdependence was first expressed as discretely different limits according to the value of other state variables. This one-at-a-time form rapidly became too cumbersome and led to the development of a criterion on the state variables in an integrated form. That is, a single equation was developed to continuously constrain all of the relevant state variables at one time.

Although the pilot's attention varies from parameter to parameter, he forms an integrated assessment of the <u>total</u> vehicle state. Evaluation is made on this combination of maneuver variables or state. That is, as the aircraft is displaced to the right there is less tolerance of velocities to the right, and right wing down bank angles. Thus, it is more representative to change the limits on each variable as a function of the other variables. Further, this interdependence is better expressed in a continuous form rather than by only a couple of discrete step changes. The continuous form better describes the pilots' evaluation characteristics.

It is well recognized that the maneuver tolerance decreases as the aircraft gets closer to touchdown. However, a three step staircase with altitude is a poor characterization of this behavior. A nonlinear or piece-wise-linear, continuous function is a more realistic description of the pilots' maneuver tolerance.

As in AC 120-29, the maneuver tolerance is best expressed as a lateral deviation boundary. This boundary is made a function of altitude to resolve ambiguities resulting from variations in the nominal glide path and course width. Then the interdependence of the maneuver variables may be brought in through sensitivity factors which trade lateral deviation for the other variables. Thus, the functional form of the maneuver, criterion that develops is:

$$Y \geq |y + K_1 \dot{y} + K_2 \ddot{y}| \qquad (3.2.2)$$

To see the interdependence of variables built into equation (3.2.2), let us take a hypothetical example. Suppose for a moment that

$Y = 50$ feet

$K_1 = 10$ feet/foot/second

$K_2 = 25$ feet/foot/second^2

Then some borderline cases are:

Case	y	$\dot{y}$	$\ddot{y}$
1	50	0	0
2	0	5	0
3	0	0	2
4	30	2	0
5	-30	-2	0
6	70	-2	0
7	5	2	1

Notice that in cases 1 - 3 the parameters yield a limit on each variable, as in the classic case, if all other variables are zero. But now in case 4, when the velocity is to the right, less lateral deviation to the right is permitted before the inequality is violated. With the velocity to the left as in cases 5 and 6, we see in case 5 that the left deviation is restricted as in case 4, but in case 6 a greater deviation to the right is permitted in the presence of a left velocity. However, the aircraft cannot satisfactorily reach the state of case 6 from an initial condition of tracking the runway centerline because the constraint inequality would have to be violated before that state is reached. Case 7 shows a further reduction from case 4 in allowable lateral deviation when acceleration to the right is combined with velocity to the right.

To gain further insight into the implications of this constraint equation, write the equation for constantly accelerated motion.

$$y = y_o + \Delta t\, \dot{y}_o + \frac{\Delta t^2}{2}\, \ddot{y}_o \qquad (3.2.3)$$

Equation (3.2.3) predicts the lateral deviation Δt seconds after the observation of the instantaneous state y_o, $\dot{y}_o$, $\ddot{y}_o$ at $\Delta t = 0$ with the assumption that the acceleration $\ddot{y}_o$ will be constant at its instantaneous value. Notice the similarity between the right hand sides of equations (3.2.2) and (3.3.3). Thus, we see that in some sense the maneuver criterion claims that the pilot cares not only about the present lateral deviation but also what it will be in the future if the present trend continues. This prediction aspect of the criterion is reasonable in view of the pilot's intuitive feel for the physical laws of motion. People have a feel for the relationship between position, velocity, and acceleration or they would be unable to walk across a busy street, drive a car, or fly an airplane. However, the exactness of the prediction depends on the person's ability to perceive the relevant variables and evaluate the prediction equation. Recognizing this uncertainty, equation (3.2.2) expresses the coefficients as K's rather than relating them to a prediction interval. This allows individual adjustment of the sensitivities without regard for prediction interval so that a better match to the

evaluation process is obtained.

Now, realizing that $\dot{y}$ is proportional to ground heading and $\ddot{y}$ is proportional to bank angle for small perturbations, equation (3.3.2) may be rewritten as

$$Y \geq |y + K_1 \quad \psi_G + K_2 \quad \phi| \qquad (3.2.4)$$

One should be cautious about extending the application of this type of criterion or placing too much faith in its absolute accuracy. It is intended for application in judging simulated autoland system response to localizer beam anomalies which are encountered on a routine basis. There are reservations about its applicability in turbulence or any attempt to implement it inflight or use it to evaluate flight data. Further study is required before extending use of this criterion beyond the current investigation.

The parameter Y is dependent on allowable runway width and airplane size at low altitude. That is, the landing gear must be over the runway. Thus Y was taken to be equal to J at low altitude.

Now the allowable deviation, Y, must vary as a function of how close the aircraft is to touchdown. For this lateral criterion, altitude has been selected as the variable to indicate the proximity to touchdown. The pilot wants the aircraft within the runway edges from 100 feet on down. Hence Y should be constant from 100 feet through touchdown. For guidance on the allowable lateral deviation, examine the FAA Category II specification for autopilot performance. The autopilot is required to track centerline within 25 microamps between 100 feet and 300 feet and within 35 microamps above 300 feet. The 25 microamps at 100 feet is about 60 feet so that at this altitude the two criteria are reasonably in line with each other for a 727 size aircraft. But we would reject the occurrence of the step change at 300 feet. There is a further problem as shown in Figure (3.2.1). It is seen that the allowable lateral deviation varies with glide slope angle and localizer beam width. The localizer beam width is determined by runway length in order to keep the beam gradient constant at threshold. It is desirable to eliminate this strong dependence on beam width and glide slope by fitting a single function of altitude through the curves. The best fit is

$$Y = \frac{h - 100}{5.3} + 60 \quad \text{for } h \geq 100 \text{ feet} \qquad (3.2.5)$$

Select K_1 such that 8 feet per second ($\psi_G = 2.56$ degrees) of cross runway velocity for 2 seconds causes violation of the maneuver criterion at low altitude. In 2 seconds the aircraft has displaced 16 feet so that $K_1 = (60 - 16)/2.56 = 17$ feet/degree. Further, select K_2 such that a 5 degree bank angle held for 2 seconds violates the maneuver criterion. After 2 seconds the aircraft has displaced 5.6 feet and has a ground heading of 1.66 degrees so that $K_2 = \left[60 - 5.6 - 17\ (1.66)\right] / 5 = 5$ feet/degree.

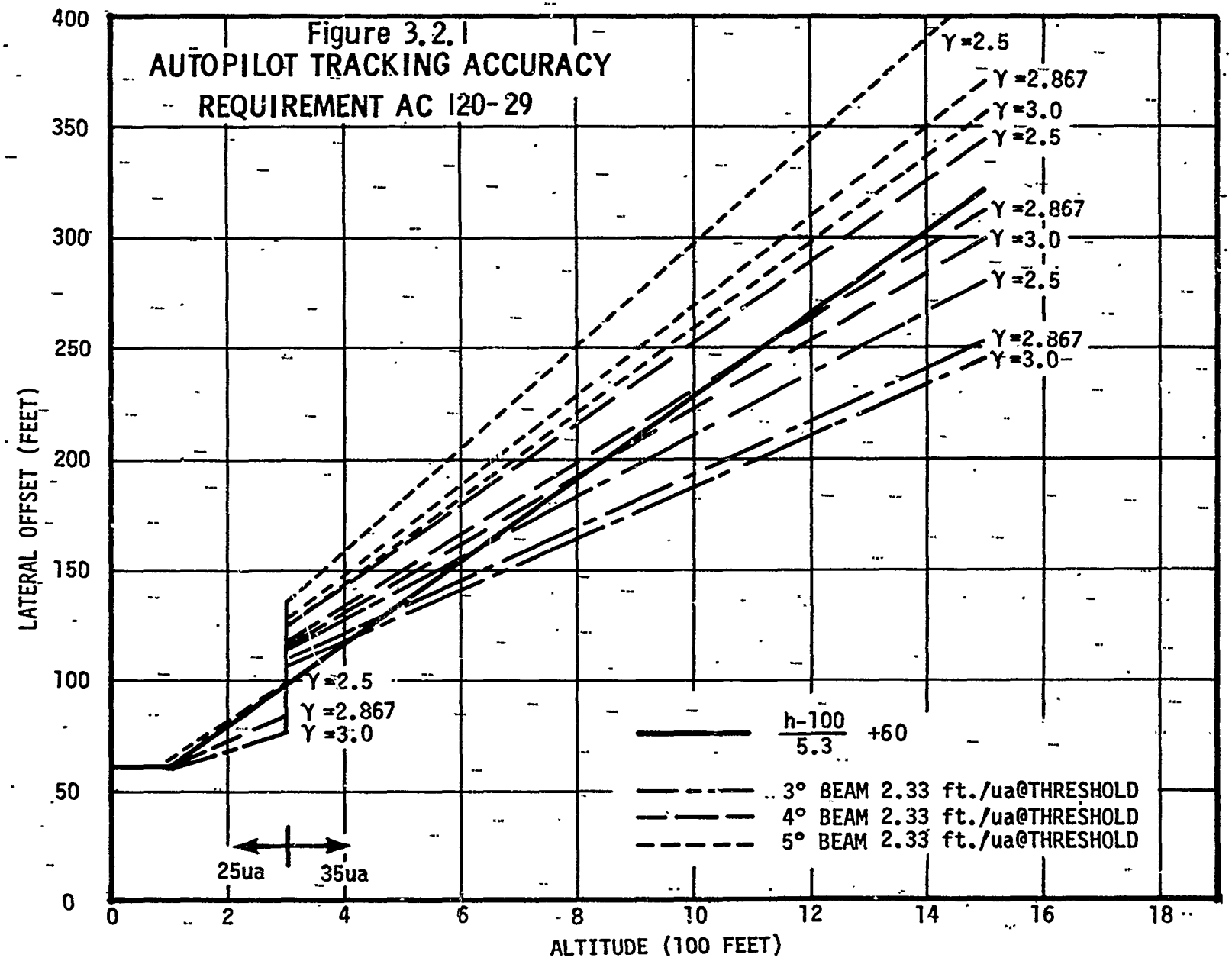
Figure 3.2.1
AUTOPILOT TRACKING ACCURACY
REQUIREMENT AC 120-29
LATERAL OFFSET (FEET)
ALTITUDE (100 FEET)
400
350
300
250
200
150
100
50
0
0
2
4
6
8
10
12
14
16
18
γ=2.5
γ=2.867
γ=3.0
γ=2.5
γ=2.867
γ=3.0
γ=2.5
γ=2.867
γ=3.0
γ=2.5
γ=2.867
γ=3.0
25ua
35ua
h-100/5.3 +60
3° BEAM 2.33 ft./ua@THRESHOLD
4° BEAM 2.33 ft./ua@THRESHOLD
5° BEAM 2.33 ft./ua@THRESHOLD

Now at 1500 feet of altitude select K_1 such that a cross runway velocity of 20 feet per second held for 4 secons will violate the maneuver criterion. Thus K_1 = 38.5 feet/degree at 1500 feet. And select K_2 so that a 10 degree bank angle held for 3.5 seconds violates the maneuver criterion. This leads to K_2 = 5 feet/degree.

Making a straight line fit between the values at 100 feet and 1500 feet yields the conclusion:

$$K_1 = 17 \text{ feet/degree for } 0 \leq h \leq 100 \text{ feet} \tag{3.2.6}$$

$$K_1 = 17 + \frac{h = 100}{65} \text{ feet/degree for } h \geq 100 \text{ ft} \tag{3.2.7}$$

$$K_2 = 5 \text{ feet/degree} \tag{3.2.8}$$

The basis for the maneuver criterion and its associated parameter values have been discussed. Although the size of the acceptable maneuver is consistent with the autopilot tracking accuracy specification of AC 120-29, the maneuver criterion used in this report has been refined by including anticipation.

3.3 Pitch Axis Footprint Criterion

Basically, the problem encountered in defining a reasonable "footprint" boundary in the 50-100 foot altitude band was one of finding the maximum allowable values for altitude and altitude rate deviations from the ideal glide slope (Δh and $\Delta \dot{h}$ respectively) such that an airplane which is equipped with reasonable flare control, and does not exceed these maximum deviations, will touchdown within the Category III dispersion limits on the runway. The "footprint" criterion problem was thus approached in the following steps.

(1) First, it was assumed that each system was provided with a flare coupler whose performance was satisfactory for Category III operation. Since this study concerns the behavior of certain autoland control laws in the presence of ILS disturbances, it will not include airplane response deviations which are not related to the G/S signal, such as the flare maneuver. Evaluating approach performance below the flare attitude would complicate even more this very difficult task. Furthermore, the actual ground effects and the action of the throttle during flare have significantly greater influence on the touchdown dispersion than does the action of the flare coupler. Consequently, the "footprint" criterion was developed without concern for problems associated with the design of flare control laws. Suffice it to assume that the flare coupler (and throttle control) will satisfy the flare requirements for Category III touchdown dispersion.

(2) Hypothetical touchdowns at the extremes of the acceptable zone (see Figure 3.3.1) were presumed. The problem was then worked backwards to determine the location of the nose of the airplane with respect to the ideal G/S which would have caused these limiting case touchdowns. This step determined the maximum and minimum Δh boundaries.

(3) The extreme $\Delta \dot{h}$ boundary of the "footprint" was defined by finding those descent rate deviations from nominal which caused the same longitudinal offsets as the maximum Δh deviations. Thus, the four points in the graph of Figure 3.3.2 were determined.

(4) To add a degree of safety to this "footprint" criterion, the extreme $\Delta \dot{h}$ points in Figure 3.3.2 were translated by 5 percent into the favorable $\Delta \dot{h}$ region as shown in Figure 3.3.3. Similarly, the extreme Δh points were moved by 5 percent into the favorable $\Delta \dot{h}$ region; and finally, for the initial trials, points were then connected as shown in Figure 3.3.4.

3.3.1 Assumptions and Constraints

In order to establish a meaningful boundary for Δh and $\Delta \dot{h}$ for the low altitude band of the G/S, certain assumptions were required. These assumptions had to be reasonable and free of arbitrary statements. For example, a particular glide slope angle may have been assumed in order to fix the geometry for an extreme, worse-case condition.

In addition, certain restriction, which hereafter will be referred to as constraints, were required in order to reduce the complexity of the problem to a level where meaningful discussion and communication may be possible. The following is a list of these assumptions and constraints.

3.3.1.1 Assumptions

(1) Each autoland system is provided with a flare coupler which will satisfy the touchdown dispersion requirements if, prior to flare, the airplane remains within the footprint. Several flare couplers have already been certified whose performance easily meets these requirements on a 2σ basis.

(2) For the shortest flare maneuvers, the worse case rate of change in descent rate is linear and can be expressed:

$$\dot{h} = m\,t \qquad (3.3.1)$$

where $\dot{h}$ = rate of change of altitude $\sim$ FPS

m = constant

t = time $\sim$ sec

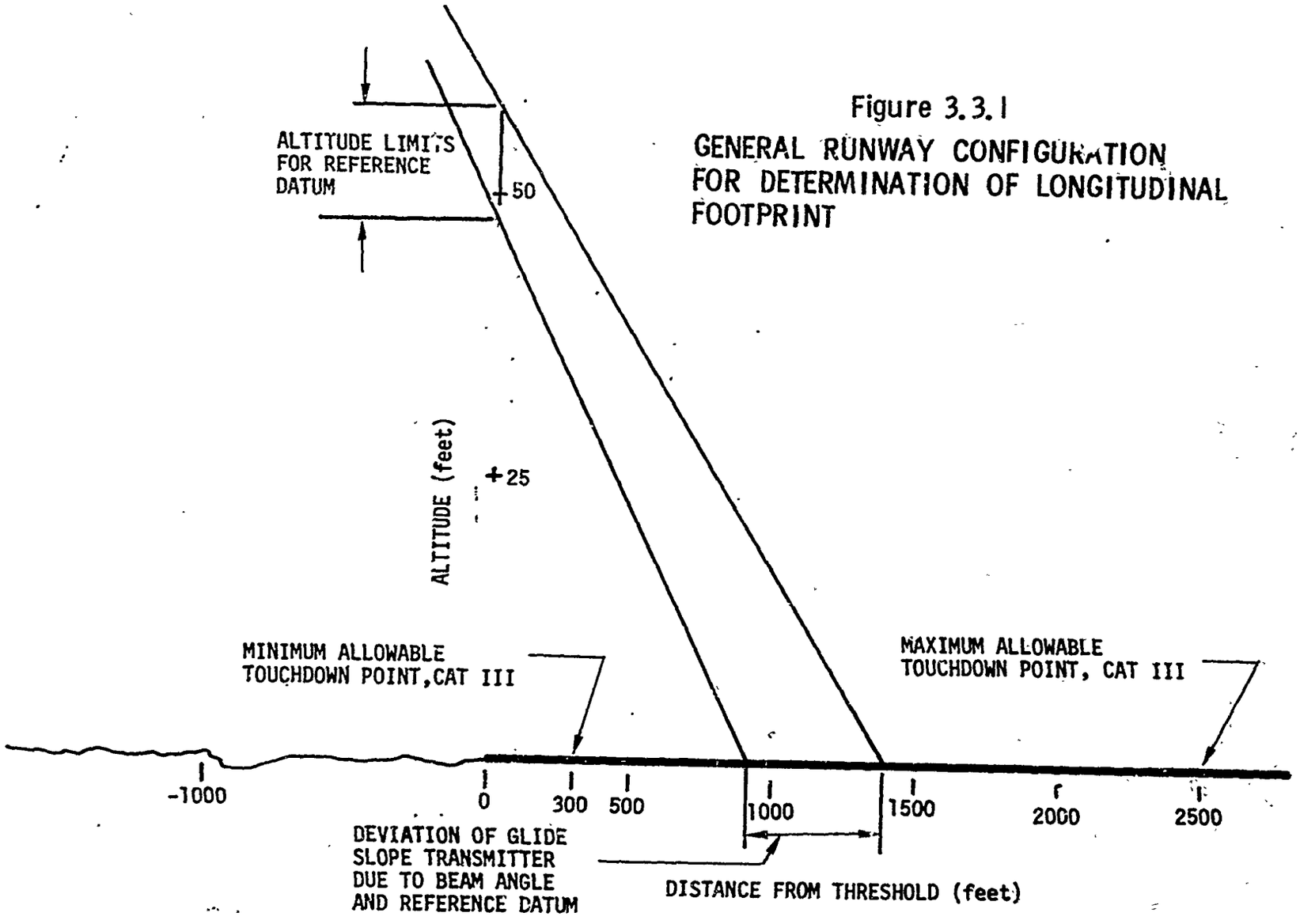

Figure 3.3.1

GENERAL RUNWAY CONFIGURATION FOR DETERMINATION OF LONGITUDINAL FOOTPRINT

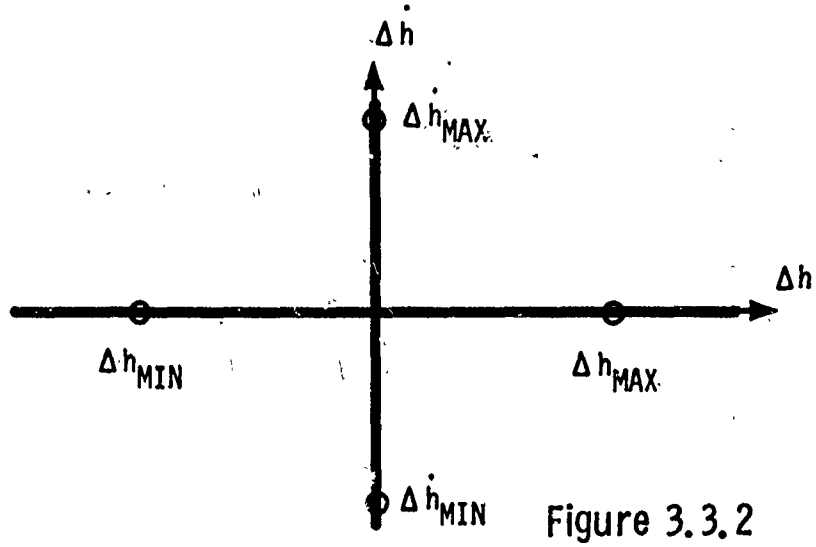

Figure 3.3.2

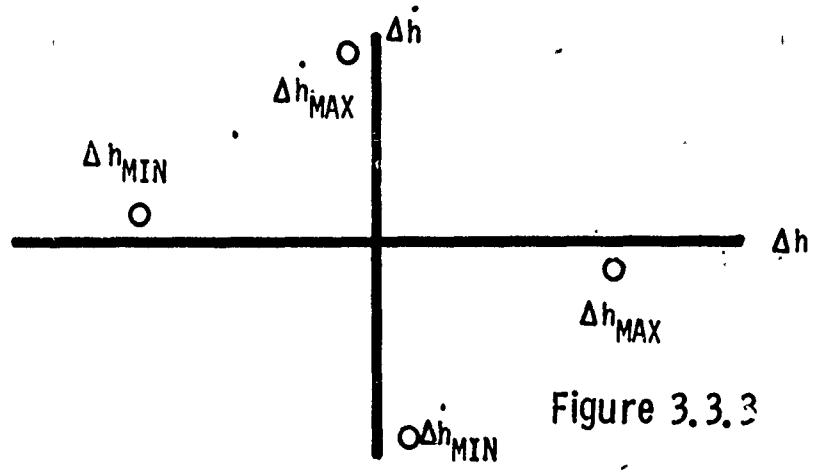

Figure 3.3.3

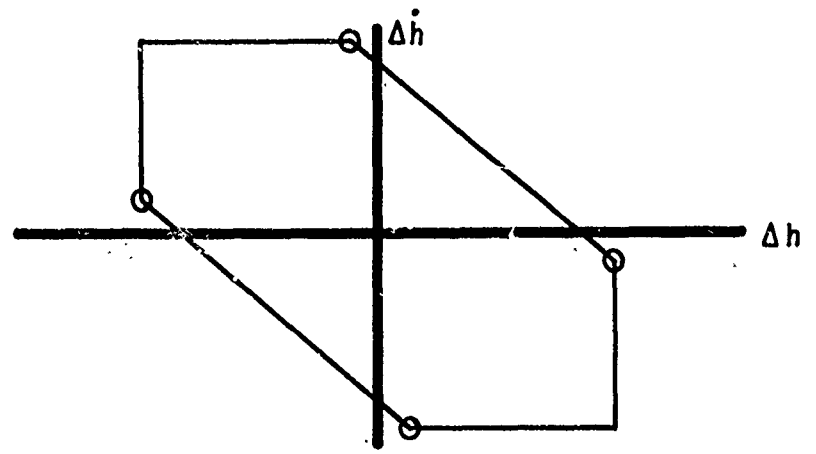

Figure 3.3.4

(3) The longest "float" caused by the flare coupler will be that demonstrated by the 747 airplane with a .95 probability. Although this probability (2σ) is considerably less than 1×10^{-6} (4.75σ), the 747 performance data are considered reasonable and valid for worse-case comparisons in that both theoretical analyses and empirical results show that the 747 touchdown dispersion is greater than that of the 727-100 (Category II) or the 367-80 (autoland research) airplanes. This is due primarily to the physical size of the 747 compared to the other two airplanes. In addition, the 747 Category III performance analysis has been documented by Boeing and approved by the FAA.

(4) The nominal touchdown point for the 727-100 airplane under certified autoland control is 357 feet beyond the G/S transmitter for a 2.5 DEG glide slope beam (Reference 1). The nominal touchdown point for any airplane under control of a particular flare coupler may be altered very easily by simply modifying the throttle control.

(5) The flare maneuver will always be executed at a gear height, above the runway level, of at least 35 ft. The normal gear height at flare for the 727-100 is 50 ft.

This assumption relates to the problem of terrain depressions in the region of the approach zone immediately preceding the runway threshold (from -1000 to 0 ft. shown in Figure 3.3.1). Depressions in this region give rise to delayed flare executions which may cause very hard touchdowns. Indeed, extremely large depressions coupled to maximum G/S deviations can cause touchdowns which may result in structural damage. Therefore, since depressions greater than 15 feet would often result in hard landings, it will be assumed that runways suitable for Cat. II and Cat. III operations will be free of depressions greater than 15 feet below runway level in the zone immediately ahead of the runway.

(6) The maximum ground speed during the flare maneuver is 240 FPS (142 Kts).

(7) The minimum ground speed during the flare maneuver is 180 FPS. (106 Kts).

3.3.1.2 Constraints

(1) Glide slope angles under consideration will be in the range

$$2.5 \leq \beta \leq 3.0^\circ$$

(2) The main landing gear must not touchdown less than 300 feet nor more than 2500 feet from runway threshold. This constraint must hold true for each facility, individually regardless of runway configuration and beam geometry.

Ref. 1 Boeing Document D6-24406, Performance Analysis of the 727-100 and 727-200 Autoland Systems, O'Toole, P. L.

(3) The greatest allowable descent rate at touchdown will be -6 FPS, a firm but safe value according to test pilot opinion, flight test results, and structural limitations.

(4) The "footprint" will be such that

$$\dot{\Delta h} < o \quad \text{when} \quad \Delta h = \Delta h \text{ MAX}$$

and

$$\dot{\Delta h} > o \quad \text{when} \quad \Delta h = \Delta h \text{ MIN}$$

NOTE: Whenever the airplane is below the beam,

$$\Delta h > 0. \text{ Whenever } \gamma < \text{G/S angle}, \quad \dot{\Delta h} < 0.$$

3.3.2 Determination of the Maximum Altitude Deviation

Determination of Δh_{MAX} (below beam deviation) for the 50-100 ft altitude band was achieved by hypothesizing a touchdown at the minimum allowable point (300 ft. in Figure 3.3.1) and then computing the most linear trajectory from that touchdown point up to the 35 ft. height above runway, as shown in Figure 3.3.5. A height of 35 ft. rather than 50 ft. was used because by Assumption No. 5, the longest delayed flare execution occurs at the lower altitude.

The most linear trajectory could be computed if the shortest longitudinal distance, ΔX in Figure 3.3.6 were known. To find this minimum ΔX, consider four extreme cases:

Case	G/S ~ Deg		V_g ~ FPS	
1	3.0	Constraint No.1	240	Assumption No. 6
2	2.5		240	
3	3.0		180	Assumption No. 7
4	2.5		180	

First, since ground speed changes less than 10% during flare, the change in sink rate is primarily due to changes in flight path. Hence,

$$\Delta X = \Delta t \cdot V_g \cos\gamma \approx \Delta t \cdot V_g \qquad (3.3.2)$$

where V_g is ground speed ~ FPS

Δt is time from execution of flare to touchdown ~ Sec

γ is flight path angle ~ DEG

The duration of the flare can be expressed

$$\Delta t = \frac{\Delta h}{\dot{h}_{AVE}} \qquad (3.3.3)$$

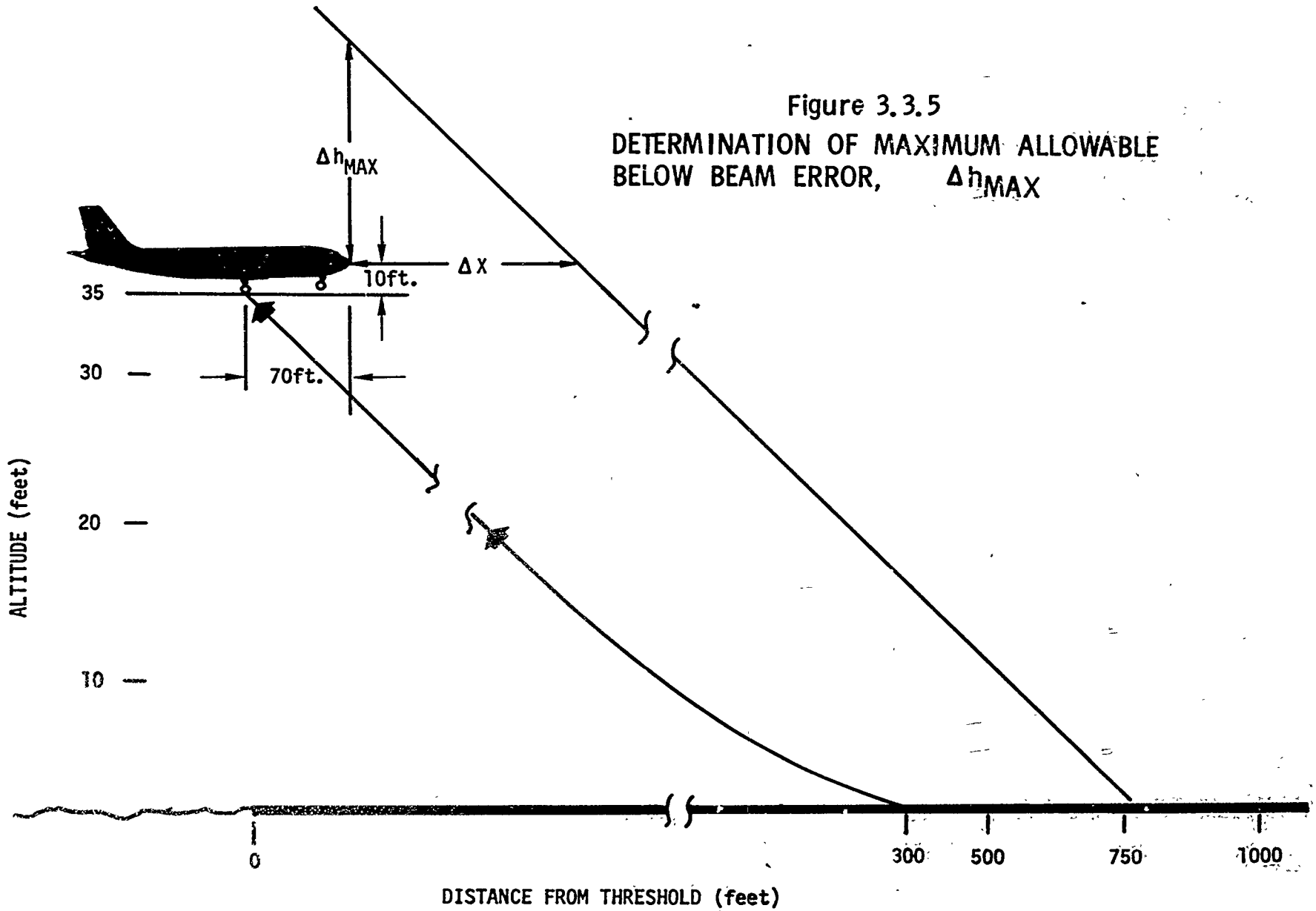

Figure 3.3.5
DETERMINATION OF MAXIMUM ALLOWABLE BELOW BEAM ERROR, Δh_{MAX}

Figure 3.3.6
GEOMETRIC DETERMINATION
OF SMALLEST ΔX (gear position
at flare)

CASE	G/S	Vg	ΔX
1	3.0	240	-905
2	2.5	240	-1020
3	3.0	180	-817
4	2.5	180	-911

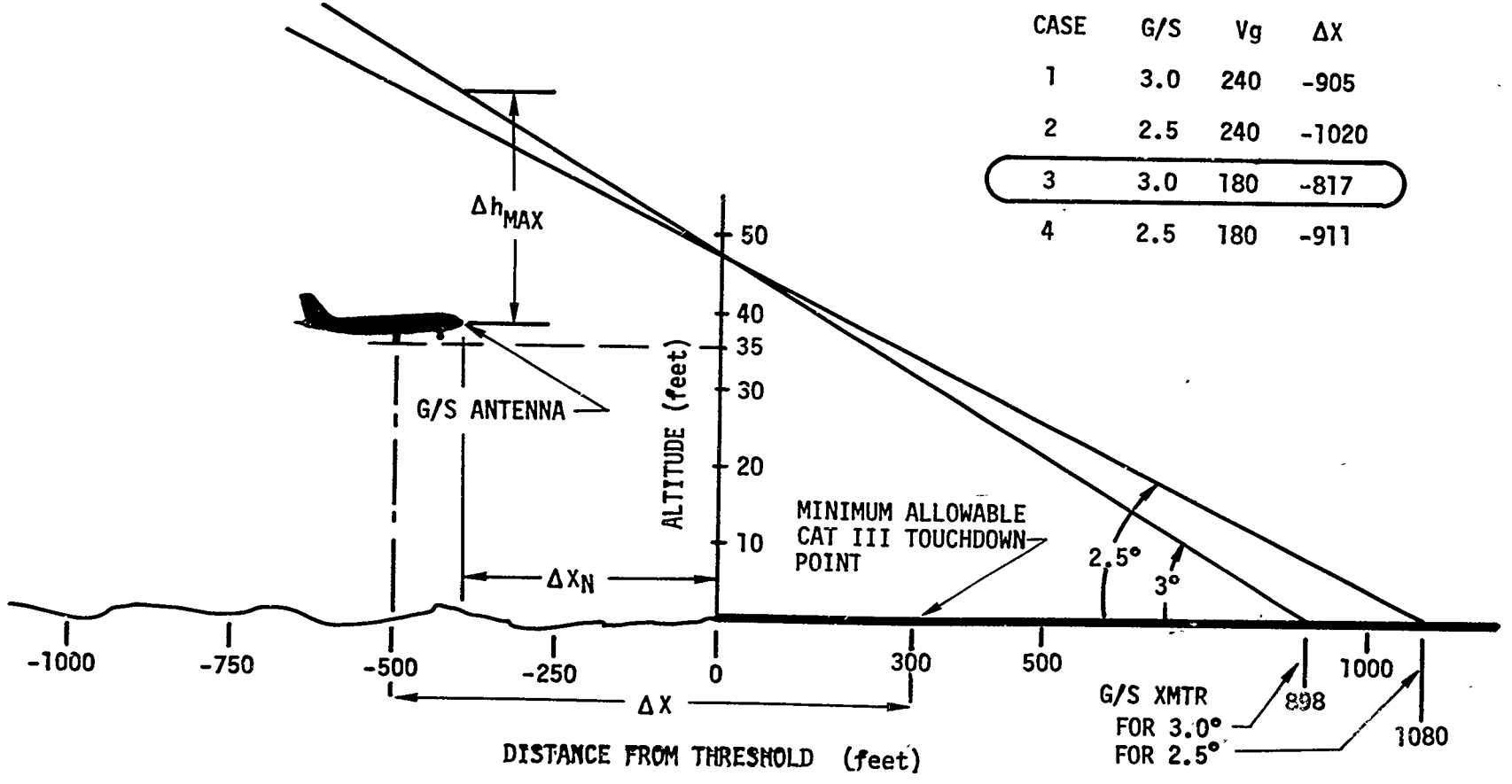

where $\dot{h}_{AVE}$ is the average descent rate during flare

Δh = vertical distance covered during flare which is 35 feet

Now, $\dot{h}_{AVE}$ is easily determined from assumption No. 2 and constraint No. 3; that is, the rate of change in $\dot{h}$ during flare is linear and the worst-case, touchdown rate is -6 FPS. Hence,

$$\dot{h}_{AVE} = \frac{\dot{h}_{FLARE} + \dot{h}_{T/D}}{2} \qquad (3.3.4)$$

$$= \frac{\dot{h}_{FLARE} - 6}{2}$$

where $\dot{h}_{FLARE}$ is the true descent rate at the execution of flare

$\dot{h}_{T/D}$ is the descent rate at the instant of touchdown

Substituting Eq. (3.3.4) into Eq. (3.3.3),

$$\Delta t = \frac{70}{\dot{h}_{FLARE} - 6} \qquad (3.3.5)$$

and substituting Eq. (3.3.5) for Δt into Eq. (3.3.2)

$$\Delta X = \frac{70Vg}{\dot{h}_{FLARE} - 6} \qquad (3.3.6)$$

Finally, in order to obtain ΔX in Eq. (3.3.6) as a function of glide slope and ground speed only, we must replace the $\dot{h}_{FLARE}$ term. According to constraint No. 4, when the altitude deviation is at maximum value, the altitude rate deviation, Δh, must be less than zero; i.e., if the airplane is below the beam the maximum distance, then it must be returning to the beam. It follows then that the very worst-case occurs when $\Delta \dot{h} = 0$.

Therefore, since we are dealing with zero altitude rate deivation,

$$\dot{h}_{FLARE} = -Vg \tan \beta \,,$$

$$\approx -Vg \quad \beta/57.3 \qquad (3.3.7)$$

where β is the glide slope angle $\approx$ DEG

Substituting Eq. (3.3.7) into Eq. (3.3.6),

$$\Delta X = \frac{70\ Vg}{-\frac{Vg\beta}{57.3} - 6} = \frac{-70}{\frac{\beta}{57.3} + \frac{6}{Vg}} \qquad (3.3.8)$$

Under FAA requirements listed in (Reference 9), the lowest possible reference datum is 47 ft. We will, therefore, apply Eq. (3.3.8) to the four cases of glide slope and ground speed shown above using the 47 ft. reference datum point. The result is shown in the Table of Figure 3.3.6.

As shown in Figure 3.3.6, case 3 yields the smallest value (-817 Ft.) for ΔX in Eq. (3.3.8). That is, the lowest speed coupled to the highest glide slope will produce the most linear trajectory from flare altitude to touchdown, and hence, the smallest value for ΔX in the four cases.

To obtain the numerical value for Δh_{MAX}, we first obtain the vertical and horizontal distance from the main gear to the G/S receiver antenna on the nose of the 727-100 airplane, which is shown in Figure 3.3.5. Numerically,

Horizontal Distance = 70 ft
Vertical Distance = 10 ft

The location of the nose ΔX_N, referred to the horizontal coordinate in Figure 3.3.6 is determined by

$$\Delta X_N = 300 + \Delta X + 70 = 300 - 817 + 70 = -447$$

The nose location above the runway is 35 + 10 = 45 ft. Consequently, since we are dealing with the 3.0 deg. beam angle,

$$\Delta h_{MAX} = \left[898 - (-447)\right] \tan (3.0) - 45 \qquad (3.3.9)$$

The 898 ft. value is the required location from threshold of the glide slope transmitter for the 3.0 deg. beam whose reference datum is 47 ft. Eq. (3.3.9) reduced to

$$\Delta h_{MAX} = 25.4 \text{ ft.} \qquad (3.3.10)$$

3.3.3 Determination of the Minimum Altitude Deviation

The same procedure used to determine the maximum allowable altitude deviation below beam is not applicable to the determination of the minimum altitude deviation, Δh_{MIN} (above beam error). This is because all flare computers to date operate "open-loop" with respect to range, i.e., there is no runway distance information input to the autopilot flare coupler. Consequently, there is no assurance that an airplane, which is tracking the beam perfectly at the beginning of flare, will touchdown less than 2500 ft. from threshold. As a result, no realistic, worse-case trajectory could be derived by simple assumptions and straightforward mathematics as was done in the minimum touchdown case.

The problem of determining Δh_{MIN}, was approached by considering the following analysis. First, the glide slope transmitter was located

Ref. 9 FAA Advisory Circular 120-29, Criteria for Approving Category I and Category II Landing Minima for FAR 121 Operators, September, 1970

hypothetically in accordance with the worse-case glide slope ($\beta = 2.5$ deg, the same glide slope to which the test airplane was subjected). The maximum reference datum height of 60 ft. was postulated and, hence, the location of the transmitter was 1375 ft. down runway from threshold, the greatest possible distance.

By assumption No. 4 (Section 3.3.1.1), the nominal longitudinal distance of the 727 flare maneuver which is initiated with zero deviation is 357 ft. Hence, the total longitudinal distance remaining, without regard for altitude deviation or dispersion of the flare maneuver (turbulence, wind shear, sensor and autopilot inaccuracies, etc.) was (see Figure 3.3.7).

$$2500 - 1375 - 357 = 768 \text{ ft.}$$

The 2500 foot figure is the maximum allowable down runway touchdown position. If a thorough statistical analysis were employed here to determine the percentage of 768 ft. that may be reserved for a Δh_{MIN}, the result would likely have been a negative quantity; i.e., the airplane should nominally be located somewhere below the beam when beginning the flare maneuver in order to maximize the probability of landing within the touchdown zone.

The "float" caused by this hypothetical flare maneuver was taken from assumption No. 3 (Section 3.3.1.1) -- the 2σ dispersion of the 747. (Reference (3) points out that the following factors contributed to 747 touchdown dispersion about the nominal.

A. Airplane Configuration; weight, c.g., flaps, etc.

B. Approach Speed

C. Beam Angle and Reference Datum

D. Receiver Centering Error

E. Path Alignment Accuracy

F. Beam Bends

G. Autopilot and Sensor Tolerances

H. Vertical Turbulence

I. Horizontal Turbulence, including Wind Shear

(Reference 3) shows that the variance (σ^2) for all the effects, A through I above, is 54,000 ft^2, but an extreme, worse case glide slope transmitter location has already been postulated. Hence, we ignore C (beam angle and reference datum). Furthermore, those variables which induce deviations only during glide slope control should be ignored. This implies that the variables D, E, F, be totally removed from the overall variance. Thus, since the variance of the sum of

Ref. 3 Boeing Document D6-33220, 747/SPZ-1 Fail-Operational Autoland System Performance Analysis

random variables is equal to the total variance,

$$\sigma_{T/D}^2 = 54{,}000 - \sigma_C^2 - \sigma_D^2 - \sigma_E^2 - \sigma_F^2 \qquad (3.3.11)$$

where

$\sigma^2_{T/D}$ is the total variance for the worse-case touchdown dispersion that we seek

σ_C^2 is the 747 variance due to beam angle and reference datum

σ_D^2 is the FAA prescribed variance due to airborne receiver centering error

σ_E^2 is the FAA prescribed variance due to path alignment

σ_F^2 is the 747 variance due to beam bends

From reference (3) the values for these variances are substituted in Eq. (3.3.11).

$$\sigma_{T/D}^2 = 54{,}000 - (5{,}850 + 2{,}700) - 100 - 4{,}550, - 400$$
$$= 40{,}400 \text{ ft}^2 \qquad (3.3.12)$$

and consequently

$$2\sigma_{T/D} = 402 \text{ ft}^{[1]} \qquad (3.3.13)$$

The value in Eq. (3.3.13) was applied as a constraint on the flare computer; i.e., performance specifications for flare couplers used in autoland systems must require that longitudinal "overshoots" remain within 402 ft. with 4.75σ probability. This requirement may be relieved depending upon the strictness of the 2500 ft. boundary.

Referring now to Figure 3.3.7, the longitudinal distance that remained on the runway for Δh_{MIN} computation was easily determined. Subtracting the maximum "float" distance in Eq. (3.3.13) from the remaining distance available on the runway, 768 ft. gave a total of 366 ft. with which to compute Δh_{MIN}. No airplane geometry enters into the computation, since as shown in Figure 3.3.7, the geometry was accounted for in the nominal distance consumed by the flare maneuver.

Recalling that the worse-case beam angle for this case is 2.5 deg

$$\Delta h_{MIN} = -366 \tan 2.5^\circ = -16 \text{ ft} \qquad (3.3.14)$$

[1] In a strict sense, this value corresponds to a 2.3σ number since the discussion concerns a single-tailed distribution.

Figure 3.3.7
DETERMINATION OF THE MAXIMUM
ALLOWABLE ABOVE BEAM ERROR, Δh_{MIN}

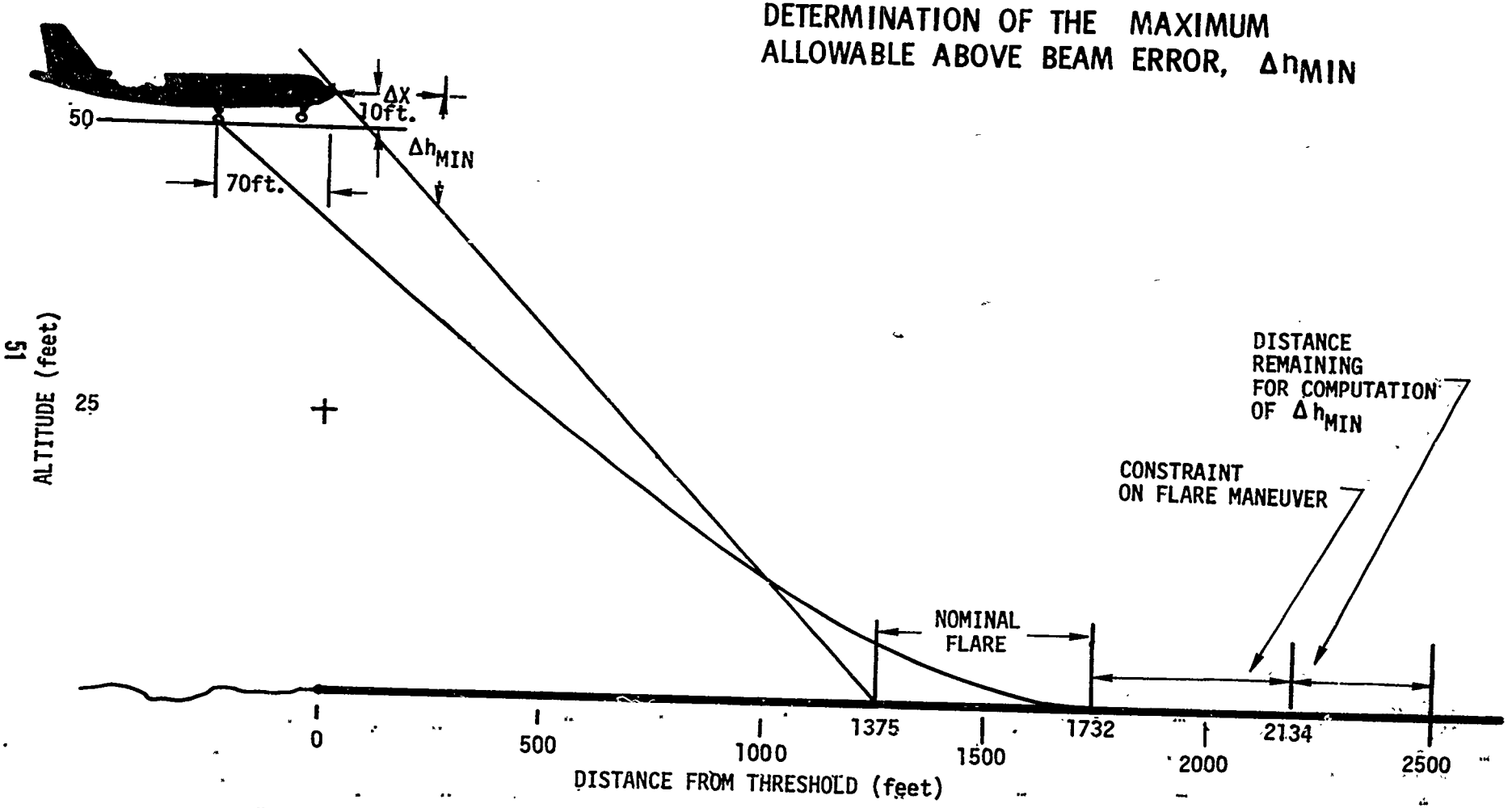

As stated briefly above, Eq. (3.3.10) and Eq. (3.3.14) essentially provide the basis on which to define the performance specifications for a Category II and Category III flare coupler. In other words, if the airplane is within the Δh_{MAX} and Δh_{MIN} boundary (and also within the $\Delta \dot{h}_{MAX}$ and $\Delta \dot{h}_{MIN}$ boundary which is derived below) at flare altitude, the flare computer must cause the airplane to touchdown between 300 and 2500 ft. on the runway.

3.3.4 Determination of the Maximum and Minimum Altitude Rate Deviations

To establish the vertical footprint boundary, the maximum and minimum descent rate deviations, the simulated 727-100 airplane was used. Stated simply, the problem was one of finding the relationship between sink rate deviations and altitude deviations.

The 727-100 airplane, equipped with the three types of longitudinal autoland systems studied in this program, was simulated and evaluated for altitude rate errors. Beginning at 100 ft (gear height) and zero beam deviation, various altitude rate deviations, $\Delta \dot{h}$, were introduced into each autopilot system until the resulting peak altitude error, Δh, reached values of -16 ft (Δh_{MIN}) and 25.4 ft. (Δh_{MAX}) for ascending and descending rate errors respectively. The values of $\Delta \dot{h}$ that caused each system to peak at these maximum and minimum altitude errors were then averaged, and this average was selected as the maximum (and minimum) altitude rate errors in the footprint. Quantitatively,

$$\Delta \dot{h}_{MAX} = 5.64 \text{ ft/sec} \qquad (3.3.15)$$

$$\Delta \dot{h}_{MIN} = -3.0 \text{ ft/sec} \qquad (3.3.16)$$

Hence, the value in Eq (3.3.15) is the largest descent rate error allowable at 100 ft. altitude and the upper limit on the vertical axis of the footprint. Similarly, Eq (3.3.16) is the lower limit on the vertical axis.

3.3.5 Complete Footprint

Plotting the values of Eq. (3.3.10), Eq. (3.3.14), Eq. (3.3.15) and Eq. (3.3.16) on rectilinear coordinates results in the X points on the axes of Figure 3.3.8. The O-points in the Figure result from translating the maximum and minimum points 5% into the favorable quadrant; i.e., the airplane will not be permitted to be at the extreme allowable altitude deviation unless the rate deviation is in the direction to decrease the error. Finally, the O-points were connected as shown in Figure 3.3.8 by the solid lines.

It should be stressed that the footprint shown in Figure 3.3.8 is the maximum allowable path variation due to all causes including beam bends, winds, offsets, etc.

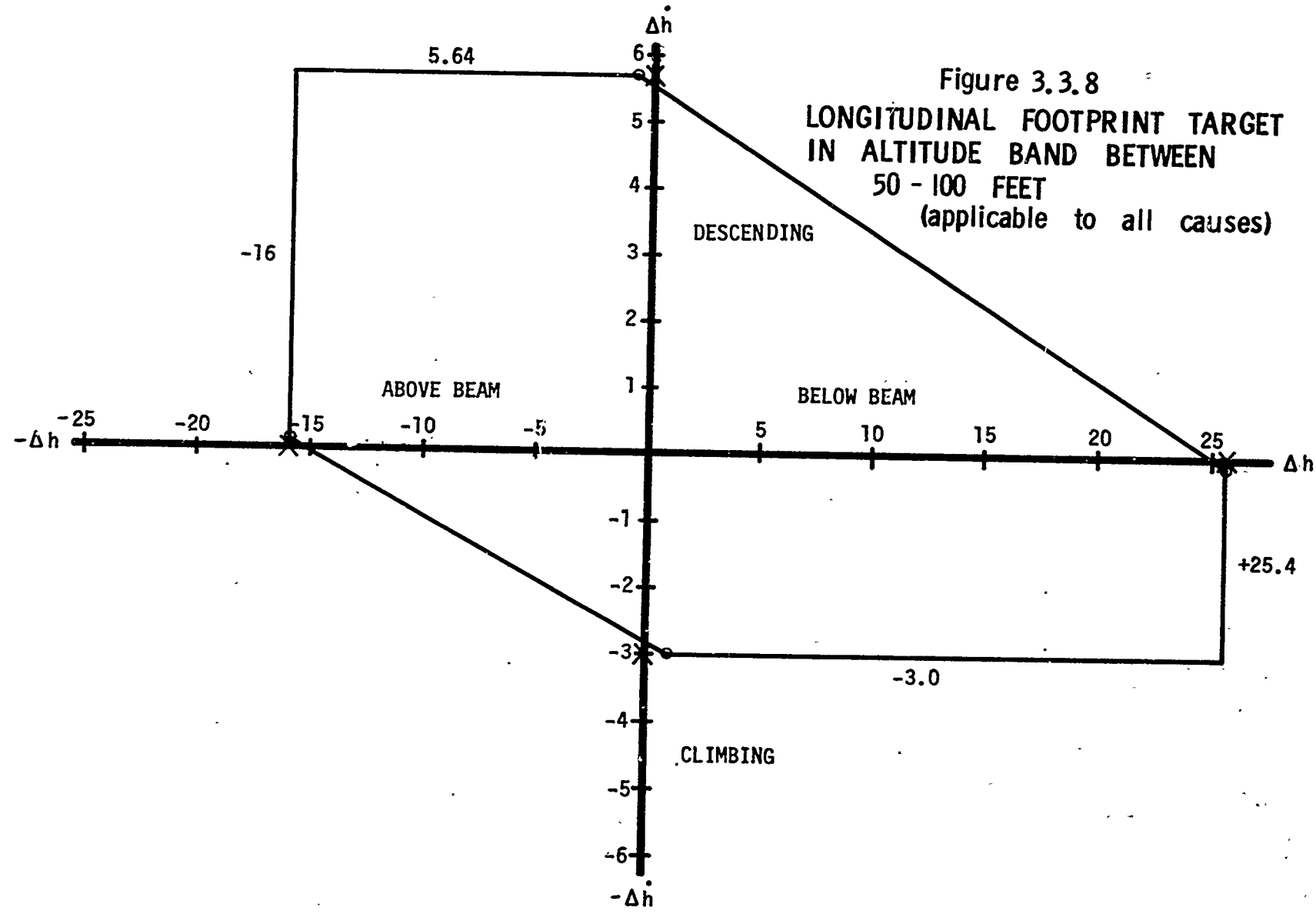

Figure 3.3.8
LONGITUDINAL FOOTPRINT TARGET
IN ALTITUDE BAND BETWEEN
50 - 100 FEET
(applicable to all causes)

3.4 Pitch Axis Maneuver Criterion

The problem in defining a reasonable maneuver criterion reduces to finding values for the coefficients C_1 and C_2 and the function F(h) in the following inequality:

$$F(h) \geq |\Delta h + C_1 \dot{\Delta h} + C_2 \dot{\theta}| \qquad (3.4.1)$$

where

$\dot{\theta}$ = pitch rate ~ DEG/SEC,

F(h) = function of altitude

It is to be noted that the terms which comprise the maneuver equation in the pitch and roll criteria do not exhibit one-to-one correspondence. In the roll axis, the third term in the maneuver equation is roll attitude. The pitch maneuver equation, (Eq (3.4.1) on the other hand, uses pitch rate to augment the maneuver description. Basically, the difference is due to the relationship between the terms in question and the inertial accelerations which result from these terms. To illustrate, the steady state, lateral acceleration is proportional to bank angle while the steady state, normal acceleration is proportional to the rate of change of pitch angle.

In developing the initial values for F(h), the Category II tracking requirements defined in FAA AC20-57 were used as a guide. However, the "all causes" F(h) was made to coincide with the smallest altitude deviation allowed by the "all causes" footprint. Moreover, the slope of F(h) was increased beyond that of the Category II tracking requirement by a factor which was approximately proportional to the ratio of the average footprint altitude deviation to the minimum tracking requirement, 12 ft.

The values of C_1 and C_2 were determined by finding a beam bend which barely induced an exceedance of the footprint boundary and then varying C_1 and C_2 until the maneuver boundary was also barely exceeded.

3.4.1 Maneuver Boundary Determination

F(h), the actual boundary, was estimated from the FAA tracking requirement of AC 20-57. This requirement stipulates that an airplane coupled to the glide slope ILS must track the beam within ± 35 ua or ± 12 ft, whichever is greater, from 700 ft. altitude to the decision height, 100 ft. Converting ua to degrees, this tracking requirement becomes ± 0.163 DEG or ± 12 ft.

The relationship between altitude deviation and glide slope deviation can be expressed

$$\Delta h_D = \left(\frac{\Delta\beta}{\beta - \Delta\beta}\right) \cdot h \qquad (3.4.2)$$

where

$\Delta\beta$ = deviation in glide slope angle $\sim$ DEG

β = actual glide slope angle $\sim$ DEG

Δh_D = deviation about the actual glide slope $\sim$ ft.

h = altitude $\sim$ ft.

Taking the nominal glide slope, $\beta = 2.75$ DEG, the FAA tracking requirement, will be converted to linear deviation, Δh_D. For the above beam case at 100 ft altitude, the negative linear deviation, Δh_{D-}, becomes:

$$\Delta h_{D-}(100) = \frac{-.163}{2.913}\ (100) = -5.6 \text{ ft}, \qquad (3.4.3)$$

and for below beam case, Δh_{D+}, the positive linear deviation is

$$\Delta h_{D+}\ (100) = \frac{.163}{2.587}\ (100) = 6.3 \text{ ft} \qquad (3.4.4)$$

At 700 ft. altitude, the above beam deviation stipulated by the FAA tracking requirement is

$$\Delta h_{D-}\ (700) = \frac{-.163}{2.913}\ (700) = -39.2 \text{ ft}, \qquad (3.4.5)$$

and the below beam deviation at 700 ft. is

$$\Delta h_{D+}\ (700) = \frac{.163}{2.587}\ (700) = 44 \text{ ft}. \qquad (3.4.6)$$

The slope of Δh_D with respect to altitude can be determined from Eq (3.4.3) through Eq (3.4.6), realizing that the altitude band covers 600 ft. The slope for above the above beam boundary is

$$\frac{-39.2 - (-5.6)}{600} = -.0560,$$

and for the below beam boundary, the slope is

$$\frac{44-6.3}{600} = .062$$

The 35 ua requirement coincides with the $\pm$ 12 ft requirement at an altitude of 214 ft in the above beam case and 190 ft in the below beam case. Therefore, the below beam deviation boundary derived from AC 20-57 is

$$\left.\begin{aligned} \Delta h_{D-} &\geq -.056h \text{ for } 214 \leq h \leq 700 \\ \Delta h_{D-} &\geq -12 \text{ ft for } h < 214 \text{ ft.} \end{aligned}\right\} \qquad (3.4.7)$$

and the above beam boundary is

$$\left.\begin{aligned} \Delta h_{D+} &\leq .062h \text{ for } 190 \leq h \leq 700 \\ \Delta h_{D+} &\leq 12 \text{ ft. for } h < 190 \end{aligned}\right\} \qquad (3.4.8)$$

To reduce the complexity of this development, the Δh_D boundary was made symmetrical about the ideal glide slope by

(1) replacing the minimum value of 12 ft. in Eq (3.4.7) and Eq (3.4.8) with the minimum altitude deviation allowed by the footprint boundary, which is 16 ft.

(2) averaging the slopes in Eq (3.4.7) and Eq (3.4.8) and then increasing this average by a factor of 1.5 to obtain a final slope of .089.

(3) finding the altitude which satisfies the equation

$$.089\, h = 16,$$

and letting this altitude replace the 214-ft. in Eq (3.4.7) and 190 -ft in eq (3.4.8).

With these refinements in Δh_D, it was thus decided to bound the maneuver criterion with Δh_D. Thus, F(h) in Eq (3.4.1) can now be expressed

$$\begin{aligned} F(h) &= .089h \text{ for } 180 \leq h \leq 700 \\ F(h) &= 16 \text{ for } h < 180 \end{aligned} \qquad (3.4.9)$$

Above 700 ft., no constraints are placed on the airplane maneuver.

3.4.2 Determination of Maneuver Coefficients

The simulation was adjusted so that the response of the A system to sinusoidal beam bends would reach a peak at 100 ft. altitude. To achieve this particular response, the height at which the bend was introduced was varied. Next, the amplitude and duration of the bend were varied until the footprint criterion was barely exceeded (at the 100 ft. height). The expression for the bend thus determined was

$$\beta_{DIST} = 0.4 \left(1 - \cos \left[\frac{2\pi}{8} \quad t \right] \right) \sim \text{DEG} \qquad (3.4.10)$$

Having determined the bend which caused marginal performance with respect to the footprint criterion, it was reasoned that this particular bend should also cause marginal performance with respect to the maneuver criterion.

To achieve marginal performance in the A system with respect to the Maneuver criterion, simulated approaches were conducted against the bend described by Eq (3.4.10), and the value of C_1 was varied until the inequality in Eq (3.4.1) barely held. Next, the value for C_2 was varied until the peak value of the right hand side of Eq (3.4.1) became insensitive to the change in C_2. Finally, C_1 was decreased until the inequality again was satisfied. The resulting values for these coefficients were

$$\left.\begin{aligned} C_1 &= 3.5 \\ C_2 &= -3.5 \end{aligned}\right\} \tag{3.4.11}$$

The maneuver criterion then, which applies to all causes during the approach, can be expressed

$$F(h) \geq |\Delta h + 3.5 \dot{\Delta h} - 3.5 \dot{\theta}| \tag{3.4.12}$$

where F(h) is described in Eq (3.4.9). Figure 3.4.1 compares the maneuver criterion boundary with the equivalent tracking boundary required by AC 120-29.

3.5 Maneuver and Footprint Criteria Application

The maneuver and footpring criteria were applied in several different ways for the purpose of illustrating the comparative performance of the three autopilots. The reasons for the varied application were related to characteristics of the criteria themselves and also the particular autopilot experiment being performed.

The maneuver and footprint criteria are a set of inequalities which define the extreme limit of allowable autopilot performance. The criteria only define a logical state in that a criterion is either being exceeded or it is not. When a criterion is exceeded, it is of interest to note how long this situation prevailed. However, on most approaches, none of the criteria are exceeded and, in such case, no information is provided as to the quality of the approach. Thus the use of the pitch and roll axis maneuver criteria equations as inequalities has only limited value. The same is true of the footprint criteria and for the same reason. To overcome this limitation, two techniques were developed to expand the usefulness of the maneuver and footprint criteria concept. These techniques are described in the following subsections.

3.5.1 Reduced Footprint Criteria for Bends Only

With the exception of the few runs made on the analog simulator to study the effects of winds and turbulence, all the simulator work was directed to the study of the effect of beam anomalies. Thus the airplane, regardless of which control law was being used, tracked beam center nearly perfectly until a beam disturbance was introduced. In actual practice, the following random variables all contribute t the difficulty of obtaining perfect performance:

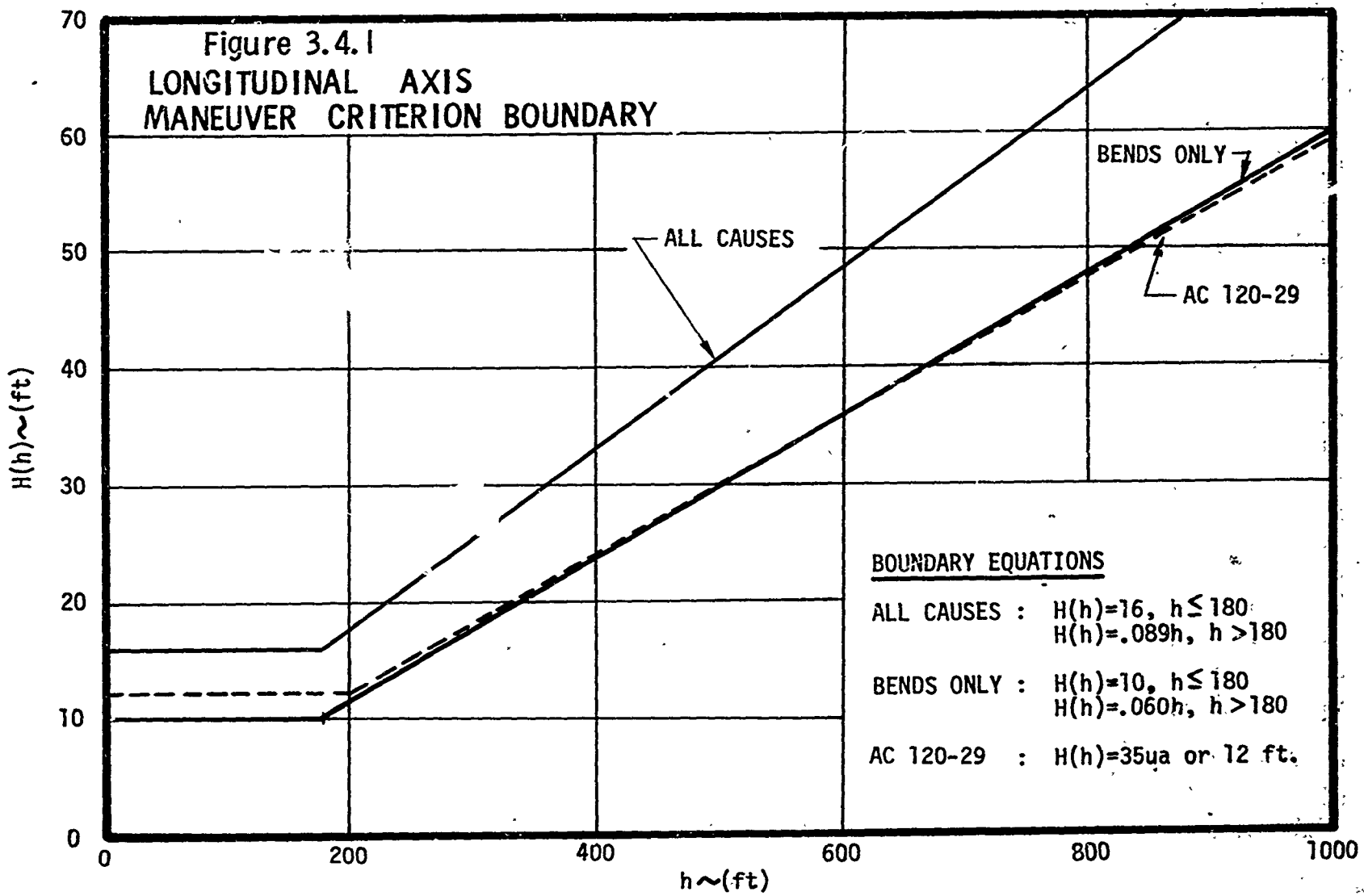
Figure 3.4.1
LONGITUDINAL AXIS
MANEUVER CRITERION BOUNDARY
BENDS ONLY
ALL CAUSES
AC 120-29
BOUNDARY EQUATIONS
ALL CAUSES : H(h)=16, h≤180
H(h)=.089h, h >180
BENDS ONLY : H(h)=10, h≤180
H(h)=.060h, h >180
AC 120-29 : H(h)=35ua or 12 ft.
H(h)~(ft)
h~(ft)
0
10
20
30
40
50
60
70
0
200
400
600
800
1000

A. Receiver Centering Error

B. Beam Alignment Accuracy

C. Beam Bends

D. Vertical Turbulence

E. Horizontal Turbulence

One object of this study was to determine an allowable footprint boundary for airplane deviations which are the result of anomalous beam behavior. Consequently, the task was to determine the percentage of the "all causes" roll and pitch axis footprint boundaries that can be applied to variables B and C above. Essentially, the effect of variables A, D and E must be subtracted from the "all causes" footprint and the remainder can be allowed for the effect of beam anomalies. A difficulty in this approach is the fact that the three autopilots do not have the same sensitivity to variables D and E.

In Section 4.1, it is shown that the effect of wind disturbances is far greater on the System A pitch and roll autopilot than it is on either System B or C autopilots. Further, the effect of winds must be described on a probability basis. This is because the required probability of a successful approach through the zone in which the footprint criteria apply is specified as 95% (2σ basis) for Cat II and 99.9999% ($4.9\ \sigma$ basis) for Cat III operation. Therefore, the amount of the footprint that must be given over for the effects of wind must be established on a probability basis before any can be allowed for the effect of beam anomalies. Clearly an autopilot to be used for Cat III operation must be far less sensitive to wind disturbances than an autopilot suitable for Cat II operation. Otherwise, more often than once in a million approaches, an approach will fall outside the footprint due to the effects of wind alone. In summary, to rigorously specify the footprint size which may be applied to the effect of beam anomalies only, it is first necessary to determine the effect of winds on autopilots A, B and C both on a 2σ and 4.9σ probability basis. In each axis, six values for the effect of winds would have to be determined and then subtracted from the "all causes" footprint criterion to specify six different footprints for the allowable effect of beam anomalies. This is burdensome, but even worse, it leads to a situation where a different "bends only" footprint would have to be dedicated on the simulator to each autopilot type and category of operation (II or III). To alleviate this problem, a single "bends only" footprint was used on the analog simulator. This footprint was appropriate for the System B autopilot in Cat II operation.

3.5.1.1 Pitch Axis "Bend Only" Footprint Criterion

The least complex method for determining a boundary for variables B and C above was to find the total variance for variables A, D and E. With this variance known, the task then reduced to finding the mean deviation that will cause the total variance of variables A, D and E to exceed the "all causes" boundary of Figure 3.3.8 once every 20 trials. A distribution, or more appropriately a density function, will

result with the following characteristics:

$$\left.\begin{aligned} \text{mean} &= \mu_{B,C} \\ \text{variance} &= \sigma^2_{A,D,E} \end{aligned}\right\} \qquad (3.5.1)$$

Refer to Figure 3.5.1. At a particular ILS facility, the mean, $\mu_{(BC)}$, is a function of the beam anomalies-bends and alignment; and the variance, σ^2_{ADE}, is a function of centering error, and vertical and horizontal turbulence. In other words, the mean will vary from facility to facility depending upon the characteristics of the glide slope beam, while the variance remains relatively constant over all the facilities. Hence, the problem was to determine μ_1 and μ_2 in Figure 3.5.1 such that a total area of 5% lay beneath both tails of each density curve P_1 and P_2 for Category II operations.

Now $$\sigma^2_{ADE} = \sigma^2_A + \frac{1}{3}\sigma^2_D + \frac{1}{3}\sigma^2_E \qquad (3.5.2)$$

where

σ^2_A = Variance of centering error

σ^2_D = Variance of vertical turbulence

σ^2_E = Variance of horizontal turbulence

The $\frac{1}{3}$ factor in the second and third term in Eq. 3.5.2 is due to the fact that turbulence is about 3 times more effective on path deviation after the airplane enters the flare maneuver than during glide slope tracking. This is very conservative because 100% of the turbulence variance was accounted for in the flare dispersion. Using the values in reference (3) and translating from ΔX to Δh through a nominal G/S angle of 2.75 DEG,

$$\sigma^2_A = \left(\frac{10}{20.8}\right)^2 = .231 \text{ ft}^2 \qquad (3.5.3)$$

$$\frac{1}{3}\sigma^2_D = \frac{1}{3}\left(\frac{71.8}{20.8}\right)^2 = 3.97 \text{ ft}^2 \qquad (3.5.4)$$

$$\frac{1}{3}\sigma^2_E = \frac{1}{3}\left(\frac{163.5}{20.8}\right)^2 = 20.6 \text{ ft}^2 \qquad (3.5.5)$$

Hence, Eq (3.5.2) becomes, in value,

$$\sigma^2_{A,D,E} = 24.8 \text{ ft}^2, \qquad (3.5.6)$$

Figure 3.5.1
DISPERSION ABOUT THE GLIDESLOPE BETWEEN
50 AND 100 FEET.

MEANS ARE FUNCTIONS OF BEAM CHARACTERISTICS.
VARIANCES ARE FUNCTIONS OF TURBULENCE AND
CENTERING ERRORS.

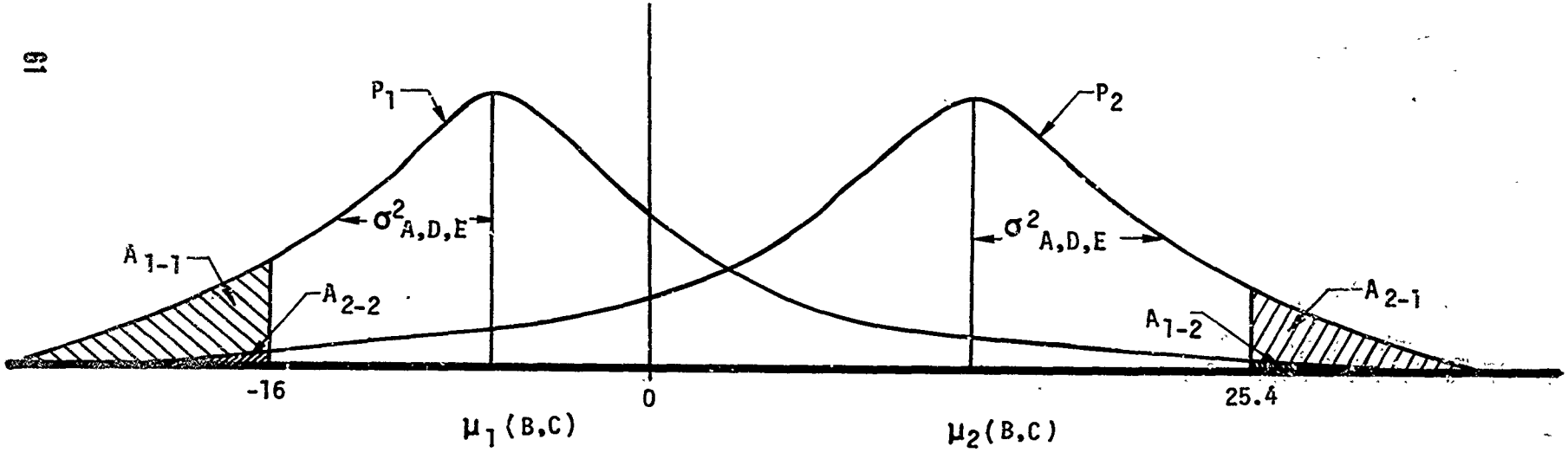

and the dispersion is

$$\sigma_{A,D,E} = 4.98 \text{ Ft.} \tag{3.5.7}$$

To determine the 5% point, one tail of each curve in Figure 3.5.1 (A_{1-2} and A_{2-2}) can be neglected because these areas result in a percentage number which is smaller than the round-off errors of Δh_{MAX} and Δh_{MIN}. Therefore, the object is to derive the multiple of sigma such that 5% of the P_1 area lies in A_{1-1} (see Figure 3.5.1), and likewise 5% of P_2 in A_{2-1}. Since single-tailed probabilities of 0.05 are desired, the sigma number which must apply is that which corresponds to the double-tailed 0.10 probability. Appropriate tables show a sigma number of 1.6.

Therefore, (Eq 3.5.7) must be multiplied by 1.6. Hence

$$1.6\ \sigma_{A,D,E} = 7.97 \text{ Ft.} \tag{3.5.8}$$

Hence, $\mu 1_{B,C}$ the mean of curve P_1, in Figure 3.5.1 is located

$$\mu 1_{B,C} = -16 + 7.97 = -8.03 \approx -8.0 \text{ Ft.} \tag{3.5.9}$$

Consequently, $\Delta h_{MIN_{ILS}}$, the minimum allowable altitude error which will apply to beam bends and alignment only becomes

$$\Delta h_{MIN_{ILS}} = -8.0 \text{ Ft.} \tag{3.5.10}$$

Similarly, subtracting the value of $1.6\ \sigma_{A,D,E}$ in Eq. (3.5.8) from 25.4 (Δh_{MAX}, all causes) yields the value for $\mu 2_{B,C}$, the mean of P_2 in Figure 3.5.1.

Thus

$$\mu 2_{B,C} = 25.4 - 7.97 = 17.43 \approx 17 \text{ ft.} \tag{3.5.11}$$

and it follows then that $\Delta h_{MAX_{ILS}}$, the maximum allowable altitude error which applies to beam bends and alignment only, will become

$$\Delta h_{MAX_{ILS}} = 17 \text{ ft.} \tag{3.5.12}$$

To complete the extreme points in the footprint for beam bands only, $\Delta \dot{h}_{MIN}$ and $\Delta \dot{h}_{MAX}$ were reduced in approximately the same proportion that Δh_{MIN} and Δh_{MAX} respectively were reduced to obtain the values in Eq (3.5.10) and Eq (3.5.12). Thus

$$\Delta \dot{h}_{MIN} = -1.5 \text{ ft/sec} \quad (3.5.13)$$

$$\Delta \dot{h}_{MAX} = 3.5 \text{ ft/sec} \quad (3.5.14)$$

Eq (3.5.10), Eq (3.5.12), Eq (3.5.13) and Eq (3.5.14) define the extreme points on the reduced footprint which will be applied to beam anomalies only. Translating these points by 5% into the "safe" quadrants, as was done in the case of the "all causes" footprint, and connecting the points linearly, resulted in the footprint boundary shown in Figure 3.5.2. This boundary governs the beam disturbance performance by each autoland system, and, if the response of the airplane to any beam upset was outside this boundary, the approach was called unacceptable.

3.5.1.2 Roll Axis "Bend Only" Footprint Criterion

The same technique used to reduce the "all causes" pitch axis footprint criterion to a "bends only" criterion is also applied to determine the "bends only" roll axis footprint. The problem is to identify the lateral displacement variance due to causes A, D and E. This is done for System B under Cat II operational conditions (2σ basis). This variance is then multiplied by 1.6 and subtracted from the "all causes" footprint displacement limit to determine the "bends only" footprint displacement limit. The .1 "g" maneuver limit which connects the displacement and displacement rate boundaries of the "all causes" footprint is retained for the "bends only" footprint.

From references (1) and (3), the variance attributable to causes A, D and E is estimated to be:

$$\sigma_{A,D,E} = 8.75 \text{ ft.} \quad (3.5.15)$$

To obtain a single-tailed probability of .05, a sigma of 1.6, which corresponds to a total probability of .1, is applied:

$$1.6\sigma_{A,D,E} = 14 \text{ Ft.} \quad (3.5.16)$$

The "all causes" footprint displacement limit is 60 Ft. (Eq. 3.1.13) and the displacement limit of the "bends only" footprint thus becomes:

$$J = 60 - 14 = 46 \text{ Ft.} \quad (3.5.17)$$

The whole of the "bends only" footprint can then be defined by equations 3.1.1, 3.1.2, 3.1.3, and 3.1.4 with J = 46 feet. This leads to the "bends only" footprint given in Figure 3.5.3. This boundary governs the beam disturbance performance by each autoland system and, if the response of the airplane to any beam upset was outside this bounary, the approach was called unacceptable.

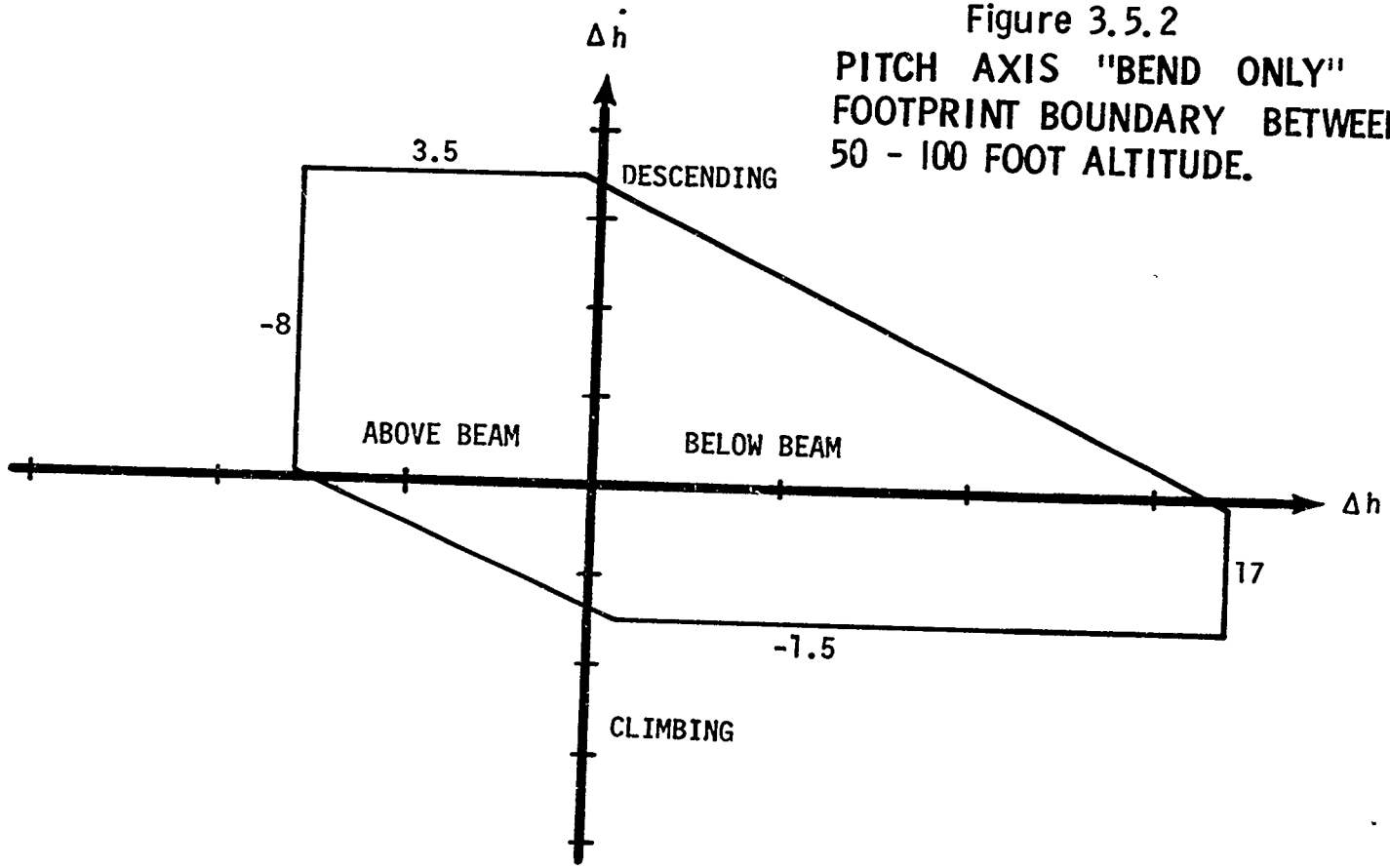

Figure 3.5.2
PITCH AXIS "BEND ONLY"
FOOTPRINT BOUNDARY BETWEEN
50 - 100 FOOT ALTITUDE.

Figure 3.5.3
ROLL AXIS "BEND ONLY"
FOOTPRINT BOUNDARY BETWEEN
0 - 100 FOOT ALTITUDE

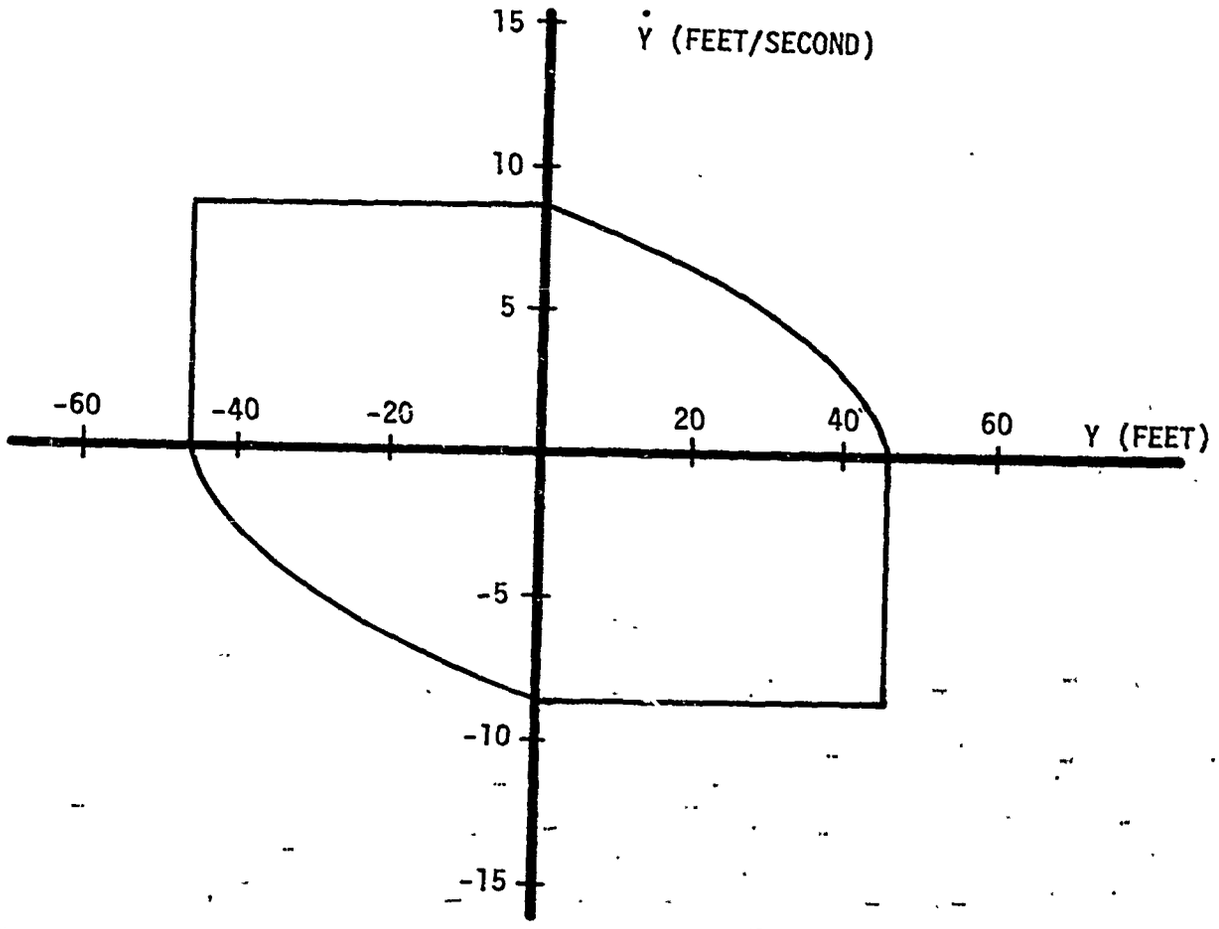

3.5.2 Reduced Maneuver Criteria for Bends Only

The same reason for the reduction of the footprint criterion boundaries to define a "bends only" criterion exists for the reduction of the pitch and roll axis maneuver criterion boundary. The "bends only" maneuver criterion is determined by reducing the threshold value of the maneuver equation inequality by the same percentage as the footprint boundaries are reduced to define the "bends only" footprint criterion. The roll and pitch axis "bends only" maneuver criteria were used exclusively on the analog simulation.

3.5.2.1 Pitch Axis "Bend Only" Maneuver Criterion

The footprint below beam deviation allowance was reduced from 25.4 feet to 17 feet in going from the "all causes" to the "bends only" footprint. See Figures 3.3.8 and 3.5.2. Thus, the "bends only" footprint is approximately 67% the size of the "all causes" footprint. Applying this 67% to equation (3.4.9) to reduce the "all causes" maneuver criterion by the same factor gives:

$$F(h) = .06\ h \text{ for } 180 \leq h \leq 700 \text{ Ft.}$$
$$F(h) = 10 \text{ for } h < 180 \text{ Ft.} \qquad (3.5.18)$$

The maneuver criterion is given by equation (3.4.12).

$$F(h) \geq [\Delta h + 3.5\ \Delta \dot{h} - 3.5\dot{\theta}]$$

The "bends only" pitch maneuver equation is defined by equations (3.4.12) and (3.5.18).

3.5.2.2 Roll Axis "Bend Only" Maneuver Criterion

The footprint displacement allowance was reduced from 60 feet to 46 feet in going from the "all causes" to the "bends only" footprint. See Figures 3.1.1 and 3.5.3. Thus, the "bends only" footprint is approximately 77% the size of the "all causes" footprint.

Applying this 77% to the Y parameter of equation (3.2.1) to reduce the "all causes" maneuver criterion by the same factor gives:

$$Y = \frac{h-100}{0.9} + 46 \text{ ft for } h \geq 100 \text{ ft.}$$
$$Y = 46 \text{ ft. for } 0 < h < 100 \text{ ft.} \qquad (3.5.19)$$

and, for clarity, repeating the rest of equation (3.2.1) to completely define the "bends only" maneuver criterion:

$$K_1 = 17 \text{ ft/degree for } 0 < h < 100 \text{ Ft.}$$

$$K_1 = 17 + \frac{(h-100)}{65} \text{ ft/degree for } h \geq 100 \text{ Ft.}$$

$$K_2 = 5 \text{ ft/degree}$$

$$Y \geq \left| y + K_1 \psi_G + K_2 \phi \right|$$

3.5.3 Maneuver Equation

By design, the maneuver equation has a continuous value. That is, at any moment in time, the maneuver equation value can be calculated. This calculation was continuously performed on the analog simulation. For the flight tests, the continuous maneuver equation value was post-flight calculated for all approaches. Thus, both for the simulator and flight data, the maneuver equation could be interpreted by noting instantaneous value or by taking average value over a period of time.

As discussed in Section 3.5.2, the maneuver equation, when it exceeds a threshold value, is said to be a criterion and this criterion was the measure most often employed on the simulator to compare autopilot performance in the presence of beam disturbances. However, there were many occasions in which the equation value did not exceed the criterion threshold, and in this case the peak value of the equation was used as the comparative measure of performance.

Throughout this report, in Figures which illustrate the path time history of the flight test airplane, a positive number referred to as the "M.E.A." is given for each trace. The M.E.A. is the average value of the maneuver equation between airplane altitudes of 350 and 50 feet. The average value of the pitch and roll axis maneuver equations, over the final portion of the approach, is a single number in each axis, which well describes the overall performance.

In summary, the peak value and average value of the pitch and roll axis maneuver equations were used to compare autopilot performance on a fine scale. This application of the maneuver equation was especially useful where no criteria violations occurred but yet a comparative measure of performance was desired.

3.5.3.1 Pitch Axis Maneuver Equation

The pitch axis maneuver equation is given as an inequality in equations (3.4.9) and (3.4.12). Combining these inequalities to form an equation gives:

$$F(h) = 16 = \left| \Delta h + 3.5\ \Delta \dot{h} - 3.5 \dot{\theta} \right| \text{ for } h < 180 \text{ Ft.} \qquad (3.5.20a)$$

$$F(h) = .089h = \left| \Delta h + 3.5 \Delta \dot{h} - 3.5 \dot{\theta} \right| \text{ for } 180 \leq h \leq 700 \text{ Ft.} \qquad (3.5.20b)$$

The flight test flight path data was plotted against range to the glide slope transmitter instead of altitude. For this reason, the functions of altitude in equation 3.5.20 are changed to functions of range with the assumption of a 2.5 degree glide slope beam angle:

$$F(\rho) = 16 = |\Delta h + 3.5\ \Delta\dot{h} - 3.5\dot{\theta}| \text{ for } \rho < 4100 \text{ Ft.} \quad (3.5.21a)$$

$$F(\rho) = .0039\rho = |\Delta h + 3.5\ \Delta\dot{h} - 3.5\dot{\theta}| \text{ for } 4100 \leq \rho \leq 16{,}100 \quad (3.5.21b)$$

Equation (3.5.21b) is simply a means of desensitizing equation (3.5.21a) when range is greater than 4100 feet (altitude greater than 180 feet). As such, the equations can be normalized to derive the maneuver equation for ranges greater than and less than 4100 feet:

$$M.E. = |\Delta h + 3.5\ \Delta\dot{h} - 3.5\dot{\theta}| \text{ for } \rho < 4100 \text{ Ft.} \quad (3.5.22a)$$

$$M.E. = \frac{16}{.0039\rho} |\Delta h + 3.5\ \Delta\dot{h} - 3.5\dot{\theta}| \text{ for } \rho \geq 4100 \text{ Ft.} \quad (3.5.22b)$$

From this equation, it is apparent that the Maneuver Equation has a continuous value that is a function displacement from the ideal glide path (Δh), displacement rate from the ideal glide path ($\Delta\dot{h}$), pitch rate ($\dot{\theta}$) and range.

The maneuver equation (3.5.22) was implemented on the analog simulator. Also, at two second intervals, the pitch axis flight data was used to calculate a maneuver equation value. For the flight data, all the maneuver equation values on an approach were averaged to determine the maneuver equation average (M.E.A). It is of interest to consider that any given M.E.A. could have been the result of standing off the ideal glide path by that number of feet. Of course, normally the average beam error was less than the maneuver equation average.

3.5.3.2 Roll Axis Maneuver Equation

The roll axis maneuver equation is given as an inequality in equation (3.2.1). Converting the inequality to a continuous equation gives:

$$60 = |y + K_1 \psi_G + K_2 \phi| \text{ for } 0 < h < 100 \text{ Ft.} \quad (3.5.23a)$$

$$\frac{h-100}{5.3} + 60 = |y + K_1 \psi_G + K_2 \phi| \text{ for } h \geq 100 \text{ Ft.} \quad (3.5.23b)$$

where:

$K_1 = 17$ ft/degree for $0 < h < 100$ Ft.

$K_1 = 17 + \frac{(h-100)}{65}$ ft/degree for $h \geq 100$ Ft.

$K_2 = 5$ ft/degree

Equation (3.5.23b) is simply a means of desensitizing equation (3.5.23a) when altitude is greater than 100 feet. As such, the equations can be normalized to derive maneuver equations for altitudes greater than and less than 100 feet:

$$M.E. = \left| y + K_1 \psi_G + K_2 \phi \right| \quad \text{for } 0 < h < 100 \text{Ft.} \qquad (3.5.24a)$$

$$M.E. = \frac{318}{h+218} \left| y + K_1 \psi_G + K_2 \phi \right| \quad \text{for } h \geq 100 \text{Ft.} \qquad (3.5.24b)$$

The maneuver equation (3.5.24) was implemented on the analog simulator. Also, at one second intervals, the roll axis flight data was used to calculate a maneuver equation value. For the flight data, all the maneuver equation values on an approach were averaged to determine the maneuver equation average (M.E.A.).

4.0 ADVANTAGES AND LIMITATIONS OF INERTIALLY SMOOTHED SYSTEM

This section will treat in detail the actual advantages and limitations of the C (inertially smoothed) system. General statements have appeared in earlier sections which imply that the C system would be highly preferred to the conventional (A) system. There are statements and illustrations in other sections which indicate that the C system rejects anomalous beam behavior a great deal more effectively than does the B system. The intent of this section is twofold: 1) to support these earlier statements by presenting discrete proof of the superiority of the C system; and 2) to show that the C system is not without problems by pointing out the operational limitations and other disadvantages.

The problems associated with the performance of all autoland systems lie in two general categories.

(1) Environmental - Winds

(2) ILS beam characteristics - bends noise, interference, etc.

There are other categories of autoland problems, but this study is confined to the comparison of control law performance. Hence, those problems which concern failure modes, redundancy, mechanization, etc., will not be included in this report.

The A autopilot, under the constraint of first generation sensors, performs marginally, with respect to these two categories of problems. Prior to the innovation of the INS, engineers, under the handicap of poor quality sensors, endeavored to resolve the major problems in the two categories above by deriving and approximating critical system variables. Now, however, the INS has introduced a second generation of critical airborne sensors, and as a consequence, path deviations resulting from wind disturbance can be greatly attenuated. Control laws similar to the inertially damped B system were the first to employ INS inputs. Soon, however, several groups in Government and industry discovered that the INS also provided the means to attenuate path deviations resulting from ILS beam anomalies. Section 2 treats the development of the C system in detail, and therefore, it will not be repeated here. However, the point is clear that the INS, working through a suitable control law, largely overcomes the environmental as well as ILS related problems and thus provides the means to achieve consistent automatic landings.

4.1 Comparative Wind Performance

To illustrate the fact that the INS provides the means to resolve the environmental problems connected with autoland performance, several response curves will be presented. Many of these responses were taken from simulation results, and although it is very difficult to validate a predicted wind response through flight tests, there is an abundance of evidence in the flight data which indicates that the simulation predictions are indeed reasonable.

Most of the wind response curves show similar responses for the B and C systems, particularly in the pitch axis. Consequently, the advantages of the inertially smoothed system in the presence of wind disturbances will be related to the A system only. However, inertial smoothing does hold improvement potential over inertial damping by virtue of the capability of inertial smoothing to employ higher gains.

Although the same general line of reasoning, regarding comparative wind performance, applies to both pitch and roll control laws, the two axes will be discussed separately, beginning with the pitch axis.

4.1.1 Pitch Axis Wind Performance

The most serious impediment to the achievement of accurate, longitudinal autoland systems is, by far, the effect of the wind shear phenomenon. Of all the random variables which affect path deviation and, hence, touchdown dispersion, wind shear has been the most difficult to deal with. Figure 4.1.1 illustrates the comparative performance of the three types of pitch autoland systems in the presence of a simulated 8 KT/100 Ft head wind shear (diminishing tail wind). This shear was introduced at 500 ft. altitude, and peaked at a value of 15 KTS. The peak offset of the A system for this wind is approximately 30 ft., substantially greater than the all "causes" boundary in the maneuver criterion and a factor of three to four times greater than the effect on the B or C systems. A simulated tail wind shear (diminishing head wind) is illustrated in Figure 4.1.2 with about the same results.

Because simulation results may leave some doubt as to conclusive findings, an attempt to duplicate the effect of a wind shear actually encountered in flight was performed. The following four figures are included to illustrate the procedure used in this effort.

Figure 4.1.3 shows the simulated response of systems A, B and C to an artificial G/S beam bend, and as expected, system C rejects about twice as much beam disturbance as do systems A or B. The flight test results for this same condition, shown in Figure 4.1.4, apparently indicate a disagreement with the simulation prediction. However, inspection of the flight data (ground speed and indicated air speed) indicated that a 4 KT/100 Ft wind shear, as depicted in Figure 4.1.5, was present during each approach. This same condition was repeated by simulation techniques, and the approximation of the wind shear was included as an additional upset. The results are shown in Figure 4.1.6. Notice that the C system response virtually doubled in amplitude as a result of the wind disturbance while the A system response more than tripled. The B system, for which response to beam bends was about the same as the A system in Figure 4.1.3, also shows a doubled response to the bend when the wind is present. Now because the A system had already saturated its beam limiter in responding to the wind upset, nearly the entire excursion of the A system can be attributed to the wind. However, systems B and C, which were holding the wind-induced deviation within controllable limits, responded partly because of the beam bend and partly because of an overshoot response to the wind.

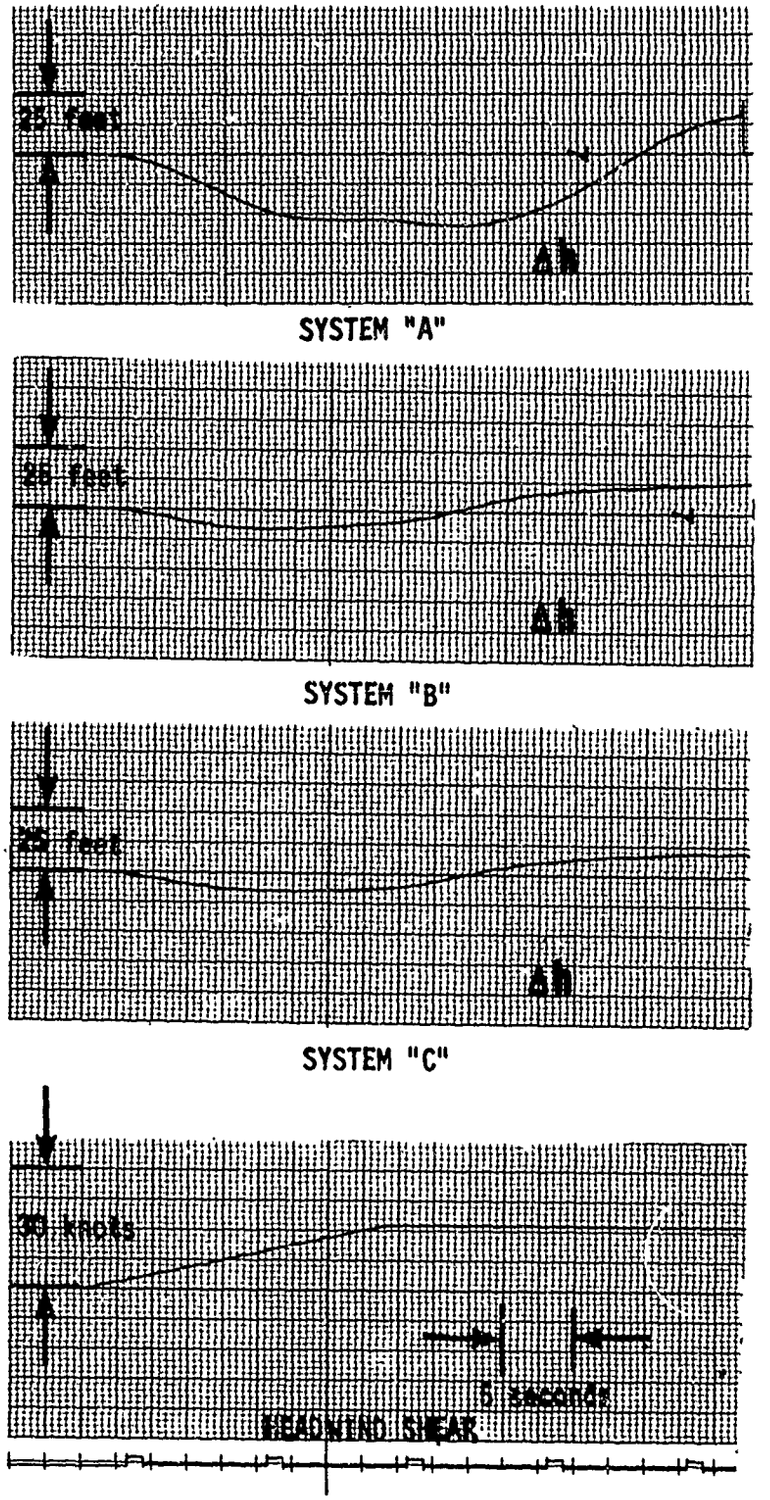

Figure 4.1.1

COMPARATIVE RESPONSE OF AUTOLAND SYSTEMS TO 8KT/100 HEADWIND SHEAR (15 KTS MAX) BEGINNING AT 500' ALTITUDE

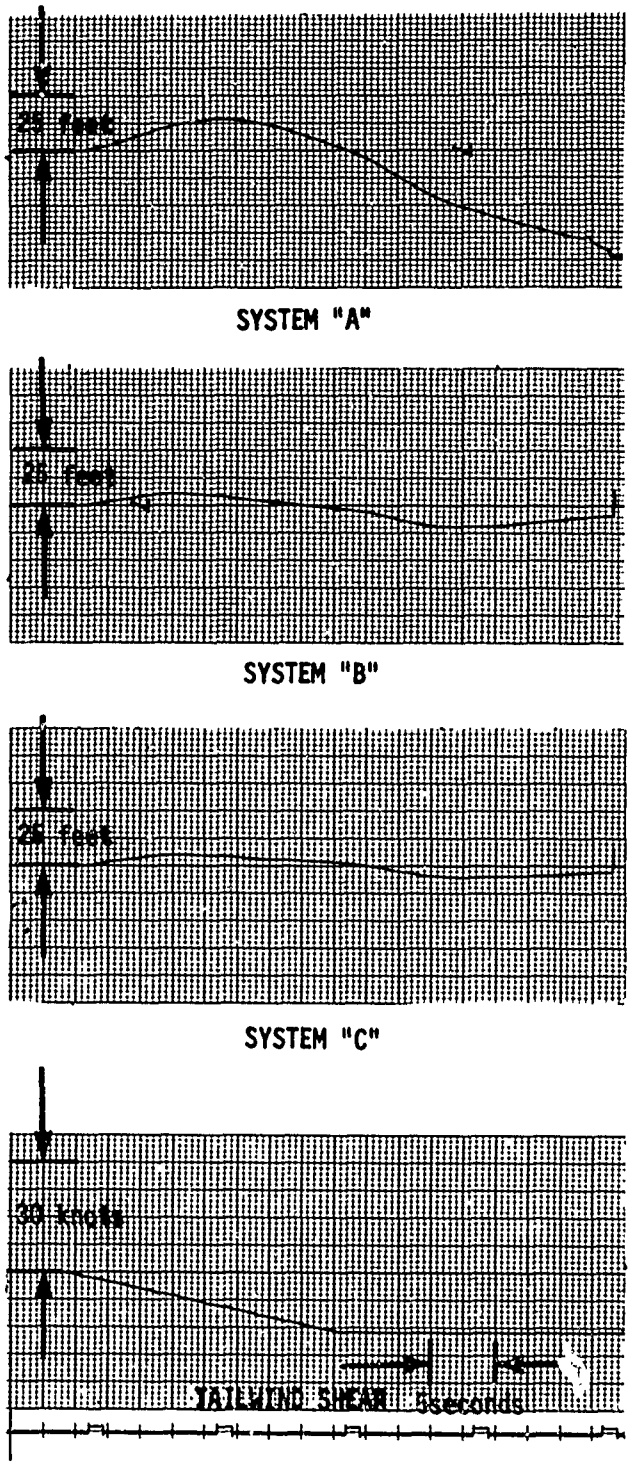

Figure 4.1.2
COMPARATIVE RESPONSE OF AUTOLAND SYSTEMS TO 8KT/100 TAILWIND SHEAR (15 KTS MAX) BEGINNING AT 500' ALTITUDE

Figure 4.1.3

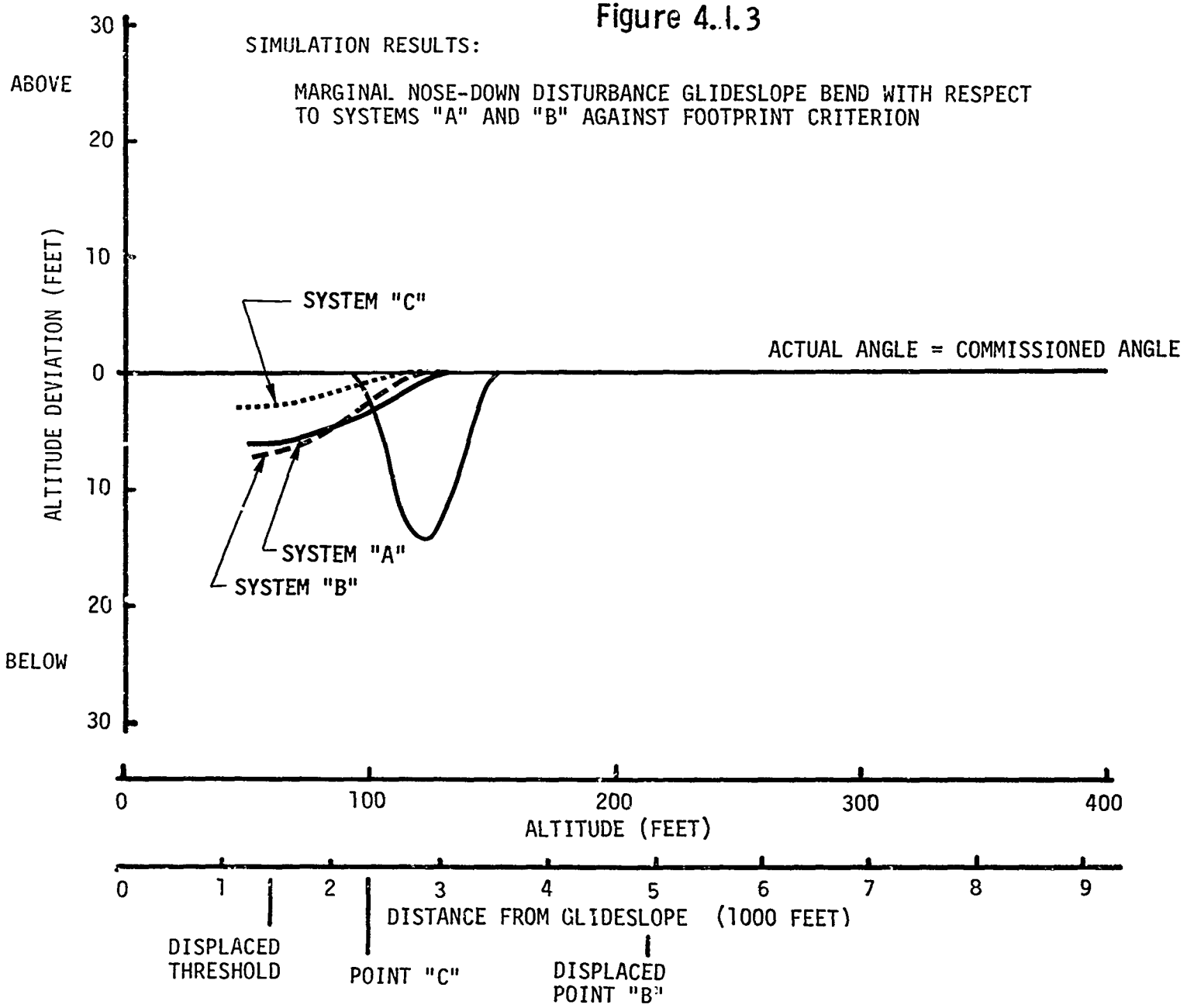
SIMULATION RESULTS:
MARGINAL NOSE-DOWN DISTURBANCE GLIDESLOPE BEND WITH RESPECT TO SYSTEMS "A" AND "B" AGAINST FOOTPRINT CRITERION
ABOVE
BELOW
ALTITUDE DEVIATION (FEET)
30
20
10
0
10
20
30
SYSTEM "C"
ACTUAL ANGLE = COMMISSIONED ANGLE
SYSTEM "A"
SYSTEM "B"
0
100
200
300
400
ALTITUDE (FEET)
0
1
2
3
4
5
6
7
8
9
DISTANCE FROM GLIDESLOPE (1000 FEET)
DISPLACED THRESHOLD
POINT "C"
DISPLACED POINT "B"

Figure 4.1.4

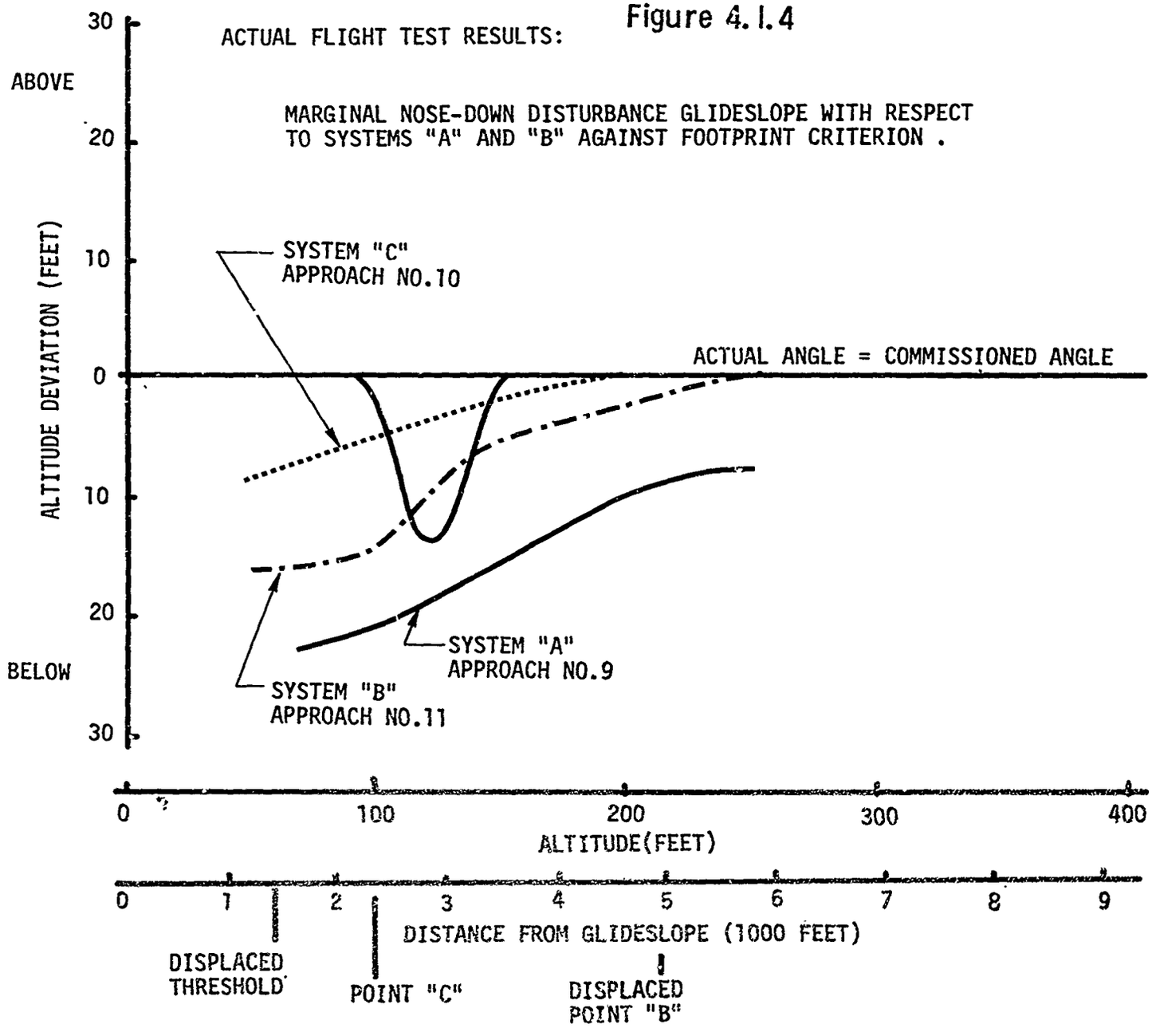
ACTUAL FLIGHT TEST RESULTS:
MARGINAL NOSE-DOWN DISTURBANCE GLIDESLOPE WITH RESPECT TO SYSTEMS "A" AND "B" AGAINST FOOTPRINT CRITERION .
ABOVE
BELOW
ALTITUDE DEVIATION (FEET)
30
20
10
0
10
20
30
SYSTEM "C" APPROACH NO.10
ACTUAL ANGLE = COMMISSIONED ANGLE
SYSTEM "A" APPROACH NO.9
SYSTEM "B" APPROACH NO.11
0
100
200
300
400
ALTITUDE(FEET)
0
1
2
3
4
5
6
7
8
9
DISTANCE FROM GLIDESLOPE (1000 FEET)
DISPLACED THRESHOLD
POINT "C"
DISPLACED POINT "B"

Figure 4.1.5

APPROXIMATE WINDSHEAR WHICH WAS PRESENT DURING BEAM BEND TESTING.

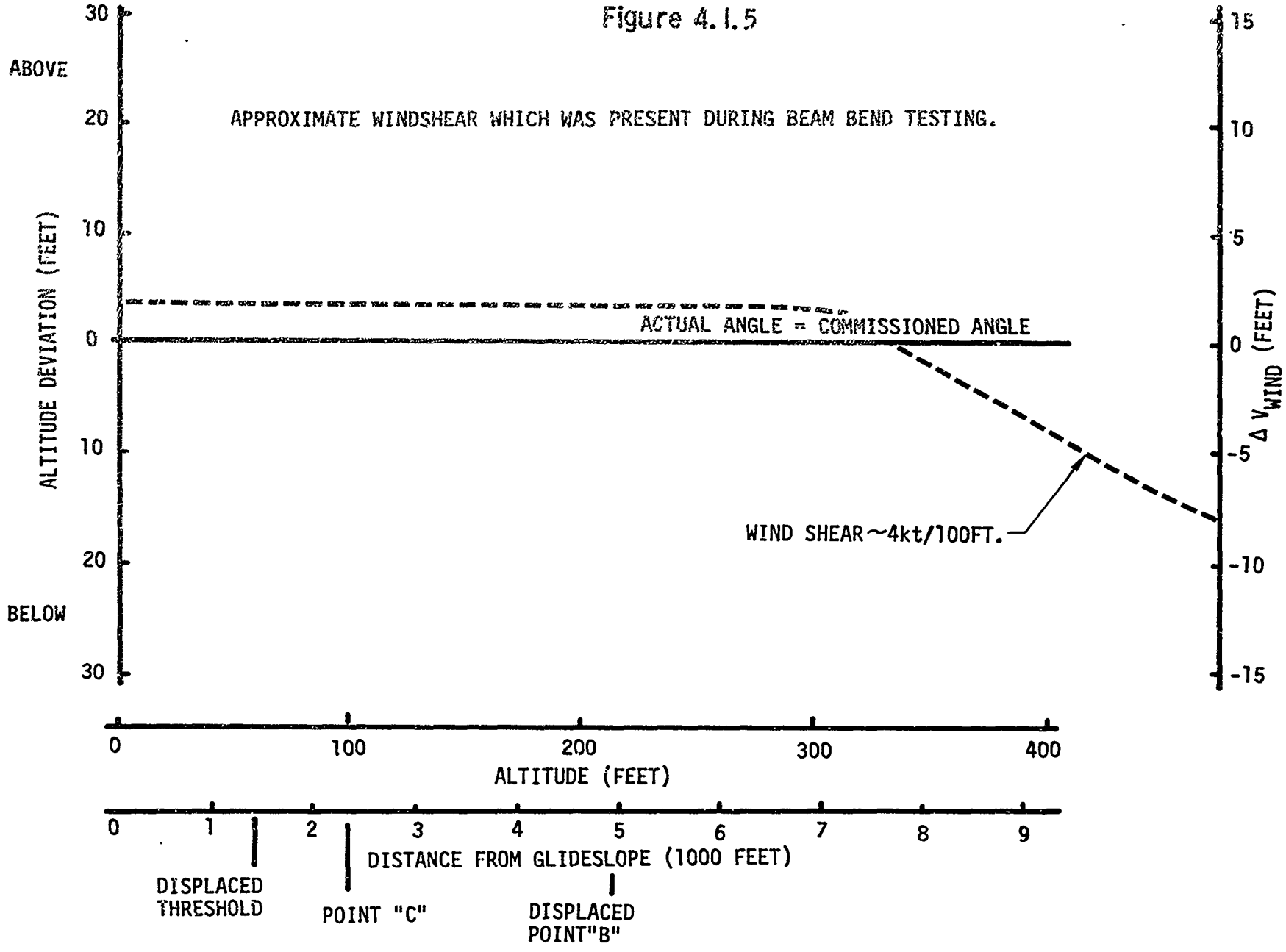

Figure 4.1.6

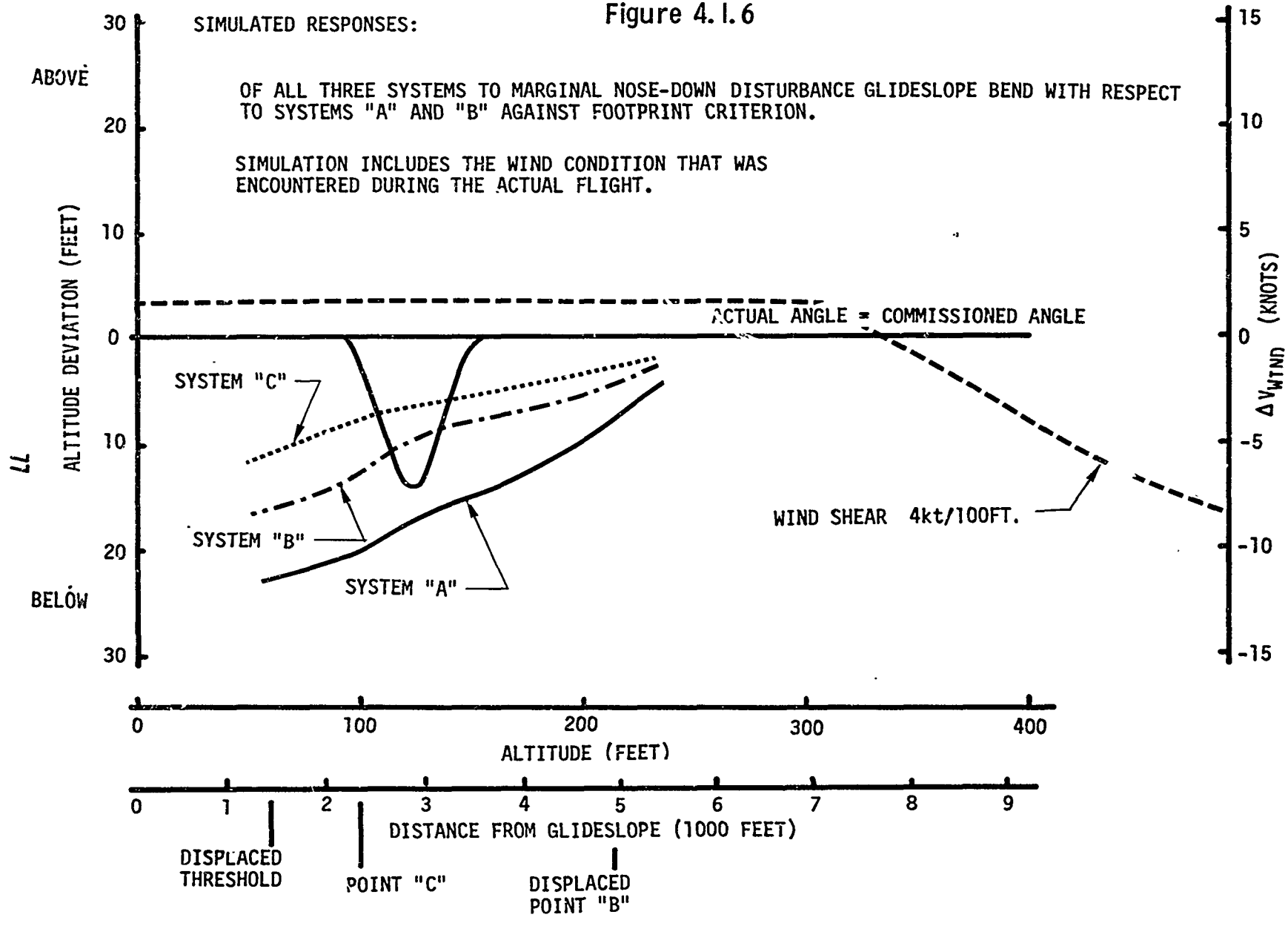
SIMULATED RESPONSES:
OF ALL THREE SYSTEMS TO MARGINAL NOSE-DOWN DISTURBANCE GLIDESLOPE BEND WITH RESPECT TO SYSTEMS "A" AND "B" AGAINST FOOTPRINT CRITERION.
SIMULATION INCLUDES THE WIND CONDITION THAT WAS ENCOUNTERED DURING THE ACTUAL FLIGHT.
ABOVE
BELOW
ALTITUDE DEVIATION (FEET)
30
20
10
0
10
20
30
ACTUAL ANGLE = COMMISSIONED ANGLE
SYSTEM "C"
SYSTEM "B"
SYSTEM "A"
WIND SHEAR 4kt/100FT.
15
10
5
0
-5
-10
-15
ΔV_{WIND} (KNOTS)
0
100
200
300
400
ALTITUDE (FEET)
0
1
2
3
4
5
6
7
8
9
DISTANCE FROM GLIDESLOPE (1000 FEET)
DISPLACED THRESHOLD
POINT "C"
DISPLACED POINT "B"

Another important point to emphasize in the preceding sequence of figures is that the responses of the A and B systems to beam bends are nearly equal in still air (Figure 4.1.3), but a substantial difference is noted when the wind shear is present (Figures 4.1.4 and 4.1.6).

The preceding sequence of figures has presented the relative performance of the three autoland systems against wind shear, the most adverse disturbance with respect to longitudinal path deviation. The remaining atmospheric disturbances - vertical gusts, longitudinal gusts, rotary winds, etc., will be regarded as one entity and referred to as random turbulence.

Figure 4.1.7 taken from the analog computer simulation, illustrates the comparative effect of random turbulence on the path deviation of each system. The peak offsets of System A, in Figure 4.1.7, are considerably greater than the peak offsets of the other two systems. This particular figure does provide an example of the relative path control capability of each system in the presence of random turbulence.

Figures 4.1.8, 4.1.9 and 4.1.10 are illustrations taken directly from flight test data. These figures show convincing evidence that systems B and C exhibit much greater wind stiffness than does System A. The environmental conditions to which each autopilot system was subjected in these figures was nearly identical because the approaches from which the data were taken occurred over a short period of time on each of three flight days. Figure 4.1.8 shows the actual flight path of system A on three approaches. Figure 4.1.9 describes the actual path of the B system for five approaches performed on the same three days, while Figure 4.1.10 describes four approach paths of the C system. Since there were no artificial beam disturbances on any of these approaches, the path deviations shown in these figures resulted principally from atmospheric disturbances.

In summarizing the comparative effect of winds on the three longitudinal autoland systems,

1. System B and C exhibit approximately the same degree of wind stiffness, owing to identical outer loop gains.
2. Path deviation variance caused by winds in the A system are approximately a factor of 3 greater than either system B or C.
3. Referring back to the discussion in Section 3.5.1.1, the variance, σ^2, for wind disturbances for a System B autopilot is 24.6 ft^2 (Equation 3.5.6). Using a factor of 2.5, a very conservative estimate for the relative performance of the A system, the A system variance would be 61.5 ft^2, and consequently, the 2σ value would be 15.7 ft. Therefore,

$$\left.\begin{aligned} 2\sigma_{B,C} &= 9.9 \text{ Ft.} \\ 2\sigma_{A} &= 15.7 \text{ Ft.} \end{aligned}\right\} \qquad (4.1.1)$$

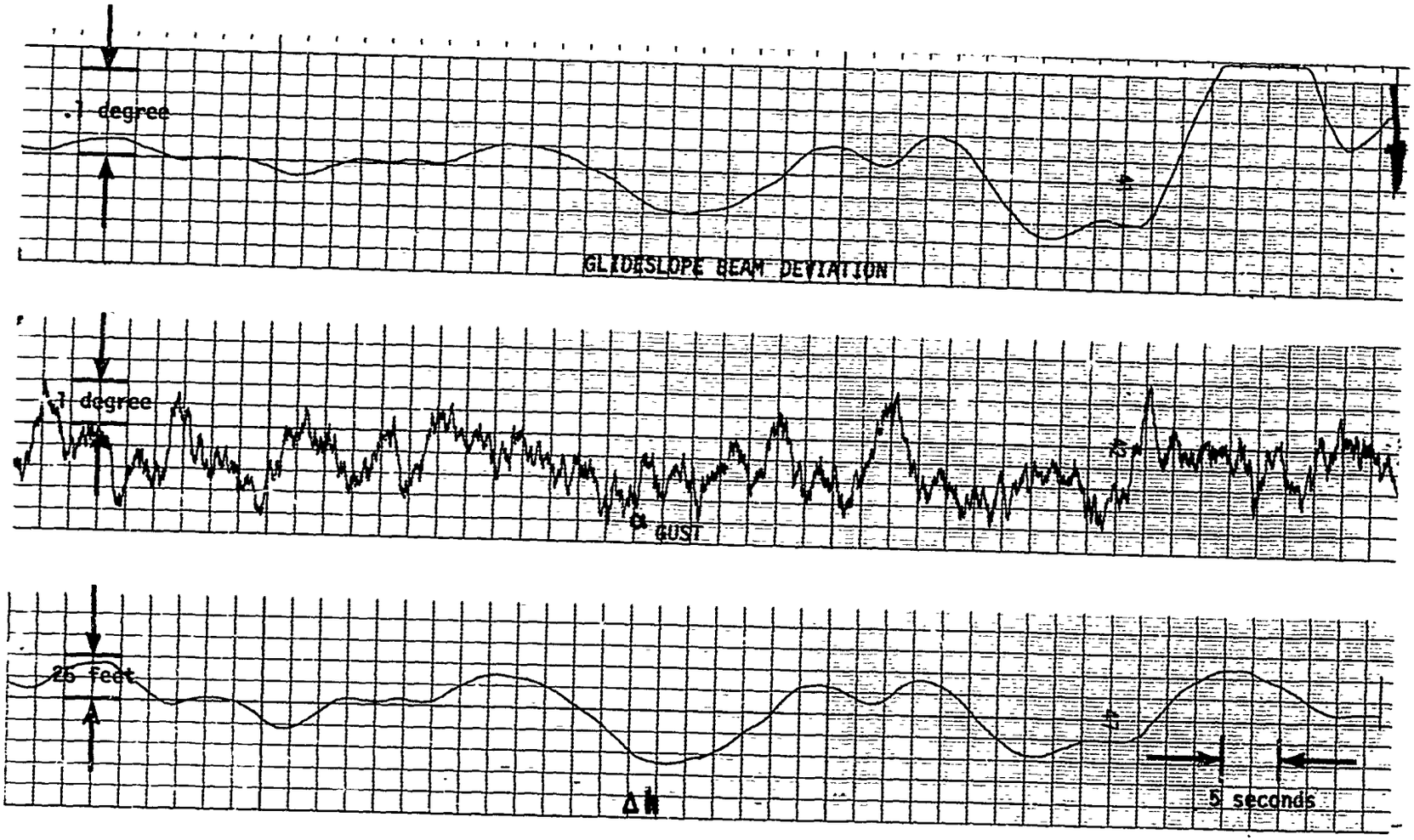

Figure 4.1.7(a)
SYSTEM "A" SIMULATED RESPONSE TO RANDOM TURBULENCE

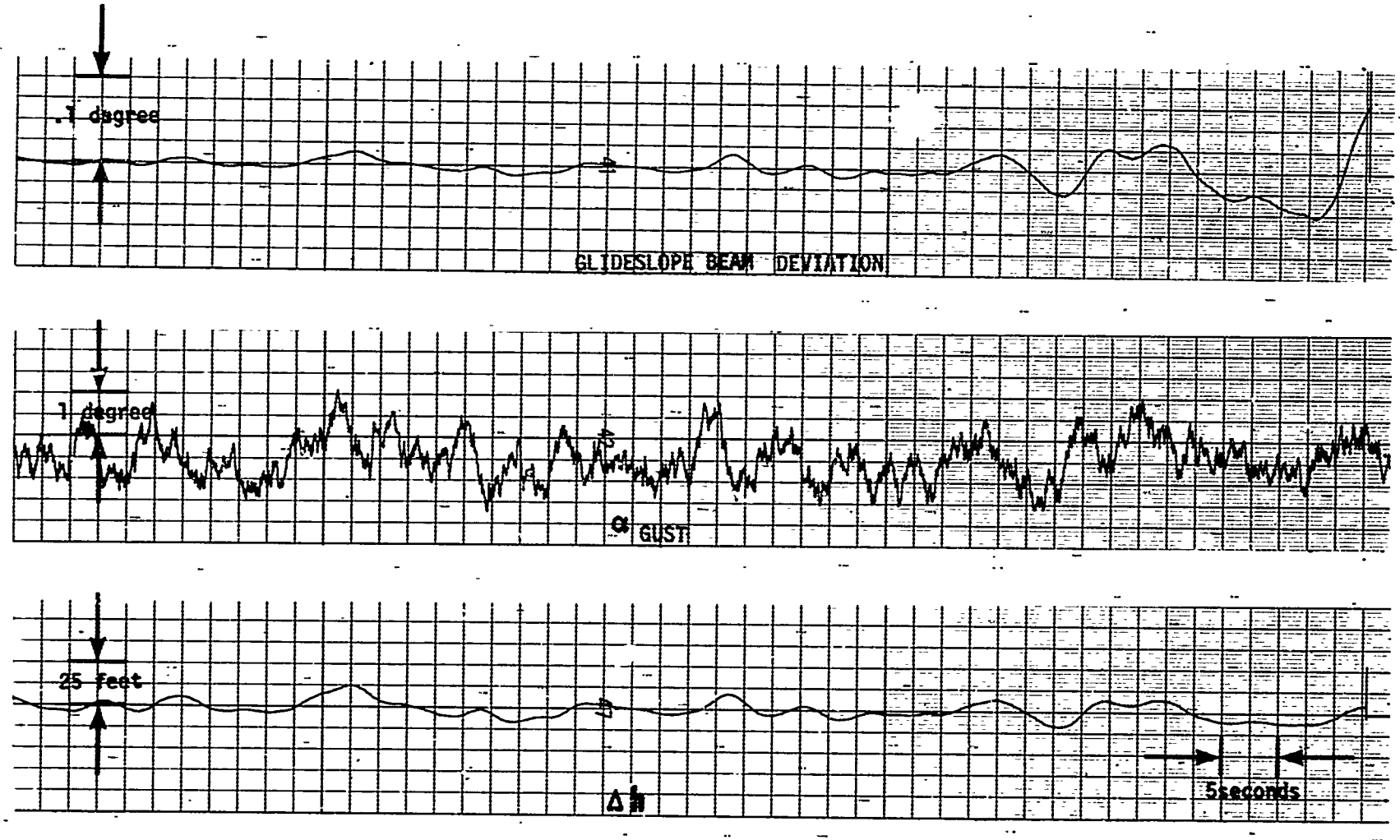

Figure 4.1.7(b)

SYSTEM "B" SIMULATED RESPONSE TO RANDOM TURBULENCE

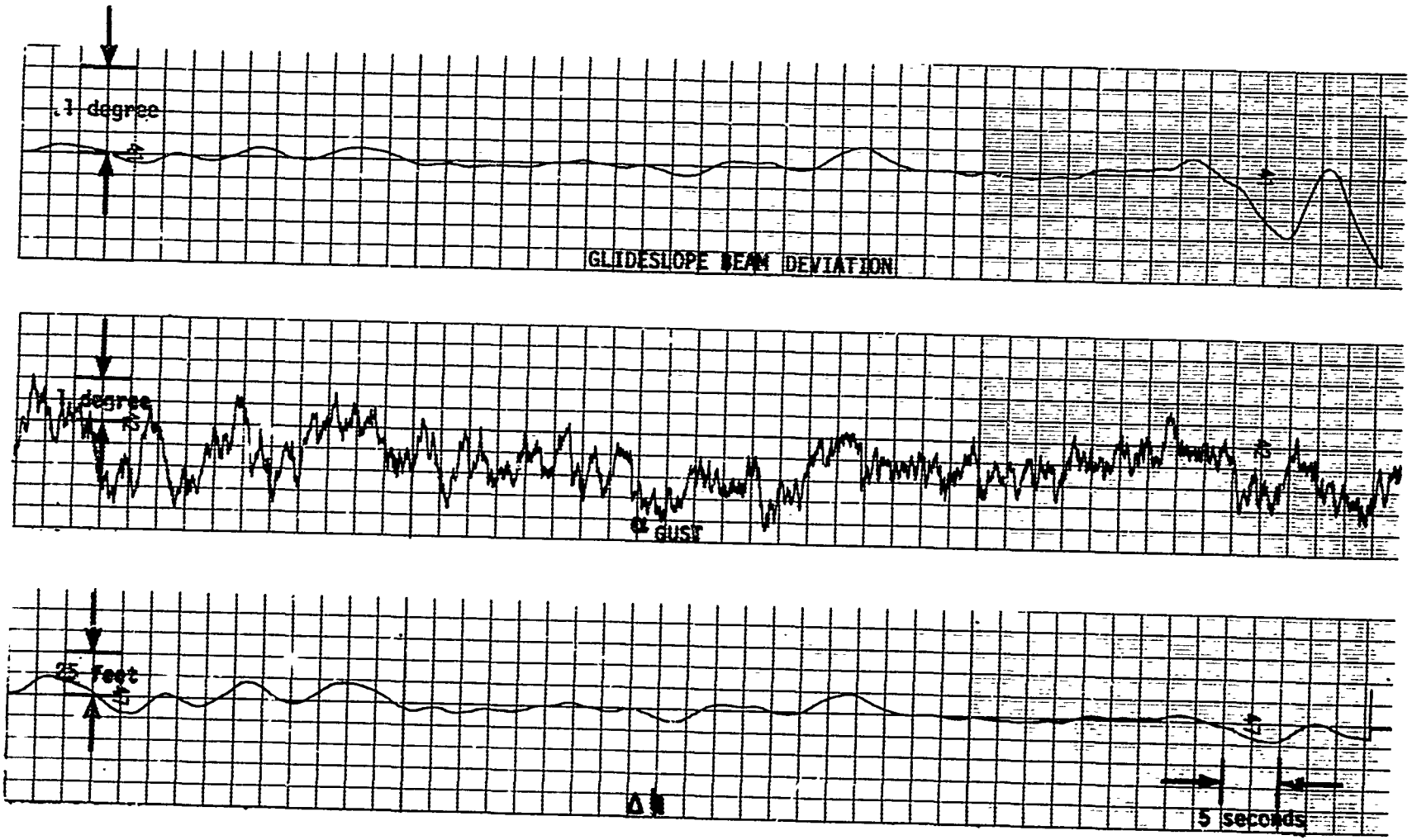

Figure 4.1.7(c)

SYSTEM "C" SIMULATED RESPONSE TO RANDOM TURBULENCE

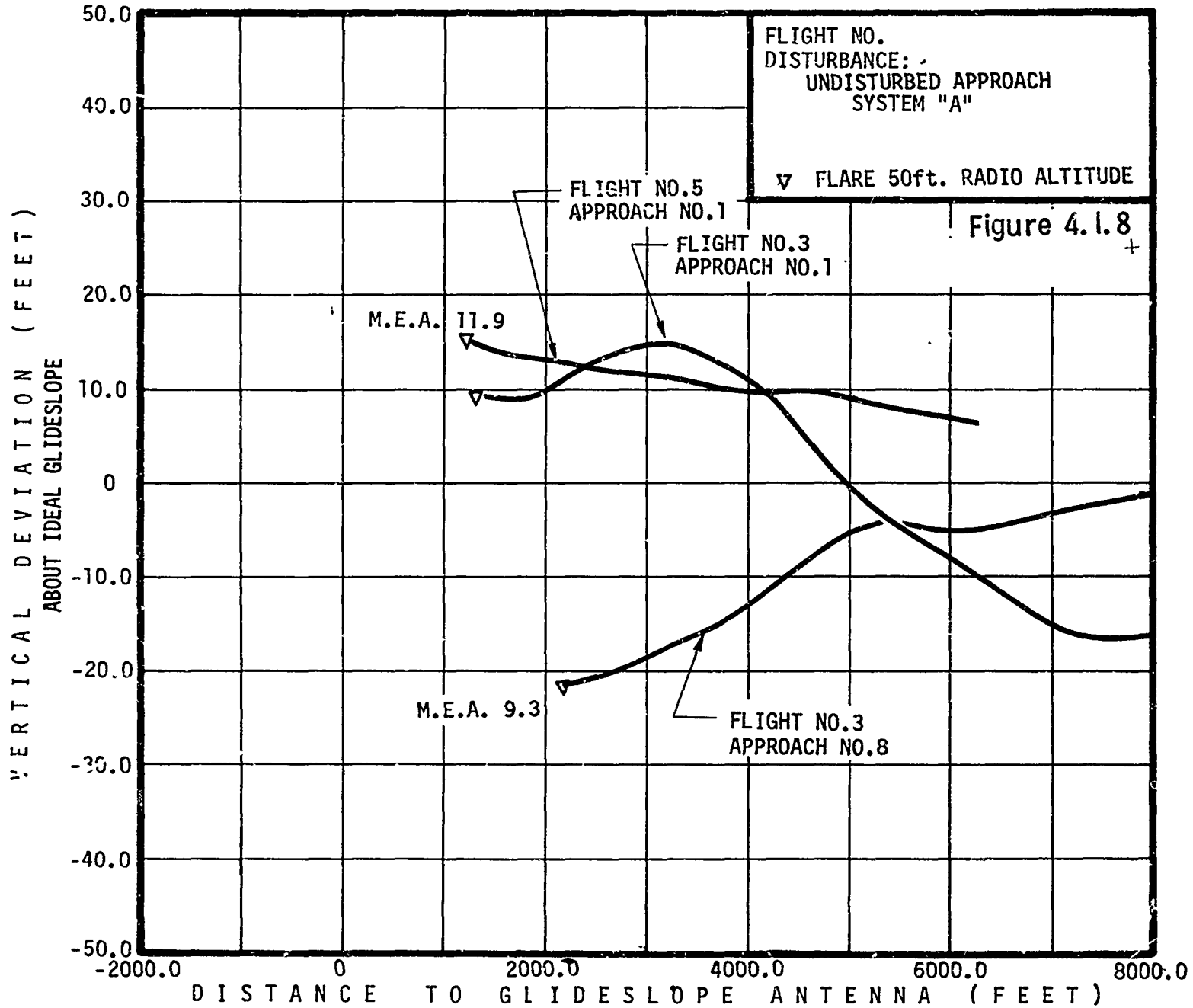
FLIGHT NO.
DISTURBANCE: -
UNDISTURBED APPROACH
SYSTEM "A"
▽ FLARE 50ft. RADIO ALTITUDE
FLIGHT NO.5
APPROACH NO.1
FLIGHT NO.3
APPROACH NO.1
M.E.A. 11.9
M.E.A. 9.3
FLIGHT NO.3
APPROACH NO.8
50.0
40.0
30.0
20.0
10.0
0
-10.0
-20.0
-30.0
-40.0
-50.0
-2000.0
0
2000.0
4000.0
6000.0
8000.0
VERTICAL DEVIATION (FEET)
ABOUT IDEAL GLIDESLOPE
DISTANCE TO GLIDESLOPE ANTENNA (FEET)

Figure 4.1.8

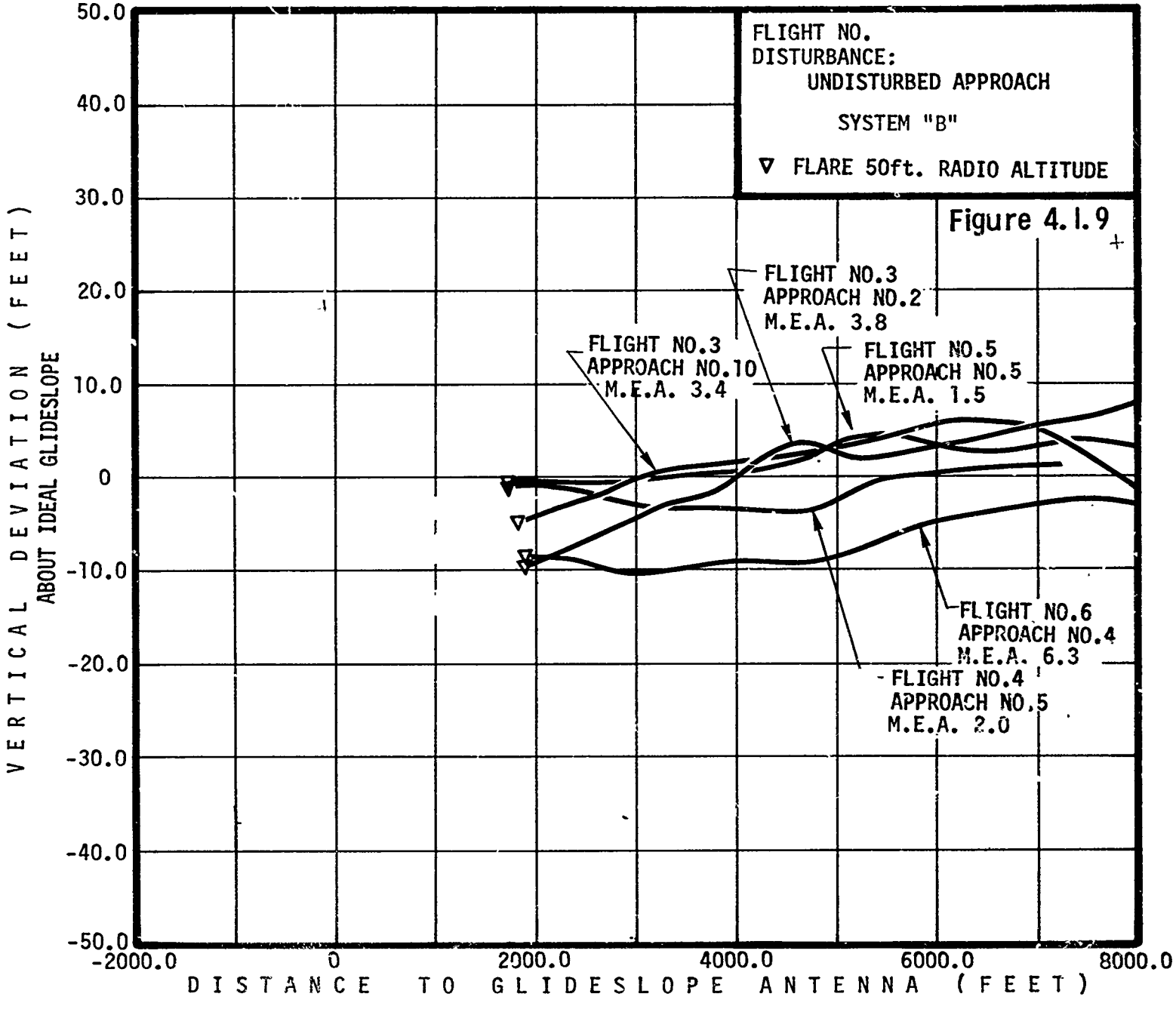
FLIGHT NO.
DISTURBANCE:
UNDISTURBED APPROACH
SYSTEM "B"
▽ FLARE 50ft. RADIO ALTITUDE
Figure 4.1.9
FLIGHT NO.3
APPROACH NO.2
M.E.A. 3.8
FLIGHT NO.3
APPROACH NO.10
M.E.A. 3.4
FLIGHT NO.5
APPROACH NO.5
M.E.A. 1.5
FLIGHT NO.6
APPROACH NO.4
M.E.A. 6.3
FLIGHT NO.4
APPROACH NO.5
M.E.A. 2.0
50.0
40.0
30.0
20.0
10.0
0
-10.0
-20.0
-30.0
-40.0
-50.0
-2000.0
0
2000.0
4000.0
6000.0
8000.0
VERTICAL DEVIATION (FEET)
ABOUT IDEAL GLIDESLOPE
DISTANCE TO GLIDESLOPE ANTENNA (FEET)

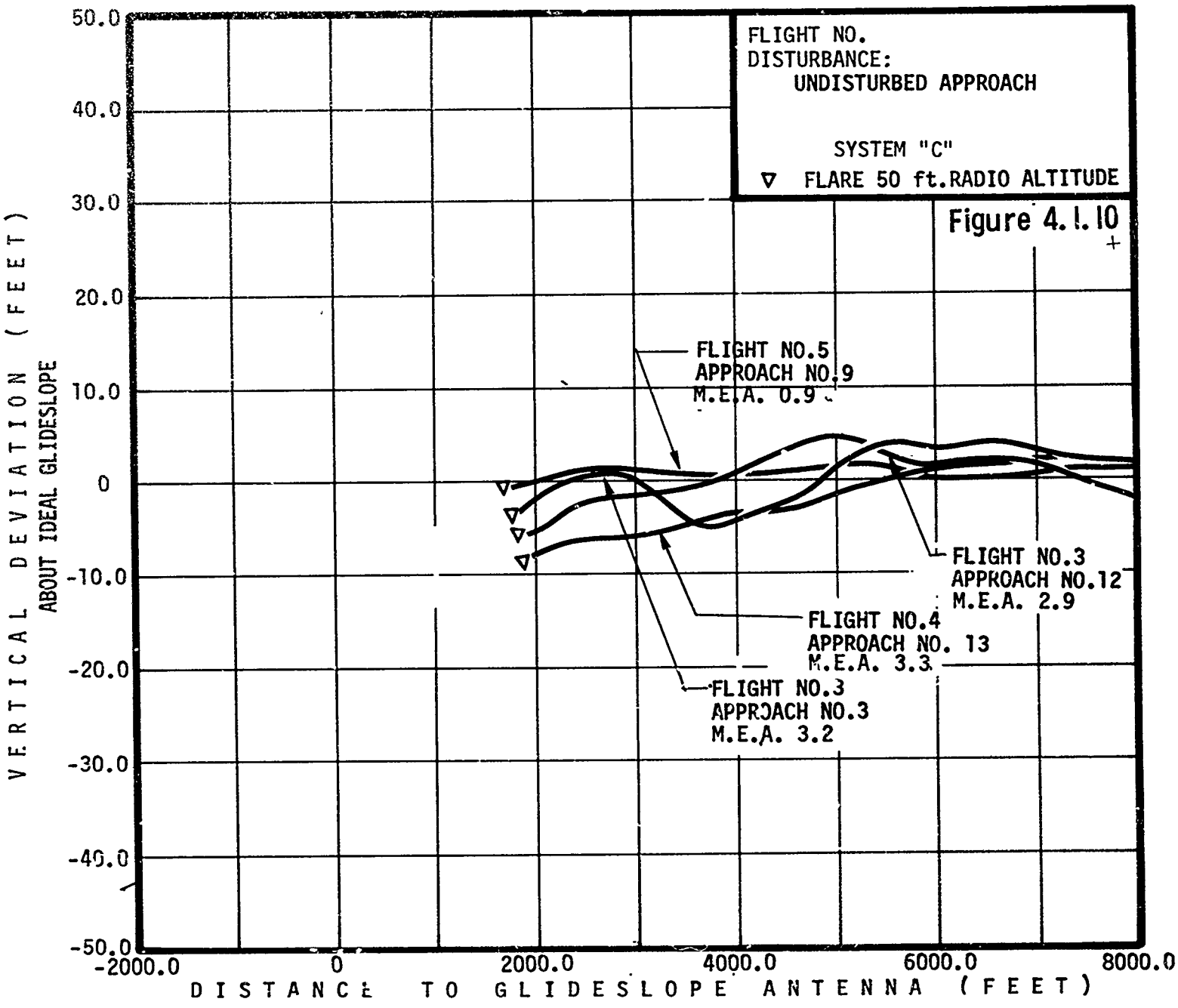
FLIGHT NO.
DISTURBANCE:
UNDISTURBED APPROACH
SYSTEM "C"
▽ FLARE 50 ft. RADIO ALTITUDE
Figure 4.1.10
FLIGHT NO.5
APPROACH NO.9
M.E.A. 0.9
FLIGHT NO.3
APPROACH NO.12
M.E.A. 2.9
FLIGHT NO.4
APPROACH NO. 13
M.E.A. 3.3
FLIGHT NO.3
APPROACH NO.3
M.E.A. 3.2
50.0
40.0
30.0
20.0
10.0
0
-10.0
-20.0
-30.0
-40.0
-50.0
-2000.0
0
2000.0
4000.0
6000.0
8000.0
VERTICAL DEVIATION (FEET)
ABOUT IDEAL GLIDESLOPE
DISTANCE TO GLIDESLOPE ANTENNA (FEET)

4.1.2 Roll Axis Wind Performance

Inertial smoothing of the localizer beam deviation has no direct impact on autoland wind performance. Linear transfer function analysis shows identical wind performance for systems with and without inertial smoothing but otherwise the same. Improved wind performance arises from high quality lateral velocity information and increased gains.

System C indirectly achieves slightly better wind performance than System B. Some of the reduction in localizer disturbance induced lateral displacement was traded to double the displacement gain in the inertially smoothed system. The increased stiffness of System C in the wind, is most noticeable for a wind shear disturbance.

The windshear performance characteristics of System A were discussed in Section 2.1.1. Figure 4.1.11 shows the simulated crosswind shear responses of the three systems. System B shows a peak lateral displacement of five feet induced by the end of the windshear, while System C shows a peak of three feet.

Observed lateral deviations caused by the wind during flight test were similar to those observed on the simulation. Figure 4.1.12 illustrates the comparative wind performance of the three systems by showing the lateral deviation of the midpoint of the line joining the main landing gear obtained by inertial smoothing of the camera tracking system data. The three lateral deviation traces were obtained with no artificial beam disturbances on the fourth, fifth, and seventh approaches during the second test flight. These three approaches were made over a time span of thirty two minutes and encountered similar wind conditions. All of the systems initially tend to track about ten feet left of centerline in the presence of ten degrees left crab because the localizer antenna was mounted on the vertical tail.

Composites of three undisturbed System A, and five undisturbed System B and C approaches are shown in Figures 4.1.13, 4.1.14, and 4.1.15 respectively. These thirteen approaches were undisturbed in the sense of there being no localizer disturbances. The lateral deviations were solely the result of winds.

The maneuver equation magnitude (MEA) was computed once per second and averaged over the final approach segment shown in the figures. This computation is discussed in more detail in Section 3.5. The composite maneuver criterion average for the three undisturbed System A approaches is 11.5 feet. The composite averages for four System B and four System C approaches are respectively 7.4 feet and 5.8 feet. The flight data indicates that System B achieves a thirty five percent reduction in maneuver criterion average compared to System A. This reduction results from inertial damping through the use of INS track angle deviation. System C exhibited only half the maneuver criterion average of System A. The maneuver criterion average of System C is eighty percent of System B. This reduction is attributable to the increased gains allowed by inertial smoothing.

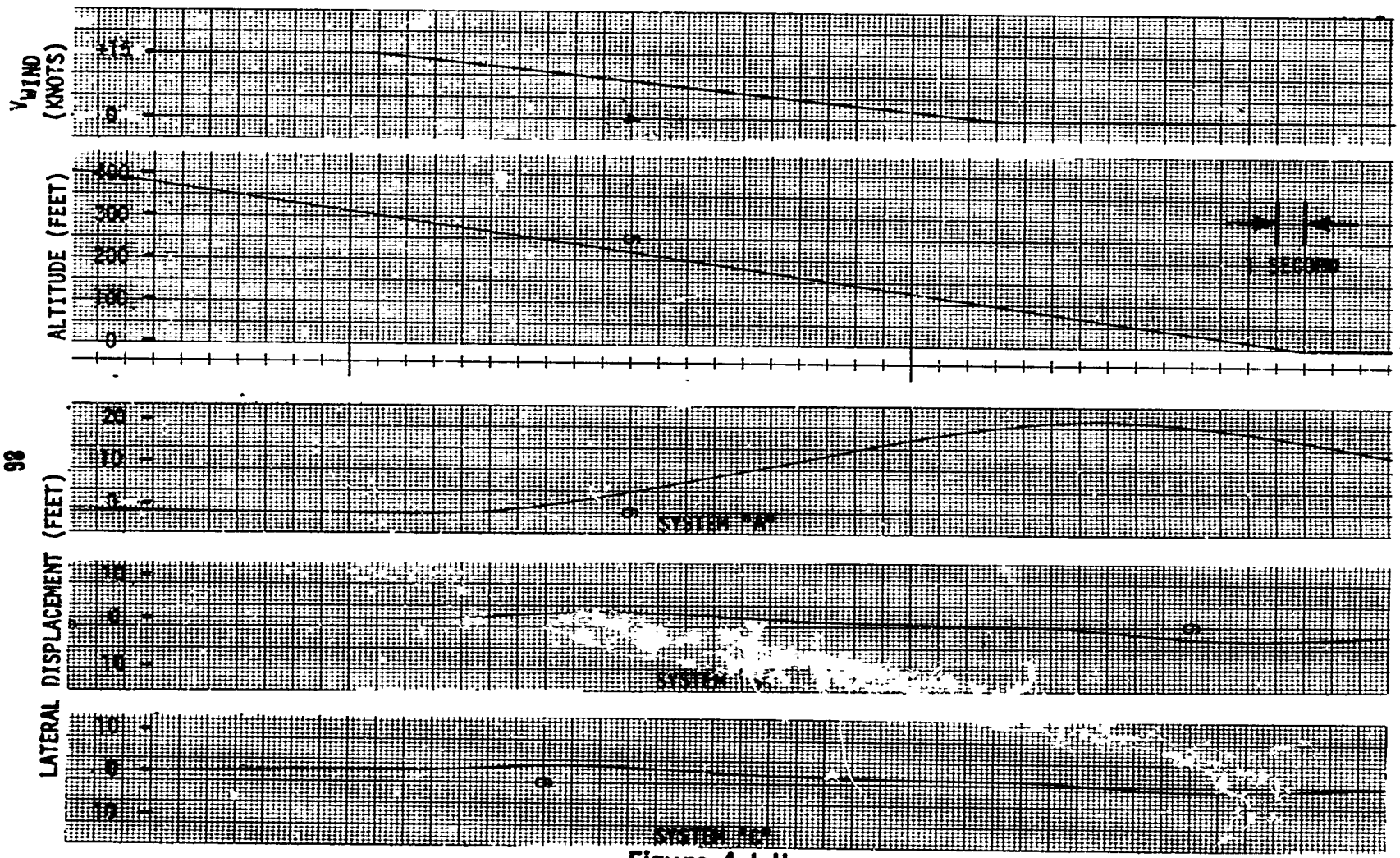

Figure 4.1.11

COMPARISON OF CROSSWIND SHEAR RESPONSES

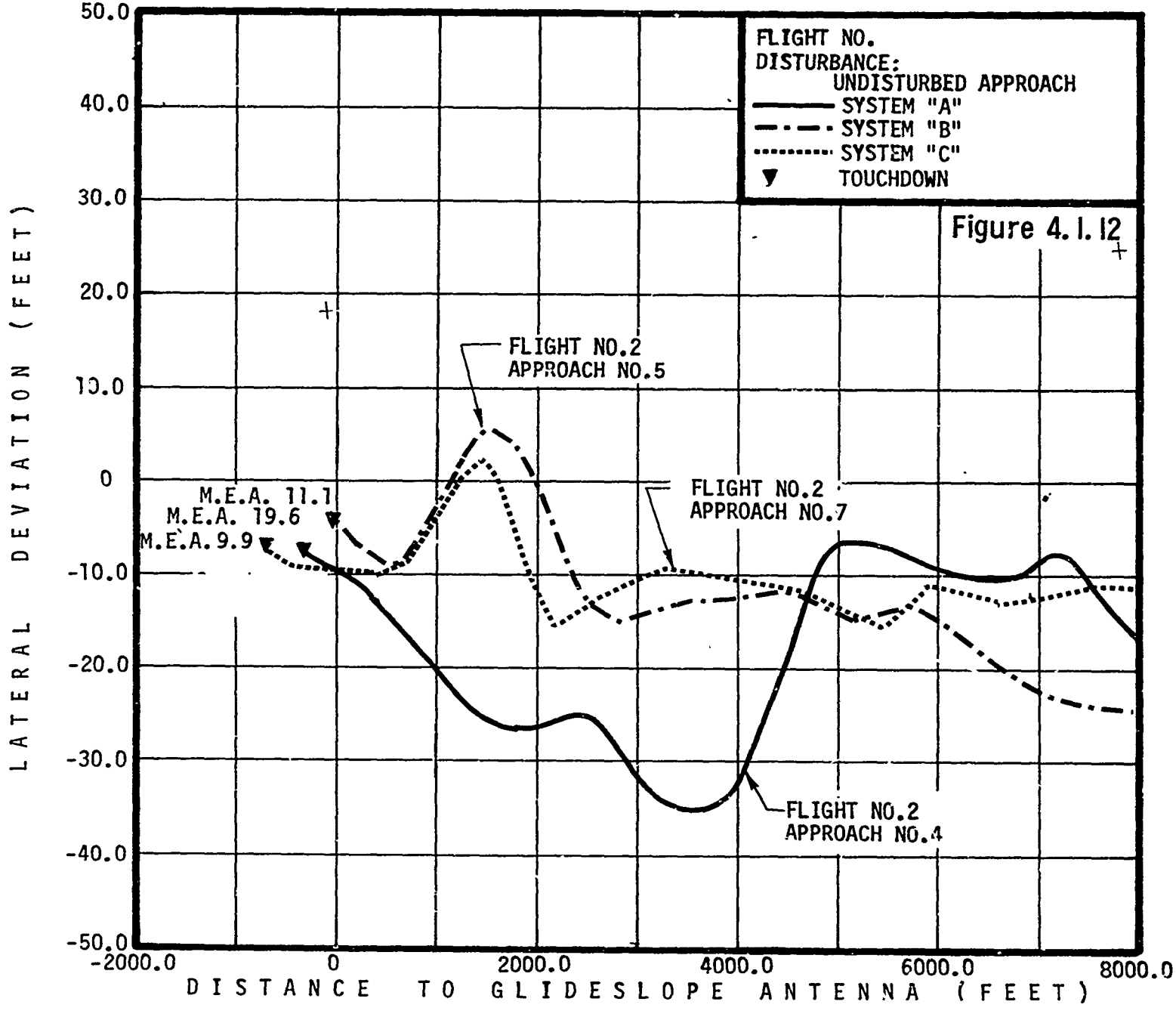
FLIGHT NO.
DISTURBANCE:
UNDISTURBED APPROACH
SYSTEM "A"
SYSTEM "B"
SYSTEM "C"
TOUCHDOWN
Figure 4.1.12
FLIGHT NO.2
APPROACH NO.5
FLIGHT NO.2
APPROACH NO.7
FLIGHT NO.2
APPROACH NO.4
M.E.A. 11.1
M.E.A. 19.6
M.E.A. 9.9
50.0
40.0
30.0
20.0
10.0
0
-10.0
-20.0
-30.0
-40.0
-50.0
-2000.0
0
2000.0
4000.0
6000.0
8000.0
LATERAL DEVIATION (FEET)
DISTANCE TO GLIDESLOPE ANTENNA (FEET)

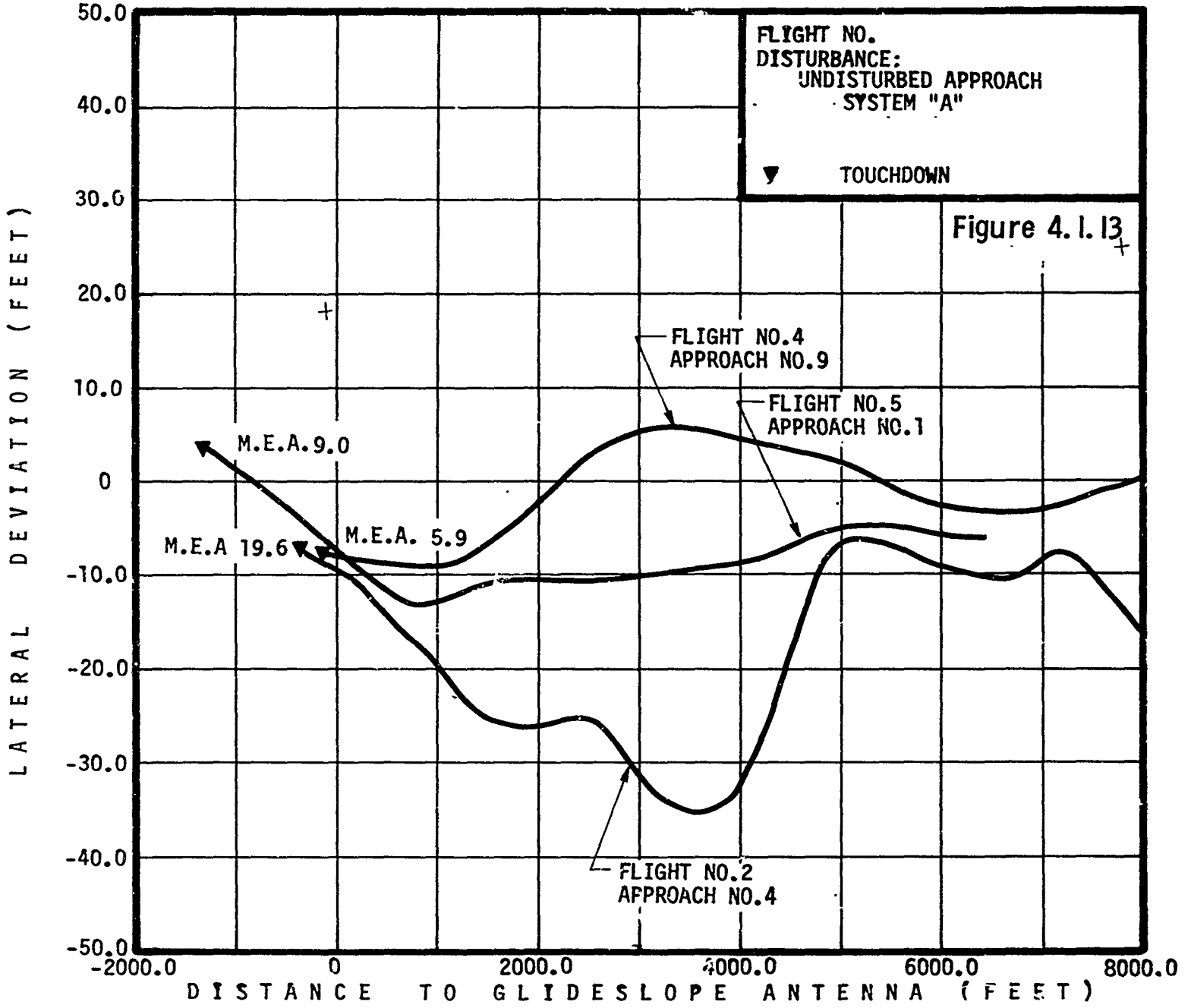
FLIGHT NO.
DISTURBANCE:
UNDISTURBED APPROACH
SYSTEM "A"
TOUCHDOWN
Figure 4.1.13
FLIGHT NO.4
APPROACH NO.9
FLIGHT NO.5
APPROACH NO.1
M.E.A.9.0
M.E.A 19.6
M.E.A. 5.9
FLIGHT NO.2
APPROACH NO.4
50.0
40.0
30.0
20.0
10.0
0
-10.0
-20.0
-30.0
-40.0
-50.0
-2000.0
0
2000.0
4000.0
6000.0
8000.0
LATERAL DEVIATION (FEET)
DISTANCE TO GLIDESLOPE ANTENNA (FEET)

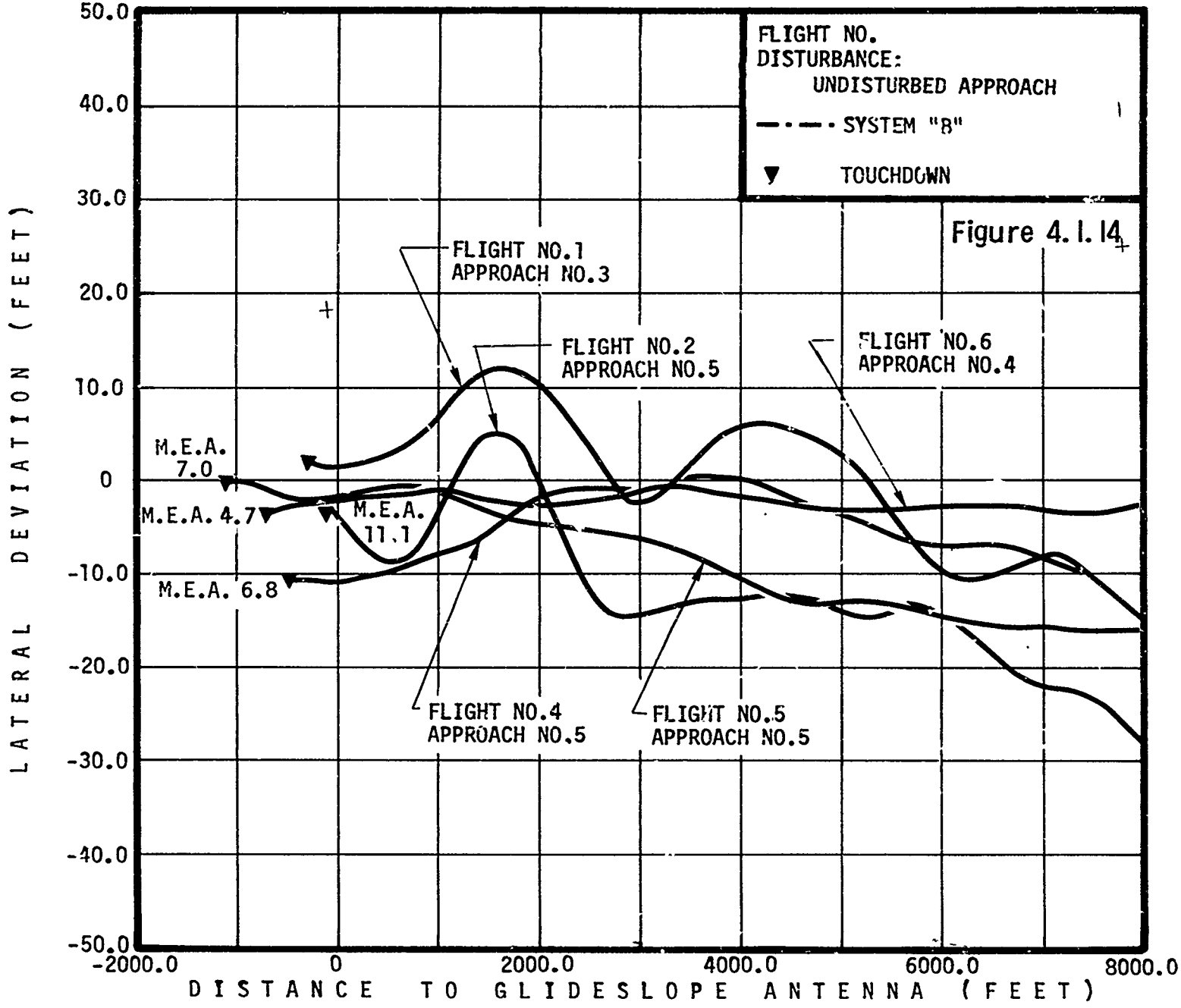
FLIGHT NO.
DISTURBANCE:
UNDISTURBED APPROACH
SYSTEM "B"
TOUCHDOWN
FLIGHT NO.1
APPROACH NO.3
FLIGHT NO.2
APPROACH NO.5
FLIGHT NO.6
APPROACH NO.4
M.E.A.
7.0
M.E.A. 4.7
M.E.A.
11.1
M.E.A. 6.8
FLIGHT NO.4
APPROACH NO.5
FLIGHT NO.5
APPROACH NO.5
50.0
40.0
30.0
20.0
10.0
0
-10.0
-20.0
-30.0
-40.0
-50.0
-2000.0
0
2000.0
4000.0
6000.0
8000.0
LATERAL DEVIATION (FEET)
DISTANCE TO GLIDESLOPE ANTENNA (FEET)

Figure 4.1.14

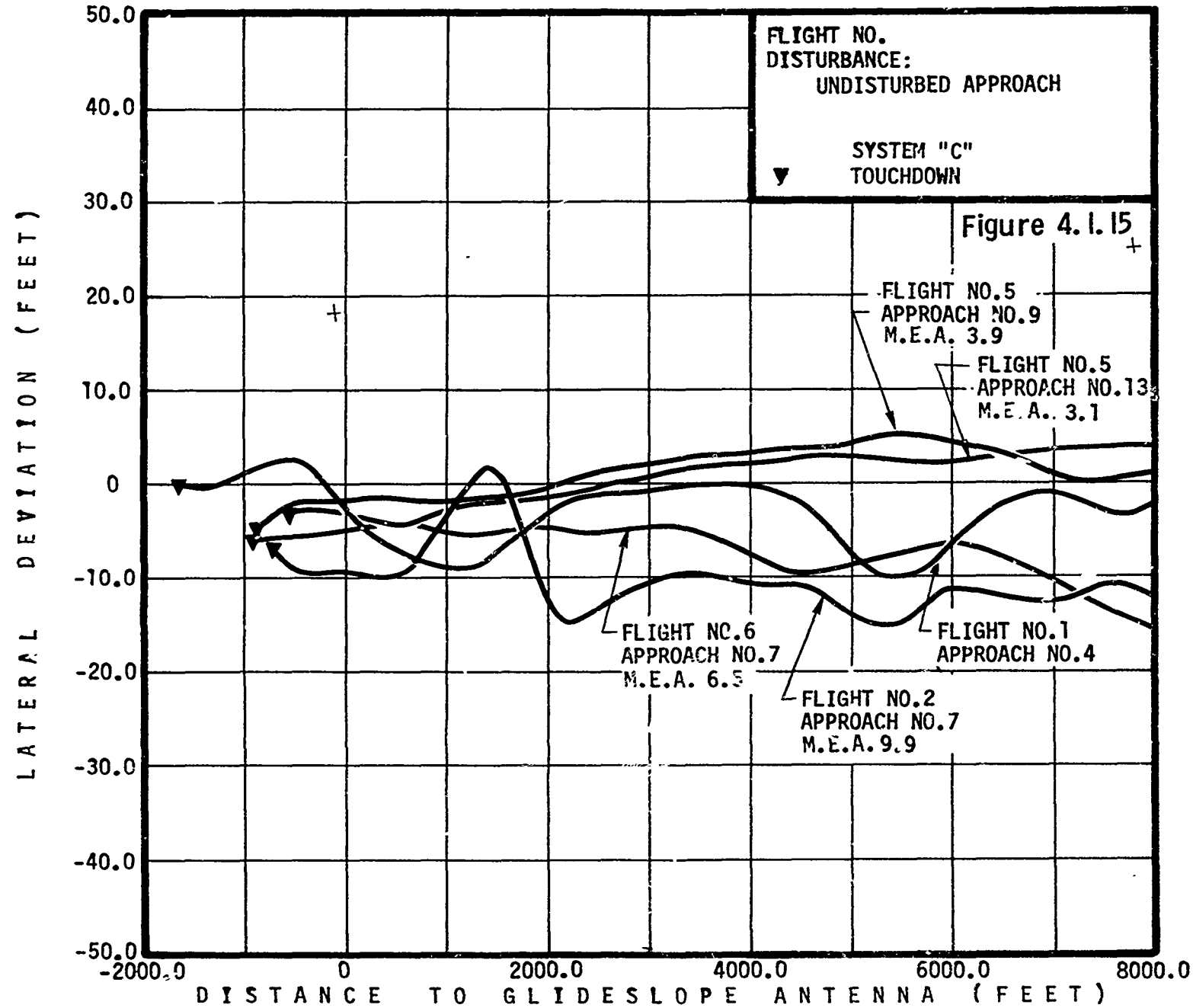
FLIGHT NO.
DISTURBANCE:
UNDISTURBED APPROACH
SYSTEM "C"
TOUCHDOWN
Figure 4.1.15
FLIGHT NO.5
APPROACH NO.9
M.E.A. 3.9
FLIGHT NO.5
APPROACH NO.13
M.E.A. 3.1
FLIGHT NO.6
APPROACH NO.7
M.E.A. 6.5
FLIGHT NO.2
APPROACH NO.7
M.E.A. 9.9
FLIGHT NO.1
APPROACH NO.4
50.0
40.0
30.0
20.0
10.0
0
-10.0
-20.0
-30.0
-40.0
-50.0
-2000.0
0
2000.0
4000.0
6000.0
8000.0
LATERAL DEVIATION (FEET)
DISTANCE TO GLIDESLOPE ANTENNA (FEET)

4.2 Beam Sinusoidal Noise Rejection

The capability of the C system to "reject" substantially more erroneous ILS information than the A or B system, without decreasing the stability margin, is probably best illustrated with the closed loop frequency response curves (Bode plots) of the three systems.

Figure 4.2.1 describes the glide slope deviation-to-ILS disturbance (β / β_{NOISE}) frequency responses of the A, B and C systems. At the lower frequencies, wherein the long term guidance information is contained, all three systems exhibit unity gain. However, the C system response to G/S beam signals beyond 0.1 rad/sec is substantially attenuated compared to the responses of the A and B systems. The A system response not only shows a tendency to resonate at 0.15 rad/sec, but also exhibits a pass band that is approximately one octave wider than the pass band of the C system. The B system response, meanwhile, shows less tendency to resonate, but exhibits a pass band that is even wider than the A system.

The two frequency response curves in Figure 4.2.2 illustrate the good G/S tracking capability of the C system. The solid curve is a duplicate of the β/β_{NOISE} response in Figure 4.2.1 and is presented only as a comparison to the dotted curve which describes the vertical deviation-to-vertical disturbance (h/h_{DIST}) response of the C system. It will be noted that the h/h_{DIST} frequency response is identical to the β / β_{DIST} response of the B system (Figure 4.2.1). This implies that the C system, in responding to actual displacement commands, will demonstrate the same, high performance tracking control as the B system. But, when subjected to the classical beam disturbances, the C system response will be greatly attenuated.

Figure 4.2.3 presents localizer deviation to ILS disturbance frequency responses of System A, B, and C. At low frequencies all three systems track the localizer beam. The response amplitude of three systems begins to rise between 0.01 and 0.1 radians per second as a result of the zero caused by proportional plus integral control. The increase in the response of System C starts at a significantly lower frequency because ILS disturbance is subject to the complementary filter lag rather than just a proportional path. The complementary filter of System C begins to significantly attenuate the response at frequencies above 0.06 radians per second. System B has almost an octave wider band pass than System C to beam disturbances with the inertial damping providing most of the response attenuation. The frequency response of System A has a broad flat peak that is almost an octave wider than the System B bandpass. The Bode plot for System A is typical of the response of a system quickened by incorporating the derivative of the disturbance. The attenuation of the System A response at high frequencies is primarily a result of decreasing lateral position response to roll command in the forward path.

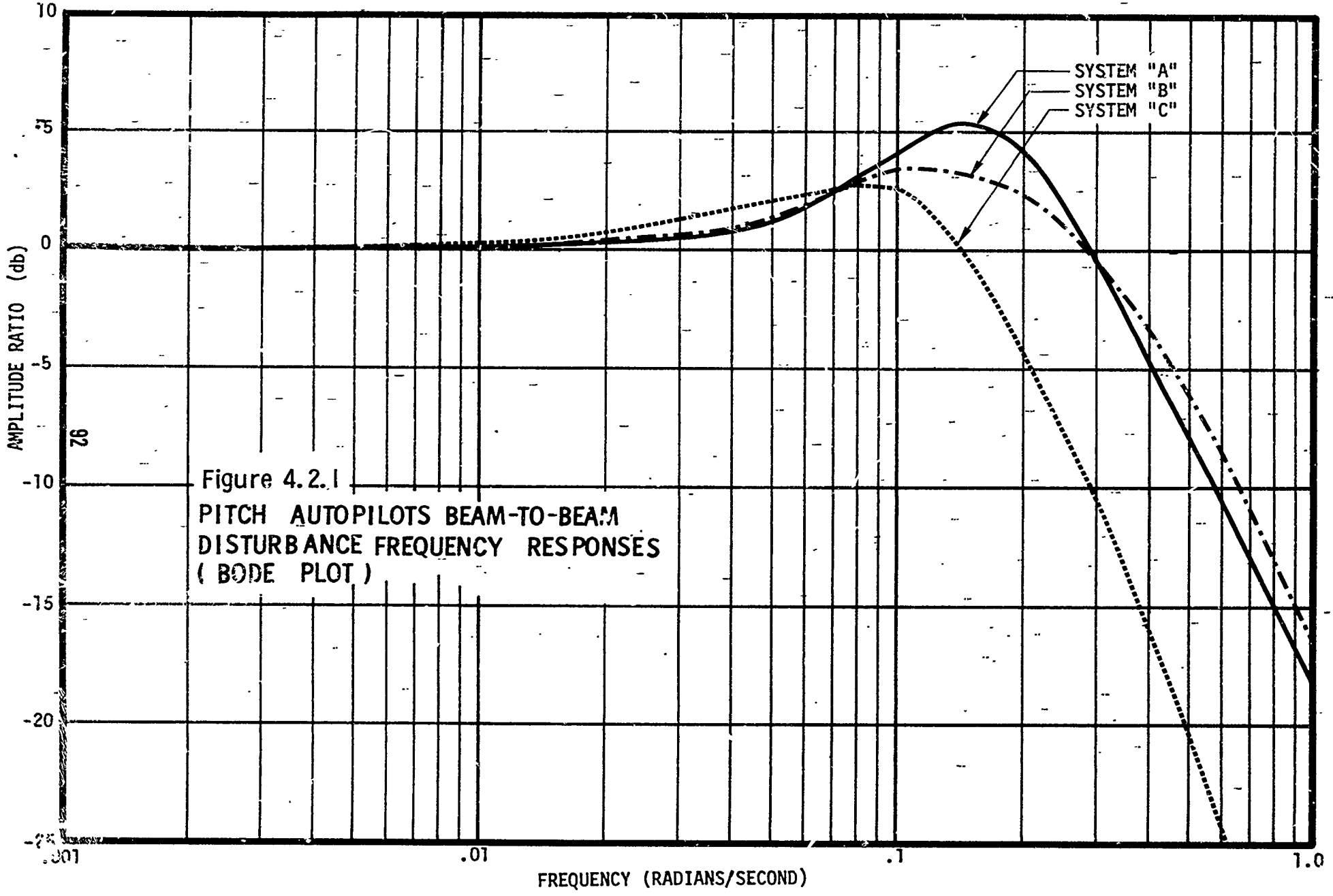

Figure 4.2.1
PITCH AUTOPILOTS BEAM-TO-BEAM DISTURBANCE FREQUENCY RESPONSES
(BODE PLOT)

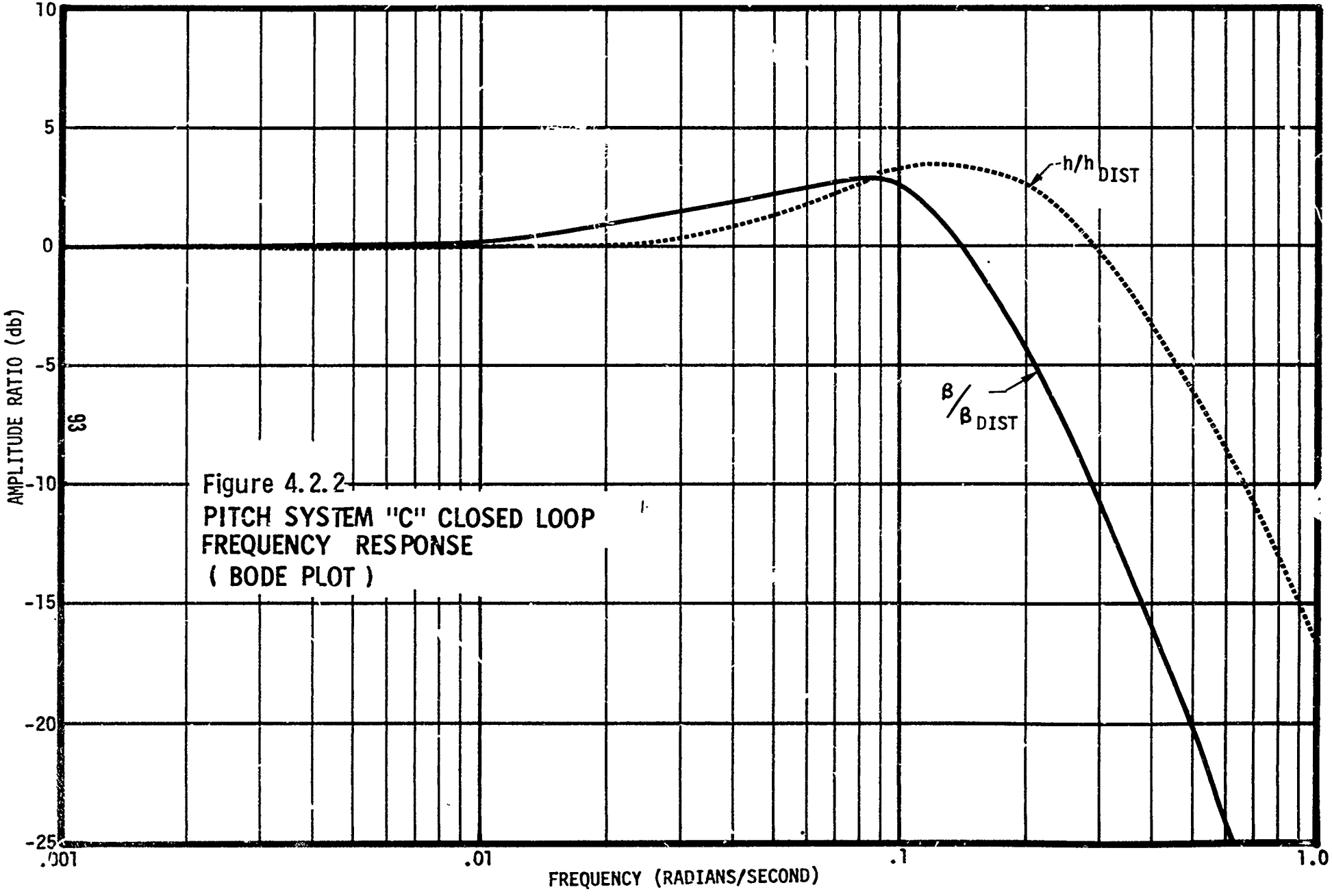

Figure 4.2.2
PITCH SYSTEM "C" CLOSED LOOP
FREQUENCY RESPONSE
(BODE PLOT)

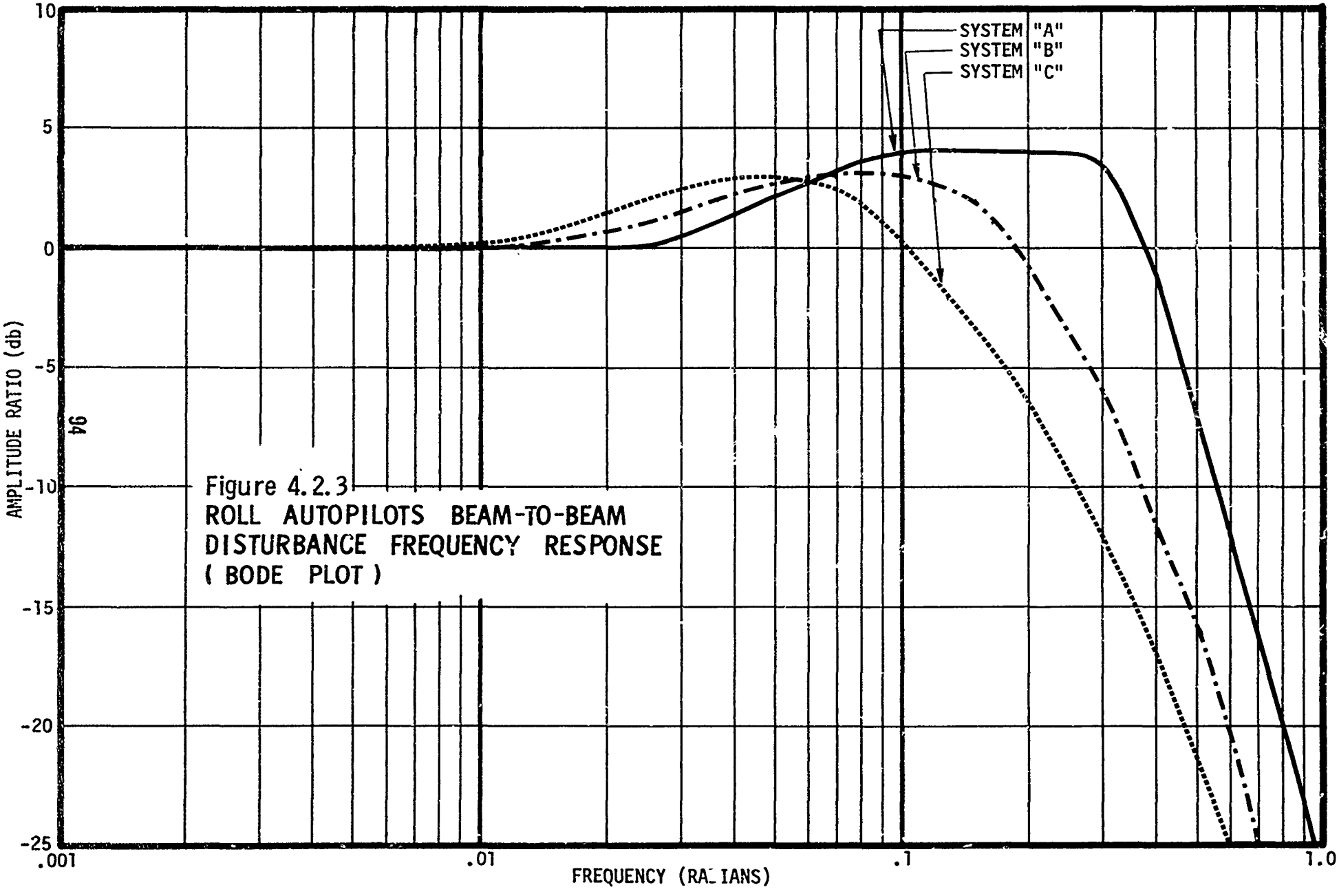

Figure 4.2.3
ROLL AUTOPILOTS BEAM-TO-BEAM
DISTURBANCE FREQUENCY RESPONSE
(BODE PLOT)

Figure 4.2.4 contrasts the ILS disturbance response with the true displacement response for System C. The curve of η/η_{NOISE} is identical to the System C response curve in Figure 4.2.3. The curve identified Y/Y_{DIST} in Figure 4.2.4 represents the lateral deviation resulting from commands equivalent to true position. The Y/Y_{DIST} bandpass of System C is slightly greater than the System B bandpass because of the higher gains. This shows that inertial smoothing does not compromise the ability to track and respond to real lateral displacements.

4.3 Comparative Response to Beam Bends

Three shapes of artificial beam bends were generally accepted as the initial disturbances to be studied on the simulation.

- o Sinusoidal $\left(1-\cos \frac{2\pi}{T} t\right)$
- o Rectangular (Step Functions, In and Out)
- o Triangular (Ramps, In and Out)

After a comprehensive study, it was decided to complete the remainder of this program using the sinusoidal disturbances only. The rectangular and triangular bends were rejected as valid upsets to the autoland systems, because neither shape possesses continuous derivatives and, hence, these disturbances caused undue response in acceleration. As a result, invalid exceedances of the maneuver criterion were observed, mainly in the A and B systems. Moreover, actual beam bends of rectangular or triangular shape are never observed in practice. In any event, Figure 4.3.1 is introduced to illustrate typical responses of all three longitudinal systems to each type of beam bend. No system was equipped with a beam limiter in the simulated runs of Figure 4.3.1 in order to demonstrate the increased amplitude of the airplane maneuver (see Eq. 3.4.21) when the rectangular or the triangular bend was used as the beam disturbance.

4.3.1 Pitch Axis Beam Bend Comparisons

As pointed out in Section 2, it was decided to mechanize each of the three systems with a beam limiter of 0.2 degrees. This, of course, rendered a degree of "fairness" or objectivity in evaluating each system's performance against beam disturbances. Flight data, however, soon revealed that the lesser performance of the A system against environmental upsets necessitated a substantially larger limiter in the A system, but since all flight testing was conducted with the 0.2-deg beam limiter installed, it became necessary to determine the extent of the effect of the limiter on each system in order to achieve a practical evaluation.

Fly down beam bend responses are illustrated in Figure 4.3.2 for the A system, Figure 4.3.3 for the B system, and Figure 4.3.4 for the

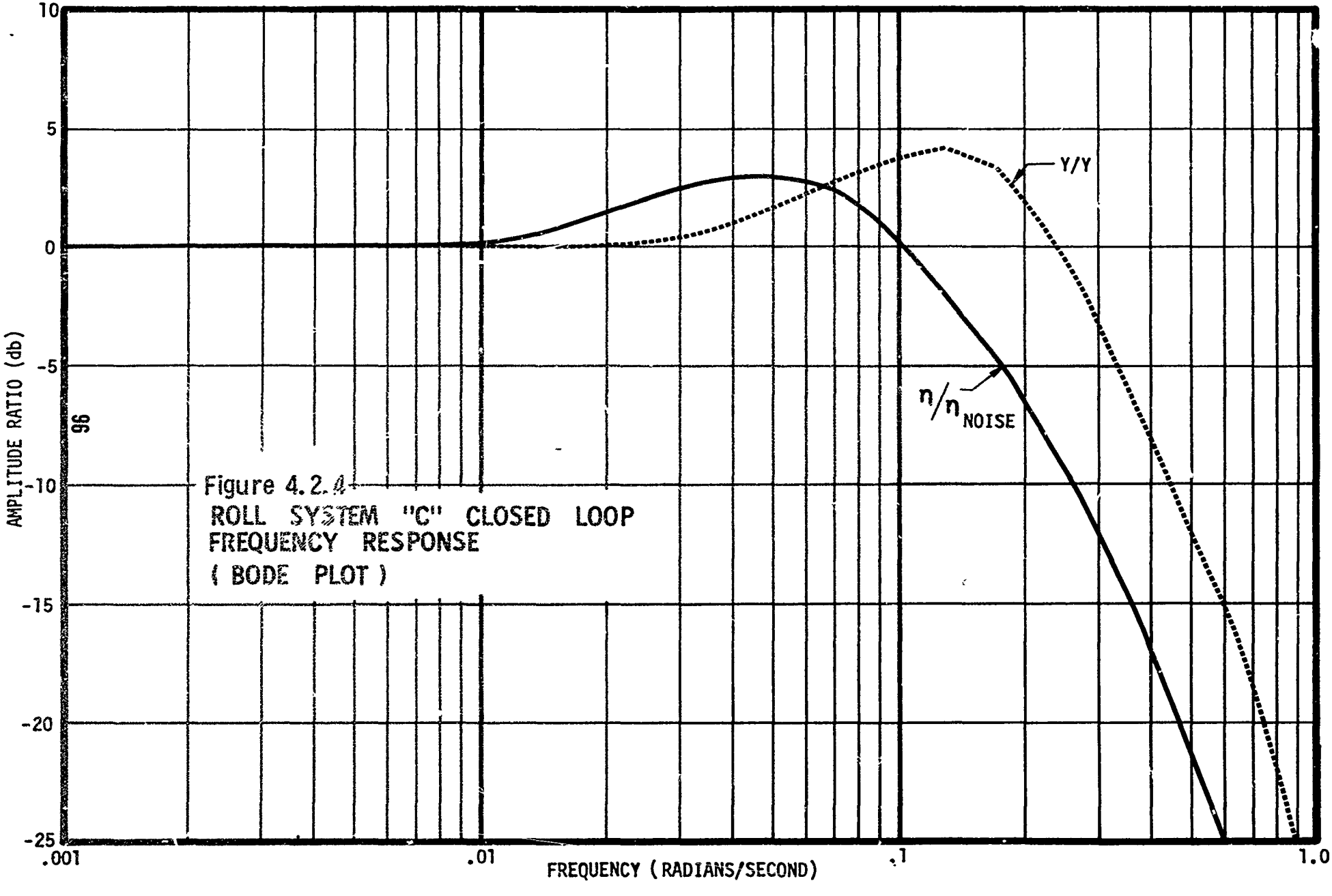

Figure 4.2.4
ROLL SYSTEM "C" CLOSED LOOP
FREQUENCY RESPONSE
(BODE PLOT)

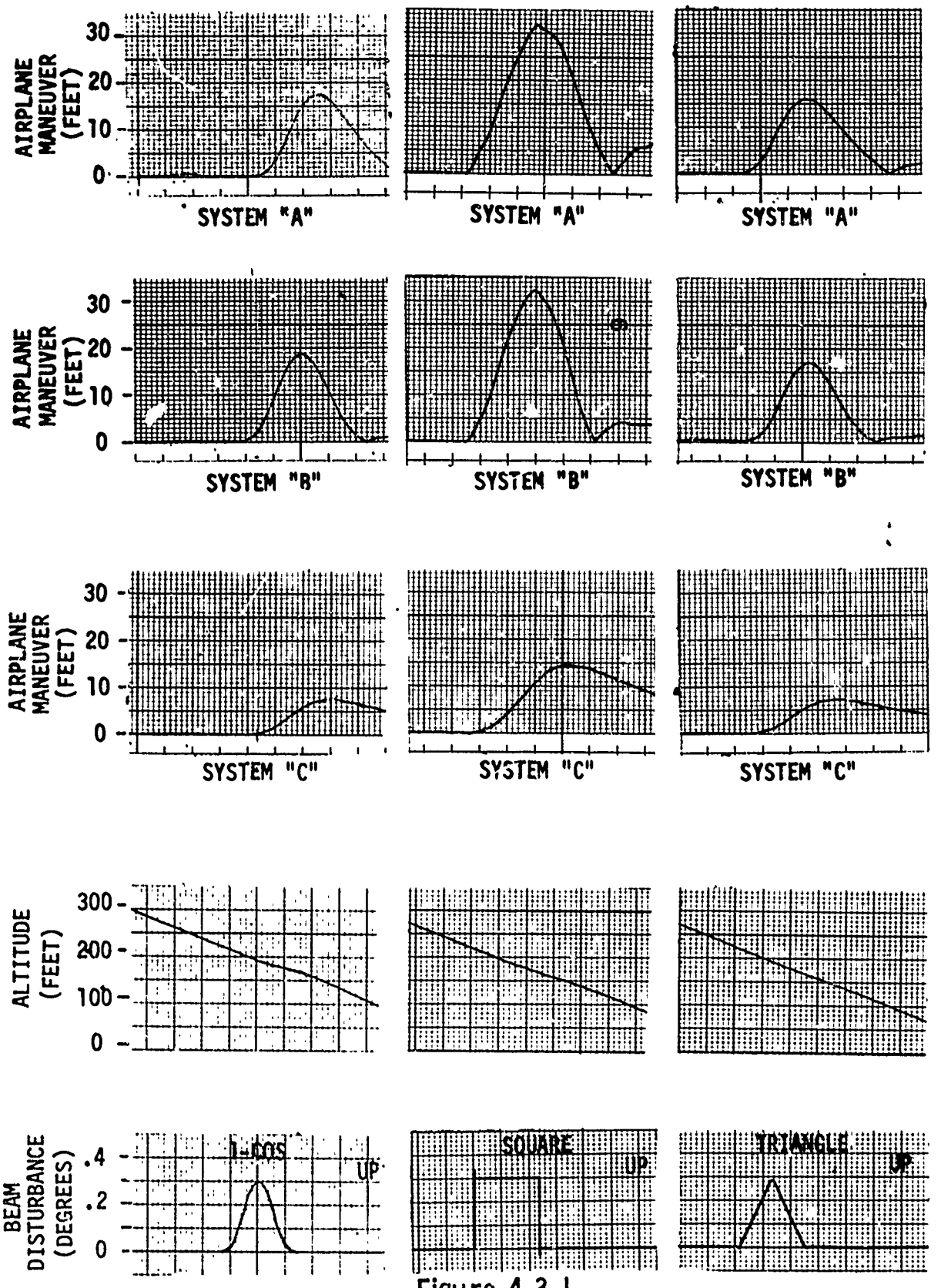

Figure 4.3.1

AIRPLANE MANEUVER RESPONSE TO THREE TYPES OF BEAM BENDS ON THREE TYPES OF CONTROL LAWS

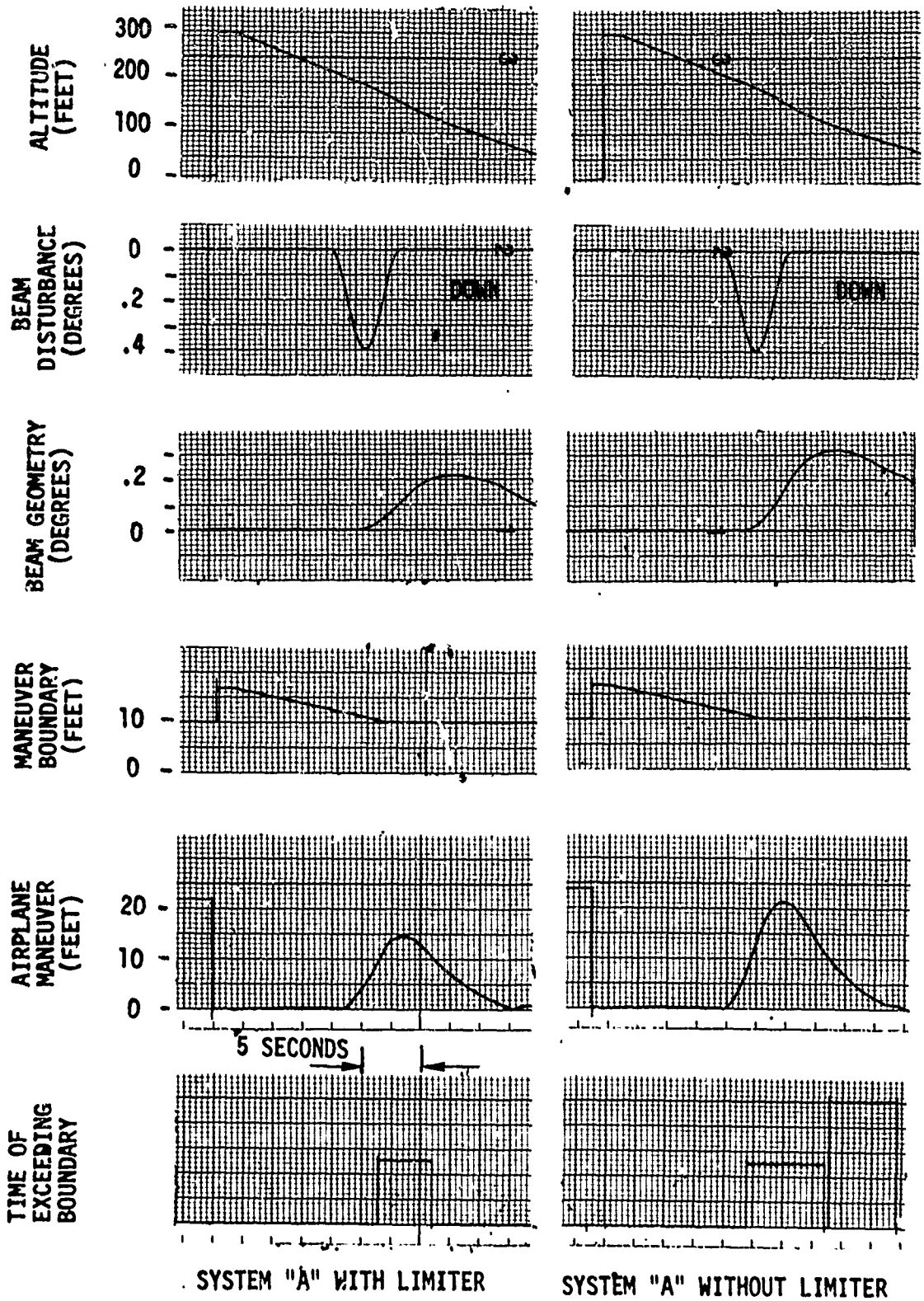

Figure 4.3.2 SYSTEM "A"
RESPONSE TO SINUSOIDAL , FLY-DOWN BEAM BEND

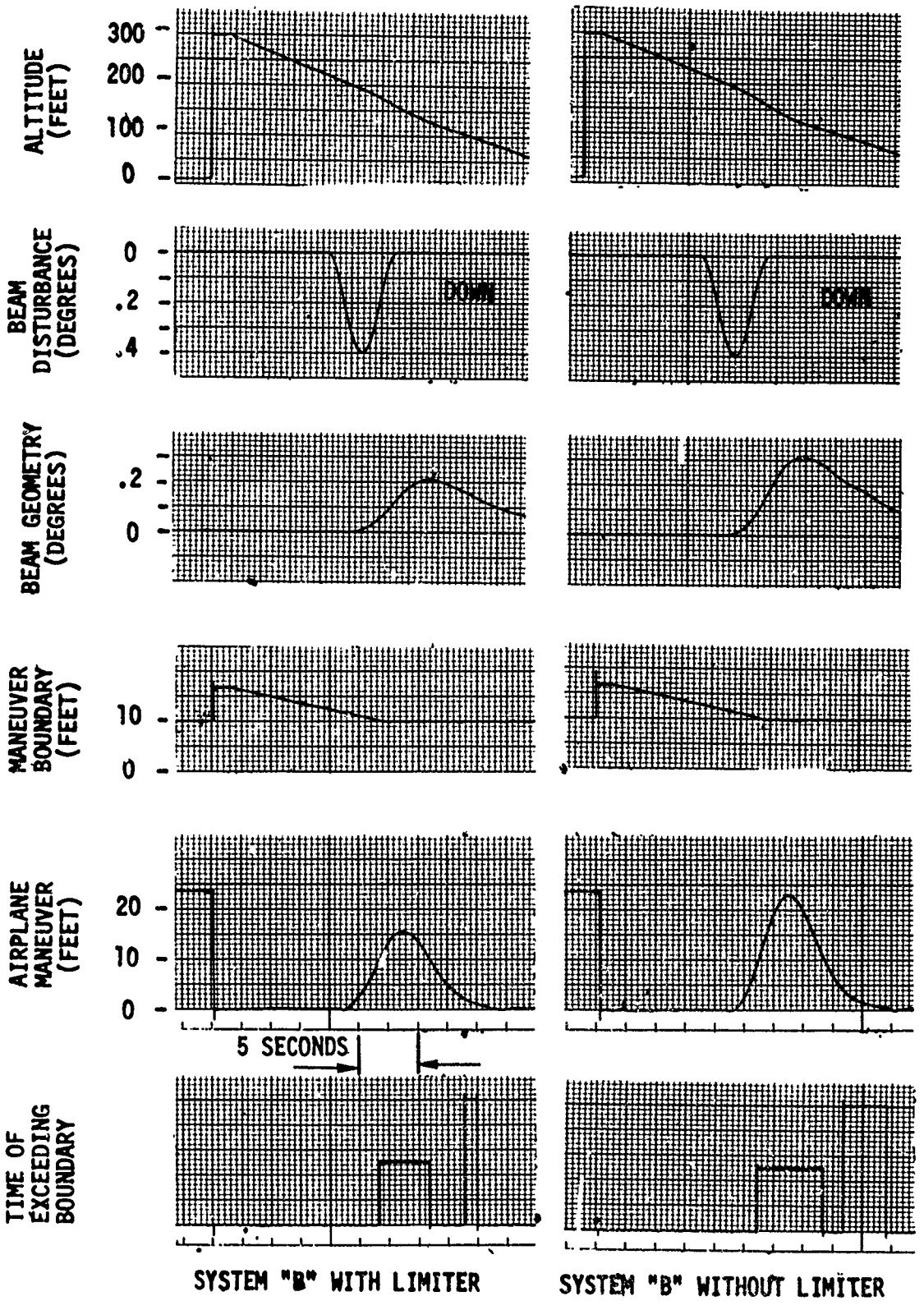

Figure 4.3.3 SYSTEM "B"
RESPONSE TO SINUSOIDAL, FLY-DOWN BEAM END

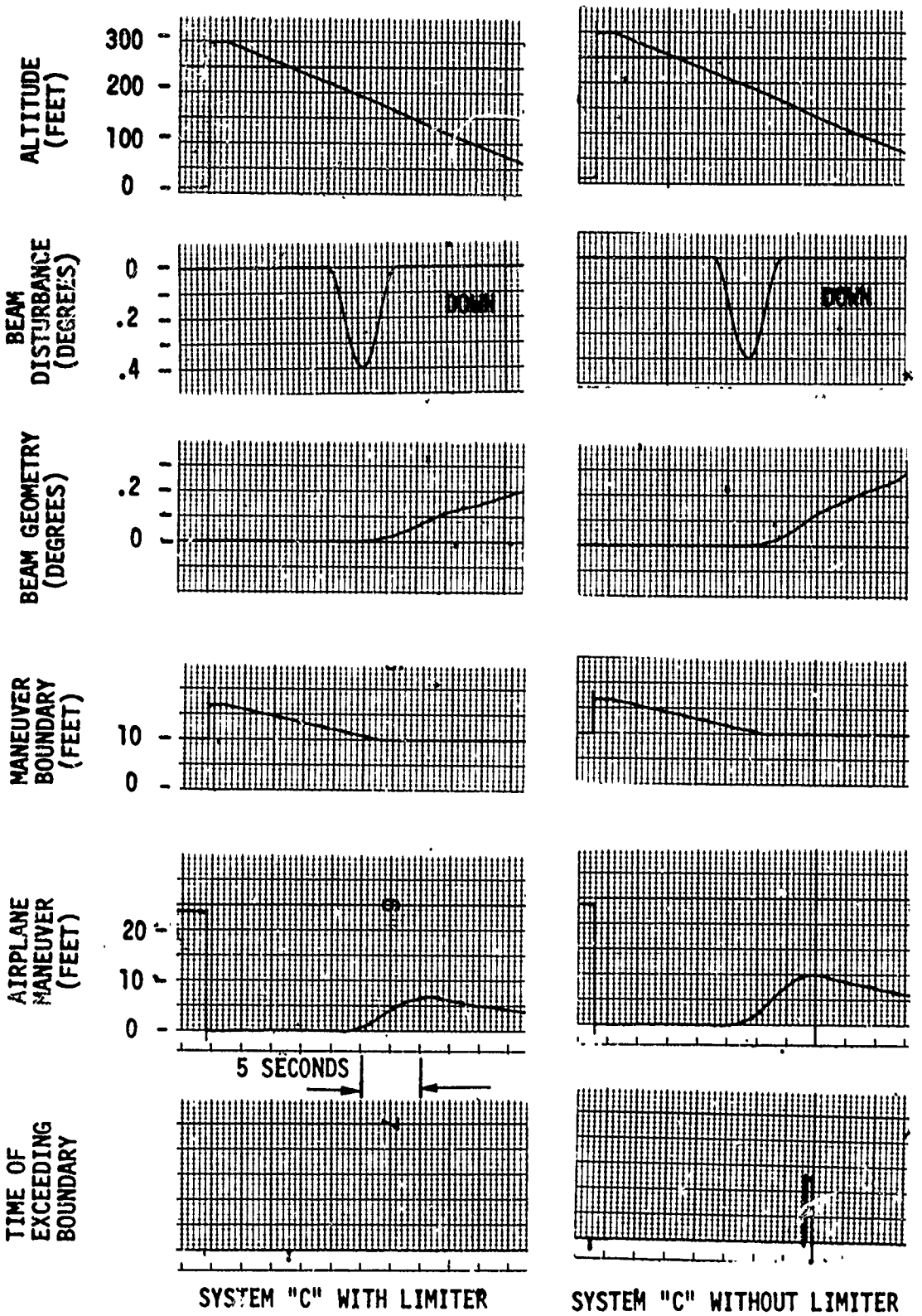

Figure 4.3.4 SYSTEM "C"
RESPONSE TO SINUSOIDAL , FLY-DOWN BEAM BENDS

C system. From the foregoing illustrations, the factor of improvement that the limiter rendered for beam bend response is shown below.

SYSTEM	IMPROVEMENT FACTOR OF LIMITER
A	1.34
B	1.34
C	1.36

These factors were obtained by averaging the peak airplane maneuvers that resulted from the "fly up" and "fly down" beam bends in each system. Thus, since the limiter improves the beam disturbance performance approximately the same factor in all three systems, and since the A system cannot perform satisfactorily with the 0.2-deg beam limit, an improvement factor other than those already mentioned must be assigned systems B and C over system A. This factor must be somewhat less than 1.34 since obviously, all beam disturbances encountered during coupled approaches are not likely to saturate the G/S receiver limiter in the A system, even in the presence of turbulence and/or wind shear. However, in considering the undisturbed flight paths on the four A system approaches as seen in Figure 4.1.5, all four approaches develop a beam error greater than the 0.2 deg. limit. Hence, the capability of the A system to provide G/S tracking is substantially reduced. Figures 4.1.6 and 4.1.7, on the other hand, demonstrate the high controllability of the B and C systems against winds in that the resulting beam error is always less than the limit in all cases. Therefore, owing to the capability of systems B and C to operate with a 0.2-deg receiver limit, a conservative improvement factor of 1.25 will be assigned systems B and C over system A. This factor is completely independent of the linear differences in beam noise rejection capability of the three systems.

The main advantage of the inertially smoothed system over a conventional system is the capability of the inertial system to reject a significantly greater portion of ILS beam bends (and other beam disturbances) than the conventional system. This statement holds for all frequencies but particularly in the pass band above 0.4 rad/sec. Figure 4.3.5 describes the ratio of the C system peak maneuver (Eq (3.4.21)) to the average peak maneuver of the A and B systems in the presence of beam bends of various amplitudes, periods and altitudes. The A and B system responses are averaged because the performance of the two systems against beam disturbances is nearly identical. Notice that the ratio in Figure 4.3.5 is less than 0.5 above 0.4 rad/sec and decreases even further with increasing frequency. Above 1 rad/sec, the decrease in the ratio of the peak maneuvers appears linear.

There is reason to believe that, in the small, low frequency region, 0 - .04 rad/sec, which is not covered by the curve in Figure 4.3.5, the C system peak maneuver may be slightly greater than that of the A or B system. However, frequencies below 0.04 rad/sec correspond to a period greater than 120 sec, which, during typical approaches covers a longitudinal distance of more than 25,000 ft. Bends of this unusual length are not likely to exist at any ILS facility which is certified

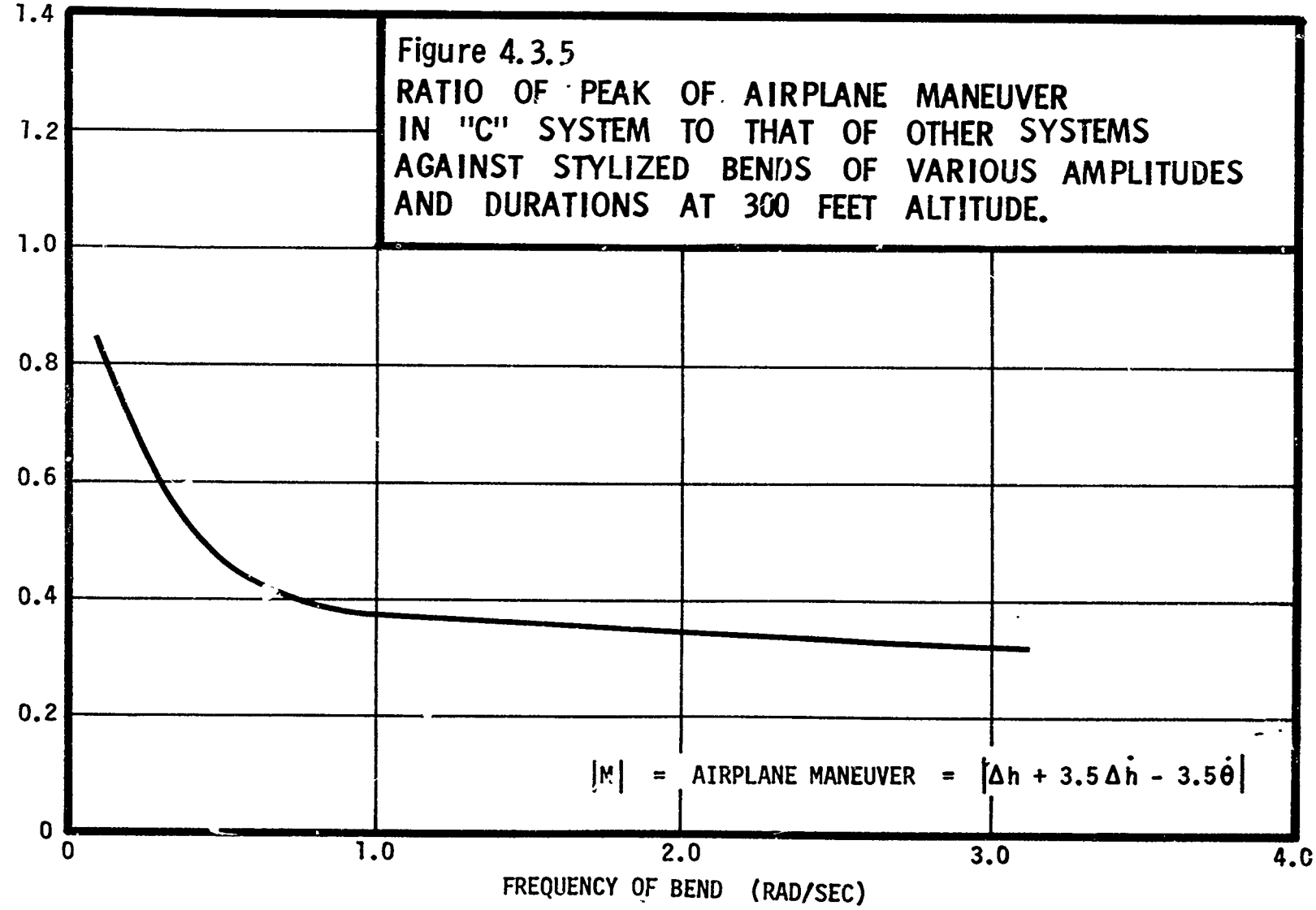
Figure 4.3.5
RATIO OF PEAK OF AIRPLANE MANEUVER IN "C" SYSTEM TO THAT OF OTHER SYSTEMS AGAINST STYLIZED BENDS OF VARIOUS AMPLITUDES AND DURATIONS AT 300 FEET ALTITUDE.
$|M_C|_{MAX} / \left|\frac{M_{A+B}}{2}\right|_{MAX}$
1.4
1.2
1.0
0.8
0.6
0.4
0.2
0
0
1.0
2.0
3.0
4.0
FREQUENCY OF BEND (RAD/SEC)
$|M|$ = AIRPLANE MANEUVER = $|\Delta h + 3.5\Delta\dot{h} - 3.5\dot{\theta}|$

for Category II or III operation. Nevertheless, this low frequency region provides the crucial test for inertial smoothing techniques. It is the supposed susceptibility of inertially smoothed systems to "memorize" these long period bends as beam center that has caused the industry in general to question the tenability of inertial smoothing.

In discussing this apparent disadvantage of the C system, it must be pointed out that the C system will not cause the airplane to deviate from the beam center any greater than the vertical distance of the peak of the bend itself. Consequently, if a long period bend exists which will cause the C system to exceed the maneuver criterion boundary, then the peak amplitude of that bend will also exceed the boundary and, hence, will cause the conventional systems to exceed the boundary also.

There has been speculation that glide slope beams similar to the sketch in Figure 4.3.6 may exist at certain facilities. The concern here is that the knee of the "dog leg" of such a bend may exist at the critical, low altitudes, causing the C system to continue on a dangerously low path completely through threshold. System A or B meanwhile with faster response characteristics will likely track the bend at the knee more closely and, thereby, will be in a more favorable position at threshold. This leads to the suggestion that the B system, with excellent wind resistance capability, will likely make consistent, satisfactory autolands against this type bend whereas the C system, with equal wind capability will be unacceptable in performance because of its low position at threshold.

According to ILS inspection requirements published by the FAA, glide slope beam limits are relatively small between 3500 ft and 4 nautical miles from threshold but can deviate rather substantially within 3500 ft of threshold. This, of course, implies that rapid changes in the glide slope are tolerated only below 175 ft altitude. Consequently, long term bends of the "dog leg" shape will not contain amplitudes greater than 20 ua (.1 DEG) above 175 ft. See Figure 4.3.7. This will pose only a minor problem for the C system. On the other hand, the graphical average path may legitimately follow the sketch shown in Figure 4.3.7, and in this case, of the three systems, only the C system could consistently make acceptable approaches on such a beam.

The overall improvement of the C system against the more frequently encountered bends may best be illustrated by relating some function of the airplane maneuver to some function describing the bend. Since the area under the curve of the (1-COSINE) function is a function of the altitude, time duration and amplitude of the bend, it was decided to plot the peak airplane maneuver against the "area" of the bend for all three systems. The derivation of the expression for the area under the bend follows.

Figure 4.3.6

HYPOTHETICAL "DOG LEG" GLIDESLOPE BEAM BEND

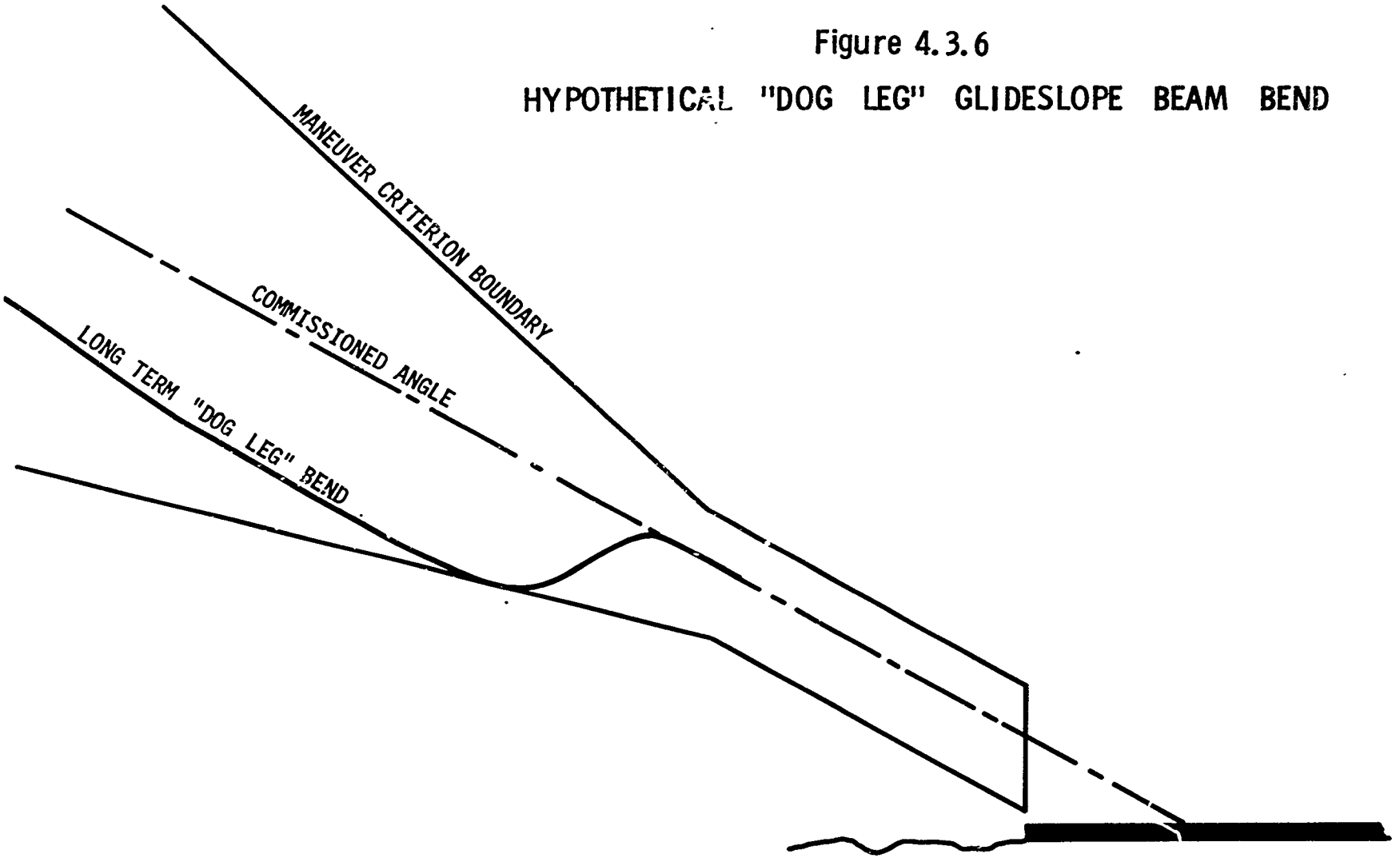

Figure 4.3.7

CAT II GLIDESLOPE BEAM INSPECTION LIMITS

(for case where actual path = commissioned angle)

comm = 2.5 deg.

ref. datum = 60 feet.

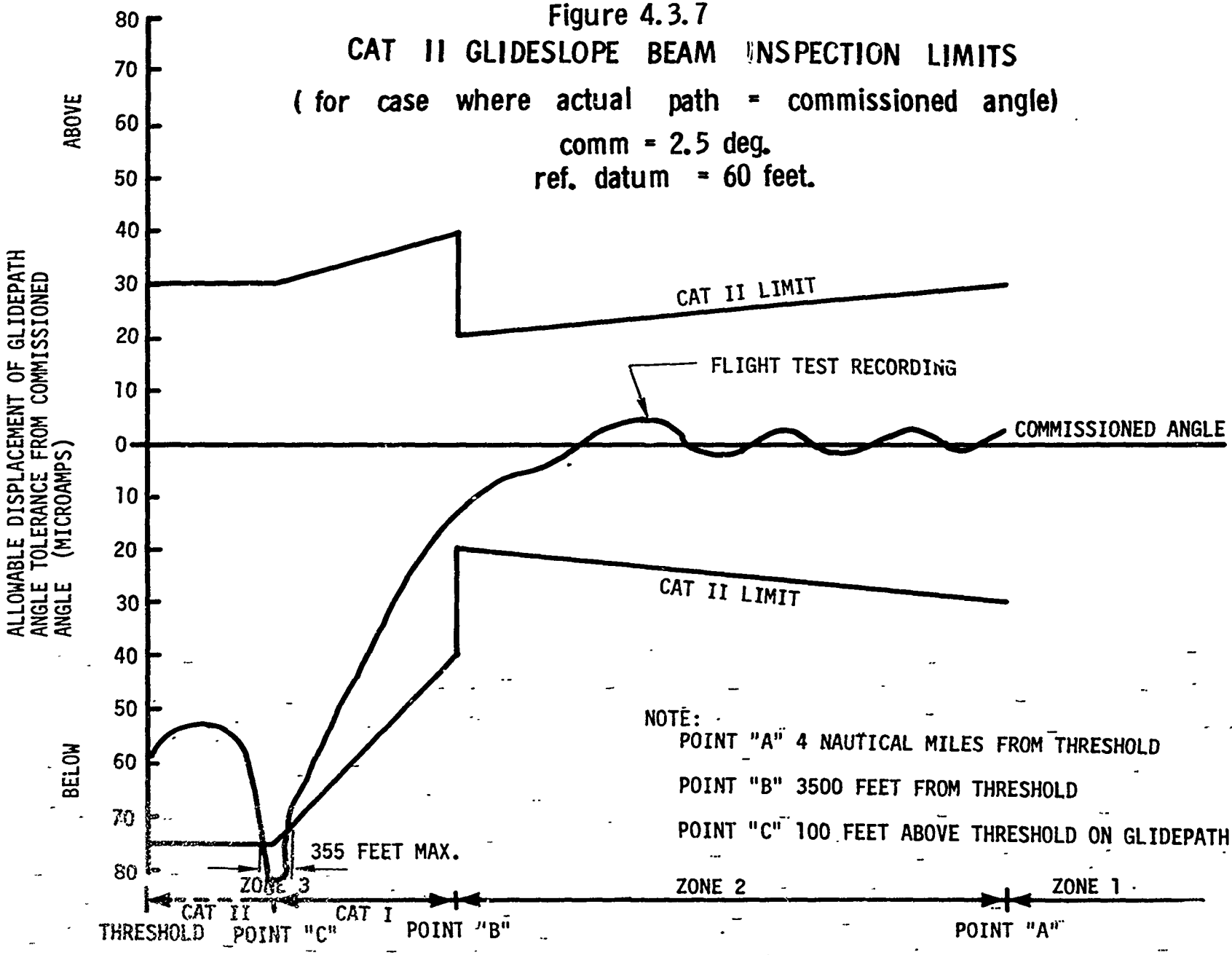

The area under the bend described by

$$\frac{\beta_{DIST}}{2}\left(1 - \cos\frac{2\pi}{T}t\right) \text{ is}$$

$$A = 1/2\,(T)\,\beta_{DIST} \tag{4.3.1}$$

where A = area under bend $\sim$ DEG-SEC

T = period of bend $\sim$ SEC

β_{DIST} = amplitude of bend $\sim$ DEG

but β_{DIST}, in equivalent feet of altitude error, is

$$\beta_{\Delta hT} = \left(\frac{\beta_{DIST}}{2.5 - \beta_{DIST}}\right) \cdot h \tag{4.3.2}$$

where $\beta_{\Delta h}$ = amplitude of bend $\sim$ feet

h = altitude of disturbance $\sim$ feet

Now h, in Eq (4.3.2), must necessarily be the average altitude, $\bar{h}$; i.e., the airplane altitude registered at the midpoint of the bend. Thus,

$$\bar{h} = \left(\frac{h_o + \dot{h}\,T}{2}\right) \tag{4.3.3}$$

where $\bar{h}$ = altitude at midpoint of bend $\sim$ ft

h_o = altitude at beginning of bend $\sim$ ft

$\dot{h}$ = nominal descent rate $\sim$ 9.2 ft/sec

Substituting Eq (4.3.2) and Eq (4.3.3) into Eq (4.3.1) results in:

$$A = 1/2\ T \left(\frac{\beta_{DIST}}{2.5 - \beta_{DIST}} \right) \left(\frac{h_o - 9.2T}{2} \right)$$

$$= \frac{T}{4} \left(\frac{\beta_{DIST}}{2.5 - \beta_{DIST}} \right) \left(h_o - 9.2T \right) \sim \text{Ft - Sec} \qquad (4.3.4)$$

The expression in Eq (4.3.4) was used to plot the independent axis in Figure 4.3.8. The C system peak maneuver (from Eq (3.4.21)) was plotted on the dependent axis along with the average peak maneuver for systems A and B. As a result, it can be seen that the improvement of the C system over the conventional systems depends upon the area of the curve. In the extremely small area (high frequency) regions, the C system improvement approaches a factor of four, while in the intermediate range, the improvement is slightly greater than two. For extremely large areas (long periods). the peak maneuvers for the three systems will converge and thus the improvement factor in the C system will vanish.

In summarizing the advantages and disadvantages of the C system against beam bends, the following conclusions are stated.

1) Under linear conditions, the C system is more than twice as effective as either the A or the B system with respect to rejection of beam bends whose periods are greater than 0.5 rad/sec and whose areas are less than 100 ft. sec.

2) For disturbances which cause beam limiter saturation, the C system improvement factor, owing to the capability to limit the G/S receiver beam error to 0.2 degrees must be increased by 1.25 over the A system.

3) The total improvement factor of the C system against the category of bends described in 1) above is 2.5 with respect to system A and 2.0 with respect to system B.

4) There is no evidence to support the supposition that the C system performance is unacceptable in the presence of the "dog leg" bend. To the extent that conventional systems are capable of satisfactory performance against the long term bend, so is the C system.

5) The C system provides the means to overcome extreme variations in the graphical average path which, while passable under flight inspection, may induce dangerous maneuvers in conventional autoland systems.

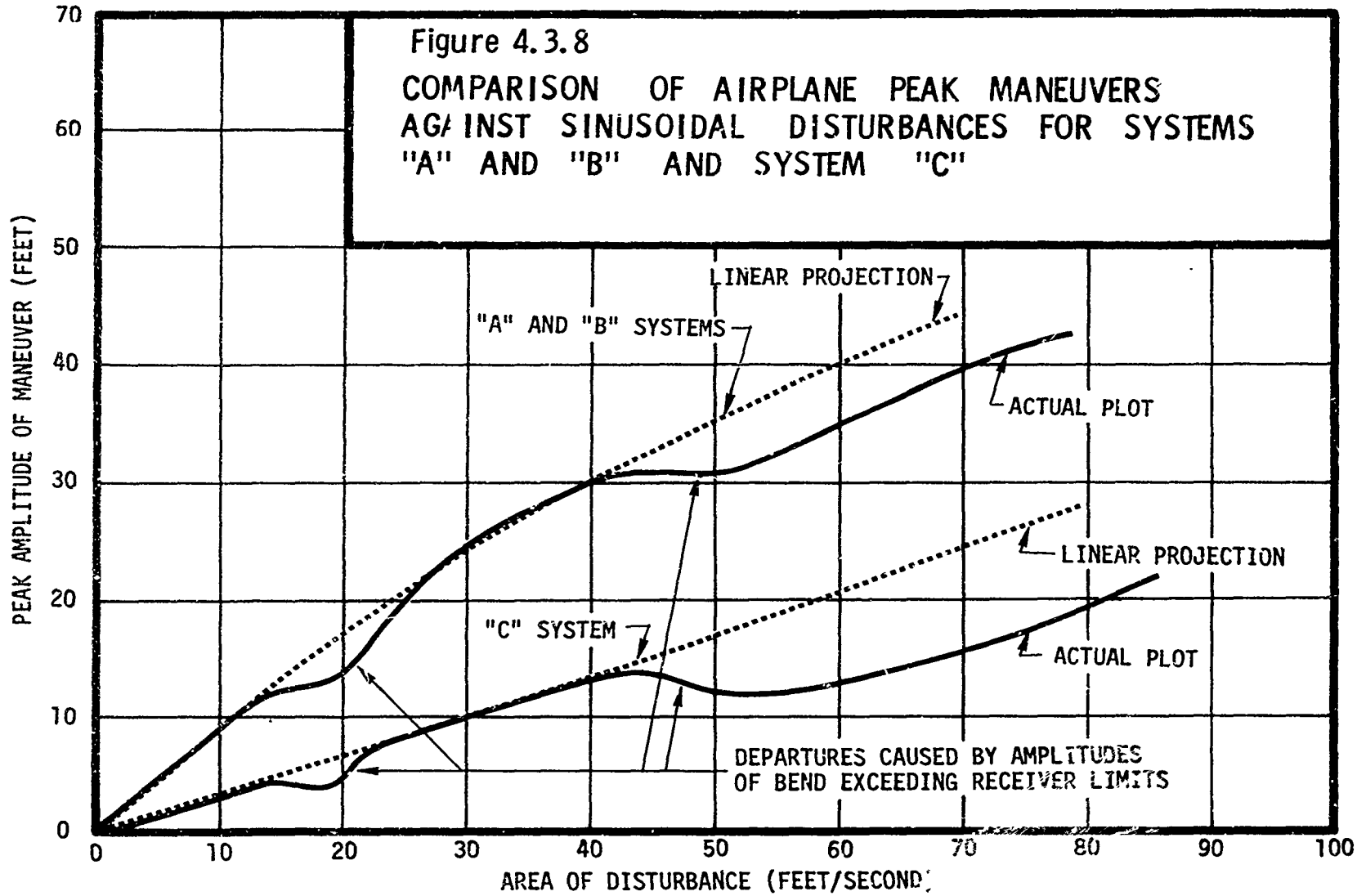
Figure 4.3.8
COMPARISON OF AIRPLANE PEAK MANEUVERS AGAINST SINUSOIDAL DISTURBANCES FOR SYSTEMS "A" AND "B" AND SYSTEM "C"
PEAK AMPLITUDE OF MANEUVER (FEET)
AREA OF DISTURBANCE (FEET/SECOND)
0
10
20
30
40
50
60
70
80
90
100
LINEAR PROJECTION
"A" AND "B" SYSTEMS
ACTUAL PLOT
LINEAR PROJECTION
"C" SYSTEM
ACTUAL PLOT
DEPARTURES CAUSED BY AMPLITUDES OF BEND EXCEEDING RECEIVER LIMITS

4.3.2 Roll Axis Beam Bend Comparisons

The response of the three systems to discrete (1-COSINE) localizer bends parallels the comparative frequency response plotted in Figure 4.2.3. For sufficiently long period bends the three systems have the same response. It is only for the shorter duration (higher frequency) bends that the three systems exhibit response differences.

Figure 4.3.9 shows the amplitude versus duration boundary of allowable (1-COSINE) localizer bends at 250 feet for the three systems. The boundary was determined by violation of the maneuver and footprint criteria reduced by the dispersion to all causes other than localizer bends. The systems were assumed to be tracking the centerline perfectly before the discrete bend was inserted at two hundred fifty feet. Figure 4.3.9 shows that inertial smoothing markedly increases the size of permissible localizer bends.

The complementary filter retains localizer beam anomalies. That is to say that the complementary filter is as slow to lose errors resulting from past localizer signals as it is to acquire errors from current localizer signals. This characteristic gives rise to a suspicion that inertial smoothing might degrade autoland performance on ILS beams which have low frequency distortions far from threshold (Zone 2) but have good characteristics in the vicinity of threshold (Zone 1). Stylized distortions of this type (shown in Figure 4.3.10) are a (1-COSINE) bend with a length over two miles, a dog leg bend, or an effective bias in Zone 2 with respect to Zone 1.

Inertial smoothing essentially does not degrade system performance in the presence of long term localizer bends in Zone 2. Because the low frequency response of the three systems is very similar, these dog leg type bends degrade all three systems in a similar manner.

Figure 4.3.11 shows the in-flight response of the three systems to the long term (1 - COSINE) bend shown in Figure 4.3.10. The amplitude of this bend exceeds the CAT II specifications but is acceptable for a CAT I localizer. The inertially smoothed System C has a response to this twenty microamps bend with a one hundred second period which is essentially the same as System B without inertial smoothing. Both System B and C display significantly more phase shift between disturbance and response than System A.

Figure 4.3.12 shows the response of the three systems to the in-flight simulation of a localizer which has a fifteen microamps bias in Zone 2 but has perfect centering in Zone 1 as shown in Figure 4.3.10. This simulated localizer exceeds CAT II specifications but is acceptable for CAT I. Again the response of Systems B and C are very much the same. This shows that inertial smoothing does not seriously degrade system performance even in the presence of such a severe dog leg type beam bend. System A did cross through center sooner than Systems B and C and returned to touchdown near the runway centerline. But the response of System A violated the reduced maneuver criterion for beam effects only.

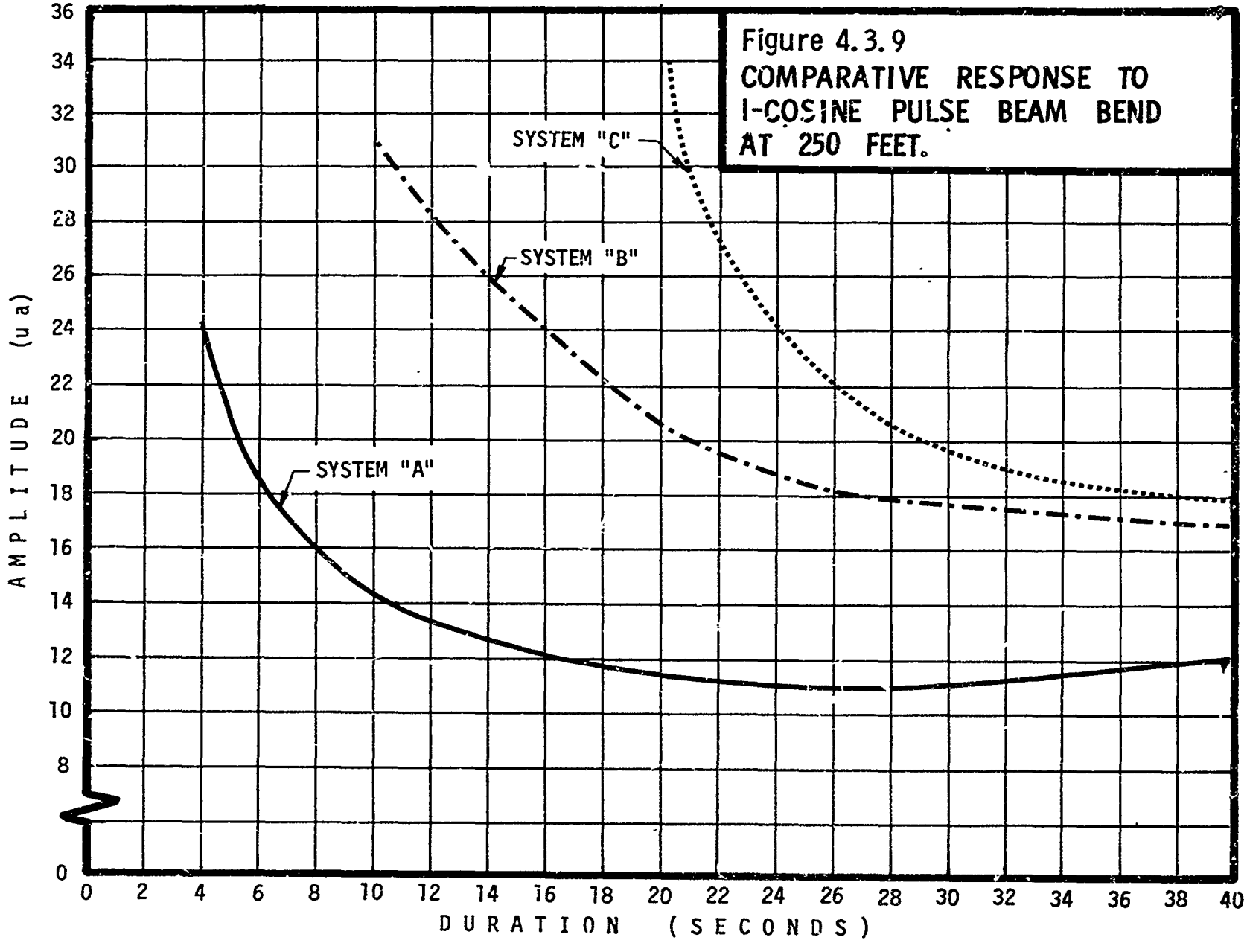
Figure 4.3.9
COMPARATIVE RESPONSE TO
I-COSINE PULSE BEAM BEND
AT 250 FEET.
SYSTEM "C"
SYSTEM "B"
SYSTEM "A"
AMPLITUDE (u a)
DURATION (SECONDS)
0
8
10
12
14
16
18
20
22
24
26
28
30
32
34
36
0
2
4
6
8
10
12
14
16
18
20
22
24
26
28
30
32
34
36
38
40

Figure 4.3.10
DOG LEG TYPE
LOCALIZER BENDS

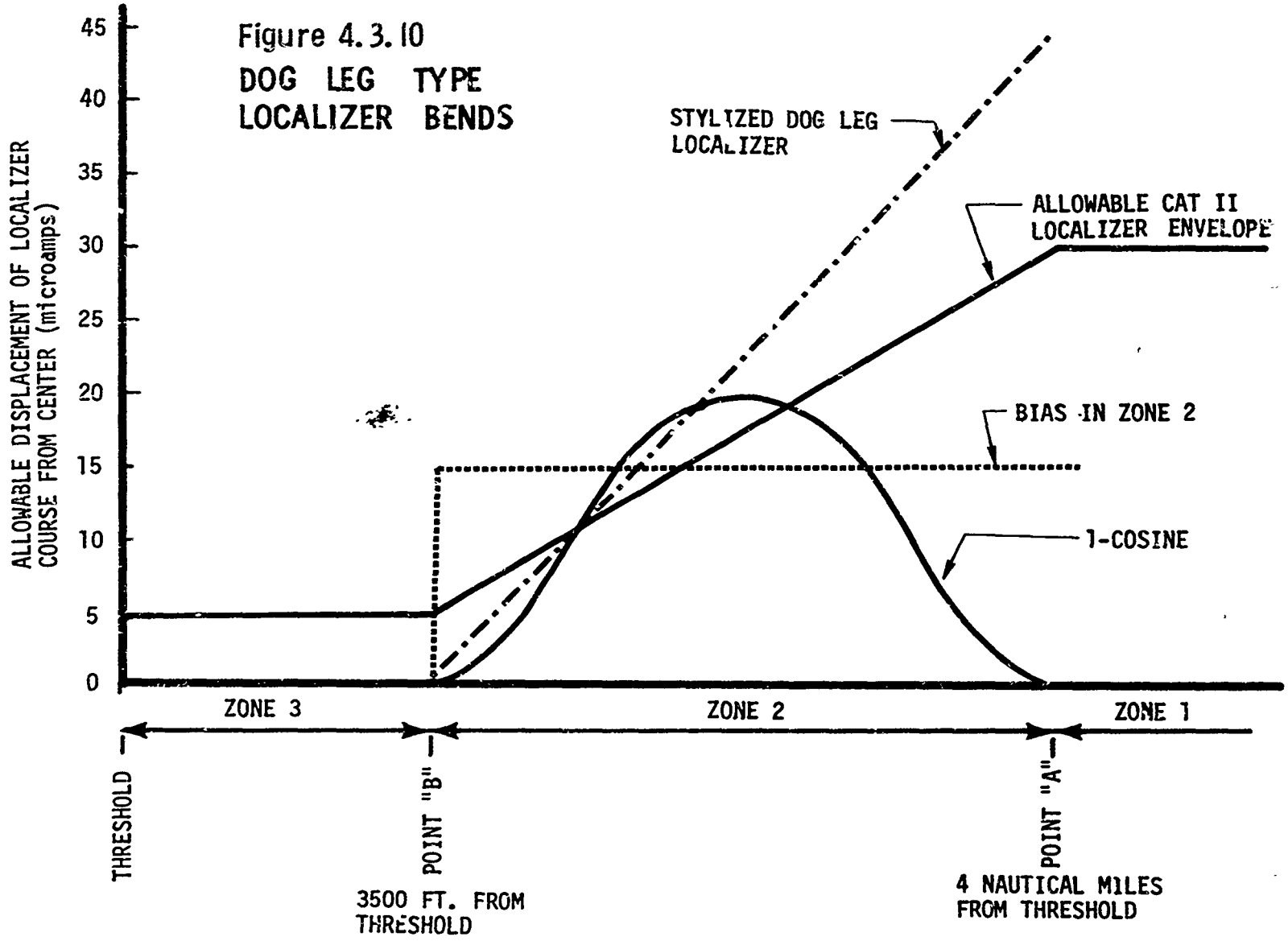

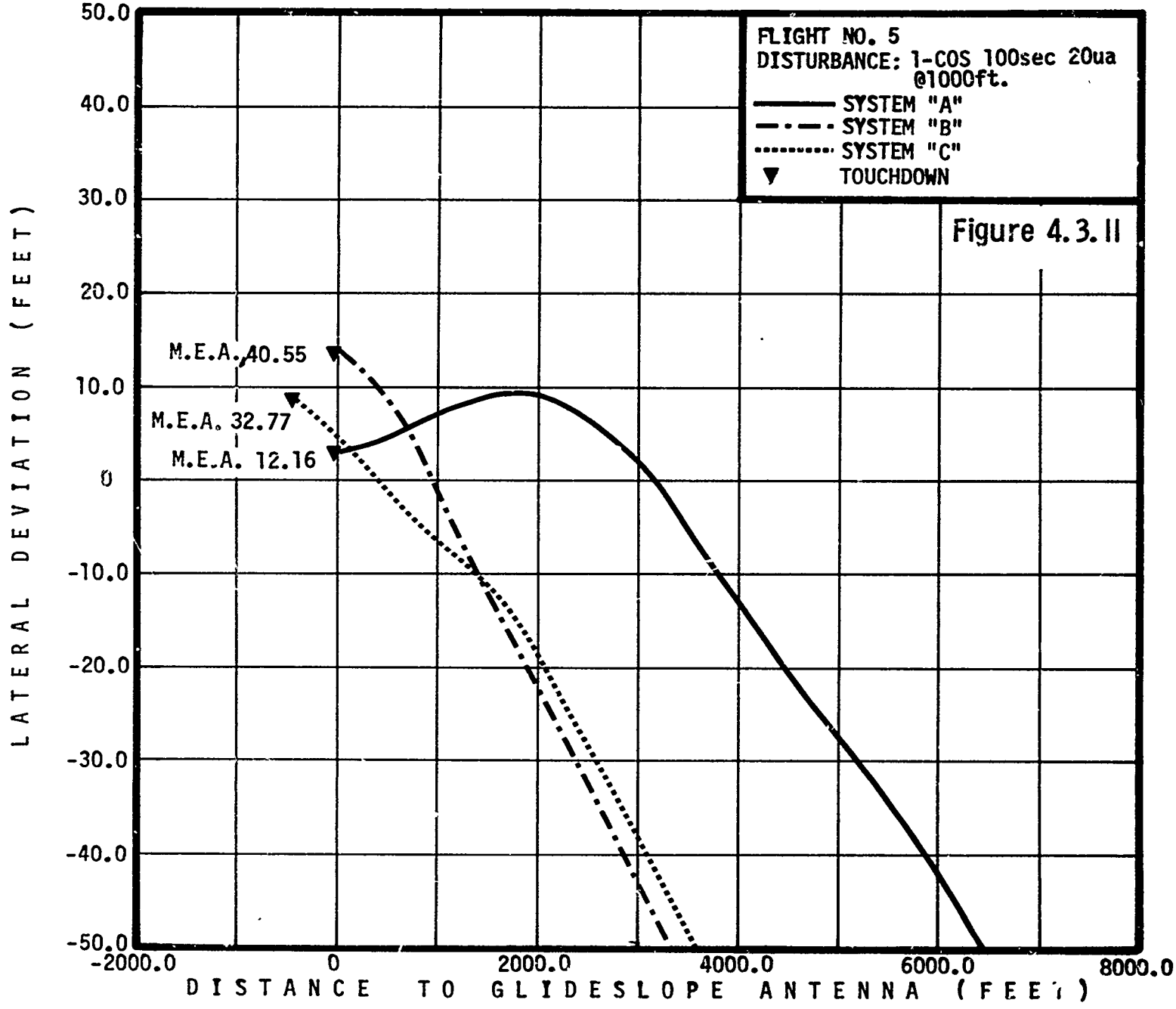
FLIGHT NO. 5
DISTURBANCE: 1-COS 100sec 20ua @1000ft.
SYSTEM "A"
SYSTEM "B"
SYSTEM "C"
TOUCHDOWN
M.E.A. 40.55
M.E.A. 32.77
M.E.A. 12.16
50.0
40.0
30.0
20.0
10.0
0
-10.0
-20.0
-30.0
-40.0
-50.0
-2000.0
0
2000.0
4000.0
6000.0
8000.0
LATERAL DEVIATION (FEET)
DISTANCE TO GLIDESLOPE ANTENNA (FEET)

Figure 4.3.11

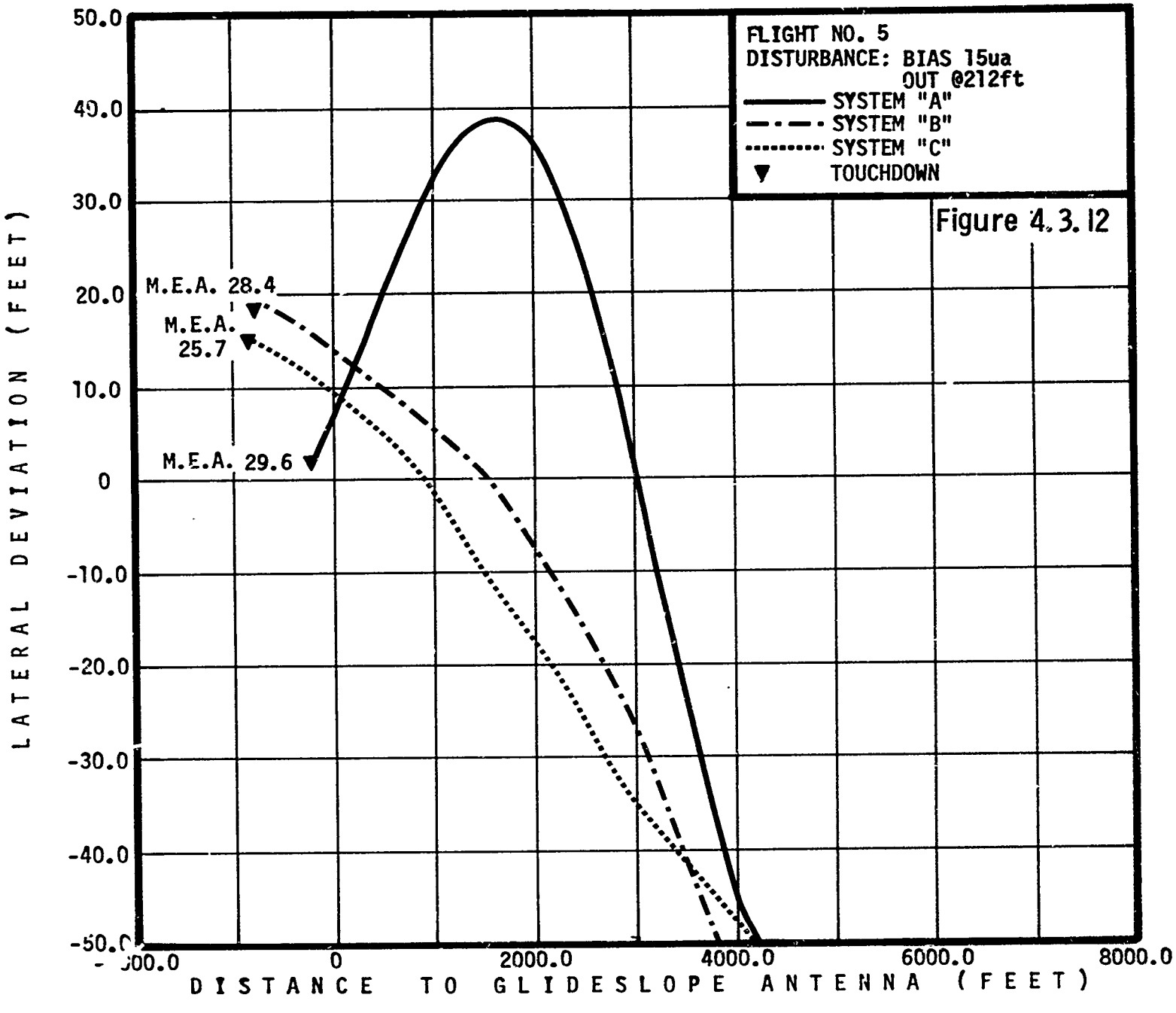
FLIGHT NO. 5
DISTURBANCE: BIAS 15ua
OUT @212ft
SYSTEM "A"
SYSTEM "B"
SYSTEM "C"
TOUCHDOWN
M.E.A. 28.4
M.E.A. 25.7
M.E.A. 29.6
50.0
40.0
30.0
20.0
10.0
0
-10.0
-20.0
-30.0
-40.0
-50.0
-2000.0
0
2000.0
4000.0
6000.0
8000.0
LATERAL DEVIATION (FEET)
DISTANCE TO GLIDESLOPE ANTENNA (FEET)

Figure 4.3.12

The dog leg shown in Figure 4.3.10 is the marginal case where the extended Zone 2 segment intersects the restricted zone at threshold. This bend is outside of both CAT II and CAT I specifications. This bend has no worse effect on the inertially smoothed System C than on the other systems.

4.4 Beam Failure Tolerances

The beam failure tolerance in this report is defined to be the length of time that the autoland system will withstand an ILS transmitter hardover without violating either the maneuver or footprint criteria. Following the hardover period the ILS beam information is returned to correct value.

In developing autoland control laws (especially for Category III performance), the vulnerability of the ground station to certain types of failure must be taken into account. Otherwise, the integrity of the redundant, airborne system may be compromised by an essentially single thread[1] ILS beam.

Since the key advantage of inertial smoothing lies in the capability to reduce path deviation in the presence of erroneous behavior of the ILS beam, including hardovers, the adverse affect of ground station hardover failure may be overcome by the application of the inertial smoothing technique. Whether this is possible depends upon limiting the duration of the hardover failure. In order for any airborne system to survive an ILS hardover-type failure, the time of the failure must be within the beam failure tolerance of that system. This section of the report will establish the beam failure tolerances for all three autoland systems.

4.4.1 Beam Failure Tolerance in the Pitch Axis

Using simulation equipment, varying durations of glide slope hardovers (both positive and negative directions) were introduced into each system at several altitudes between 50 and 700 feet. That duration of G/S hardover which caused each system to barely remain within the limits of the maneuver criterion boundary was plotted against the altitude at which the hardover was introduced. (It is to be noted that the A system was not equipped with a beam limiter during these simulated trials).

Responses to beam failures of less than 10 seconds duration become critical with respect to the footprint criterion below 300 ft. altitude. Consequently, while simulating beam failures below 300 ft., it was discovered that the beam failure tolerance decreased below that value determined by the maneuver criterion, as shown in Figure 4.4.1. For all three systems, the footprint criterion dominates the tolerance curves at the lower altitudes. From the figure, it can be concluded that the

[1] Although switching arrangements are provided within ILS transmitter stations where a "back-up" system may be placed on line for a detected malfunction, there is no simultaneous redundancy and, hence, the transmitters are single thread devices.

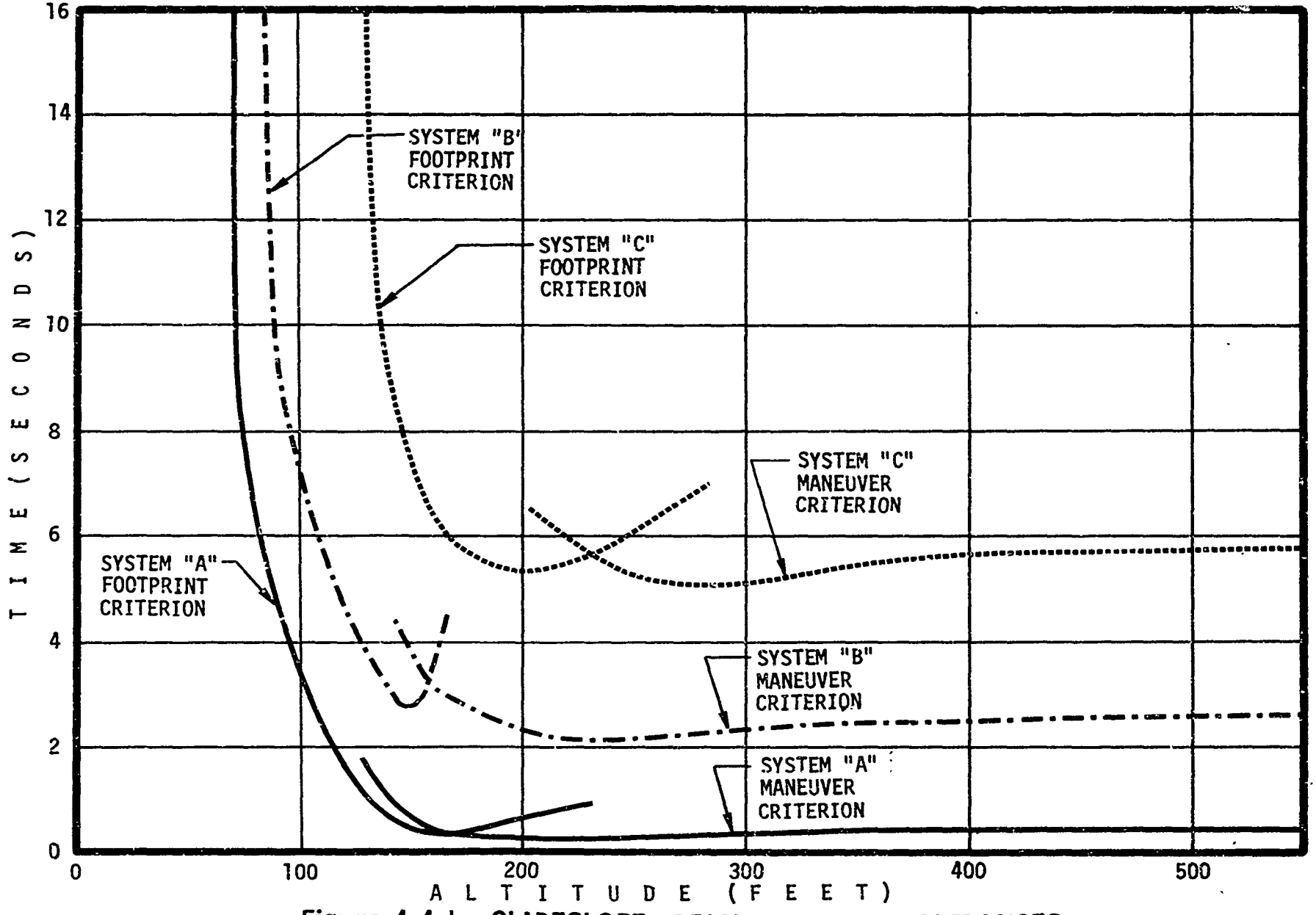

Figure 4.4.1 GLIDESLOPE BEAM FAILURE TOLERANCES

beam failure tolerances for all three systems are as follows:

- o System A - .25 sec.
- o System B - 2 sec.
- o System C - 5 sec.

This particular study also revealed the altitude below which each system becomes independent of the G/S beam; that is, the altitude at which the worse case beam disturbance (hardover) does not induce an exceedance of either the footprint or the maneuver criterion. Table 4.4.1 contains the values for these particular altitudes. From the Table, it can be concluded that unacceptable airplane response will occur for glide slope beam hardovers introduced before the airplane has descended below an altitude of

1) 70 ft. for System A
2) 87 ft. for System B
3) 130 ft. for System C

TABLE 4.4.1

Altitudes below which beam anomalies cannot induce violations in the system.

BEAM DISTURBANCE	AUTOPILOT SYSTEM		
	A	B	C
FLY UP			
Maneuver Criterion	76	118	166
Footprint Criterion	70	87	130
FLY DOWN			
Maneuver Criterion	78	124	166
Footprint Criterion	78	132	178

4.4.2 Beam Failure Tolerance in the Roll Axis

Localizer hardovers (150 ua) of varying duration were introduced to the simulated aircraft and automatic landing system at altitudes between 50 and 550 feet. The maximum hardover duration that each system could tolerate without violating the maneuver or footprint criteria was determined. The allowable localizer hardover duration as a function of altitude is plotted for all three systems and both criteria in Figure 4.4.2. The curves in Figure 4.4.2 are terminated at low altitude under the circumstance that the violation occurs at touchdown. Rollout guidance was not a topic of consideration in this report.

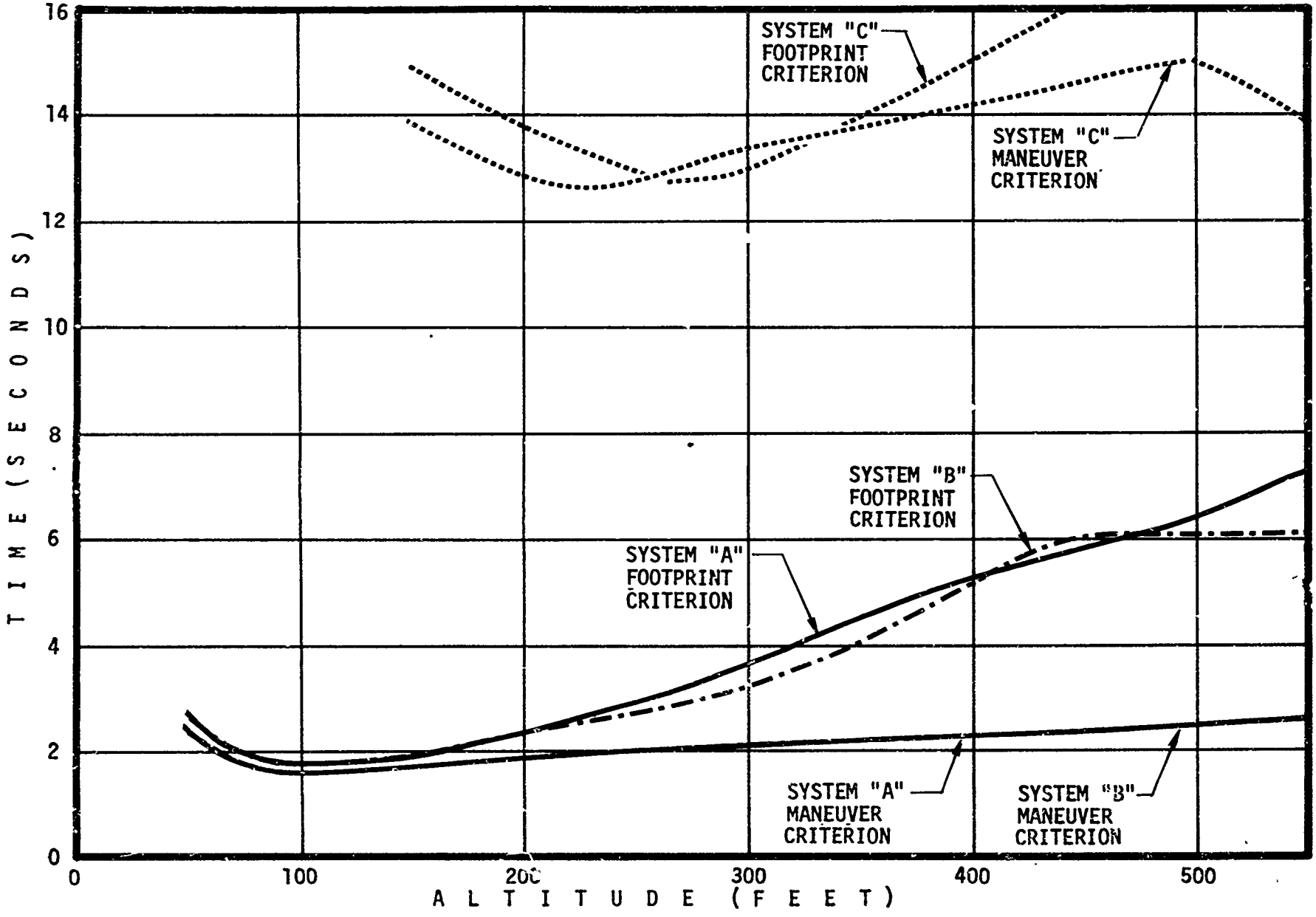

Figure 4.4.2 LOCALIZER BEAM FAILURE TOLERANCES

The allowable hardovers determined by the maneuver criterion for Systems A and B are identical. The hardover input is so severe that the response of Systems A and B is determined solely by the roll rate and bank angle command limiters and is independent of other aspects of control law configuration. For both System A and B, the allowable hardover duration determined by the footprint criterion is always longer than that allowed by the maneuver criterion because the maneuver criterion anticipates that the footprint criteria will be violated. For both Systems A and B, the maximum allowable localizer failure duration is 1.7 seconds determined at the most critical altitude of 100 feet.

For System C, the allowable hardover duration determined from the footprint criterion is less than that determined from the maneuver criterion only near 300 feet altitude. In this situation, the aircraft departs from the footprint with an acceptable maneuver above 100 feet but does not re-enter the footprint until the aircraft is below the 100 feet. System C can withstand localizer failure durations up to 12.7 seconds at the 250 ft. worst case altitude.

4.5 Effects of Overflight Interference

Overflight interference is a serious problem only on the localizer although the same effect on a much smaller scale has been observed on the glideslope. Inertial smoothing has the advantage of significantly reducing nuisance wheel and bank angle activity and lateral path deviations resulting from overflight interference. There are no disadvantages to the use of inertial smoothing in the presence of overflight interference.

The overflight signature is produced by a moving reflector causing multipath interference. The localizer signal reflected from a moving aircraft adds to the direct signal at the approaching aircraft to cause erroneous deviations. The overflight signature is a function of the phase shift, signal strength ratio and relative differential depth of modulation between the direct and reflected signals. The overflight interference signatures are grouped into two broad categories: "high altitude overflight" and "low altitude overflight".

The high altitude overflight signature is produced when the reflected signal is relatively weak compared to the direct signal. The reflected signal interferes with the direct signal to cause an oscillatory disturbance on the localizer deviation that would have otherwise been received. The frequency of the oscillatory error increases as the disturbance progresses and the amplitude envelope is nearly symmetric. A high altitude overflight disturbance was observed on about one third of the approaches made during the flight test program. This disturbance occurs frequently in service, especially at airports with heavy traffic.

Figure 4.5.1 shows the typical signature of the high altitude overflight disturbance. The upper trace is an actual disturbance recorded during flight test. The lower trace is the simulated disturbance which

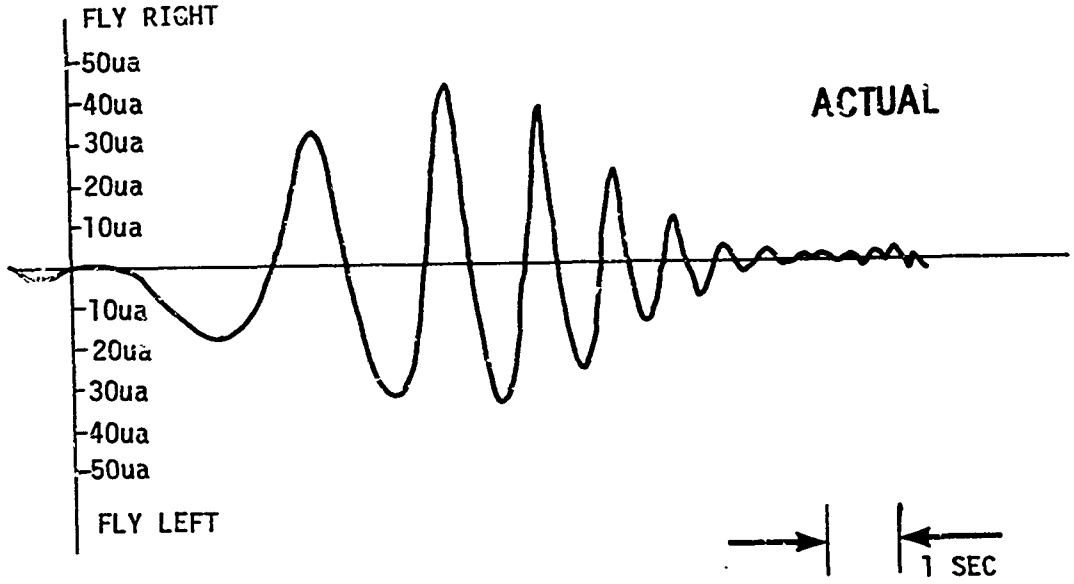

LOCALIZER OVERFLIGHT DISTURBANCE
FLIGHT NO.6
RECORDED AT 15:04:34 ALT. ≈ 1400 FT.
OBSERVED AIRCRAFT TAKING OFF AHEAD
NOV. 19,1971

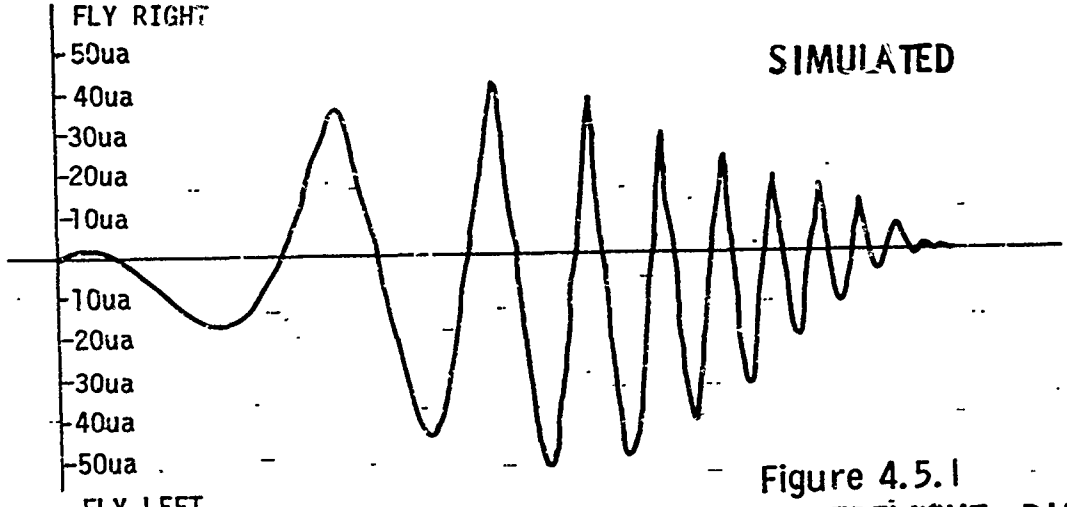

SIMULATED LOCALIZER OVERFLIGHT DISTURBANCE
SCHEDULED TEST INPUT FOR FINAL DISTURBANCE DATA .

Figure 4.5.1
HIGH ALTITUDE OVERFLIGHT DISTURBANCE

was used to obtain comparative flight test data. It is evident that the simulated overflight disturbance is a good model for the observed phenomenon.

The response of each of the three systems to the high altitude overflight localizer disturbance is shown in Figure 4.5.2. The disturbance causes System A to oscillate the ailerons violently, even to full authority or hardover. Inertial smoothing significantly decreased the wheel activity of System C. Since the overflight has more area in the fly left direction than the right, the aircraft deviated to the left. System C exhibits only one-fourth the lateral deviation of System A. Figure 4.5.3 shows the residual overflight induced lateral deviations in the touchdown zone. System A did not recover prior to touchdown from the overflight disturbance at 750 feet. Systems B and C did recover before touchdown, however, System C exhibits a five foot standoff. This standoff is most likely the result of an INS tilt error as explained in Section 4.6. The maneuver equation average for System A is three times that of System C.

The low altitude overflight interference signature is shown in Figure 4.5.4. This signature is produced when the reflected signal is relatively strong compared to the direct signal. The disturbance oscillation is about the apparent deviation of the reflected signal rather than the direct signal. This results in a more one sided character of the low altitude overflight; that is, the increasing frequency oscillating error typically does not pass through zero for a long portion of the disturbance.

The response of the three systems to the low altitude overflight disturbance which was simulated during flight test is shown in Figure 4.5.5. The lateral deviation induced by the disturbance was thirty five feet for System A. The maneuver equation peaked at fifty two feet, violating the "bends only" maneuver criterion, and the M.E.A. was 13.6 feet. The peak value of the maneuver equation was fifty four feet for System B at touchdown, also violating the "bends only" maneuver criterion. System C with inertial smoothing shows very small but distinct path deviations resulting from the low altitude overflight disturbance. The peak value of the maneuver equation for System C was thirty three feet, and the M.E.A. was 9.4 feet. An obvious feature of the lateral deviation trace of System C in Figure 4.5.5 is the tendency to track at an angle to the runway centerline. Systems A and B show a similar tendency. The angular tracking is only two tenths of a degree which is probably the combined result of several causes and accounts for about one half of the System C.

Inertial smoothing dramatically reduces the activity and path deviation of System C in the presence of both high and low altitude localizer overflight disturbance. For all disturbances of this type, System C shows superior performance over that of either System A or System B.

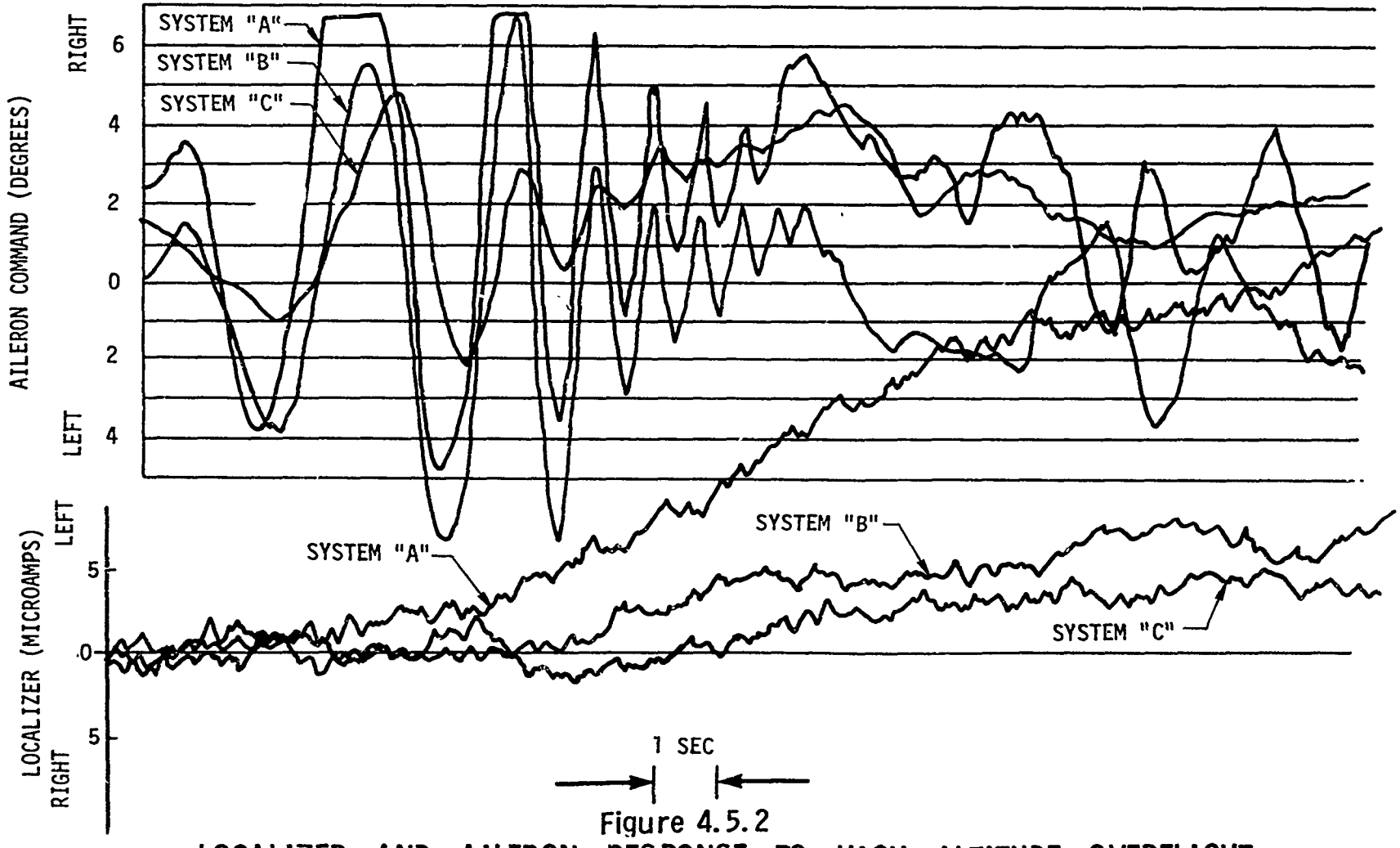

Figure 4.5.2

LOCALIZER AND AILERON RESPONSE TO HIGH ALTITUDE OVERFLIGHT

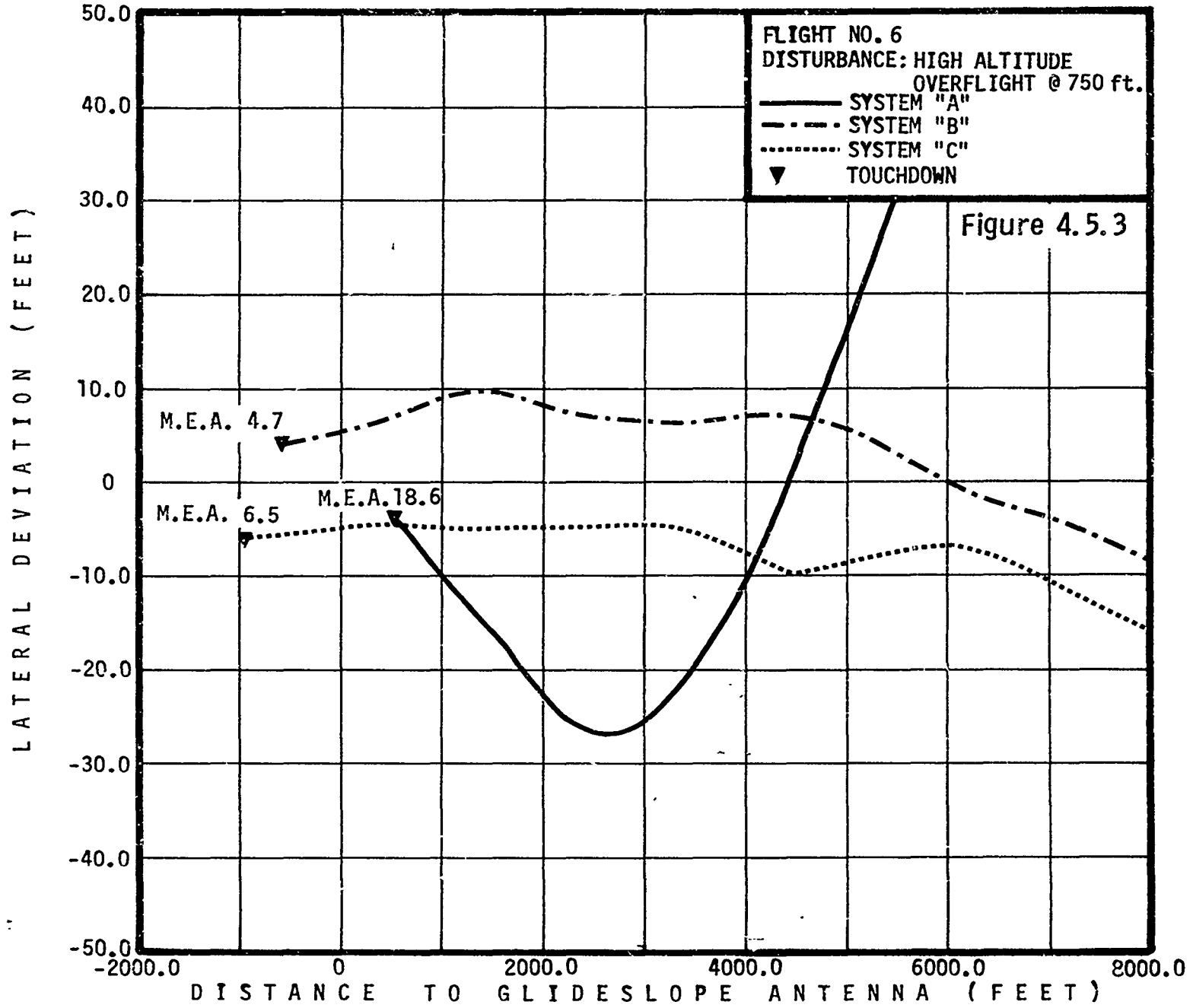
FLIGHT NO. 6
DISTURBANCE: HIGH ALTITUDE OVERFLIGHT @ 750 ft.
SYSTEM "A"
SYSTEM "B"
SYSTEM "C"
TOUCHDOWN
M.E.A. 4.7
M.E.A. 6.5
M.E.A. 18.6
50.0
40.0
30.0
20.0
10.0
0
-10.0
-20.0
-30.0
-40.0
-50.0
-2000.0
0
2000.0
4000.0
6000.0
8000.0
LATERAL DEVIATION (FEET)
DISTANCE TO GLIDESLOPE ANTENNA (FEET)

Figure 4.5.3

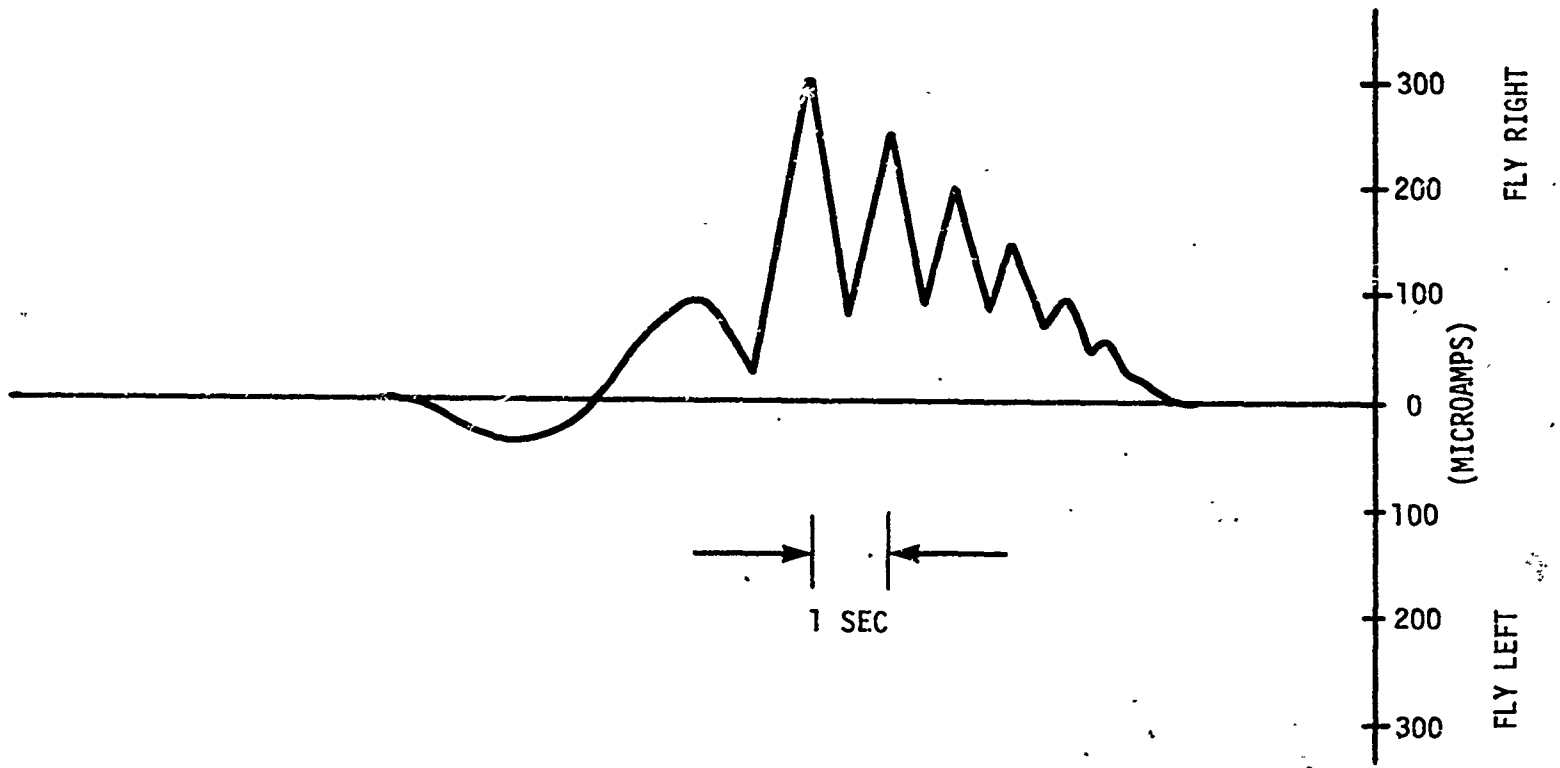

Figure 4.5.4
LOW ALTITUDE OVERFLIGHT DISTURBANCE

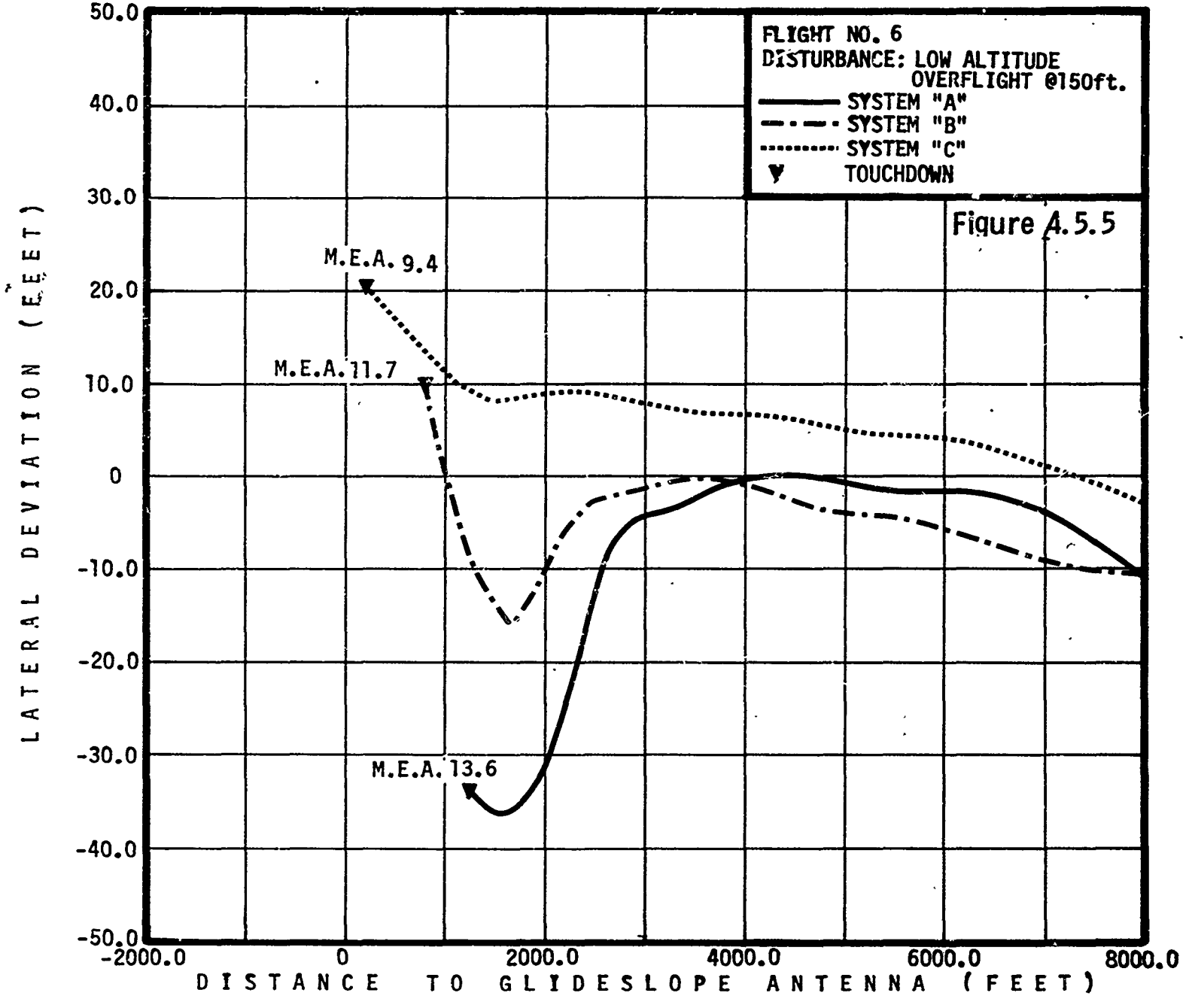
FLIGHT NO. 6
DISTURBANCE: LOW ALTITUDE OVERFLIGHT @150ft.
SYSTEM "A"
SYSTEM "B"
SYSTEM "C"
TOUCHDOWN
M.E.A. 9.4
M.E.A. 11.7
M.E.A. 13.6
50.0
40.0
30.0
20.0
10.0
0
-10.0
-20.0
-30.0
-40.0
-50.0
-2000.0
0
2000.0
4000.0
6000.0
8000.0
LATERAL DEVIATION (FEET)
DISTANCE TO GLIDESLOPE ANTENNA (FEET)

Figure A.5.5

4.6 Sensor Imposed Limitations

The quality of the sensor information provided to an autoland system may have a critical effect on the performance of that system. As pointed out in the roll axis analysis of Appendix B, the innovation of the INS provided a second generation of airborne sensors, and as a consequence, a number of limitations imposed by the first generation of sensors were lifted. However, the INS platform is not without errors, and therefore, certain limitations still exist, though on a much smaller scale. The effects of certain INS errors on the performance of the system C autopilot are discussed in this section.

Of the three autopilots used in this program, System A is least sensitive to the quality of inertial information. A platform such as conventional vertical gyro may be marginally suitable for use with an inertially damped control law as basic stability becomes a problem. As for the inertially smoothed System C, virtually no maneuver dependent error is tolerable. Thus, only an inertial navigation system is suitable as the source of inertial data for a first order complementary filter type smoothed system.

All autoland autopilots have some degree of dependency on attitude, acceleration and velocity information. To be useable, all this information must be in the same coordinate system. The coordinate system is oriented with respect to local true vertical and runway azimuth. Thus, the fundamental problem in providing attitude, acceleration or velocity, is a knowledge of airplane orientation with respect to this coordinate system. A platform is the device which operates on some inertial principle and provides this orientation information. The platform may be a set of conventional vertical and directional gyros or, at the other extreme (with regard to accuracy), an inertial navigation system.

The potential performance of all autoland autopilots is constrained, among other things, by quality of the inertial reference information they are provided. The quality of the inertial information may be characterized by the extent of maneuver dependent errors, maneuver independent errors and signal format limitations.

The influence of maneuver independent errors and signal format limitations on the performance of the roll axis System C are discussed in subsection 4.6.2. It is shown that a significant offset at touchdown results from the INS mis-estimate of vertical (tilt error). Further, that this offset increases with the amount of complementary filtering.

The pitch axis System C is less dependent upon highly accurate inertial data than the roll axis. However, care must be taken in the control law mechanization to minimize the effect of certain sources of error. For System C, there is no significant path offset attributable to inertial information errors.

4.6.1 Sensor Limitations in the Pitch Axis

The derivation of the change in altitude rate presents the only serious concern for sensor quality in the pitch axis. The limitations of the sensors which produce the necessary variables for this derivation are best understood by simple mathematical analyses.

The change in altitude rate or vertical speed is expressed

$$\Delta\dot{h} = \dot{h}_c - \dot{h}_D, \tag{4.6.1}$$

where

$\Delta\dot{h}$ is the change in vertical speed,

$\dot{h}_c$ is the vertical speed command,

$\dot{h}_D$ is the derived vertical rate.

But

$$\dot{h}_c = V_g \tan \beta , \tag{4.6.2}$$

where V_g is ground speed from the INS

β is the actual glide slope angle;

and

$$\dot{h}_D = \frac{\dot{h}_{ADC}}{\tau S+1} + \frac{\ddot{h}\,\tau}{\tau S+1} , \tag{4.6.3}$$

where

$\dot{h}_{ADC}$ is vertical speed from the air data computer,

$\ddot{h}$ is vertical acceleration from the INS,

τ is the time constant of the derived altitude rate network = 20 sec.

Both $\dot{h}_{ADC}$ and $\ddot{h}$ in Eq (4.6.3) are highly sensitive to the sensor quality which produces them.

To illustrate, Eq (4.6.2) will be rewritten to express $\dot{h}_{c_f}$, the vertical speed command as fed into the autopilot. Thus

$$\dot{h}_{c_f} = (V_{g_o} + \Delta V_g + E_{v_g}) \sin(\beta + \Delta\beta), \qquad (4.6.4)$$

where V_{g_o} is the initial ground speed at glide slope capture,

ΔV_g is the change in ground speed during the approach,

E_{v_g} is the ground speed error,

$\Delta\beta$ is the difference between the nominal glide angle and the actual angle.

Upon simplifying, Eq (4.6.4) becomes

$$\dot{h}_{c_f} = \left\{ (V_{g_o} + \Delta V_g)\frac{\beta}{57.3} \right\} + \left\{ V_{g_o}\frac{\Delta\beta}{57.3} + E_{v_g}\frac{\beta+\Delta\beta}{57.3} + \Delta V_g\frac{\Delta\beta}{57.3} \right\}$$

$$= \left\{ \dot{h}_c \right\} + \left\{ \dot{h}_{c_E} \right\}, \qquad (4.6.5)$$

where the terms are grouped to indicate the true vertical speed command, $\dot{h}_c$, and the associated error, $\dot{h}_{c_E}$.

Examining the three terms which comprise the error in the vertical speed command, the first two terms are constant values and are, therefore, washed out through the path integrator during the initial transient. Consequently, the only limitation with respect to the constant errors is the time duration that may be available to wash out a given amplitude of $\Delta\beta$ and E_{v_g}.

The third term in the error expression of Eq (4.6.5) is dynamic and depends on the change in ground speed. Exact limitations due to this error are unknown; however, the entire error can be totally eliminated simply by including the actual glide slope angle as an input to the autopilot.

Examining Eq (4.6.3), the derived vertical rate feedback expression, a time lag of 20 sec is incorporated to provide good attenuation of the noise from the air data system. Hence, no limitations can now be attributed to this particular source. However, this large time constant gives rise to the need for compensation which is provided by the second term in Eq (4.6.3). Since $\ddot{h}$ in this term is provided by the vertical accelerometer in the INS, D.C. offsets must be considered. Consequently, the vertical accelerometer output is washed out with a

100-sec time constant and, hence, Eq (4.6.3) is more accurately expressed

$$\dot{h}_D = \frac{1}{\tau S+1} \left(\dot{h}_{ADC} + \frac{100 \tau S \ddot{h}}{100S+1} \right) \tag{4.6.6}$$

Although this washout circuit satisfactorily removes the DC errors, it unfortunately introduces a long term stand-off of the beam after glide slope capture. Hence, in order to prevent this standoff, another compensation circuit (lead/lag) was required on the altitude rate from the air data computer. The total expression then for the derived altitude rate feedback is

$$\dot{h}_D = \frac{1}{20S+1} \left(\frac{120S+1}{100S+1} \dot{h}_{ADC} + \frac{2000 S \ddot{h}}{100S+1} \right) , \tag{4.6.7}$$

which, for the low pass band where

$$h = \int_0^t \dot{h}_{ADC} \, dt \tag{4.6.8}$$

can be reduced to

$$\dot{h}_D = \frac{(120S\dot{h} + \dot{h} + 2000S^2\dot{h})}{(20S+1)(100S+1)}$$

$$= \dot{h} \left(\frac{2000S^2 + 120S+1}{(100S+1)(20S+1)} \right) = \dot{h} \tag{4.6.9}$$

Eq (4.6.9) simply implies that the derived altitude rate network produces a signal which is an excellent approximation of true vertical speed.

With the possible exception of the small dynamic errors associated with the vertical accelerometer, no limitations are imposed on the system as a result of deriving the altitude rate feedback in the manner described.

Another aspect of the sensor considerations is the requirement for proper pre-glide slope capture synchronization of the glide path computational blocks. Owing to the 100-second lag on both the vertical acceleration and the vertical velocity signals (see Figure 2.3.4), the computation cannot be placed in operation at an arbitrary time, such as glide slope capture. In fact, to insure that accelerometer errors do not aggravate the glide slope capture transient, the 100 second lags should be in the "compute" mode more than 6 minutes prior to glide slope capture. When digital autopilots are utilized to implement the control laws, the altitude rate circuit might be energized and remain in a "compute" mode throughout the flight. Although this requirement applies to both the B and C systems, the complementary filter in the C system greatly magnifies the need for "pre-synchronization" of the derived vertical rate network.

4.6.2 Sensor Limitations in the Roll Axis

System C implemented inertial smoothing with signals from an ARINC 561-2 Inertial Navigation System. This INS has no maneuver dependent errors which have a significant effect on inertial smoothing or control system gains. The effect of the other errors are not negligible. The maneuver independent errors may be modeled as a bias and ramp error in track angle. The track angle signal format properties are granularity, data rate, and computational time delay.

Bias errors in the track angle deviation signal would produce a standoff from localizer center except that the path integrator develops an output to cancel the bias error and return the aircraft to the centerline. The dynamics of the bias error cancellation are dependent on the low frequency path mode. System C also propagates the bias error through the complementary filter gain and time constant to achieve inertial smoothing. The approximate transfer function between track angle error and gain programmed beam error is

$$\frac{\eta_P}{\psi_{G_E}} = \frac{K_{\psi G_C} S}{K\eta_C \left(\frac{K\eta_C}{K_{I_C}} S + 1 \right)} + \frac{K_{\psi G_{COMP}} S}{K\eta_C \left(\frac{K\eta_C}{K_{I_C}} S + 1 \right)\left(\tau\eta_{COMP} S + 1 \right)} \quad (4.6.1)$$

The transfer function indicates that the steady state of no offset due to bias error would be nearly achieved in three to four minutes of tracking the localizer, since the two time constants are both twenty seconds for System C.

Equation 4.6.1 shows that a localizer standoff will be induced by ramp errors in track angle deviation. The ramp errors result from platform tilt and accelerometer biases. Inertial smoothing increases the displacement due to tilt as a function of the complementary filter time constant as shown in Figure 4.6.1. Inertial damping alone gives a displacement sensitivity to tilt of five feet per milliradian. Inertial smoothing increases the sensitivity by 0.5 feet per milliradian for each second of the complementary filter time constant. A one milliradian tilt error is essentially worst case and causes a fifteen foot standoff for System C. The postflight processing of inertial and camera systems data modeled the inertial errors and estimated the magnitude of tilt errors encountered during flight test. The standard deviation of the actual tilt errors was on the order of 0.2 milliradian (three feet) and the largest tilt was 0.5 milliradians (7.5 feet).

Increasing the complementary filter time constant reduces the path deviations due to ILS bends while paying a penalty in deviations induced by inertial errors. This trade between ILS and INS induced errors determines the optimum amount of inertial smoothing. However, the trade study cannot accurately be made because of the lack of an adequate knowledge of the ILS short term anomalies.

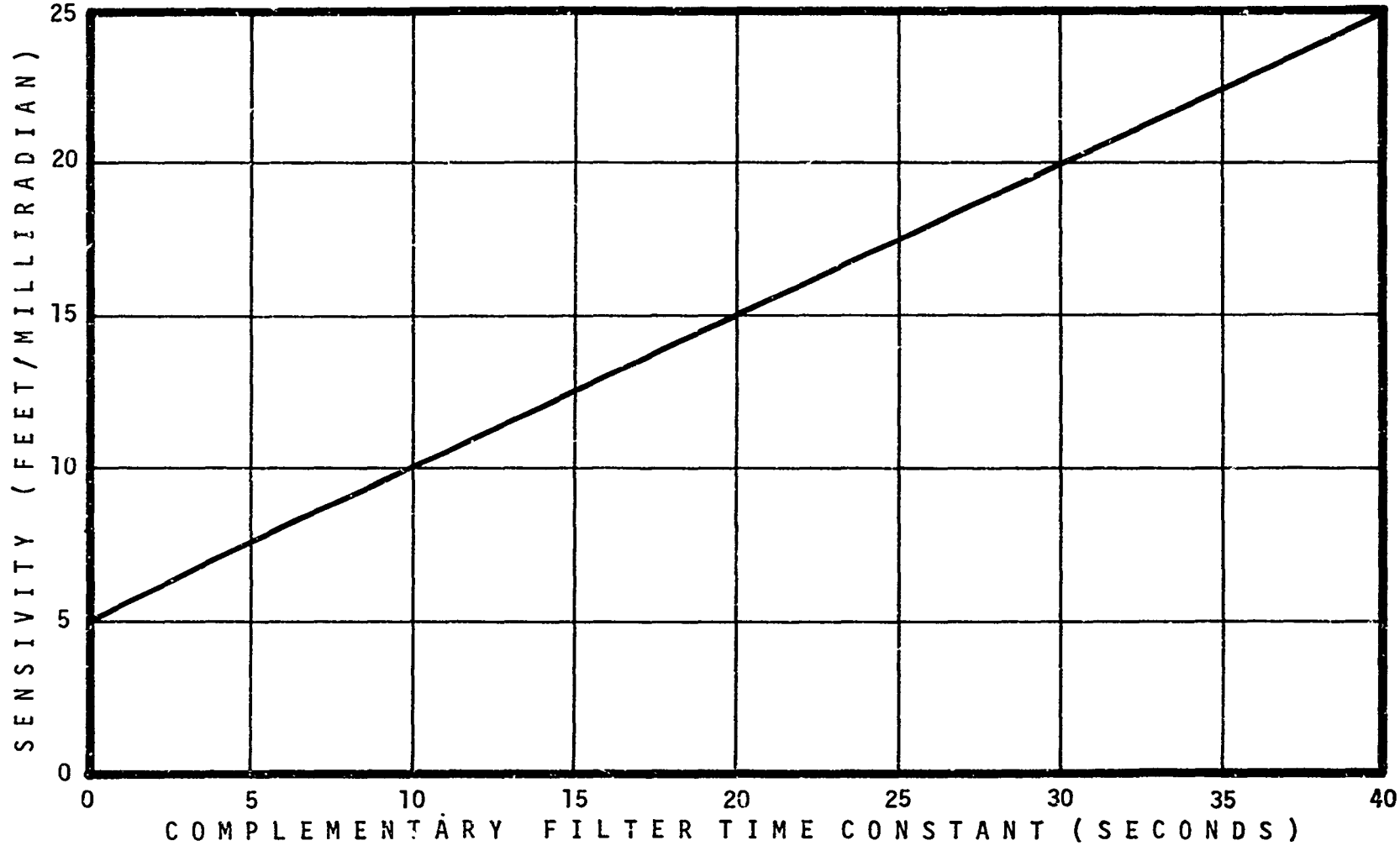

Figure 4.6.1 SENSITIVITY TO TILT ERRORS AS A FUNCTION OF COMPLEMENTARY FILTER TIME CONSTANT

The INS used for flight test was the Delco Carousel IV. This system rotates the horizontal accelerometers about the vertical axis at one revolution per minute. Thus, bias errors in the accelerometers cause a sinusoidal track angle error of one cycle per minute. At aircraft approach velocity, one cycle per minute covers a distance of two nautical miles along the localizer. Equation 4.6.1 shows that at this frequency System C has a sensitivity to accelerometer biases of seven feet per milli g. The average accelerometer bias vector determined from flight data was 0.1 milli g (less than one foot) and the largest estimated bias was 0.3 milli g (two feet).

A test was run on the analog simulator to determine the lag that could be imposed on an otherwise perfect track angle signal before any degradation in the B or C autopilot performance was noticeable. It was found that a time constant of .4 seconds or less had virtually no effect on system stability. The track angle signal from the hardware used in flight test had a granularity of 0.044 degrees, a data rate of five per second, and a staleness of 37 milliseconds at the time of output. These characteristics were considered the equivalent of a .4 second lag. The standard INS digital output program does not provide data at five per second and had to be reprogrammed as described in Appendix D in order to meet the requirements of Systems B and C.

4.7 Operational Requirements

There are essentially no operational requirements peculiar to the inertially smoothed autoland system. Conversely, the inertially smoothed system does not alleviate or reduce any operational requirements now in existence. Localizer intercept angles are functions of the course width and airplane velocity as in all autoland systems. Glide slope captures may be attained through the same range of speed and flight path variations as conventional systems.

One factor which must be considered, however, is the probability distribution of the error in the outer loop damping signal; i.e., ground heading in the roll axis and vertical speed in the pitch axis. Because the time required to washout these errors is a function of system gains, a maximum time can be established. Further, the largest error can be determined from probability considerations and, hence, for a given speed, the minimum capture distance can be established. This determination applies more specifically to the lateral axis, but by the same reasoning, a minimum capture distance can be determined in the longitudinal axis.

5.0 FLIGHT TEST PROGRAM

The schedule, equipment, techniques, and results of the flight test program are discussed in this section.

The test vehicle was the Boeing 727-E2 airplane (Figure 5.0.1). The airplane was based at Boeing Field, Seattle. A short cruise flight of approximately twenty five minutes was made to Grant County Airport, in Central Washington, where the autoland experiments were conducted. Typically, twelve approaches were made at Grant County Airport before returning to Boeing Field, which resulted in an average flight duration of three and one-half hours. Six such test flights were made between October 20 and November 19, 1971. In a total flight time of twenty two hours, 65 automatic landings were made, including five on return to Boeing Field.

The Boeing 727-E2 airplane is normally used for crew training purposes and, thus, its avionics configuration is standard. For the flight experiments, a digital autopilot and associated equipment were configured in such a manner as to permit functional substitution for the airplane's existing autopilot. In addition, the digital autopilot was programmed to permit selection of A, B or C autopilot control law in either axis. Automatic landings were made on successive approaches under the control of any of the three control laws, as selected by the digital autopilot operator.

The flight tests were divided into five categories. These categories are listed in Table 5.1. Also shown are the number of flight hours and approaches, and the dates on which the various experiments were conducted. Functional tests required almost five hours of flight time. The specific items checked for proper operation and correspondence with the simulation are listed in the Table. The second category of tests was intended to establish the baseline performance of the complete system while using the Grant County Airport ILS beams. During these tests, adjustments were made to the autopilot mode switching. Inspection of the localizer and glide slope instrumentation traces revealed that the ILS beams were satisfactorily free of noise, bends and offsets. It was necessary that the beams be of high quality in order that the results of the subsequent flight experiments would be as expected. The next tests were made to check the correlation between simulator predicted and actual flight recorded responses to certain square disturbance inputs. The simulator predictions were validated on six approaches.

The performance and disturbance data categories of flight experiments were the principle subjects of the flight program. The forty two approaches made in the last three flights provided the sought-after data regarding the comparative autopilot's performance in the presence of both environmental and ILS beam disturbances. In each flight, the sequence of conditions was as follows: an approach on autopilot A, B or C, in both pitch and roll axes, was made with no

Figure 5.0.1

BOEING 727-E2 TEST AIRCRAFT

TABLE 5.1

Flight Test Program Summary

	Approx. Flt Hrs.	Approaches	Dates (1971)
1. Functional Check (Total)	(4.62)	(5) total	
a. Inner Loops	3.25	3/4 Complete	10/20
b. Stability and control coef.			
c. Track, altitude hold			
d. Glide slope, localizer			
e. Disturbance inputs			
f. Instrumentation system	1.37	1/4 remaining	10/26
2. Baseline Data (Total)	(3.91)	(12)	
a. Average performance	1.91	6	10/26
b. Autopilot variations			
c. Moses Lake beam anomalies	2.0	6	11/3
3. Validation Data (Total)	(2.0)	(6)	11/3
a. Square, pulse inputs			
b. Footprint Criteria			
4. Performance Data (Total)	(3.4)	(13)	
a. Moses Lake beam anomalies	1.4	5	11/10
b. Close-in capture	1.0	4	11/16
c. Left-right captures	1.0	4	11/19
d. Additional average performance			
5. Disturbance Data (Total)	(8.3)	(29)	
a. Comparative autopilot response	2.6	10	11/10
b. Maneuver criteria	2.4	10	11/16
c. Superposition and stationarity	3.3	9	11/19
Grand Total	22.23	65	

NOTE: The return automatic landings at Boeing Field are included in the totals.

artificial beam disturbance input; the next three approaches were then made, one on each control law, with the same localizer and glide slope beam disturbances introduced on each approach. This grouping of four approaches was repeated three times on each flight. The objective of this sequencing arrangement was to expose the three control laws to nearly identical conditions. Thus, differences in results were almost entirely attributable to the performance capabilities of three control laws.

5.1 Experimental Test Equipment

No alterations to the airplane's autopilot wiring were permitted because of cost considerations and the fact that the airplane was to remain available, except on test flight days, for crew training. This circumstance dictated a palletized experimental equipment configuration in which the experimental autopilots and instrumentation could be plugged in as a temporary substitute to the existing standard autopilots. The substitution arrangement is illustrated in Figure 5.1.1. The instrumentation, autopilot and INS pallets were located in the cabin section of the airplane. The modified autopilots were engineering units that were physically interchangeable with the airplane's standard autopilot boxes. For non-experimental airplane use, the standard airplane autopilots were retained in their normal racks. For the autoland experiments the standard autopilot boxes were removed and the modified autopilot boxes substituted in their stead. A wire bundle ran from the modified boxes to the autopilot pallet and it was through these wires that electronic connection was made between the pallets and the airplane controls and sensors. The switchover from standard to experimental configuration could be made in about five minutes. The experimental equipment pallets were left on the airplane through the full five week flight test period. Laboratory checkout of the pallets was performed on a 727 autopilot test bench. An analog computer simulated airplane dynamics and generated autopilot feedback signals. The test bench contained all the wiring existent in the actual airplane. Consequently, when the palletized equipment was moved to the airplane, checkout on the airplane itself took only two days. On the first flight, four automatic landings were made.

5.1.1 Experimental Autopilot and INS

The autopilot and associated equipment were functionally and physically separated into three groups: the experimental autopilot pallet which housed the digital autopilots and signal distribution panel; the INS pallet which contained the INS navigation, control and display units; and the modified autopilot boxes which effectively coupled all the test equipment to the airplane.

A picture of the autopilot pallet as installed in the airplane is shown in Figure 5.1.2. Three prototype General Electric variable increment digital computers were positioned one above the other on the right-hand side. The upper and middle computers provided roll and pitch axis computation respectively. The lower computer was carried as a spare. Analog signal demodulation/modulation/isolation was performed by signal conditioner electronics in the lower left of the

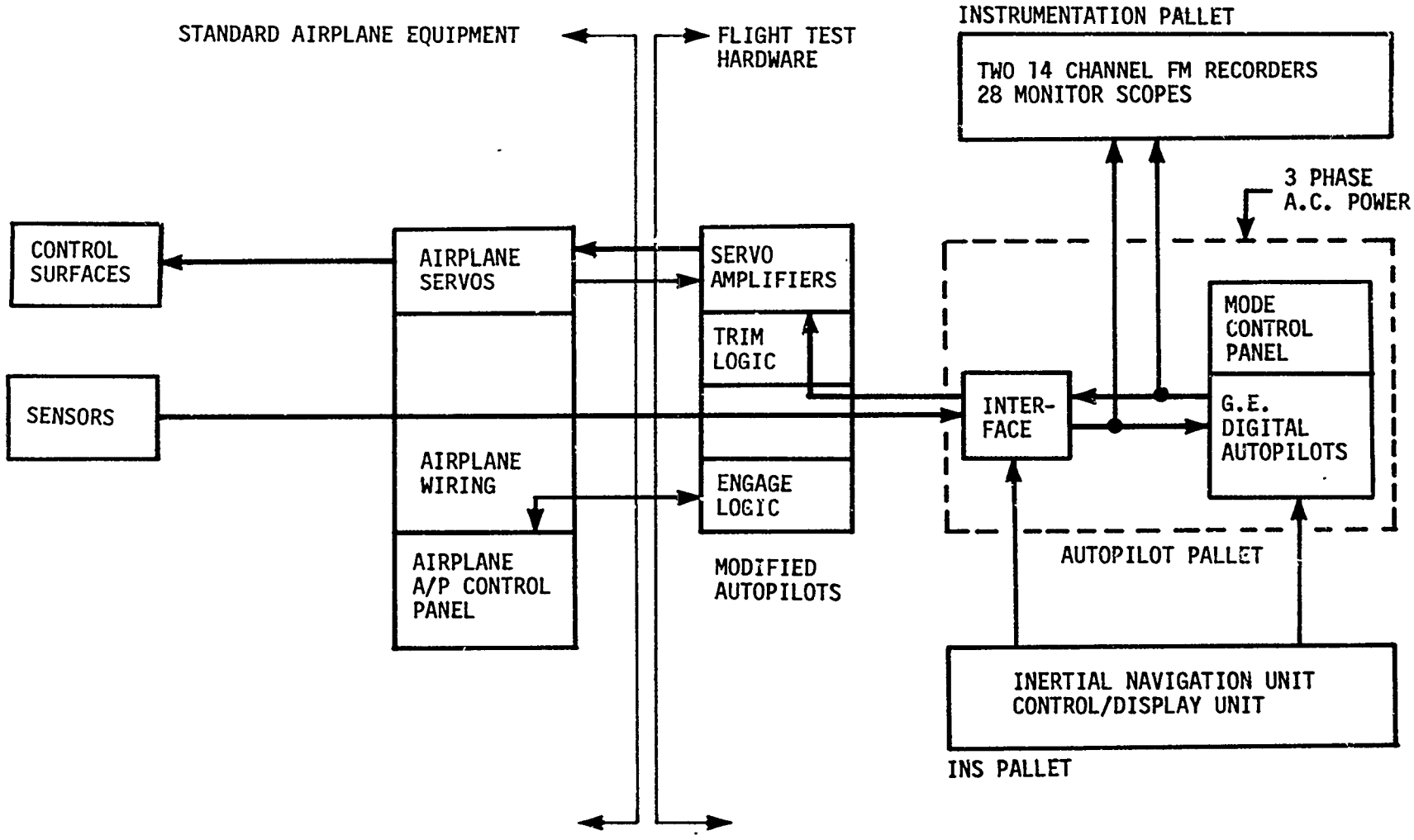

Figure 5.1.1
EXPERIMENTAL FLIGHT TEST EQUIPMENT

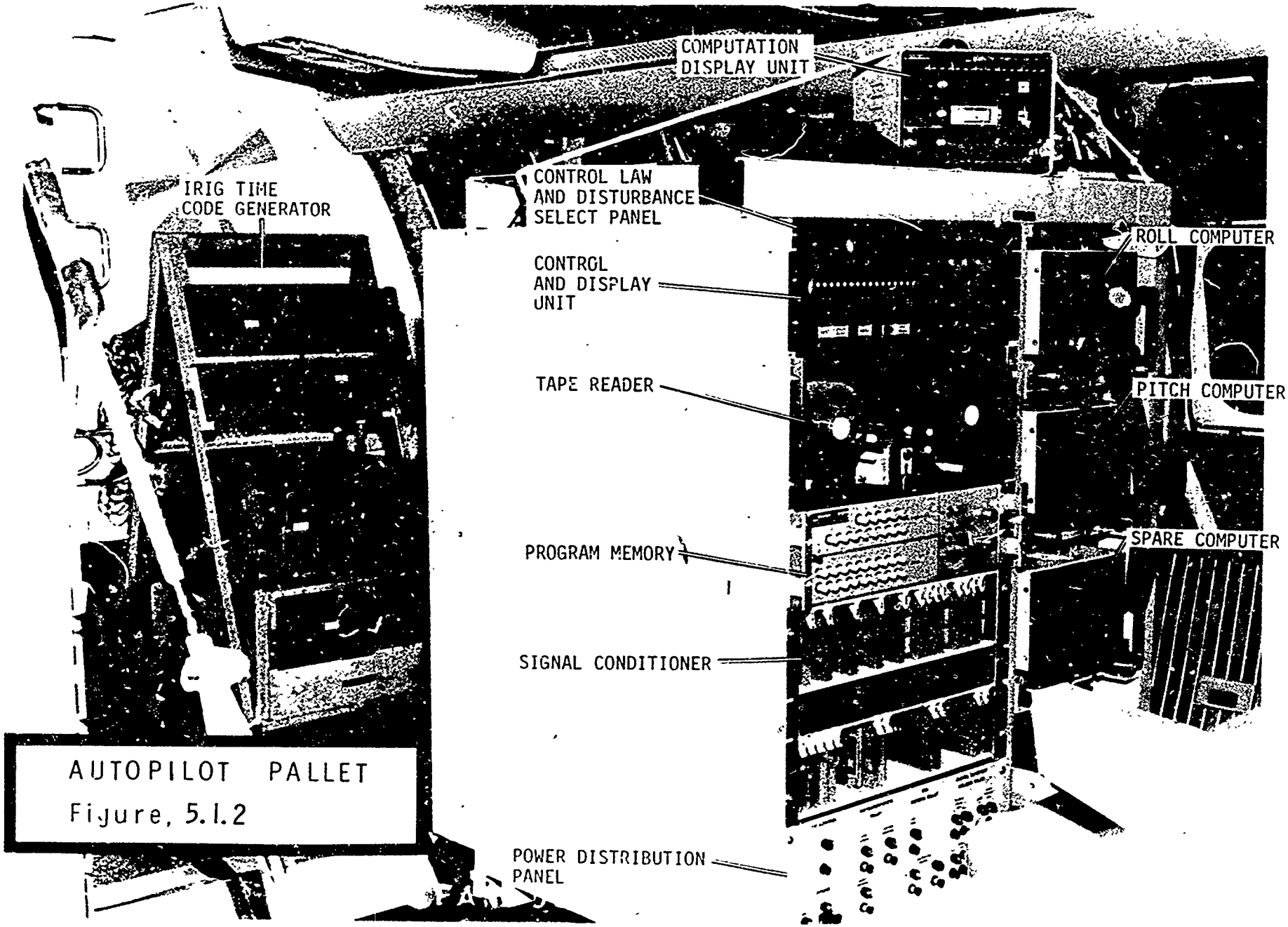

AUTOPILOT PALLET

Figure, 5.1.2

pallet. A digital program memory (middle left side) simultaneously stored all three pitch and roll control laws and the equations that defined the beam disturbance inputs. This alterable digital program memory was conveniently loaded through the punched paper tape reader above it. Complete reloading of the program could be accomplished in about twenty minutes. The alterable memory control and display unit, in the upper left of the pallet, contained provisions for hand loading changes to the memory. Thus, minor changes to the program could be made, even while in flight, by the computer operator. Any such changes could be post-flight incorporated into a revised punched paper tape.

At the very top left of the pallet was the control law and disturbance input selection switch panel. The control select switches on this panel permitted independent selection of the A, B or C control law in both pitch and roll axes. The disturbance select switches permitted selection of the type of beam disturbance and axis to which the disturbance was to be inserted. The beam disturbances were introduced by simply adding to the localizer and glide slope signal inputs to the autopilots. The beam disturbances were automatically initiated as the airplane descended through a preselected radio altitude. Termination occurred after a preset period of time. The flight instruments in the cockpit did not "see" the disturbance; they did, however, reflect the airplane response to a disturbance.

All the units comprising an AC Electronics Carousel IV inertial navigation system were mounted on a single pallet. The inertial equipment was standard in hardware and only slightly modified in software for compatibility with the requirements of the inertially-aided control laws. The software alterations are discussed in detail in Appendix D. Of the various INS analog outputs available, only pitch and roll attitudes and vertical acceleration were used and these were unmodified. The digital output line software was altered principally to increase the data rate of the track angle output from once every 600 milliseconds to once every 200 milliseconds. No change to the navigation program was made and thus the alteration had no effect on the operation or performance of the system. Ground speed and track angle, in digital format from the INS, were routed directly to the experimental autopilots.

One set of standard 727 airplane pitch and roll autopilot units was modified to provide airplane sensor and control signal routing to the autopilot pallet. The modified 727 autopilots also provided control of the airplane elevator and aileron autopilot servos. The modified units were inserted in the existing standard autopilot trays for the test flights.

5.1.2 Instrumentation

Two fourteen-channel, FM tape recorders were mounted in the instrumentation pallet as shown in Figure E.1. All signal inputs to the recorders were conditioned to a continuous DC analog format. A time code generator (in background of Figure 5.1.2) supplied a time

record on one channel of each recorder.

The recorded data was made available within one day of the flight in oscillograph strip-out form. Thus preliminary analysis of results could be accomplished in time to generate any required change of plans to the flight test scheduled for the next week. The tape data was also "digitized" on a small computer to make the data compatible with a 6600 digital computer. Within this 6600 computer, data processing was performed to convert all data to engineering units, to Kalman filter the INS data with the ground camera position estimates, to compute the maneuver criteria values, and to determine the center and gradient of the Moses Lake airport localizer and glide slope beams.

5.1.3 Camera Tracking System

Four ground-based cameras were used to determine aircraft true position with respect to the runway during the last one and one-half miles of the final approach. The camera control equipment was synchronized to the IRIG time code generator in the airplane and a picture was taken every two seconds. Space position data was calculated through post-flight photo reading (azimuth and elevation) and a digital computer triangulation program. This estimate of airplane position was then combined with INS data in a Kalman filtering technique to improve overall accuracy. Essentially, the Kalman filtering removed much of the randomness from the camera data. The net result was a vertical and lateral position estimate that was accurate to within one foot for the last 4500 feet of the approach. A discussion of the camera tracking system and Kalman filtering technique is given in Appendix C.

5.2 Grant County Airport ILS Beam Characteristics

The usefulness of much of the flight test data was fundamentally predicated upon the assumption of the principle of superposition. That is to say that the ILS beam must be free of multipath distortion in order that beam disturbances artificially introduced within the autopilot could be validly "added" to the received beam deviation. There existed no means to compensate for beam distortion. Fortunately, the Grant County Airport ILS beams were found to be free of any noticeable distortion or roughness.

The analog simulation was programmed with the assumption of nominal ILS beam course widths and the published Grant County 2.5 degree glide slope angle. One to one correspondence of the simulation and flight test results depended upon nominal course width and course center values for the Grant County ILS beams. However, off nominal values could be taken into account and thus there was no absolute requirement for nominal values. The ILS beams were found to be off-nominal but satisfactory for the flight tests.

Both of the aircraft's Collins 51RV-1 ILS receivers were calibrated before any flight tests were made. Centering offsets were less than 1 ua and sensitivities correct to within three percent.

5.2.1 Glide Slope Beam

The glide slope beam was found to be marginally satisfactory for the purposes of the flight tests. Beam centering and slope were close to published value but sensitivity was far below allowable tolerance. The beam was free of any noticeable roughness or bends.

The location of beam center, as shown in Figure 5.2.1, was calculated from camera data. The instantaneous values of beam error were superimposed on the camera data to construct the beam center estimate. Data from one steady approach on each of the last three flights were used for the beam center calculations. The agreement between the data was within a band of 4 feet of altitude and thus the beam appeared quite stationary over a week's period of time. The straight line average in Figure 5.2.1 is drawn with reference to a plane inclined at 2.5 degrees that intersected the runway at the glide slope antenna station. The beam appeared to emanate from a point seven feet underground and had a slope of 2.46 degrees. At the Grant County facility, the base of the glide slope antenna is approximately five feet lower in elevation than the runway centerline. The reason for the extended beam center estimate failing by two feet to intersect the antenna base remains unexplained.

The sensitivity of beam in microamps per degree of actual deviation from center was found to be 150 ua per degree instead of the nominal of 215 ua per degree. This fact resulted in larger excursions in feet from beam center than had been expected. The tolerance specification on beam sensitivity would allow a minimum of 168 ua per degree; thus the beam, in this respect, was out of tolerance.

The beam center estimate was used as the reference path for computation of the pitch axis maneuver criterion.

5.2.2 Localizer Beam

The localizer beam was found to be entirely satisfactory for the purposes of the flight tests. The beam was free of any noticeable roughness or bends.

The localizer beam center with respect to runway centerline was statistically estimated from over 1000 samples taken at one second intervals on 25 approaches. This was done by calculating, from the camera data, the equivalent degrees of deviation from centerline and plotting it against the recorded localizer beam deviation signal. Drawing a straight line for a least square fit gave a localizer offset of less than .14ua and a gradient of 91.2 ua per degree. Converted to dimensions of feet, these ua figures are equivalent to a .41 foot left bias offset and a 2.88 foot per ua sensitivity at runway threshold. The measured sensitivity is 19 percent lower than is nominal for Cat II localizer beams. Therefore, deviations in feet from centerline, for all causes, were slightly higher than would have occurred at a Cat II facility with nominal sensitivity.

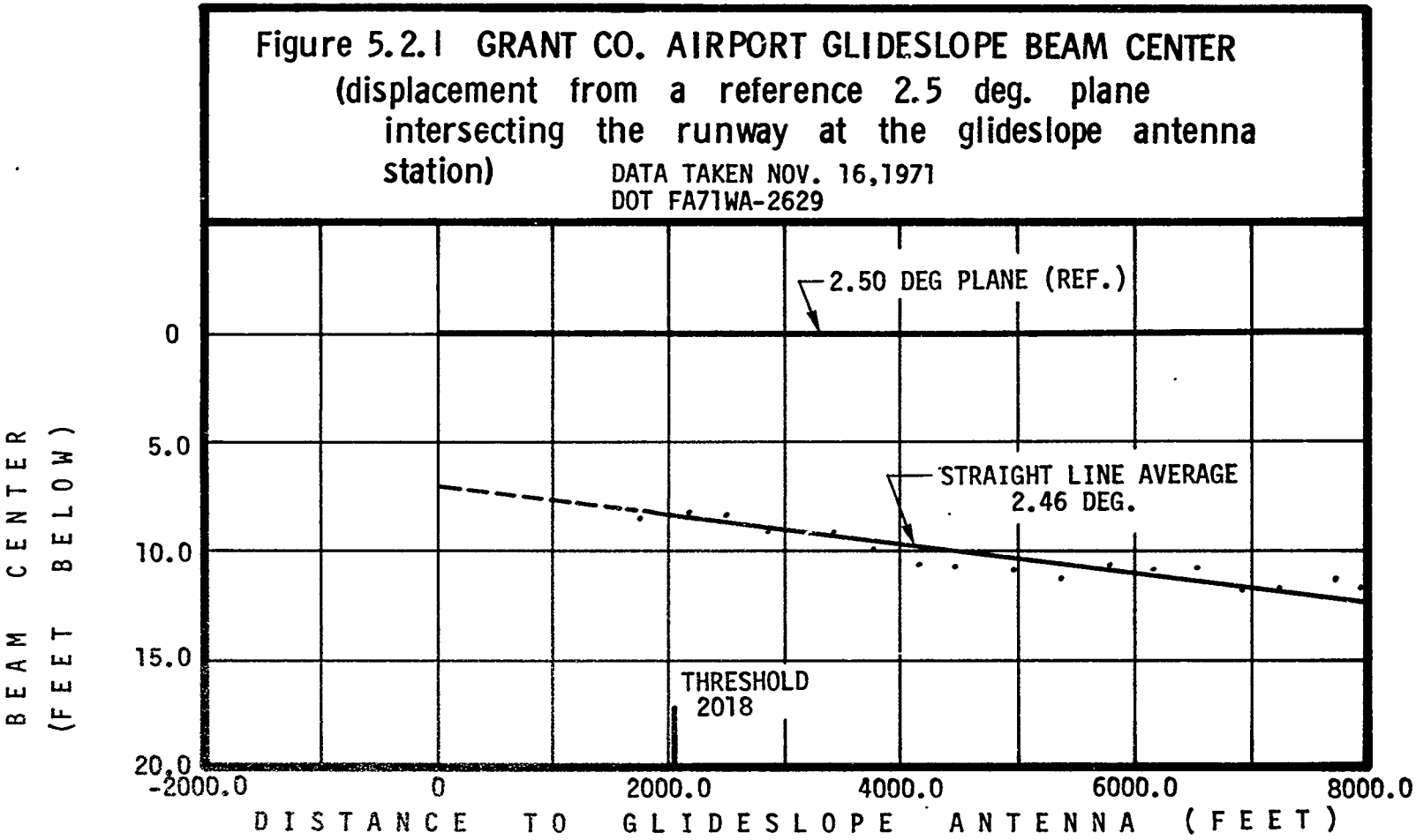
Figure 5.2.1 GRANT CO. AIRPORT GLIDESLOPE BEAM CENTER
(displacement from a reference 2.5 deg. plane intersecting the runway at the glideslope antenna station)
DATA TAKEN NOV. 16,1971
DOT FA71WA-2629
2.50 DEG PLANE (REF.)
STRAIGHT LINE AVERAGE
2.46 DEG.
THRESHOLD
2018
BEAM CENTER (FEET BELOW)
0
5.0
10.0
15.0
20.0
-2000.0
0
2000.0
4000.0
6000.0
8000.0
DISTANCE TO GLIDESLOPE ANTENNA (FEET)

5.3 Simulation Validation

In general, good agreement was obtained between the simulation and the flight test results throughout all six flights. However, owing to wind gusts and shear, some response shapes from the flight data were more difficult to correlate than others. In the pitch axis, for example, the three beam disturbances, which were planned as validation disturbances on the third flight, were coincident with substantial environmental activity, and as a result, correlation with the simulation was very difficult to achieve. Consequently, it was decided to use the fifth flight, which was conducted under unusually calm winds to show validation of the pitch axis simulation. The roll axis flight test results, on the other hand, correlated very well with the simulation results on the third flight as intended.

5.3.1 Simulation Validation in the Pitch Axis

Excellent correlation between the simulated and the flight test responses against stylized beam bends was obtained on the second, third and fourth approaches of flight number 5. The evidence of this agreement is contained in Figures 5.3.1, 5.3.2 and 5.3.3, where each system response against a common bend is depicted. This common bend was a 50 ua, 16-sec, sinusoidal fly-down disturbance inserted at 200 ft altitude. The ground speed for these approaches ranged between 118 and 128 KTS which compared favorably with the 125 KTS used on the simulation.

It will be noted that in Figure 5.3.1, the A system responses, that the airplane had been tracking slightly below the G/S prior to the introduction of the beam disturbance; hence, the slight disagreement between the two responses. A similar condition is shown in the B system response of Figure 5.3.2, while the C system, responses in Figure 5.3.3 are almost coincident.

5.3.2 Roll Axis Simulation Validation

Close correlation between simulator predicted airplane response and that actually obtained inflight is evident by inspection of Figures 5.3.4, (System A), 5.3.5, (System B), and 5.3.6 (System C). A five second, 16 ua, square localizer disturbance was used as the forcing function and is shown on the figures for reference. The dotted line is the airplane response as determined on the simulator under no wind conditions with a 125 knot approach speed.

During flight number 3, when all the flight data shown in these figures were taken, a 15 knot tailwind existed which resulted in 140 knot ground speed. Because of this 15 KT increase in speed, the flight responses "lag" those of the simulator. The significant factors that indicate the close correlation are: the peak change in cross track position due to the disturbance is very nearly the same for simulator and flight data; the rate of divergence from original path is also the same for simulator and flight data. Further, a high confidence in the correlation is established by the repeatability of the flight data.

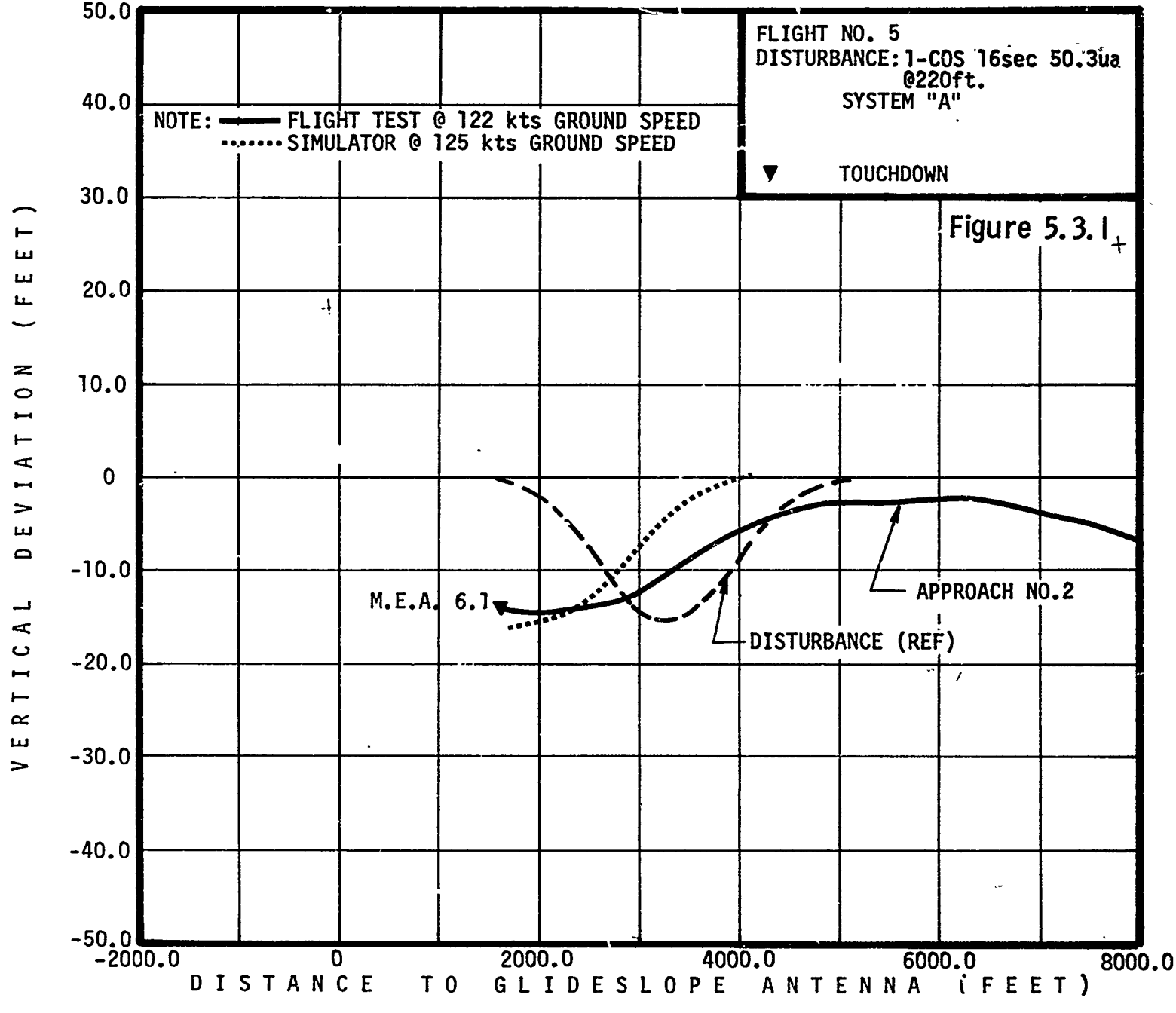
FLIGHT NO. 5
DISTURBANCE: 1-COS 16sec 50.3ua
@220ft.
SYSTEM "A"
NOTE: FLIGHT TEST @ 122 kts GROUND SPEED
SIMULATOR @ 125 kts GROUND SPEED
TOUCHDOWN
Figure 5.3.1+
M.E.A. 6.1
APPROACH NO.2
DISTURBANCE (REF)
VERTICAL DEVIATION (FEET)
50.0
40.0
30.0
20.0
10.0
0
-10.0
-20.0
-30.0
-40.0
-50.0
-2000.0
0
2000.0
4000.0
6000.0
8000.0
DISTANCE TO GLIDESLOPE ANTENNA (FEET)

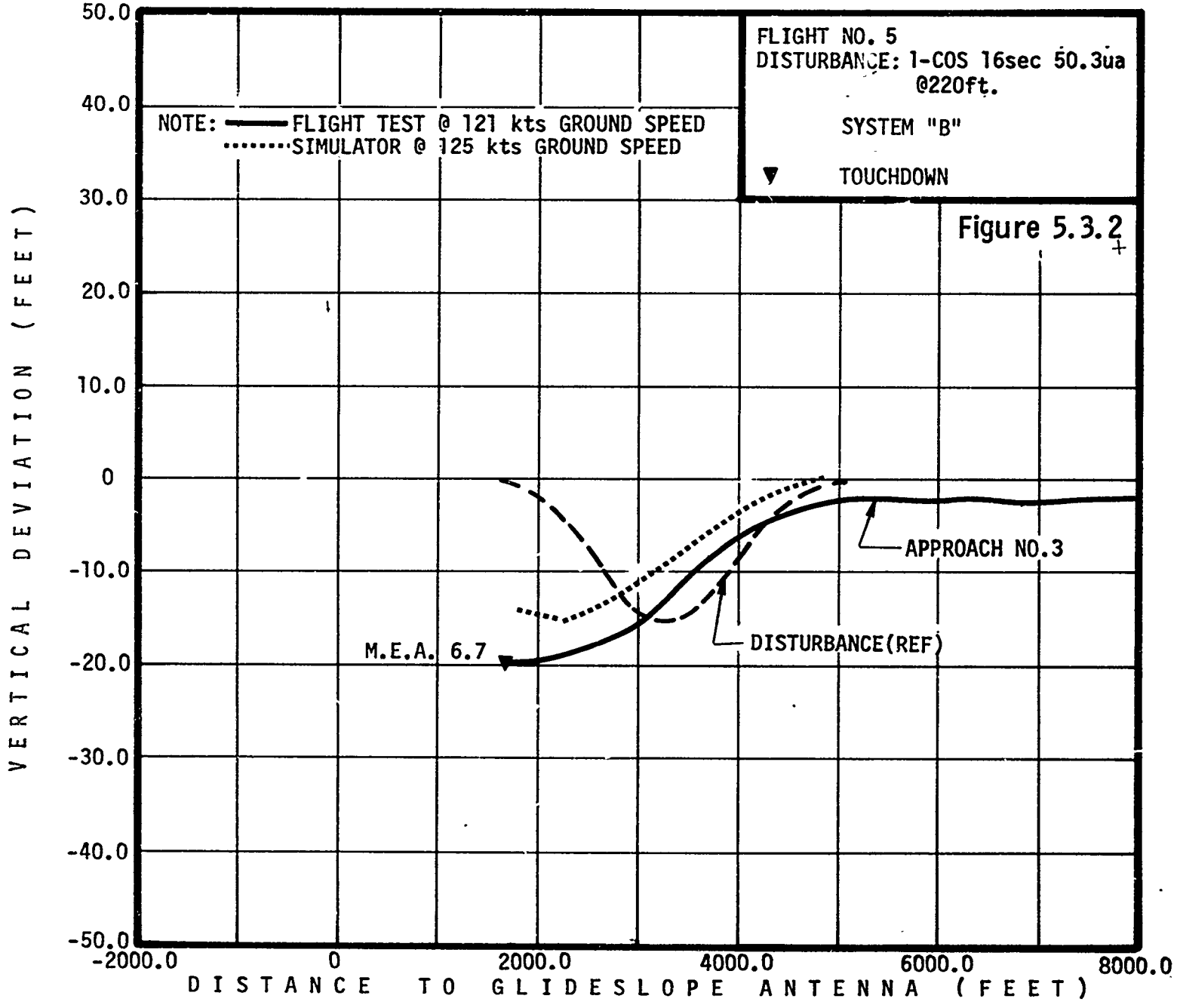
FLIGHT NO. 5
DISTURBANCE: 1-COS 16sec 50.3ua @220ft.
SYSTEM "B"
TOUCHDOWN
NOTE: FLIGHT TEST @ 121 kts GROUND SPEED
SIMULATOR @ 125 kts GROUND SPEED
Figure 5.3.2
APPROACH NO.3
DISTURBANCE(REF)
M.E.A. 6.7
VERTICAL DEVIATION (FEET)
50.0
40.0
30.0
20.0
10.0
0
-10.0
-20.0
-30.0
-40.0
-50.0
-2000.0
0
2000.0
4000.0
6000.0
8000.0
DISTANCE TO GLIDESLOPE ANTENNA (FEET)

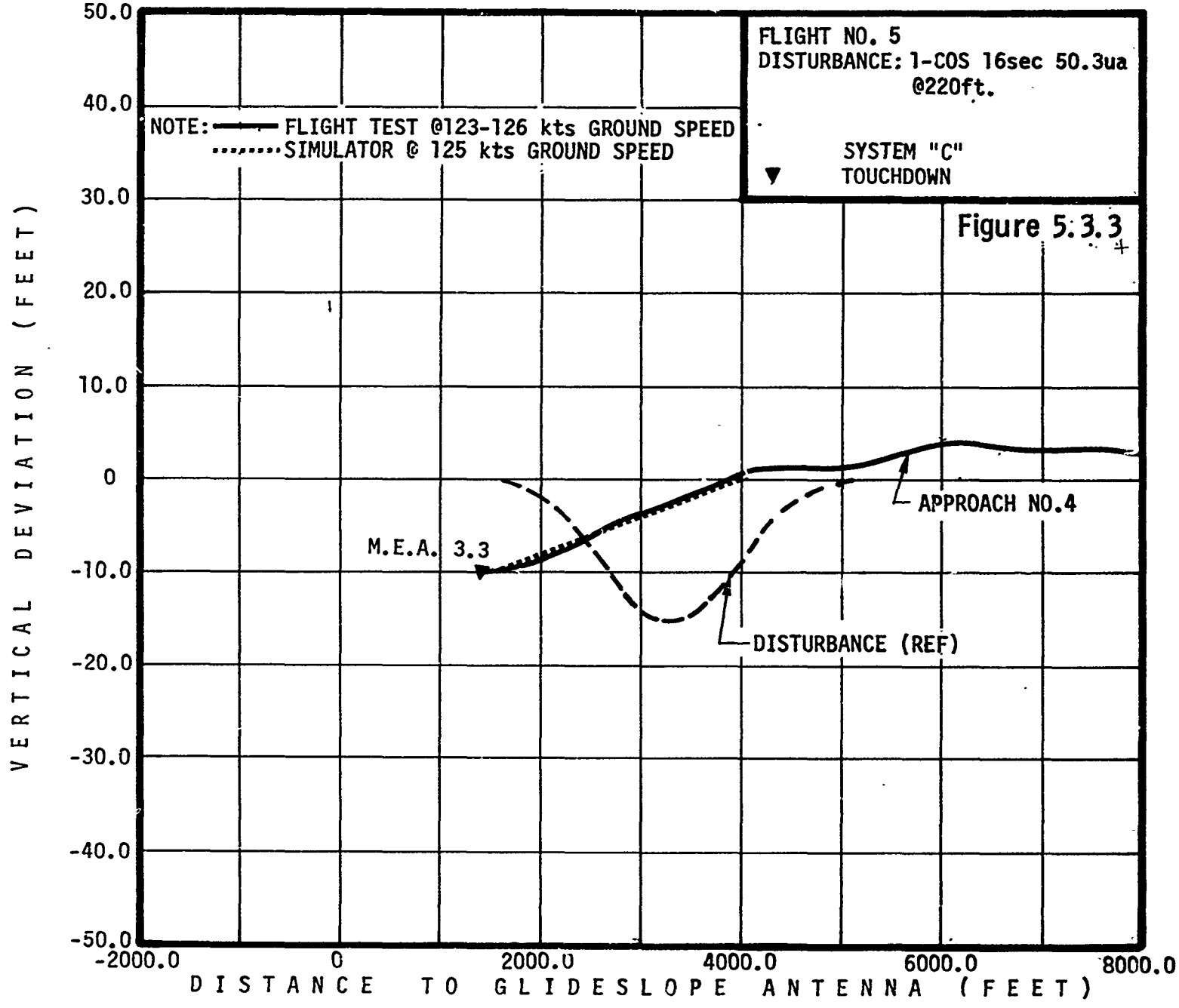
FLIGHT NO. 5
DISTURBANCE: 1-COS 16sec 50.3ua
@220ft.
NOTE: FLIGHT TEST @123-126 kts GROUND SPEED
SIMULATOR @ 125 kts GROUND SPEED
SYSTEM "C"
TOUCHDOWN
Figure 5.3.3
APPROACH NO.4
M.E.A. 3.3
DISTURBANCE (REF)
VERTICAL DEVIATION (FEET)
50.0
40.0
30.0
20.0
10.0
0
-10.0
-20.0
-30.0
-40.0
-50.0
-2000.0
0
2000.0
4000.0
6000.0
8000.0
DISTANCE TO GLIDESLOPE ANTENNA (FEET)

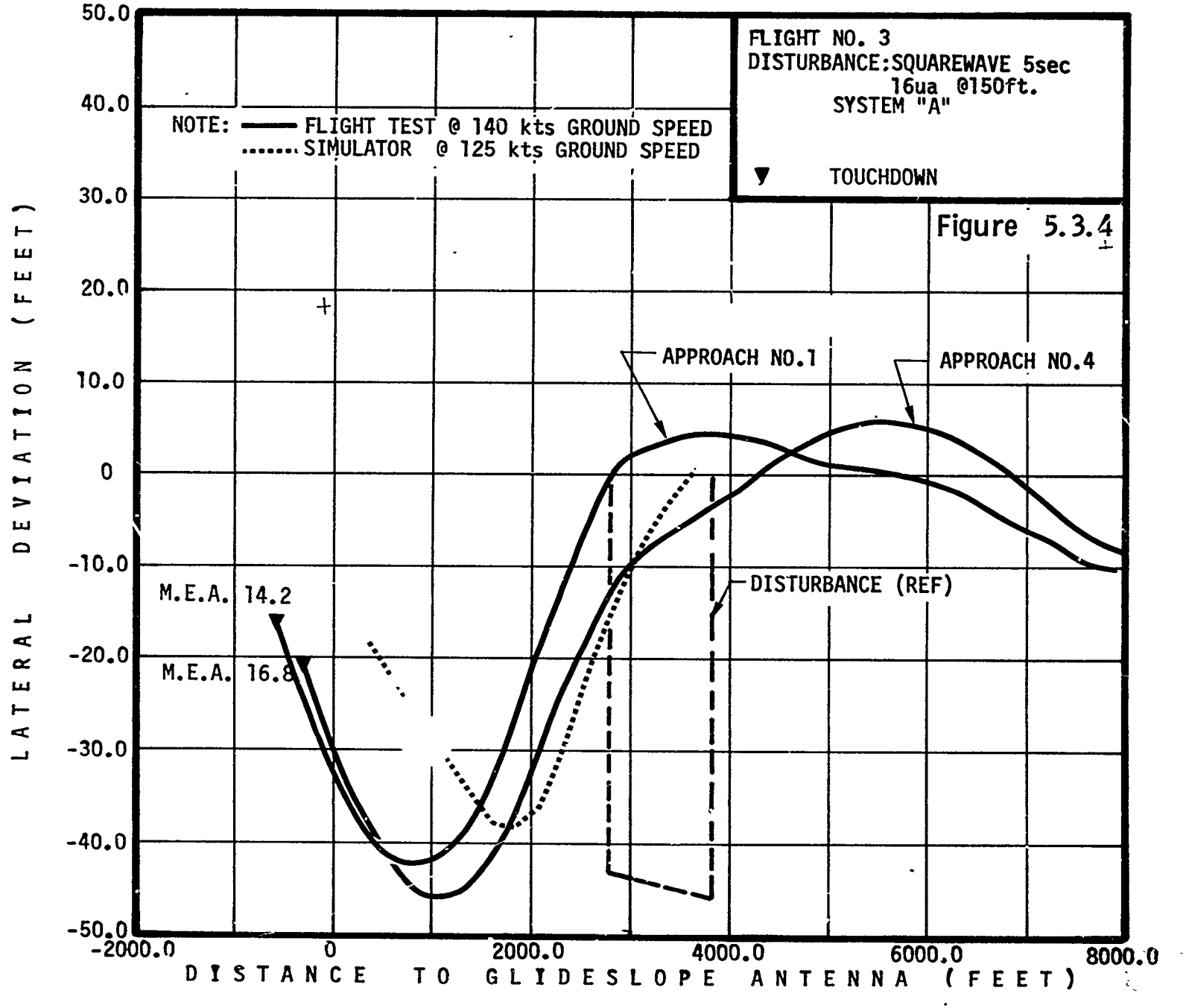
FLIGHT NO. 3
DISTURBANCE:SQUAREWAVE 5sec
16ua @150ft.
SYSTEM "A"
NOTE: FLIGHT TEST @ 140 kts GROUND SPEED
SIMULATOR @ 125 kts GROUND SPEED
TOUCHDOWN
APPROACH NO.1
APPROACH NO.4
DISTURBANCE (REF)
M.E.A. 14.2
M.E.A. 16.8
LATERAL DEVIATION (FEET)
50.0
40.0
30.0
20.0
10.0
0
-10.0
-20.0
-30.0
-40.0
-50.0
-2000.0
0
2000.0
4000.0
6000.0
8000.0
DISTANCE TO GLIDESLOPE ANTENNA (FEET)

Figure 5.3.4

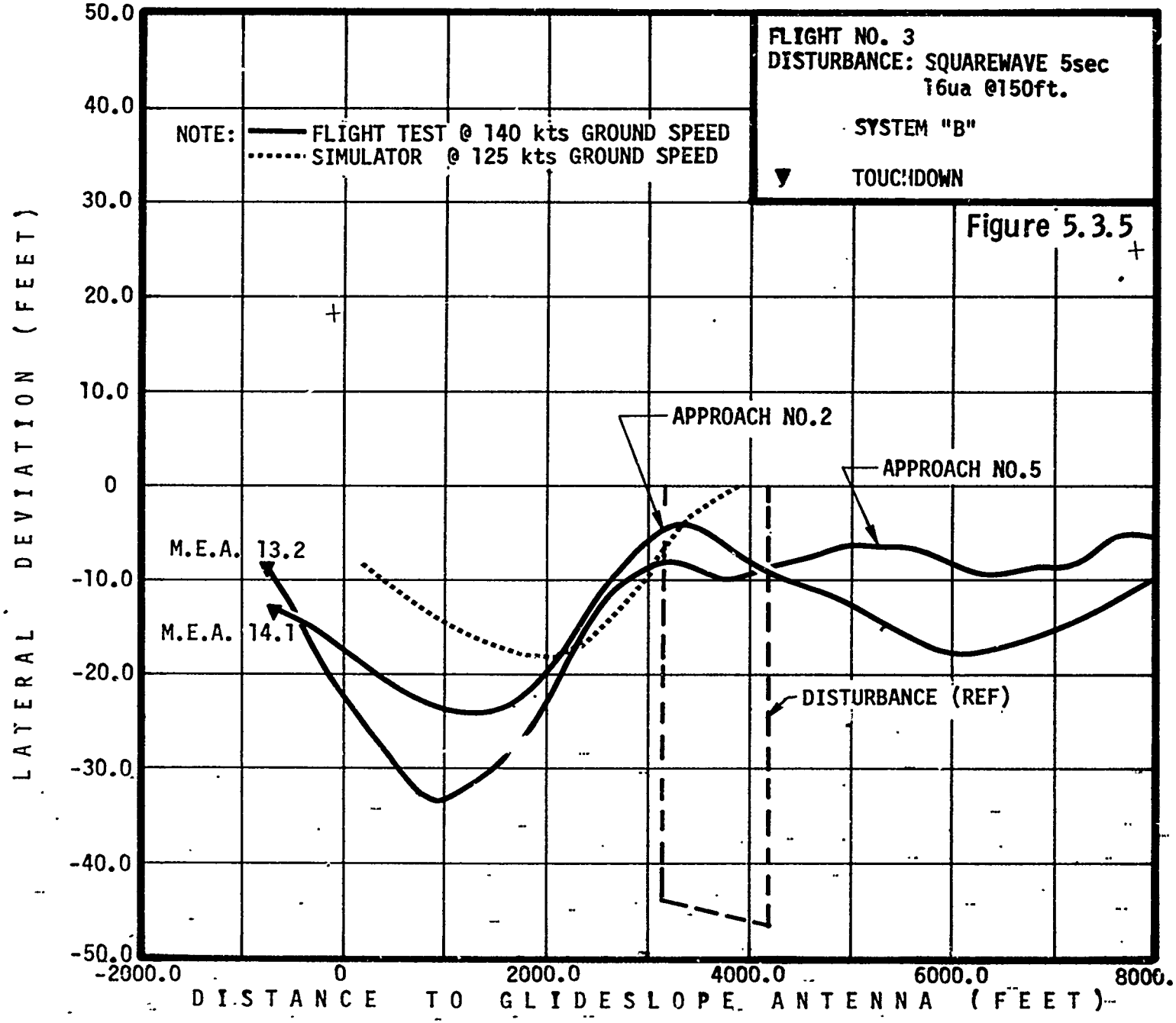
FLIGHT NO. 3
DISTURBANCE: SQUAREWAVE 5sec
16ua @150ft.
SYSTEM "B"
TOUCHDOWN
NOTE: FLIGHT TEST @ 140 kts GROUND SPEED
SIMULATOR @ 125 kts GROUND SPEED
Figure 5.3.5
APPROACH NO.2
APPROACH NO.5
M.E.A. 13.2
M.E.A. 14.1
DISTURBANCE (REF)
LATERAL DEVIATION (FEET)
50.0
40.0
30.0
20.0
10.0
0
-10.0
-20.0
-30.0
-40.0
-50.0
-2000.0
0
2000.0
4000.0
6000.0
8000.0
DISTANCE TO GLIDESLOPE ANTENNA (FEET)

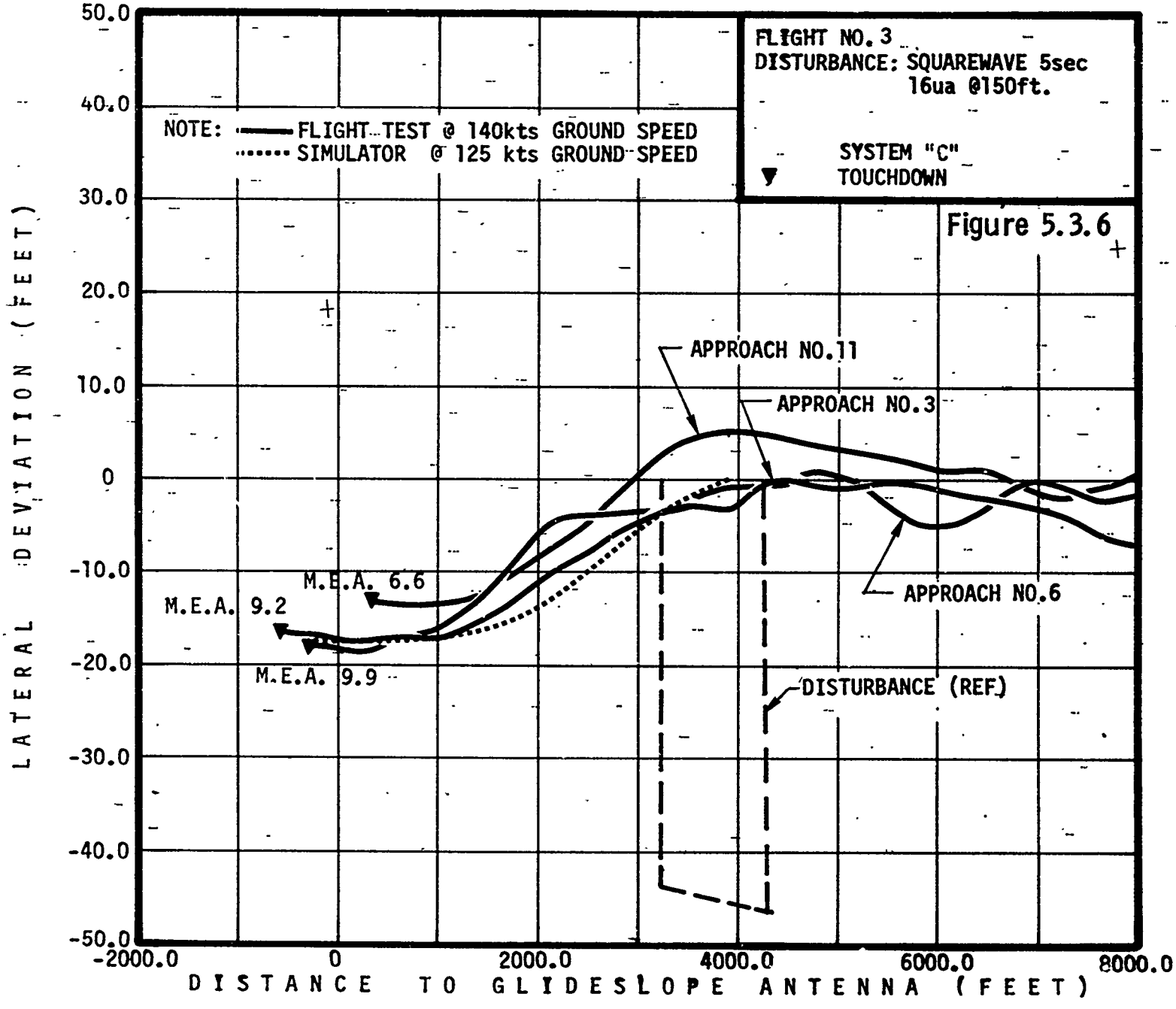
FLIGHT NO. 3
DISTURBANCE: SQUAREWAVE 5sec
16ua @150ft.
NOTE: FLIGHT TEST @ 140kts GROUND SPEED
SIMULATOR @ 125 kts GROUND SPEED
SYSTEM "C"
TOUCHDOWN
Figure 5.3.6
APPROACH NO.11
APPROACH NO.3
APPROACH NO.6
M.E.A. 6.6
M.E.A. 9.2
M.E.A. 9.9
DISTURBANCE (REF.)
LATERAL DEVIATION (FEET)
50.0
40.0
30.0
20.0
10.0
0
-10.0
-20.0
-30.0
-40.0
-50.0
-2000.0
0
2000.0
4000.0
6000.0
8000.0
DISTANCE TO GLIDESLOPE ANTENNA (FEET)

5.4 Flight Test Performance Analysis

Beginning with the third flight of Nov. 3, 1971, and through the sixth flight of Nov. 19, 1971, those ILS disturbances, which either produced marginal responses on the simulation or were otherwise selected for specific test objectives, were introduced into the various autoland systems during live approaches. In addition, to isolate the effects of non-ILS perturbations, several undisturbed approaches were conducted on each of the three systems, thus making available a broad spectrum of response data. These flight data then provided the basis for demonstrating the technique by which the performance of any autoland system may be analyzed.

In this analysis, both performance criteria are employed, and since the data were taken from actual approaches, the "all causes" boundaries apply.

To obtain a quantitative measure of relative performance of the three autopilot control laws the average value of the maneuver equation, M.E.A. (see Section 3.5.3), was calculated from the data provided by the camera tracking system and airborne instrumentation. These calculations were made over a range of 0-8000 ft. from the G/S transmitter, where the camera tracking coverage was provided.

Below 100 ft. altitude, where the footprint criteria apply, the state of the airplane's position and rate of displacement from the desired path provide a sound basis for judging the performance of each system individually. Thus, a qualitative measure of system performance was obtained by plotting the deviation and rate of deviation from the commanded path in both pitch and roll below 100 ft. The footprint criteria boundaries are given on these plots and any violation of the criteria is readily apparent.

5.4.1 Flight Test Performance in the Pitch Axis

Table 5.4.1 contains the descriptions of the glide slope beam disturbances which were selected for the flight test performance analysis. The rationale behind each disturbance is stated under REMARKS where marginal performance is noted against the maneuver criterion, M.C. or the footprint criterion, F.C. These twelve disturbances were used to perturb the various autoland systems during coupled approaches at Grant County Airport. A total of 45 such approaches were conducted, 12 of which were unperturbed, and the resulting performance of the three systems was evaluated quantitatively with respect to the maneuver criterion and graphically with respect to the footprint criterion.

An autothrottle was used on all approaches. On flight number 3 very poor performance was noted in that the unit permitted airspeed to fall up to 10 knots below commanded value. Also, whenever the aircraft descended below beam, an unusually high nose up pitch attitude was developed by the autopilot in an attempt to return. The autothrottle was removed after the flight and recalibrated. Performance was improved during the remainder of the flights. However, performance was not as good as the autothrottle used on the simulator.

TABLE 5.4.1
GLIDESLOPE DISTURBANCES SELECTED FOR FLIGHT TESTING

	DESCRIPTION OF DISTURBANCE					
DIST.NO.	SHAPE	AMPLITUDE (ua)	PERIOD (sec)	ALTITUDE (feet)	DIRECTION	R E M A R K S
1	1-COS	50	16	220	Down	Produces marginal performance against M.C. in System "C"
2	1-COS	30.5	16	220	Down	Maximum allowable bend under Cat II requirements
3	1-COS	56	66	350	Down	Maximum graphical path allowable below ideal glide slope
4	1-COS	26	66	350	Up	Produces marginal performance against F.C. in System C
5	1-COS	39	12	250	Up	Maximum graphical path allowable above glide slope
6	1-COS	65	6	150	Down	Produces marginal performance against F.C. in Systems A & B
7	Square	22	4	250	Up	Obtain indicial response characteristics
8	Square	65	8	220	Down	Produces marginal performance against "all causes" F.C. in System A
9	Square	47	6	150	Up	Produces marginal performance against F.C. in System B
10	1-COS	21.5	10	250	Up	Obtain indicial response characteristics
11	Square	220	6	200	Up	Simulates beam hardover failure for 6 sec.
12	Square	220	∞	100	Down	Simulates beam hardover failure

The quantitative evaluation is summarized in Table 5.4.2. All the approaches, for which the aircraft equipment and ground cameras were operating properly on flight number 3 through 6, are included.

The values in this table represent the average value of the maneuver equation, M.E.A. (see section 3.5.3) for each system as accumulated on each approach. A composite average, or "mean", was calculated for both the aggregate of perturbed approaches and the unperturbed approaches with each system and is shown in the lower table.

For those approaches on which a violation of the "all causes" maneuver criterion occurred, an asterisk is shown following the M.E.A. value. It will be noted that, whereas System A exhibits a composite average for both aggregates that is more than the predicted factor of 2 (see page 78) greater than the C system composite, the B system composite averages are only slightly greater than that of the C system. The primary reason for this failure to achieve the full predicted improvement in the C system over the B system is that, in most cases, the deviation due to atmospheric upsets was significantly greater than that attributable to the artificial beam disturbance. However, a comparison of the performance of the three systems is more accurately illustrated in the M.E.A. of disturbances No. 1, No. 2 and No. 3. These beam disturbances were introduced on the fifth flight where the wind conditions were known to be calm and, hence, had minor effect on the M.E.A. value. In these cases, the results of the relative performances come very close to expectations.

The autopilot's performance in the presence of these artificial beam disturbances is illustrated graphically in Figure 5.4.1 (System A), Figure 5.4.2 (System B) and Figure 5.4.3 (System C). These figures describe the trajectories of the airplane deviation and rate of deviation from ideal glide path for that period of time during which landing gear height above the runway elevation was between 100 and 50 feet. This is the altitude band in which the footprint criterion applies. The "all causes" footprint criterion boundary is shown on each figure for reference. The number associated with certain trajectories refers to the disturbance number which perturbed that particular approach. The results shown in these figures substantiate the general predictions in relative performance of the three systems. Note the absence of any concentration or "aim point" in the trajectories of System A. It should also be noted that 6 of the total A system approaches violated the footprint boundary (5 of these violations were perturbed approaches). Systems B and C, on the other hand, not only reflect a definite concentration of trajectory points near the origin, but only one approach in the B system, and one in the C system, exceeded the footprint criterion boundary. Furthermore, the one C system approach which exceeded the boundary was caused by disturbance number 8. Disturbance number 8 was a validation input that is similar to an eight second hardover.

5.4.2 Flight Test Performance in the Roll Axis

Table 5.4.3 contains the descriptions of the localizer beam disturbances which were selected for the flight test performance analysis.

TABLE 5.4.2
QUANTITIVE EVALUATION OF THE FLIGHT TEST PERFORMANCE IN THE PITCH AXIS

DISTURBANCE NO.	SYSTEM "A" M.E.A.	FLT/APP	SYSTEM "B" M.E.A.	FLT/APP	SYSTEM "C" M.E.A.	FLT/APP	REMARKS
1	6.05*	5/2	6.68*	5/3	3.35	5/4	
2	2.32	5/8	2.28	5/6	1.22	5/7	Nearly calm wind conditions
3	3.64	5/12	2.31	5/11	.56	5/13	
4	13.53*	6/2	3.63	6/3	6.02	6/1	
5	11.33*	6/6	2.83	6/5	3.81	6/7	4 Kn/100 Ft increasing headwind, 18 Kn total change
6	20.18*	6/9	9.72*	6/11	4.96	6/10	
7	5.25*	3/4	2.27	3/5	3.10	3/6	Winds variable & gusty
8	21.40*	3/7			8.12*	3/11	Not included in composite due to malfunctioning autothrottle
9			1.89	3/9			
10			2.27	4/3	1.31	4/2	
11	7.52*	4/7	6.34*	4/6	1.44	4/8	Light winds with minor gusts
12	3.74	4/10	1.92	4/11	3.13	4/12	
Unperturbed Approaches	9.29*	3/8	3.82	3/2	3.26	3/3	Winds variable and gusty
			3.41	3/10	2.93	3/12	
			2.03	4/5	3.34	4/13	
↓	11.91*	5/1	1.48	5/5	.92	5/9	Nearly calm wind conditions
			6.27	6/4			
Composite Average for Perturbed Approaches	8.17		3.83		2.89		NOTE: *Denotes violation of maneuver criterion
Composite Average for Unperturbed Approaches	10.6		3.40		2.61		

Figure 5.4.1
PITCH SYSTEM "A"
"ALL CAUSES" FOOTPRINT PERFORMANCE
(flights 3 through 6)

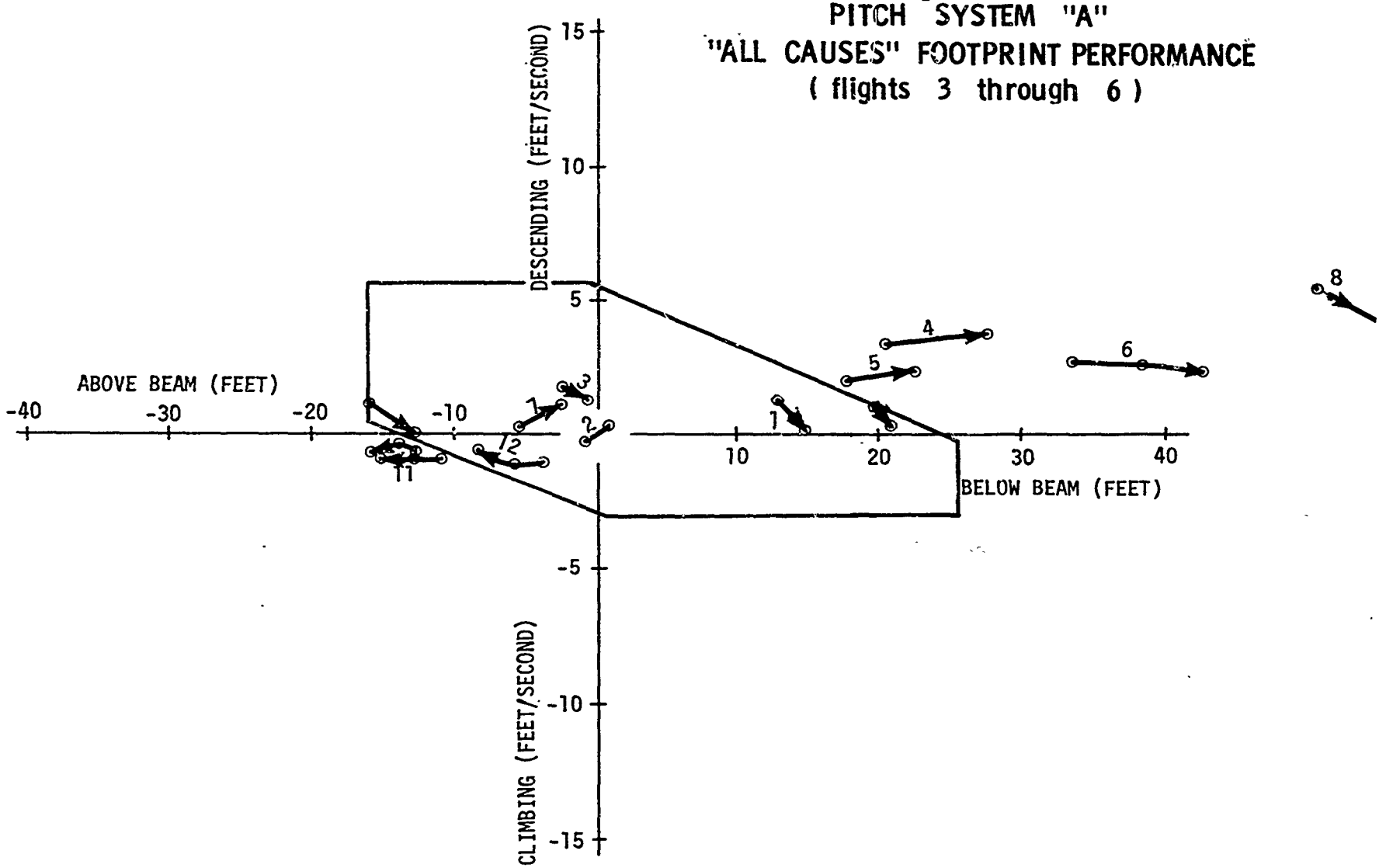

Figure 5.4.2
PITCH SYSTEM 'B'
"ALL CAUSES" FOOTPRINT PERFORMANCE
(flights 3 through 6)

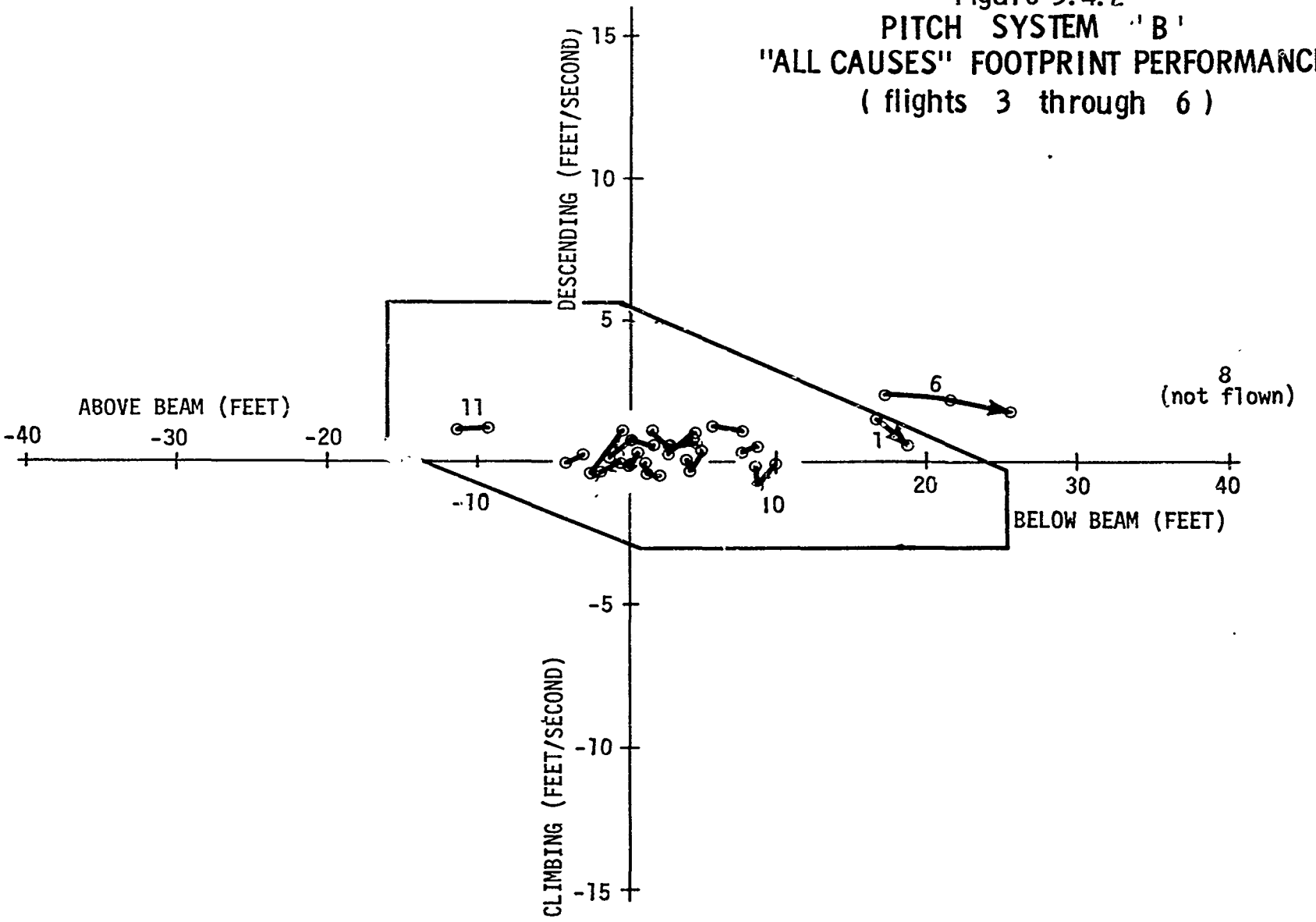

Figure 5.4.3
PITCH SYSTEM "C"
"ALL CAUSES" FOOTPRINT PERFORMANCE
(flights 3 through 6)

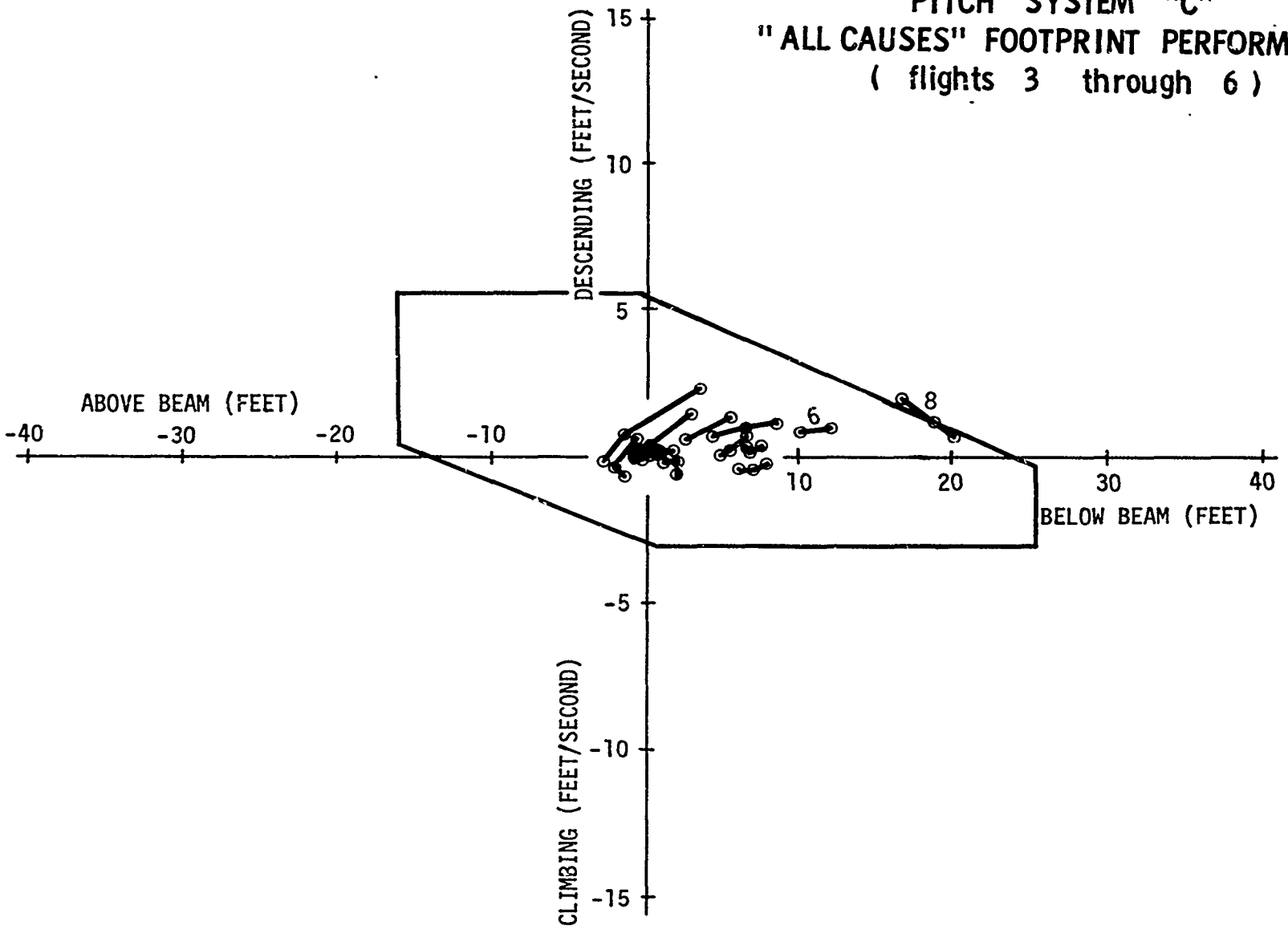

TABLE 5.4.3
LOCALIZER DISTURBANCES SELECTED FOR FLIGHT TESTING

	DESCRIPTION OF DISTURBANCE					
DIST.NO.	SHAPE	AMPLITUDE (ua)	DURATION (sec)	ALTITUDE (feet)	DIRECTION	R E M A R K S
1	Square	16	5	150	Left	Simulation validation
2	Square	16	10	150	Left	Simulation and Footprint Validation
3	1-Cosine	25	10	250	Left	Bend exceeding Cat I requirements
4	1-Cosine	35	3	150	Left	Maximum allowable short bend under Cat I and Cat II requirements
5	1-Cosine	20	100	1000	Left	Very long bend
6	1-Cosine	25	10	1000	Left	High altitude maneuver criterion
7	Bias	15	Until	212	Left	Worst case dog leg
8	Bias + 1-Cosine	8 +8	Always +8 Sec	200	Left + Left	Maximum allowable misalignment + bend under Cat II requirements
9	High Altitude Overflight 750 Ft.					Typical in commercial service
10	Low Altitude Overflight 150 Ft.					Typical in commercial service
11	1-Cosine	14	10	150	Left	Maximum Allowable bend under Cat I requirements

The rationale behind each disturbance is stated under REMARKS. The disturbance set included localizer beams good at high altitude but bad at low altitude and those bad far out and good near threshold. Each of the eleven disturbances was summed with the received localizer signal to simulate a distorted beam during coupled approaches with all three systems at Grant County Airport. The resulting performance of the three systems was evaluated quantitatively with respect to the maneuver criterion and the footprint criterion.

The quantitative evaluation of roll axis performance is summarized in Table 5.4.4. All the approaches, for which the aircraft equipment and ground cameras were operating nominally on flight number 3 through 6, and 3 unperturbed approaches from flight number 2 are included in the Table. The numerical values in the Table are the average value of the maneuver equation, M.E.A. (see Section 3.5.3) for each of the 47 approaches including 9 which were unperturbed. The M.E.A.'s are ordered by system and disturbance (see Table 5.4.3). An asterisk (in Table 5.4.4) is used to indicate violation of the maneuver criterion.

The M.E.A. values for each system may be compared on a given disturbance to indicate relative performance against localizer beams which may be stylized as the simulated one. The relative performance of the three systems agreed with expectations. Disturbance 8, which included a bias affects the three systems about the same. Disturbance 7 produces a slightly lower M.E.A. for System C because, although System A crosses through runway centerline quickly, it overshoots more than 50 feet to the right of centerline. System A exhibits a considerably smaller M.E.A. for disturbance number 5, the long term 1-COSINE bend, because it has less phase shift at this frequency than System B or C. The 8 matched M.E.A. values for disturbances 1, 2, 3, 4, 6, 9, and 10 were averaged to produce a composite M.E.A. for System A, B, and C of 17.8, 10.1, and 8.3 feet respectively. Although these numbers are not statistically significant because of the limited sample size, the trend of performance improvement is strongly revealed. The composite M.E.A. for the two matched sets of undisturbed approaches of System A, B, and C is 11.5, 7.4, and 5.8 respectively.

The performance of Systems A, B, and C is depicted graphically with respect to the lateral footprint in Figures 5.4.4, 5.4.5, and 5.4.6 respectively. Twelve of the matched sets of approaches listed in Table 5.4.4 were used for the Figures. The second set of disturbance number 1 approaches was not used. These Figures describe the trajectories of aircraft lateral deviation and rate of deviation with respect to the extended runway centerline with a point plotted each second between 100 feet gear height above runway elevation and touchdown. This is the altitude band in which the footprint criterion applies. The "all causes" footprint criterion is shown on each Figure for reference. The disturbance number appears next to the appropriate trajectory when possible. The results shown in these Figures substantiate the general prediction of relative performance of the three systems. System A distinctly violates the all causes footprint for disturbance numbers 2, 3, and 7, and has a marginal violation for disturbance number 1. System B almost violates the footprint criterion

TABLE 5.4.4
QUANTITIVE EVALUATION OF THE FLIGHT TEST PERFORMANCE IN THE ROLL AXIS

DISTURBANCE NO.	SYSTEM "A" M.E.A.	FLT/APP	SYSTEM "B" M.E.A.	FLT/APP	SYSTEM "C" M.E.A.	FLT/APP	R E M A R K S
1	16.8	3/4	14.1	3/2	9.9	3/6	
	14.2	3/1	13.2	3/5	9.2	3/3	
	15.7	3/7			6.6	3/11	
2	23.7*	3/8	13.5	3/10	9.6	3/12	
			11.9	3/9			
3	34.1*	4/14	13.6	4/3	13.5	4/2	
4	14.8	4/10	6.3	4/11	5.3	4/12	
5	12.2	5/2	40.5*	5/3	32.8*	5/4	
6	6.4	5/12	4.0	5/11	3.1	5/13	
7	29.6	5/8	28.4	5/6	25.7	5/7	
8	29.4*	6/2	31.0	6/3	32.0	6/1	
9	18.6	6/6	4.7	6/5	6.5	6/7	
10	13.6	6/9	11.7	6/11	9.4	6/10	
11	14.1	4/7			9.2	4/8	
	19.6	2/4	11.1	2/5	9.9	2/7	
Unperturbed	5.9	4/9	6.8	4/5			
Approaches	9.0	5/1	7.0	5/5	3.9	5/9	
			4.7	6/4			

NOTE: * Denotes violation of maneuver criterion

Figure 5.4.4
ROLL SYSTEM "A"
"ALL CAUSES" FOOTPRINT PERFORMANCE
(flights 3 through 6)

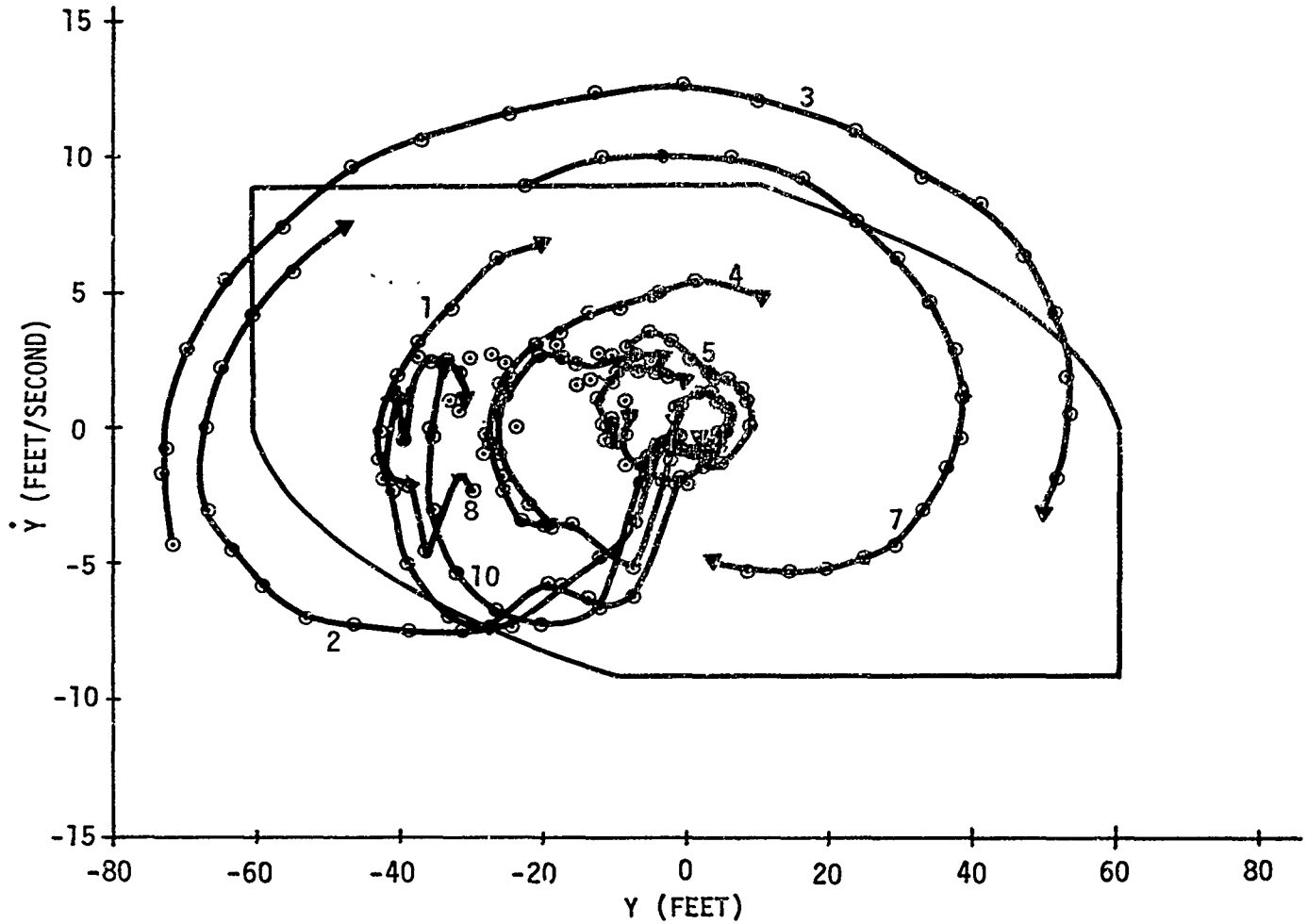

Figure 5.4.5
ROLL SYSTEM "B"
"ALL CAUSES" FOOTPRINT PERFORMANCE
(flights 3 through 6)

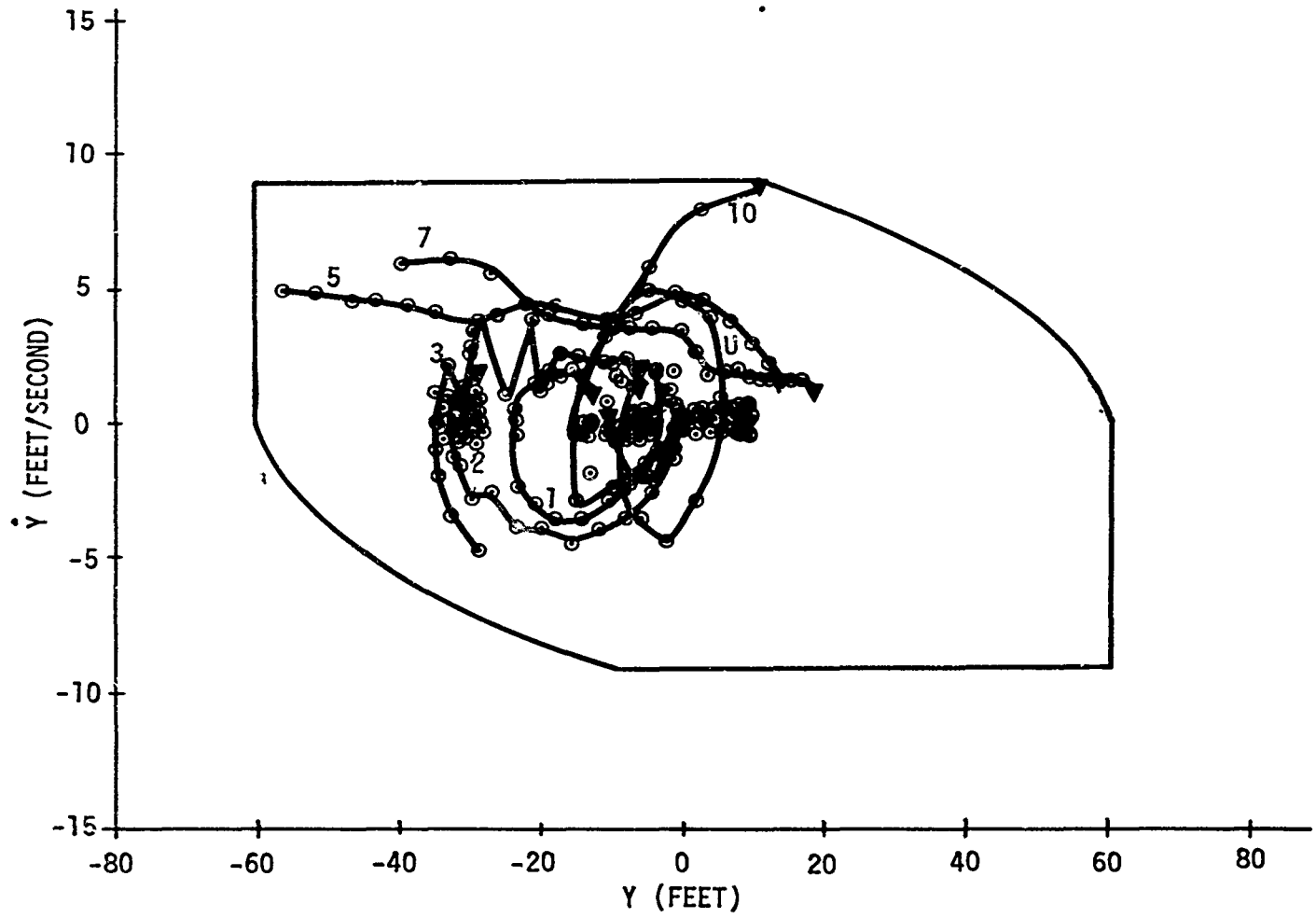

Figure 5.4.6
ROLL SYSTEM "C"
"ALL CAUSES" FOOTPRINT PERFORMANCE
(flights 3 through 6)

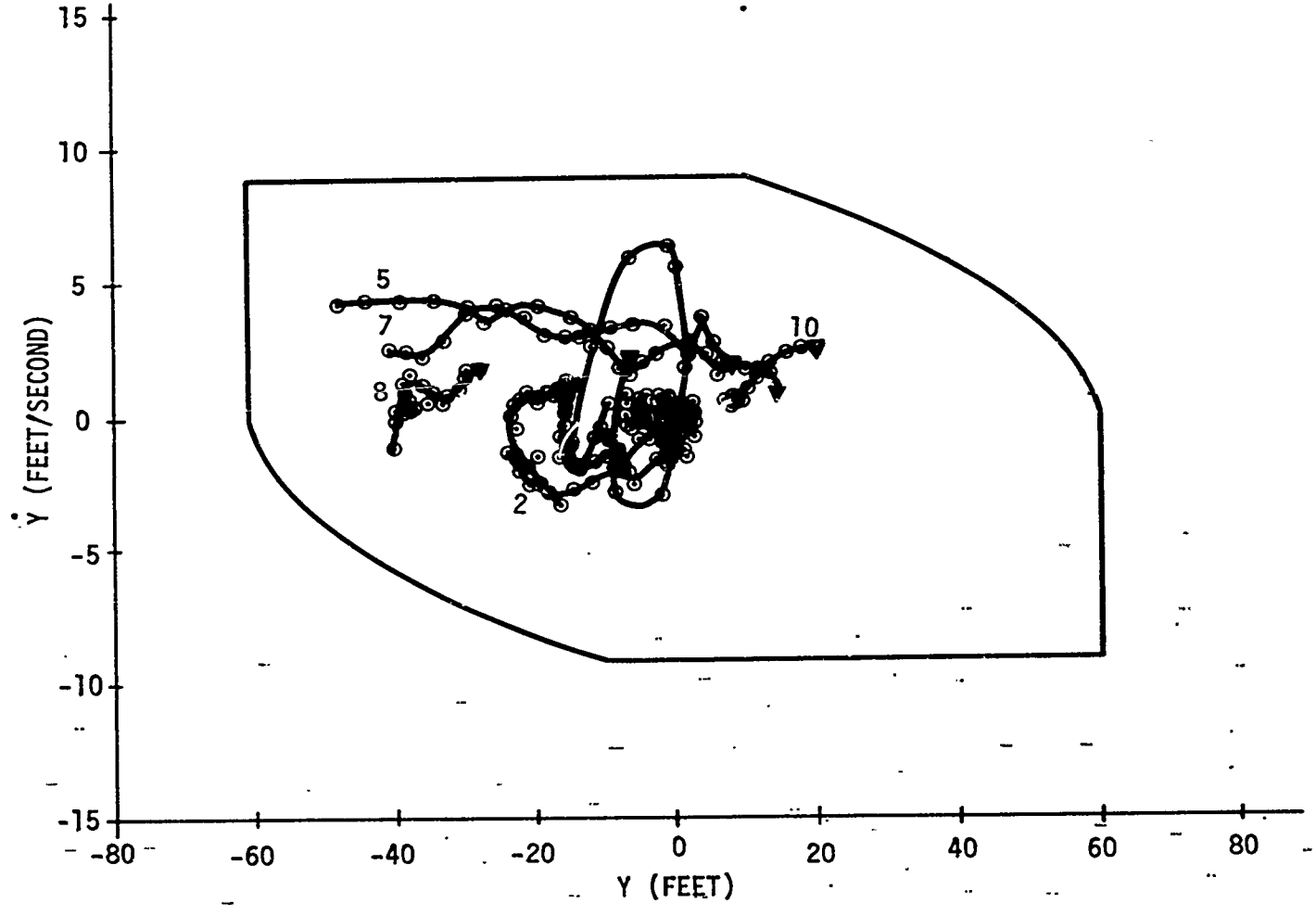

for disturbance number 10. All approaches with System C lie well within the lateral footprint. Note that the trajectories of System A are widely scattered rather than clustered near the origin. System B and C data points are progressively more clustered around the origin. If the trajectories produced by disturbance numbers 5, 7, and 8 (worst case long term high altitude localizer beam anomalies) did not appear in Figure 5.4.6, the clustering of System C responses around the origin would be even more apparent! This graphical comparison of approach data against the footprint criterion clearly shows the performance improvement trend predicted by simulation and analysis.

6.0 ILS BEAM REQUIREMENTS

The discussion in this section is intended to provide an insight into the ILS beam quality requirements as a function of the type of autopilot control law used and the type of operation (Cat II or Cat III). The type of operation dictates the required probability of successfully completing the approach without violating either the maneuver or footprint criteria. As previously noted, these success rates are 95% for Cat II operation and 99.9999% for Cat IIIA operation. Cat IIIA operation or performance is referred to in this section to indicate that rollout control is outside the scope of this study.

In order to maximize the relevance of the beam quality requirements, the beams are categorized in the context of the existing Cat I and Cat II beam inspection specifications (Reference 2). No new beam specifications that are independent of existing specifications are proposed. However, an improved Cat II beam which would result in an across-the-board improvement in performance of all autopilots is defined to ease the difficulty of achieving Cat III performance.

A three dimensional matrix of performance requirement, beam quality and autopilot system would describe the dimensions of the next problem. The concern is whether the required performance can be attained under the various combinations of beam quality and autopilot control laws. Some of the combinations result in an obvious answer. For example: Cat III performance cannot possibly be achieved with a System A autopilot on a Cat I quality beam. At the other extreme, it is expected that Cat IIIA performance can be achieved with a System C autopilot on an improved Cat II Beam.

A statistical approach is taken in this section to define the size of six "bends only" footprint criteria for autopilots A, B and C under both Cat II and Cat IIIA performance conditions. This is done, just as in Section 3.5, by subtracting from the "all causes" footprint criteria an amount which takes into account the deviation variance attributable to all causes except beam bends. Once the six "bends only" footprint criteria in each axis are known, the actual size of the allowable bends can be estimated from analog simulator data. Many hundreds of approaches on each autopilot were made on the simulator during which the approximate airplane response to a wide variety of discrete beam anomalies was determined. The result of this investigation is an approximate definition of the maximum allowable discrete beam anomalies which are tolerable to each of the three autopilots under Cat II and Cat IIIA performance requirements.

The reader is cautioned that this statistical approach to the definition of a group of "bends only" footprint criteria has accuracy limitations and, as such, has limited absolute validity. There are two

Ref. 2 United States Standard Flight Inspection Manual, 217 Instrument Landing System (ILS), OAP 8200.1 CHG 17, October 26, 1970.

principal reasons for this: firstly, the statistical estimate of the effect of "all other causes" is subject to considerable error because very limited flight test data exist and secondly, no account is made for the observation that improbable events occur far more frequently than would be predicted by a Gausian extrapolation from a small sampling. The conclusion is that it is not possible, from a statistical analysis, to be highly confident that any autopilot is capable of landing within the touchdown zone 999,999 times out of one million attempts. This is so because it is equivalent to being confident of the value of a number that is in the sixth significant place. However, it is possible to be reasonably confident about the predicted probability of a given level of performance on a 19 out of 20 basis.

6.1 Cat II Performance on Cat I Beam

The potential of each of the three autopilot control laws to provide Cat II performance while approaching on ILS beams of Cat I quality is considered in this subsection. By definition, Cat II performance results a 95 percent success rate under all combinations of atmospheric and beam disturbances.

6.1.1 Longitudinal Axis

For Category II consideration, the "bends only" footprint (Figure 3.5.2) applies as a valid criterion to the B and C systems because:

(1) it was developed on the basis of 95% probability, and

(2) flight results suggest that the predicted wind dispersion is approximately correct.

This footprint cannot apply to the A system, owing to the poor wind performance. An appropriate CAT II footprint for the A system may be derived by considering the 2 σ wind dispersion derived in Section 4.1.1. Utilizing the same method as that in Section 3.5.1, the "all causes" footprint is reduced to yield an applicable CAT II "bends only" footprint for System A.

These CAT II beam bend footprints for System A, B and C are shown in Figure 6.1.1. The reader is reminded that whenever the airplane trajectory lies within these footprint boundaries, the probability that the airplane will not exceed the "all causes" boundary is greater than .95.

Figure 6.1.2 describes the actual flight traces recorded on a C system approach to Boeing Field on Nov. 10, 1971. This facility is certified for Category I operations to a minimum height of 400 ft. and exhibits a "diving" bend at approximately 3000 ft, range from threshold. It is to be noted from the figure that this particular beam fails to meet Category I or II requirements because of the excessive slope reversal. The System C performance against this beam was excellent according to the remaining flight traces as well as pilot opinion.

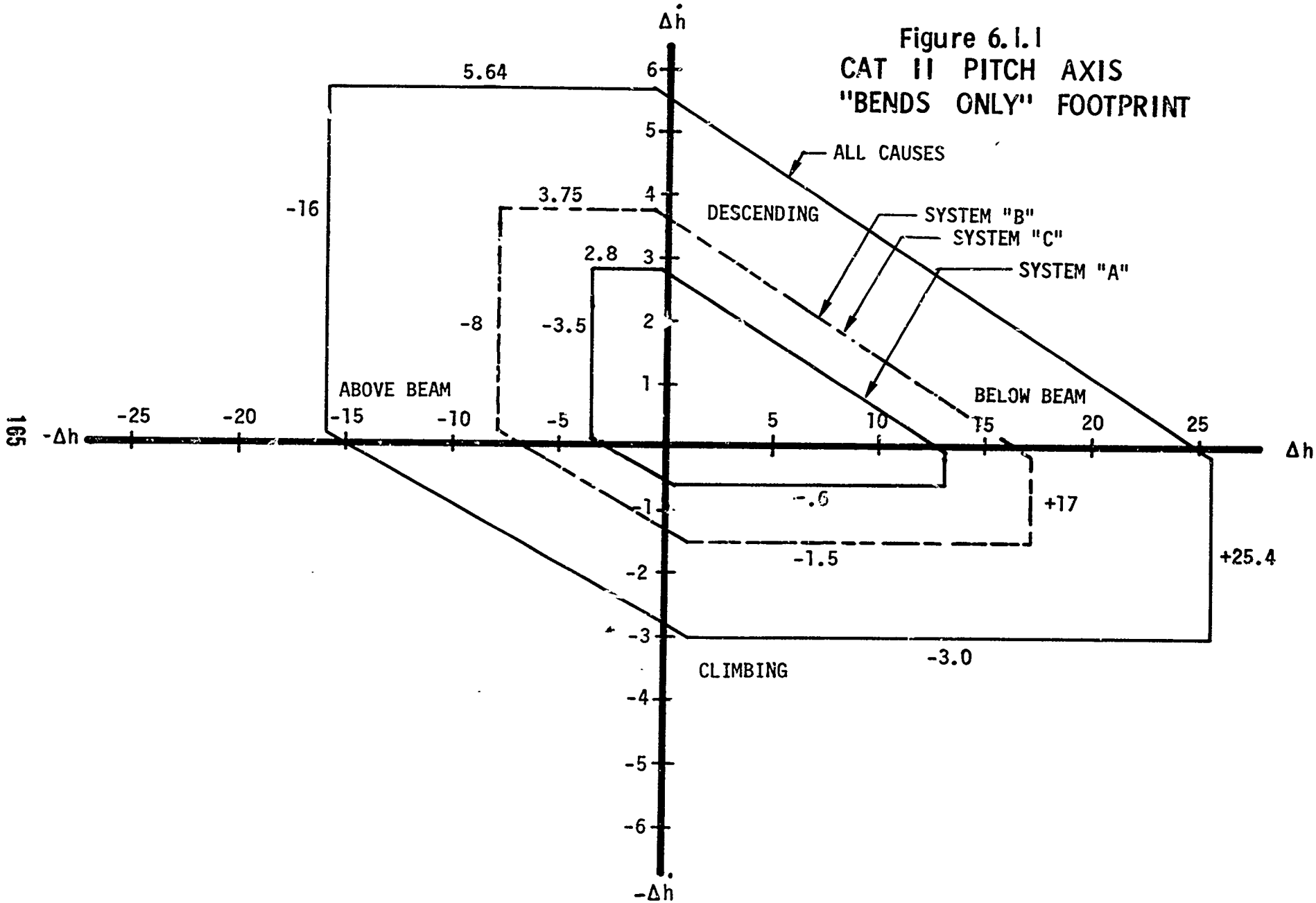

Figure 6.1.1
CAT II PITCH AXIS
"BENDS ONLY" FOOTPRINT

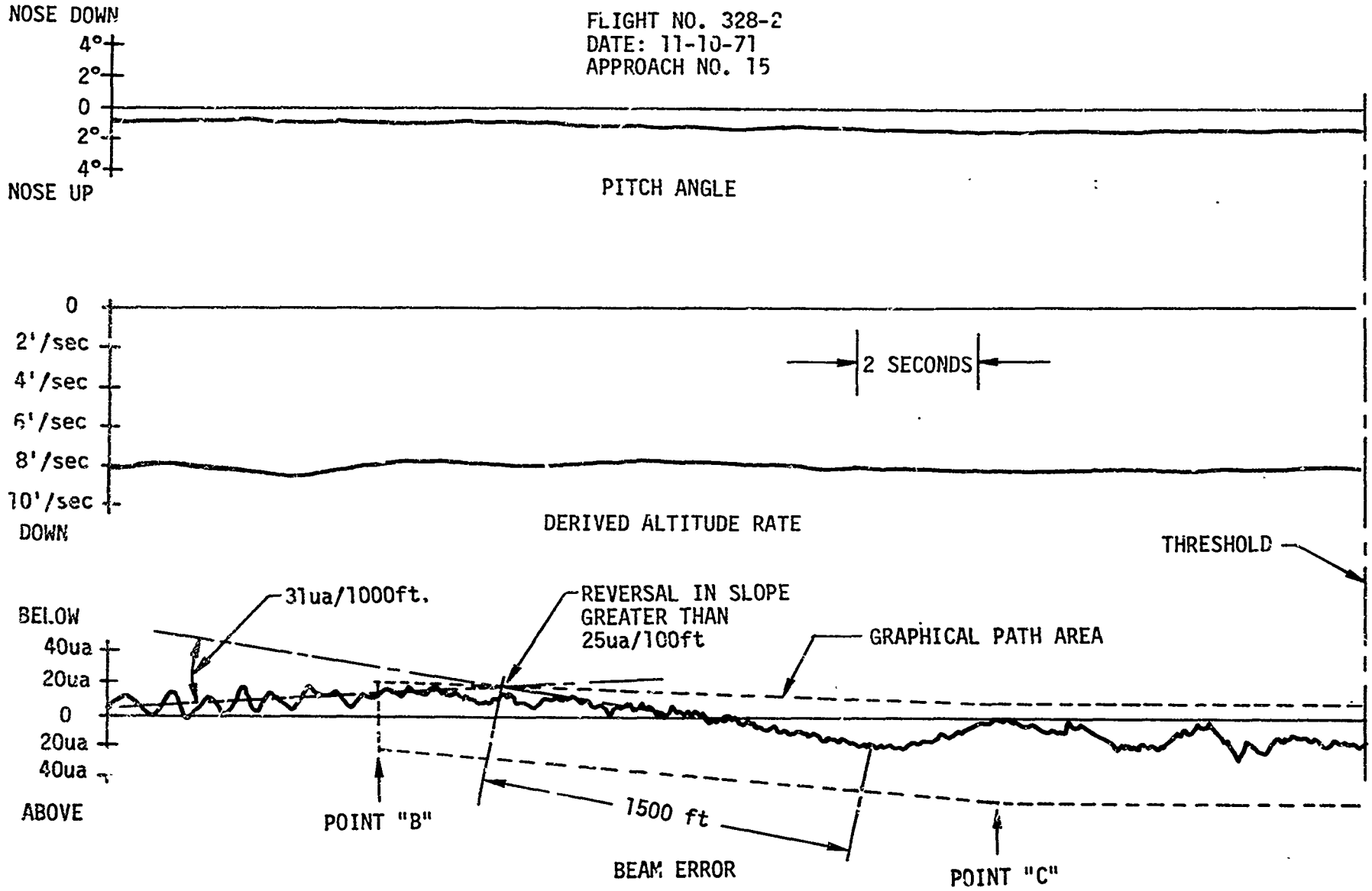

Figure 6.1.2
SYSTEM "C" APPROACH TO BOEING FIELD

6.1.2 Cat II Performance on Cat I Localizer Beam

Achieving Cat II automatic landing performance on Cat I localizer beams is a function of the performance requirements, the characteristics of the Cat I localizer, and the sensitivity of the autoland system to localizer anomalies. Cat II performance is specified by the footprint and maneuver criteria. The characteristics of Cat I localizers must meet the specifications of reference (2). Specific beam signatures meeting the Cat I requirements were hypothesized and the response to these signatures was used to estimate the likelihood of each system achieving the desired performance.

The roll axis "bends only" footprint for System B with the Cat II success rate was determined in Section 3.5.1.2. This reduced footprint allowed the determination of permissible localizer anomalies by constraining autopilot response to them as presented in Section 4.3.2. The maximum allowable average touchdown displacement resulting from deterministic localizer misalignment and bends was determined from autopilot dispersion to all other causes and the required success rate. Recall, from Section 3.5.1.2, that the width of the all causes footprint was reduced by a factor corresponding to the required success rate times the autopilot standard deviation to all other causes. For the Cat II success rate of 19 out of 20 the factor 1.6 is used to multiply the standard deviation. Also the maximum allowable velocity was reduced to the value at which the parabolic constraint in the first and third quadrants intersect the ordinate.

The best estimates of the standard deviation of each system to all causes other than localizer misalignment and bends are:

σ_A = 11.1 feet

σ_B = 8.75 feet

σ_C = 8.0 feet

These estimates are based on (references 1 and 3) together with simulation and flight test experience.

The appropriately reduced footprint widths for Cat II performance are presented in Table 6.1.1.

SYSTEM	CAT II WIDTH
A	42 Feet
B	46 Feet
C	47 Feet

Table 6.1.1. Cat II Roll Axis "Bends Only" Footprints

The "bends only" footprint for System B is shown in Figure 3.5.3. The equivalent footprint for System A would be contracted by four feet

everywhere along the right and left hand boundaries and for System C would be similarly expanded by one foot. The all causes maneuver criterion must be reduced in the same proportion as the footprints (see Section 3.5.2.2).

Figure 6.1.3 shows the Cat I localizer beam specifications from (reference 2). Point A is four nautical miles from threshold. Point B is 3500 feet from threshold and Point C is where the glide path is 100 feet above threshold. Localizer beam center is defined as the average deviation in the region 1500 feet on each side of Point B. The beam center is allowed to vary ± 15 ua from extended runway centerline. The allowable localizer beam bends are specified with respect to beam center. The allowable bends decrease linearly in Zone 2 from 30 ua at Point A to 15 ua at Point B. The specification remains constant at 15 ua from Point B to Point C (Zone 3 for Cat I) and 30 ua beyond Point A (Zone 1). No specification is placed on the Cat I localizer between Point C and the localizer antenna.

The 15 ua allowable misalignment between localizer beam center and extended runway centerline is equivalent to 35 feet for the tailored course width. With bends of an additional 15 ua, the aircraft would have to be outside the all causes footprint to have zero localizer deviation. If the 15 ua bend occurs on a localizer with no misalignment, the problem is less serious.

The comparative response on the simulation to a 25 ua 1-COSINE bend starting at 100 feet and lasting for 10 seconds is shown in Figure 6.1.4. This places localizer zero 58 feet from runway centerline at threshold and is within the Cat I localizer specifications. System A violates the maneuver and footprint criteria. System B does not violate the criteria but comes close. System C performance is well within the acceptable limits with the response less than half of the maximum allowed for "bends only".

Figure 6.1.5 shows an automatic approach and landing made by System C on the return to Boeing Field (BFI) at the end of the fourth test flight. The BFI localizer is at the edge of the Cat I tolerance with a 15 ua beam bend in Zone 3. Pilots report that System A performance on this localizer is marginal since frequently this beam bend causes the aircraft to be outside the extended runway edges between altitudes of 200 to 100 feet. System C shows outstanding performance with the pilot commenting that the approach shown was the best automatic landing that he has seen at BFI.

Performance on Cat I localizers with Cat II success rates is highly dependent on the combination of misalignment and bends at a particular facility. System A is unlikely to make Cat II performance on more than a few Cat I beams. System B is likely to achieve Cat II performance on a fair number of Cat I beams. System C is likely to achieve Cat II performance on almost all Cat I beams and some beams that have short term bends exceeding Cat I tolerances but good alignment. Figure 6.1.6 shows comparative flight data for a well aligned

Figure 6.1.3

CAT I LOCALIZER SPECIFICATIONS

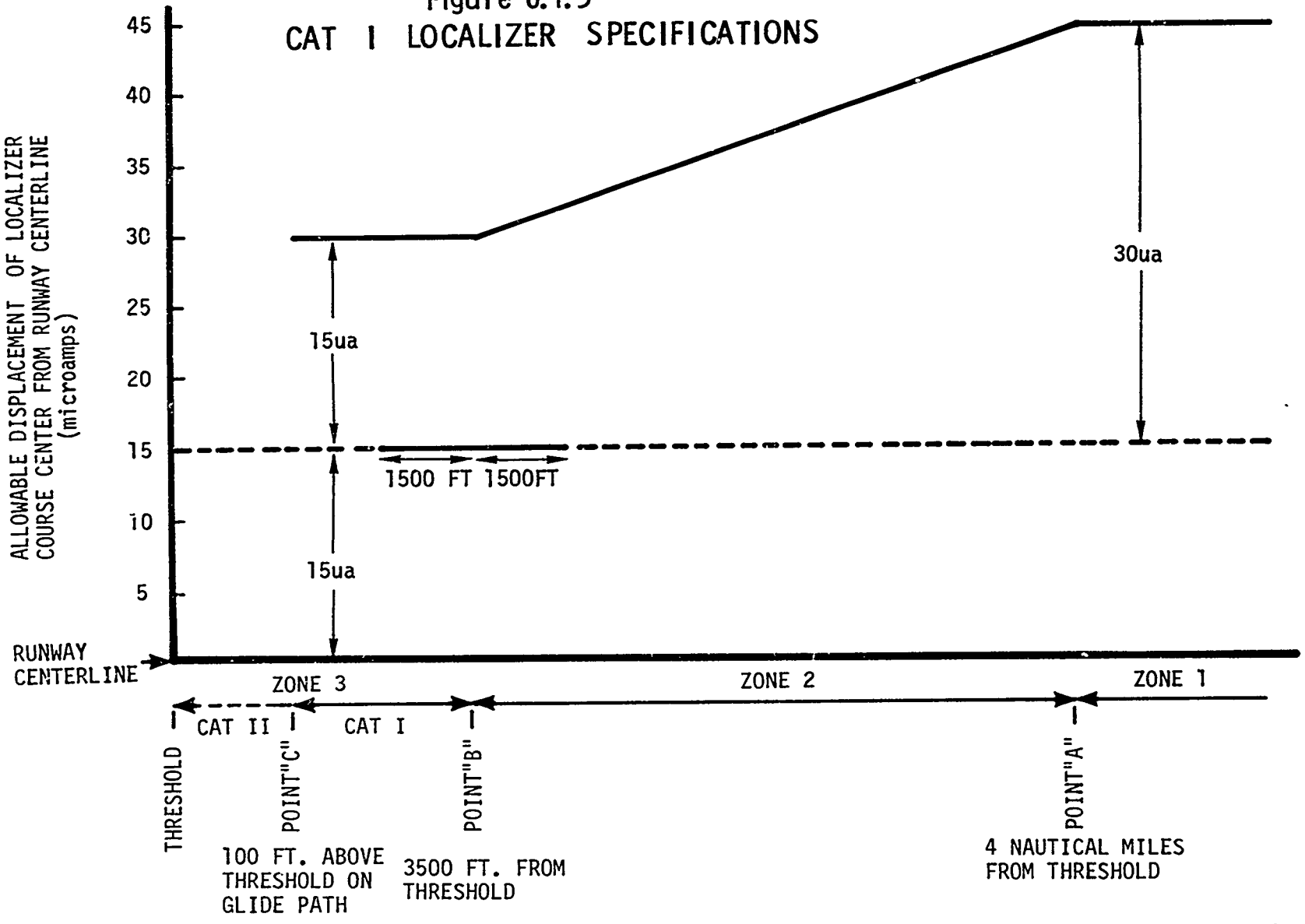

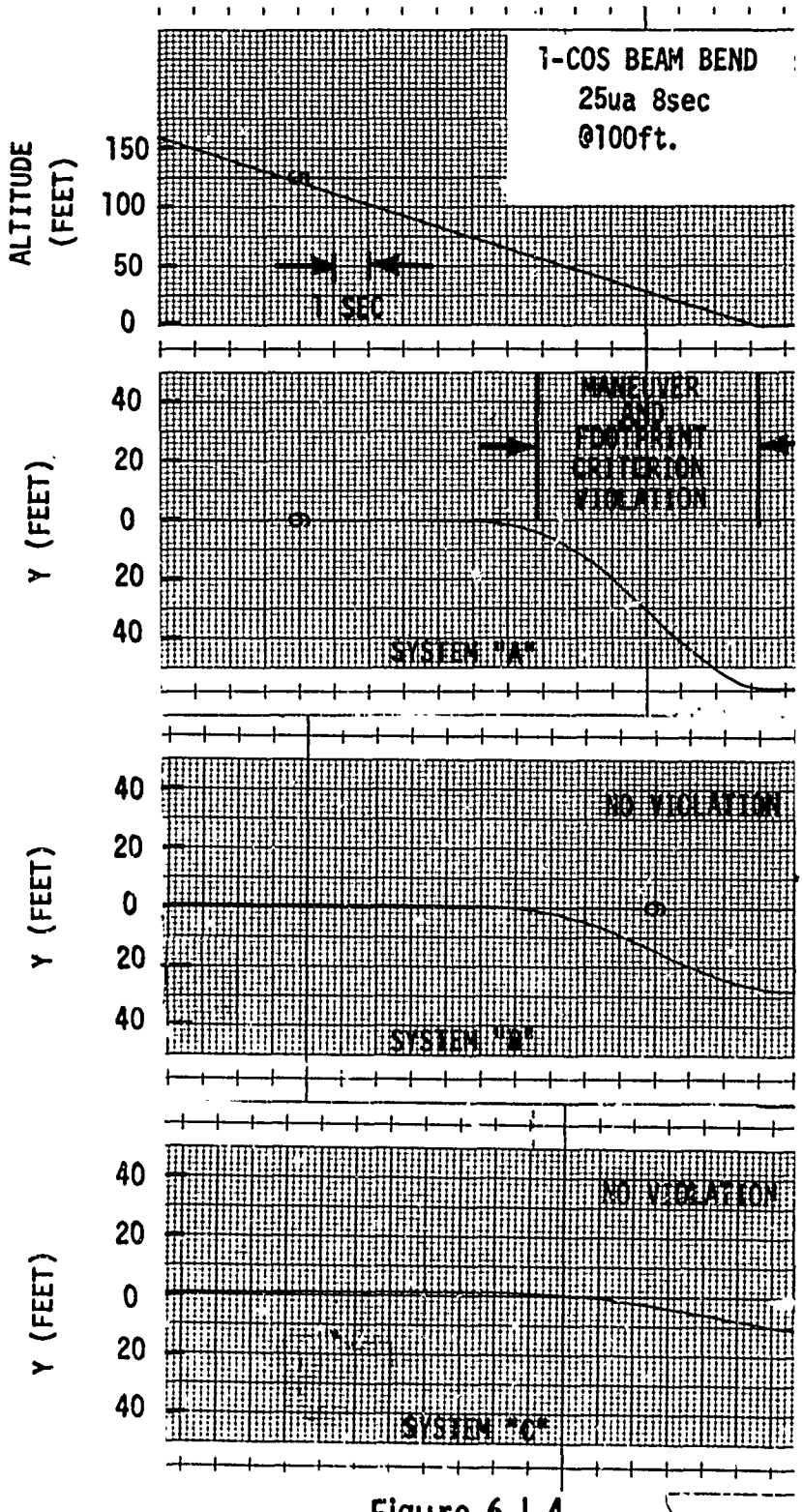

Figure 6.1.4
SIMULATION RESPONSE TO CAT I LOCALIZER BEND

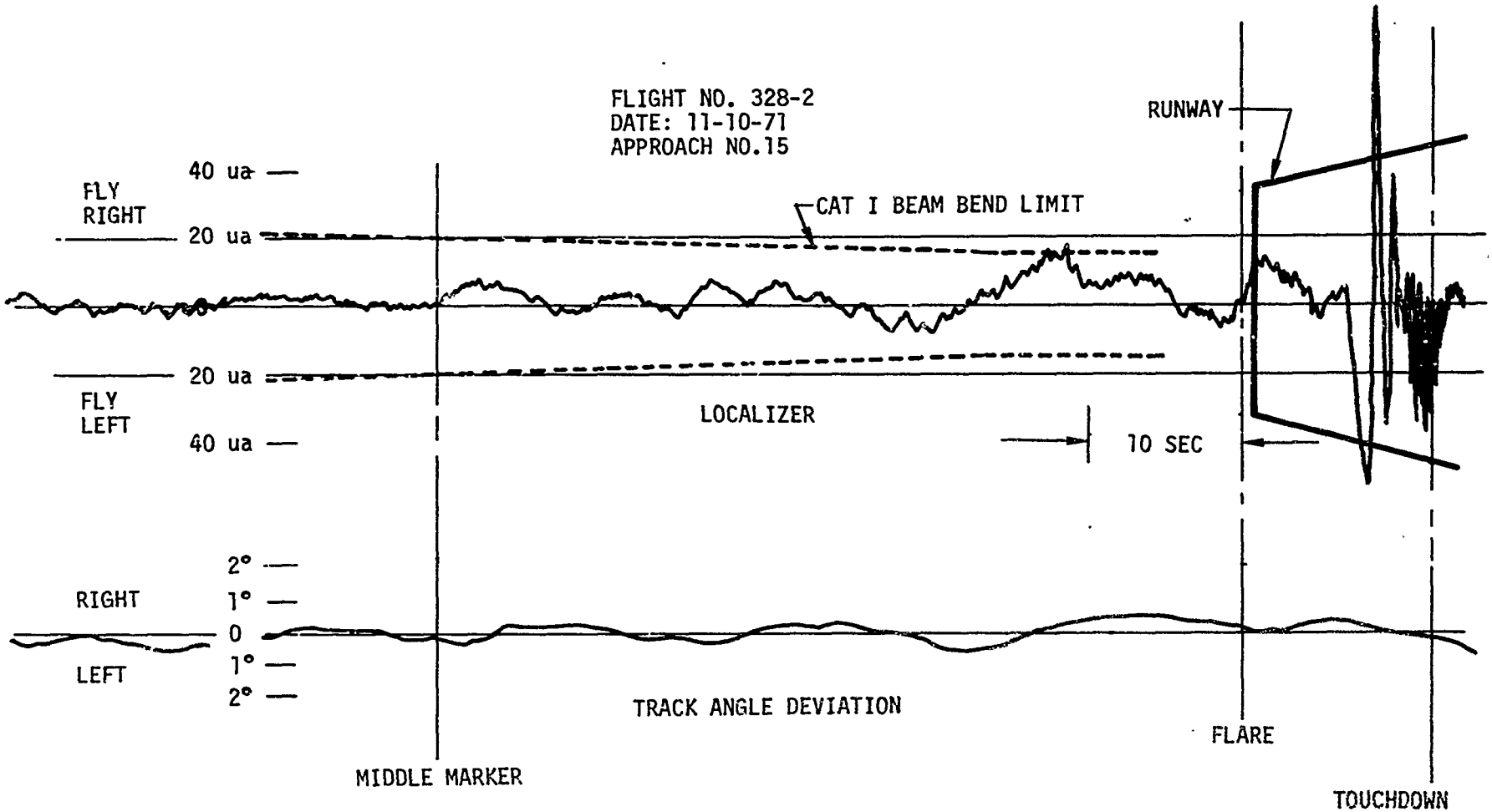

Figure 6.1.5
SYSTEM 'C' APPROACH TO BOEING FIELD

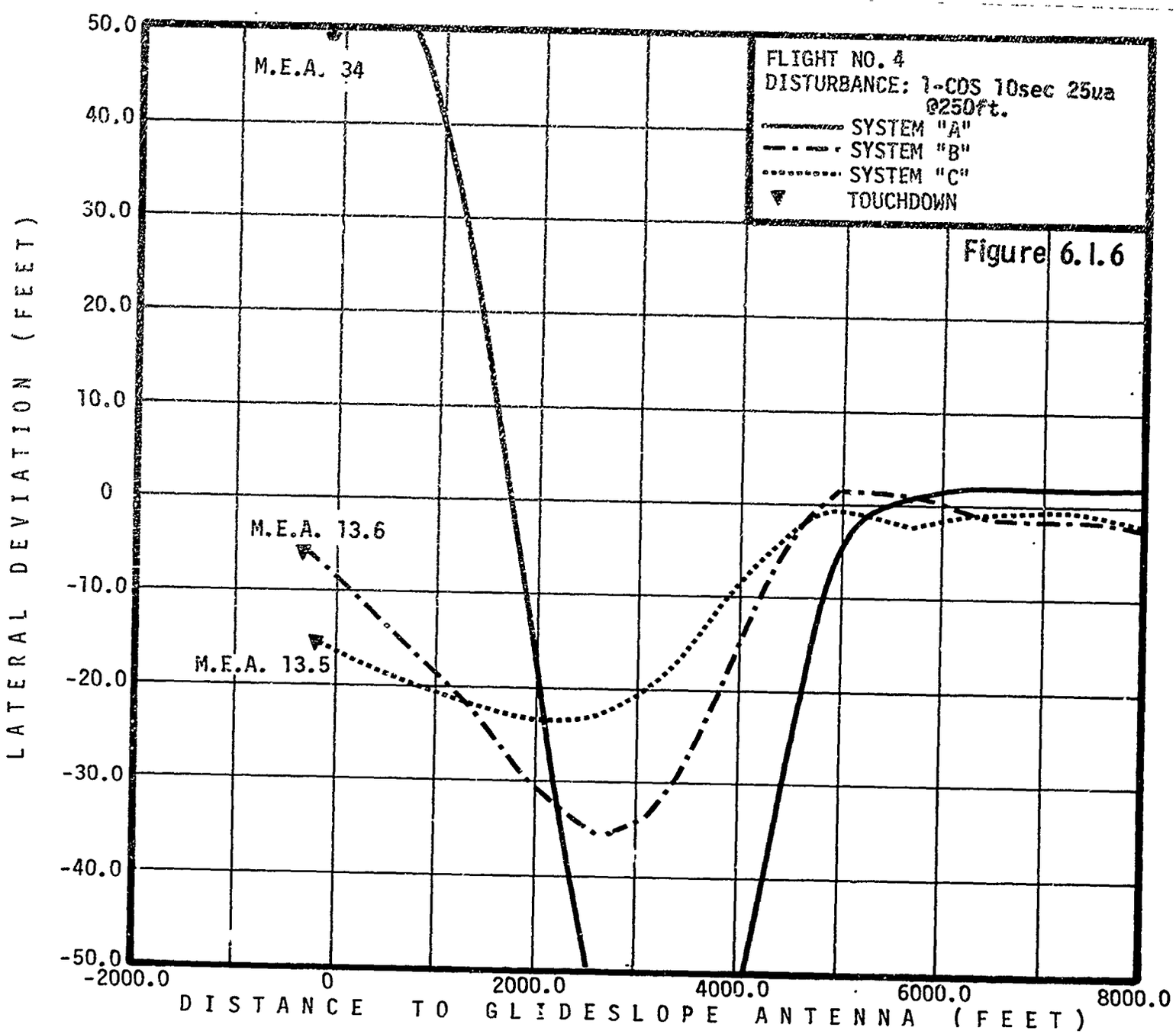
FLIGHT NO. 4
DISTURBANCE: 1-COS 10sec 25ua @250ft.
SYSTEM "A"
SYSTEM "B"
SYSTEM "C"
TOUCHDOWN
M.E.A. 34
M.E.A. 13.6
M.E.A. 13.5
50.0
40.0
30.0
20.0
10.0
0
-10.0
-20.0
-30.0
-40.0
-50.0
-2000.0
0
2000.0
4000.0
6000.0
8000.0
LATERAL DEVIATION (FEET)
DISTANCE TO GLIDESLOPE ANTENNA (FEET)

Figure 6.1.6

localizer with a simulated bend which exceeds Cat I specifications. The System C response to this bend is less than half the maximum allowed by the Cat II footprint and maneuver criteria.

6.2 Cat II Performance on Cat II Beam

The potential of each of the three autopilot control laws to provide Cat II performance while approaching on ILS beams of Cat II quality is considered in this subsection.

6.2.1 Longitudinal Axis

In order to test each system against a Category II quality beam, the long term beam disturbance, illustrated in Figure 6.2.1, was introduced into each of the three simulated systems. This particular disturbance represents the maximum allowable graphical path average under Category II specifications. The system responses, in vertical deviation, to this particular disturbance are shown in Figure 6.2.2. As noted, when compared to the Category II performance footprints in Figure 6.1.1, the A system exceeded the boundary, the B system was marginally acceptable, and the C system was well within the footprint.

Several other comparisons were evaluated on the analog computer with the same results. Thus, it is concluded that against Category II beams, the A system may result in unacceptable performance at some facilities, the B system performance may be marginal at some facilities, and the C system performance is acceptable at all Cat II facilities. However, the reader is cautioned against basing operational conclusions on the foregoing discussion, chiefly because the pitch axis criteria in this report were derived assuming worst case combinations of beam angle and threshold crossing height. For example, it will be shown later that the glide slope configurations may be more optimally designed, thereby expanding the performance criteria boundaries for all systems. Further discussion of this subject is reserved for Section 7.2 but it is emphasized here that System A may meet Category II performance at a given facility, depending upon the beam angle, reference datum and the beam deviations within the graphical path average area.

6.2.2 Lateral Axis

The Cat II localizer specifications given in (reference 2) are shown in Figure 6.2.3. The localizer beam center is defined as the average indicated deviation between Point B and threshold (Zone 3 for Cat II). Beam center must be within 11 ua of extended runway centerline. In Zone 1, beam bends up to 30 ua from beam center are allowed (this is the same as Cat I). In Zone 2, the allowable bends decrease linearly from 30 ua at Point A to 5 ua at Point B and remain constant at 5 ua in Zone 3.

The 11 ua allowable misalignment translates to 26 feet at tailored course width. Similarly the allowable 5 ua bends are equivalent to 12 feet. The combination of allowable misalignment and bends for the Cat II localizer is about half of that specified for Cat I.

Figure 6.2.1
CAT II GLIDESLOPE BEAM INSPECTION LIMITS
(for case where actual path = commissioned angle)

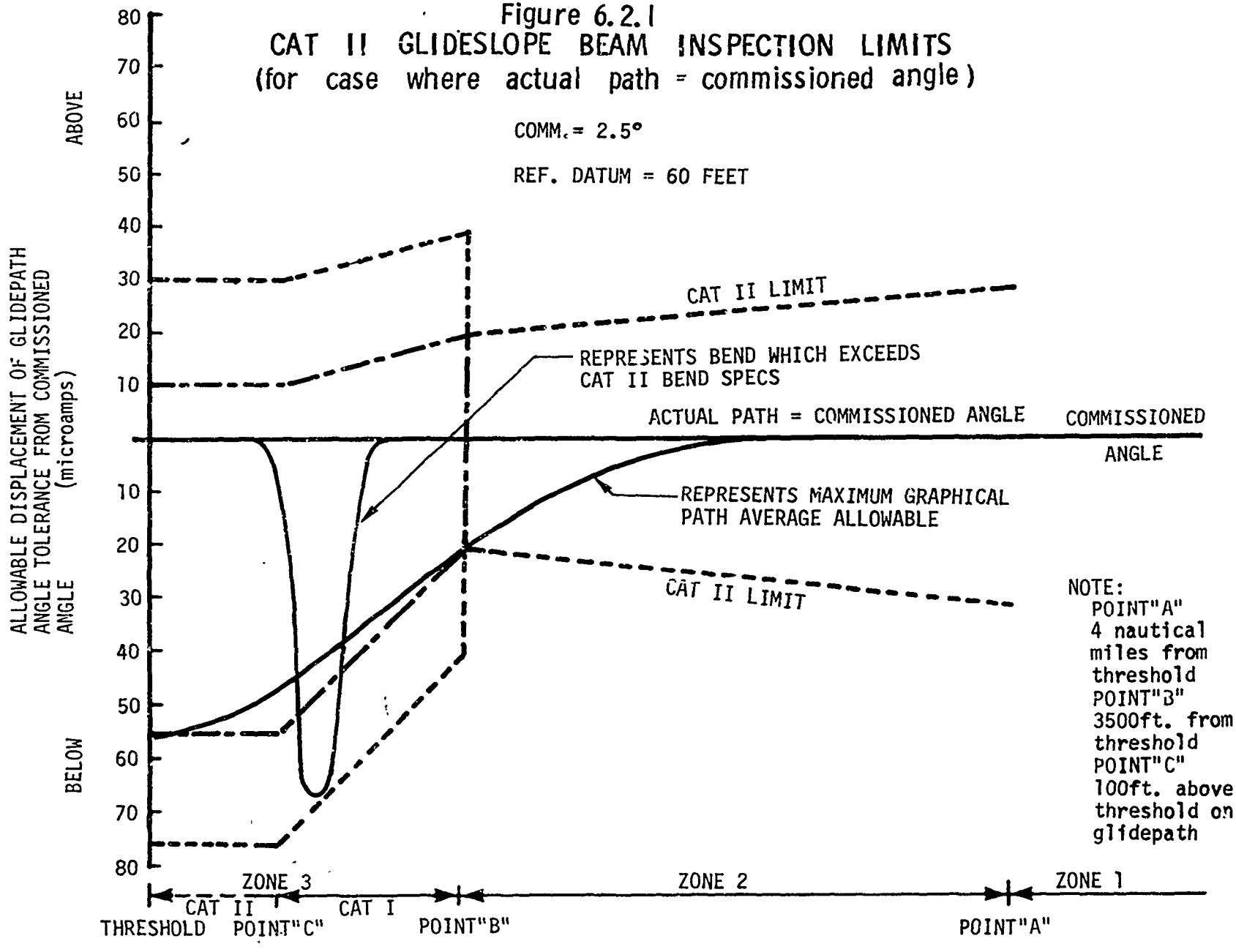

Figure 6.2.2

RESPONSES TO MAXIMUM GRAPHICAL PATH AVERAGE
FOR THE LONGITUDINAL AUTOLAND SYSTEMS.

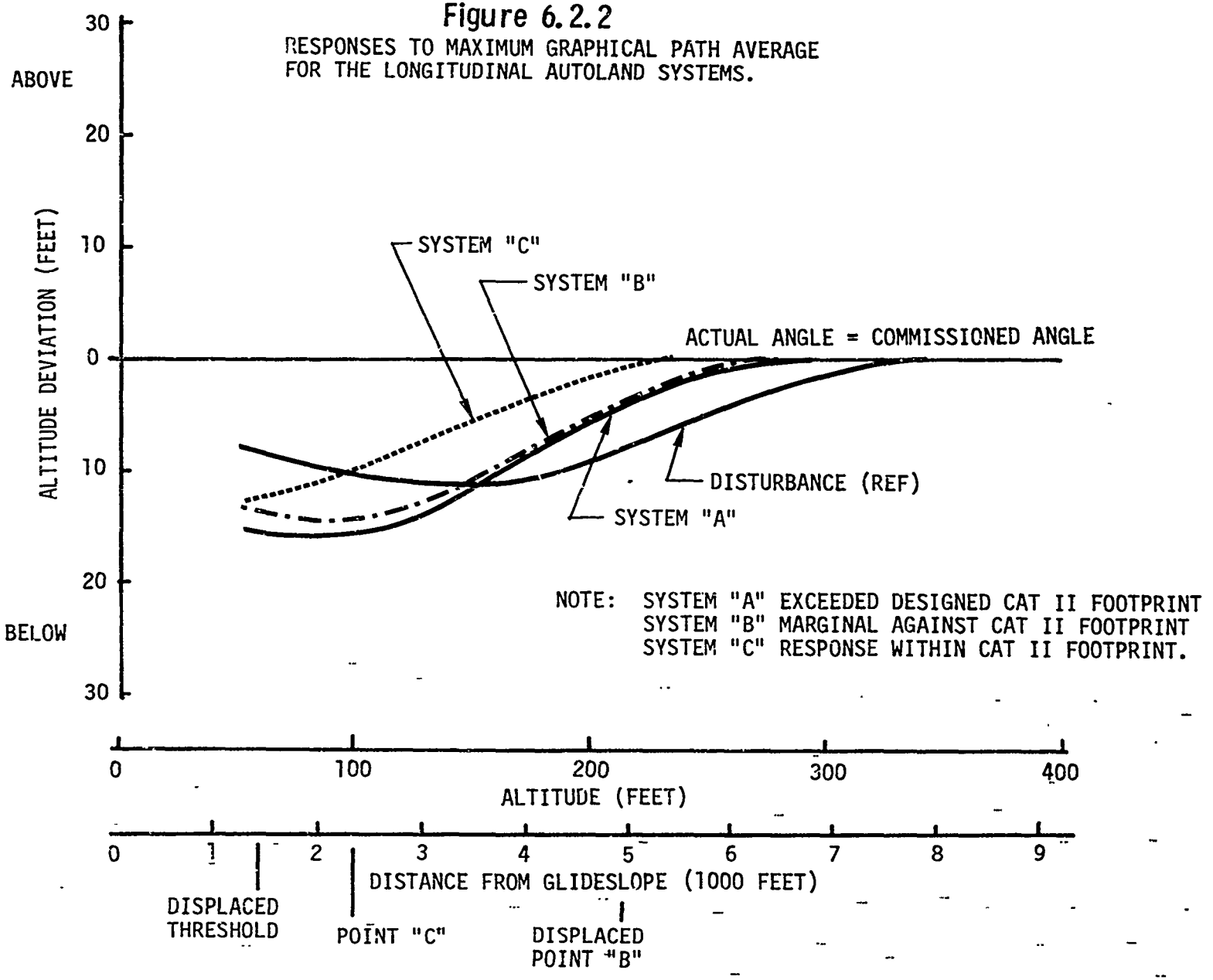

Figure 6.2.3
CAT II LOCALIZER SPECIFICATIONS

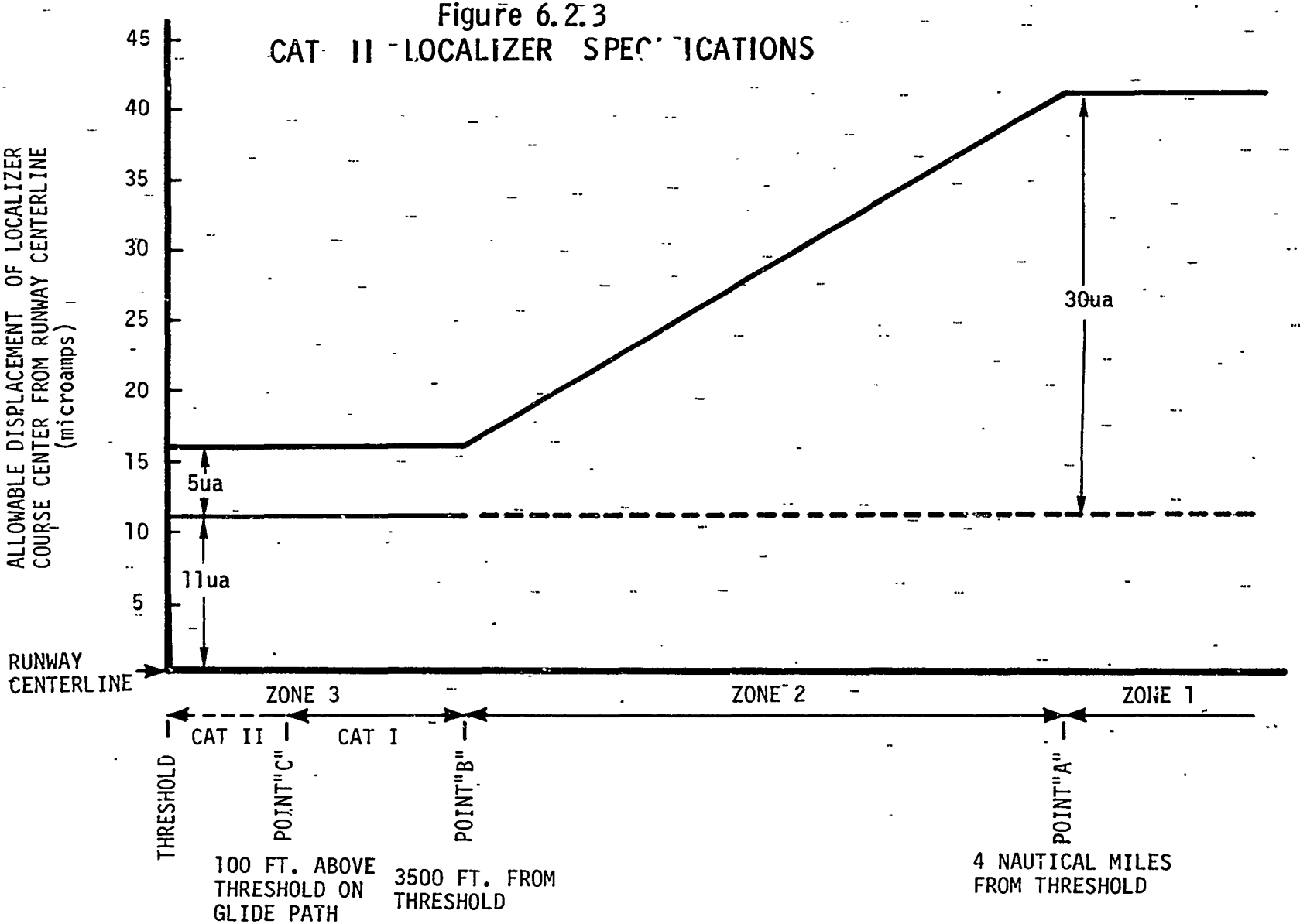

In general, all three systems can make Cat II performance on Cat II localizer beams. However, System A meets the performance level with almost no margin. System B has more margin than System A. And System C has sufficient margin that it can achieve Cat II performance on a Cat I localizer beam.

The difference in performance margin is apparent when a misalignment is combined with the permissible bends. Figure 6.2.4 shows the flight data from a simulated localizer misalignment of 8 ua in addition to an 8 ua 1-COSINE bend with 8 second period starting at 200 feet of altitude. This localizer is within Cat II tolerances because the bends are allowed to exceed the specified level for 2 seconds out of each 10 second interval for an aircraft with a ground speed of 100 to 110 knots. System A does not meet Cat II performance on this simulated localizer which is within Cat II specifications. System A violated the all causes maneuver criterion as well as its Cat II "bends only" footprint. System B and C suppress the response to the bend so that the affect of the misalignment predominates. Both System B and C satisfied their Cat II "bends only" footprint and maneuver criteria.

6.3 Cat II Operation on Out-of-Spec Cat II Beam

The possibility of relaxing some of the Cat II beam inspection limits without incurring a serious penalty in resultant autopilot performance is considered in this subsection.

6.3.1 Longitudinal Axis

The performance of the three systems against a glide slope beam which fails to meet Category II inspection requirements is illustrated in Figure 6.3.1. A comparison of the system responses against the short term bend of Figure 6.2.1. It can be seen in Figure 6.3.1 that all three systems remain within their respective Category II performance criteria boundaries. However, it is especially emphasized that the response of the C system is negligible and, hence, will easily tolerate bends of much greater amplitude and duration.

The bend used in this comparison was introduced at an altitude of 150 feet. Thus, the relatively small responses by all three systems testify for the hypothesis that beam information has minor effect at these low altitudes. Thus, all three systems perform satisfactorily against this particular disturbance. However, at higher altitudes, the A and B systems would easily exceed the maneuver criterion boundary when subjected to this same disturbance, while the C system would likely be quite satisfactory.

This single illustration points out one important fact. The use of an inertially smoothed control law opens the possibility of achieving Category II performance on certain ILS beams where the transmitted signal cannot be retained within Category II limits. Whether this can actually be achieved depends, of course, on the exact discrepancy that causes the problem. A careful flight check with an inertially smoothed autopilot at each problem facility would have to be made to confirm performance.

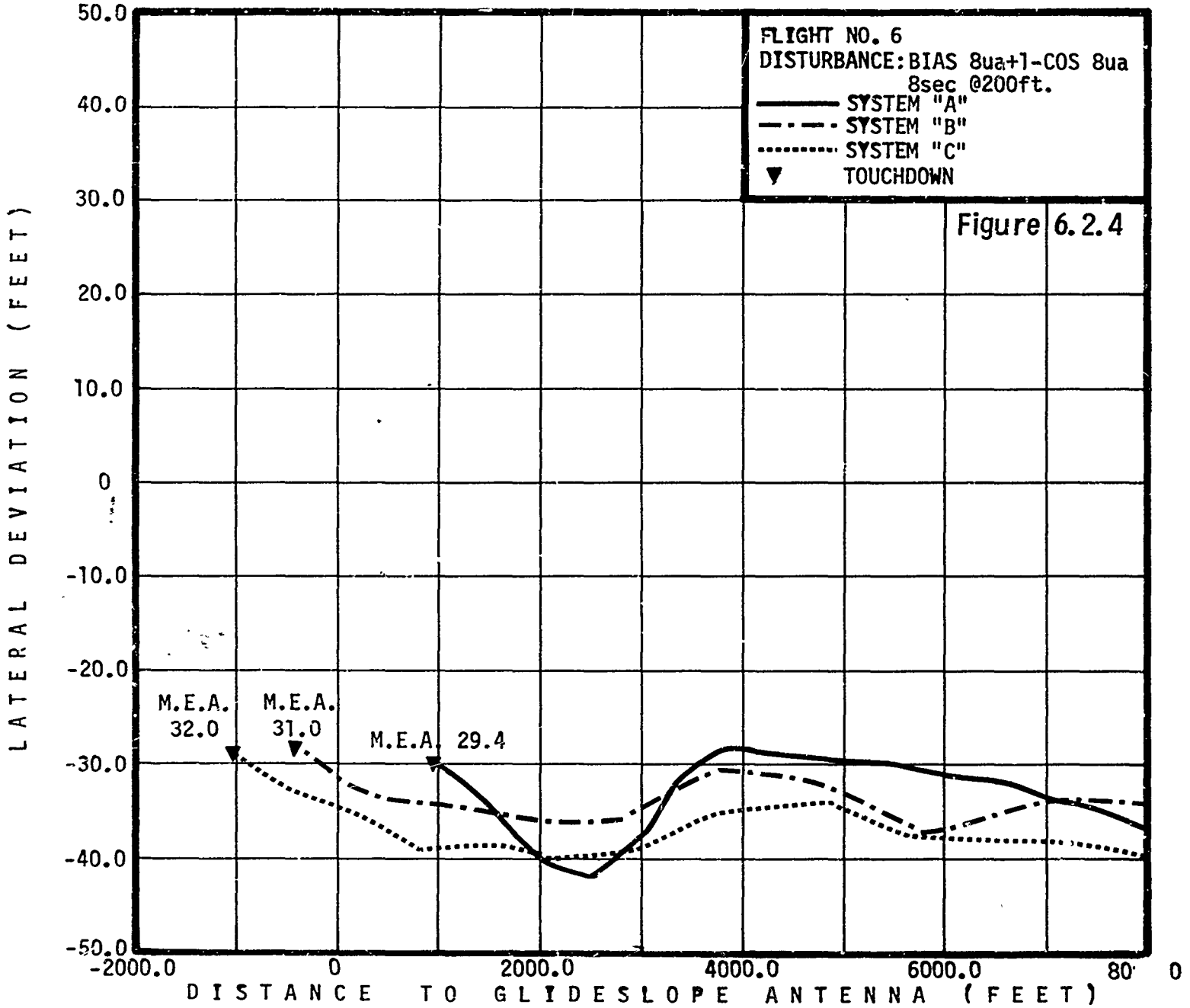
FLIGHT NO. 6
DISTURBANCE: BIAS 8ua+1-COS 8ua
8sec @200ft.
SYSTEM "A"
SYSTEM "B"
SYSTEM "C"
TOUCHDOWN
Figure 6.2.4
LATERAL DEVIATION (FEET)
50.0
40.0
30.0
20.0
10.0
0
-10.0
-20.0
-30.0
-40.0
-50.0
M.E.A. 32.0
M.E.A. 31.0
M.E.A. 29.4
-2000.0
0
2000.0
4000.0
6000.0
80
0
DISTANCE TO GLIDESLOPE ANTENNA (FEET)

Figure 6.3.1

RESPONSES OF THE THREE SYSTEMS TO A BEAM BEND WHICH EXCEEDS CAT II ALLOWANCES.

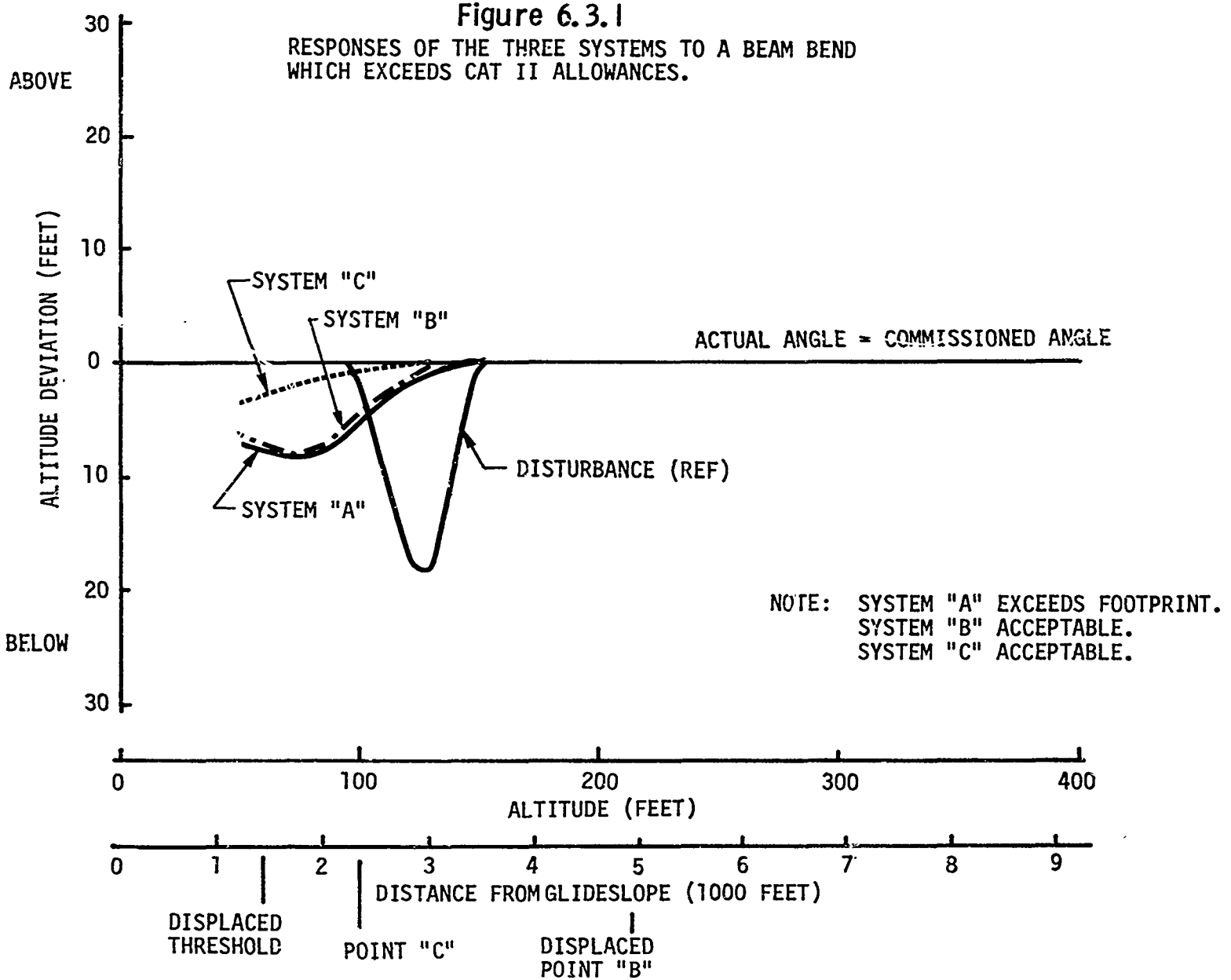

6.3.2 Lateral Axis

The out-of-spec Cat II beam decreases the margin in Cat II performance. The margin of each system in achieving Cat II performance on a Cat II localizer which is within Cat II tolerances was presented in Section 6.2.2. The small margin of System A does not permit Cat II performance if the localizer is much outside the Cat II specifications. In fact, some localizers within Cat II specifications prevent System A from achieving Cat II performance. System B has a larger footprint and reduced sensitivity to beam bends which allow System B to meet Cat II performance requirements on localizer beams further outside Cat II tolerances than the beams on which System A is successful. System C can achieve Cat II performance on Cat I localizers so the out-of-spec Cat II localizer could be as bad as Cat I tolerances and still permit System C to meet Cat II performance requirements.

6.4 Cat IIIA Performance on Cat II Beam

The potential of each of the three autopilot control laws to provide Cat IIIA performance while approaching on any Cat II ILS beam is considered in this subsection.

6.4.1 Longitudinal Axis

The "all causes" footprint cannot be reduced in a practical sense to cover Category IIIA operation. That is, the variance of a 4.9 σ distribution for the "all causes" footprint is less than the variance of the wind-induced deviation, even for systems B and C. Hence, no allowance can be made for the beam irregularities. Thus, none of the three autoland systems is capable of meeting the Category IIIA performance requirements as measured by the "all causes" footprint boundary in this report.

6.4.2 Lateral Axis

The three roll axis "bends only" footprints for the Cat II success rate were determined in Section 6.1.2. Now for Cat IIIA, the success rate is 999,999 out of 1,000,000 approaches and the multiplying factor on the standard deviation is 4.75. Using the autopilot standard deviations listed in Section 6.1.2, the appropriately reduced footprint widths for Cat IIIA performance are presented in Table 6.4.1.

SYSTEM	CAT IIIA WIDTH
A	7
B	18
C	22

TABLE 6.4.1. CAT IIIA ROLL AXIS "BENDS ONLY" FOOTPRINTS

The three Cat IIIA "bends only" footprints together with the all causes footprint are shown graphically in Figure 6.4.1. The all causes maneuver equation must be reduced in the same ratio as the footprints (see Section 3.5.2.2).

The Cat IIIA "bends only" footprint for System A is only 7 feet wide. This is equivalent to 3 ua on the tailored course width for the combined effects of misalignment and bends. Thus, it is highly unlikely that System A can achieve Cat IIIA performance on Cat II localizers.

Neither System B nor System C can achieve Cat IIIA performance on all Cat II localizers since a misalignment of 25 feet is within specifications and there is no requirement to reduce such a misalignment.

6.5 Cat IIIA Performance on Improved Cat II Beam

The potential of each of the three autopilot control laws to provide Cat IIIA performance while approaching on an improved CAT II ILS beam is considered in this subsection.

6.5.1 Longitudinal Axis

To achieve good performance, all autopilots fundamentally rely upon accurate adjustment of the ILS beam average center and sensitivity. It is clear, for instance, that if a localizer beam is biased off runway center 10 ua all along the approach course, the airplane will, on average, land offset by the equivalent number of feet; 23 feet in this instance. It is possible to say 23 feet because the localizer beam sensitivity is purposely adjusted to provide a standard sensitivity (feet to microamps) in the touchdown zone at all facilities. Considerable effort is made to accurately position the course center and adjust the sensitivity of localizer beams to a common standard for all facilities. This effort has its reward in providing a near zero mean for lateral axis displacement error. Also, because of standardized beam sensitivity, approach coupler gain programming can be provided nearly constant lateral guidance feedback gain to the autopilot. This provides for uniform autopilot tracking performance at all facilities. To a large degree, because of this care in localizer beam centering and sensitivity, the B and C system autopilots, as pointed out in Section 6.4.1, may well be capable of Cat IIIA performance on Cat II or Cat III beams.

Glide slope beams, by comparison to localizer, are permitted to have a wide variation in the position of average beam center and also in sensitivity. Figure 6.5.1 illustrates the extreme glide slope beam angle and threshold crossing height allowable by Cat II specifications. The pitch axis footprint and maneuver criteria developed in Section 3.3 were derived by assuming that the maximum allowable above ideal path error was constrained by a 2.5 degree beam with a threshold crossing height of 60 feet. Similarly, the maximum allowable below beam error was constrained by a 3.0 degree beam with a threshold crossing height of 47 feet. The resulting footprint was then appropriate for

Figure 6.4.1
CAT III A ROLL AXIS "BENDS ONLY" FOOTPRINTS

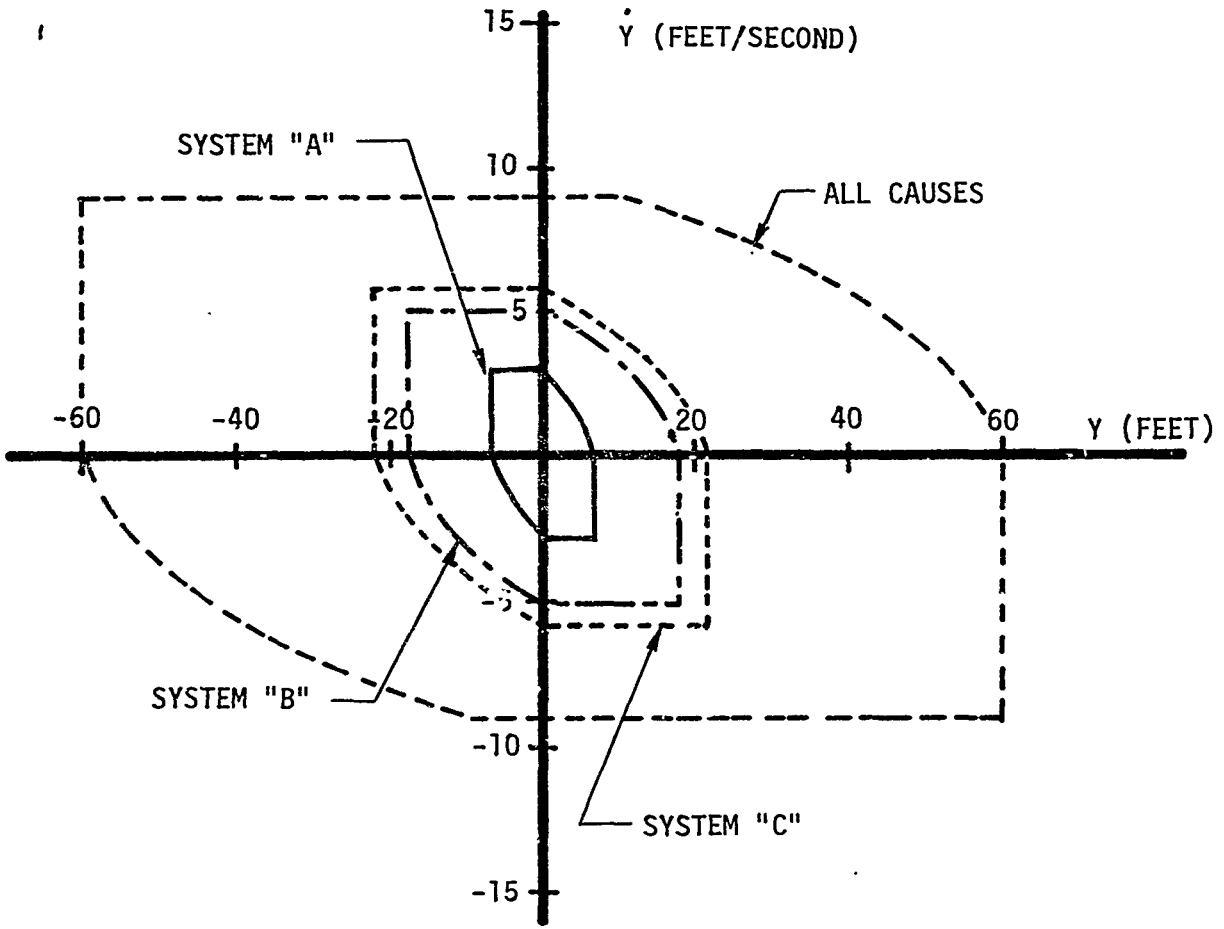

Figure 6.5.1
CAT II GLIDE PATH SITING EXTREMES

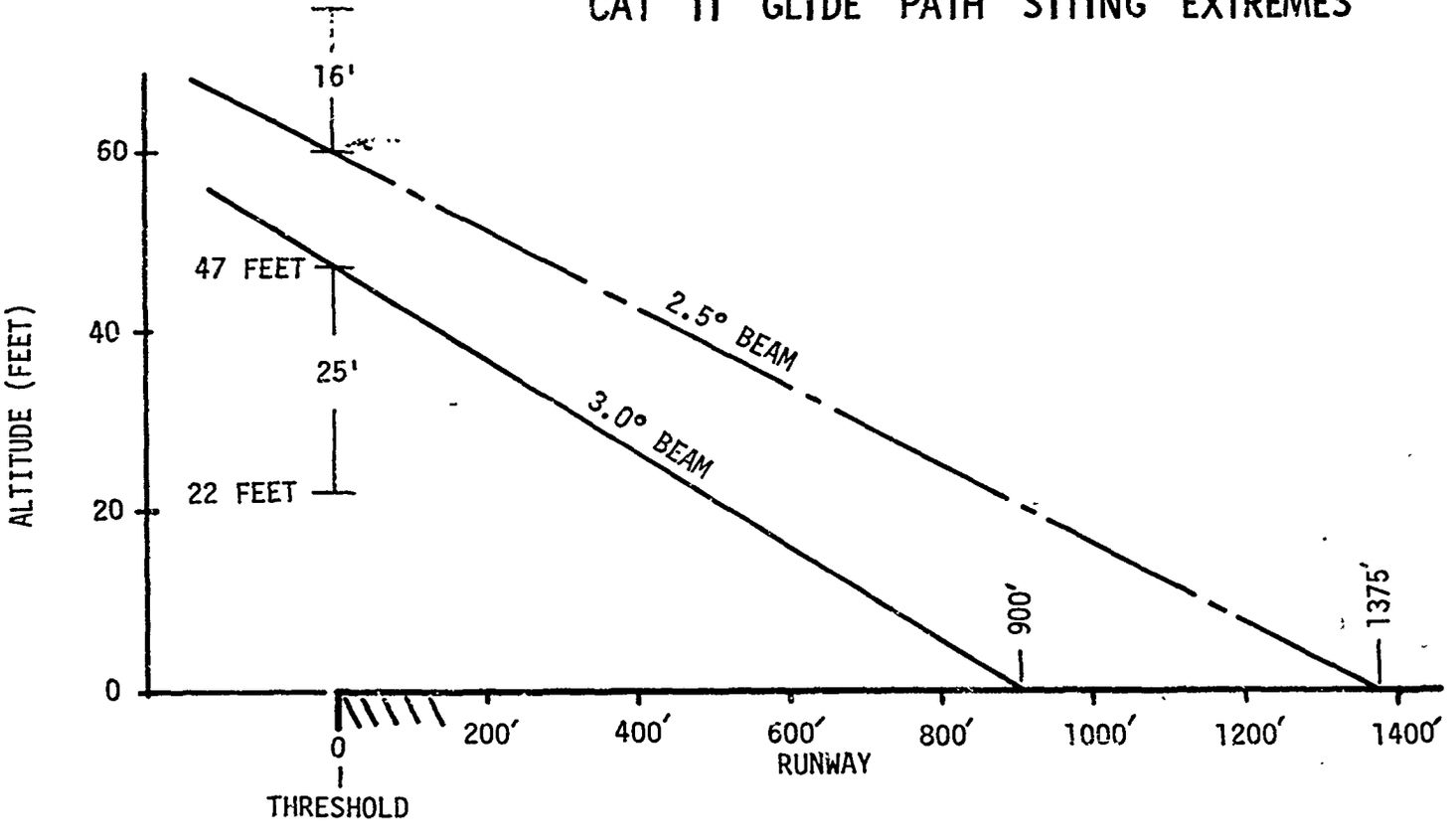

the worst case sites in the whole population of Cat II glide slope beams. The footprint is so confining that a performance success rate of 99.9999 percent is not possible with any of the three autopilots.

In view of the fact that the footprint which applies to the whole population of Cat II glide slope facilities is so confining, it is of interest to consider the advantages that would accrue from a standardization of glide slope beam sites. In Figure 6.5.2 a 2.5 degree and a 3.0 degree "optimally" located glide slope beams are illustrated. The apparent point of emination of these two beams is approximately 1170 feet down runway. At this location, and with the given threshold crossing heights, the probability of landing between 300 feet and 2500 feet down runway is maximized. This statement is predicated upon the use of a flare coupler with performance as specified in Section 3.3. Were all 2.5 and 3.0 degree beams sited as in the Figure, the resulting maximum allowable above and below beam displacement error limits for corresponding footprints would be as shown. These limits were calculated with the same equations as were used to determine the far more confining "all facilities" footprint.

The threshold crossing heights in Figure 6.5.2 were purposely chosen to allow a larger below beam error than above beam error. This is because autopilots will fall below beam more often than above. This is a result of gain programming as a function of radio altitude. If the airplane is below beam, the glide slope feedback gain is low and oppositely when above beam. Thus, if the airplane is below beam, it will not climb back up to the beam as rapidly as it would descend if it were above beam.

For an "optimally" located 2.5 degree beam, the top to bottom footprint dimension is 54 feet as opposed to 41 feet for the "all facilities" footprint. For an "optimally"located 3.0 degree beam, the top to bottom footprint is 69 feet.

The "optimally" located 3.0 degree beam leads to the footprint shown in Figure 6.5.3. The corresponding "bends only" footprint, determined by taking into account all other causes on a 4.75σ basis is also shown in the Figure. This Cat III "bends only" footprint is nearly the same size as the Cat II "bends only" footprint applicable to all facilities as given in Figure 6.1.1. That is to say that the bends allowance on a Cat III Beam can be the same as presently apply for Cat II beams if a standard 3.0 beam with a 60 foot threshold crossing height is used. There is then, a great potential advantage in standardizing the siting of glide slope beams.

6.5.2 Lateral Axis

It is unlikely that localizer installations in general could be improved to meet the 3 ua requirement for combined effects of misalignment and bends which would enable System A to meet Cat IIIA performance. A localizer improved to maintain alignment within 11 feet of runway centerline and with the presently specified 5 ua bends in Zone 3 would allow System B to achieve Cat IIIA performance. A localizer improved to maintain alignment within 15 feet would allow System C to achieve Cat IIIA performance even if the Zone 3 bend specification were relaxed to 10 ua.

Figure 6.5.2
OPTIMUM GLIDEPATH LOCATION

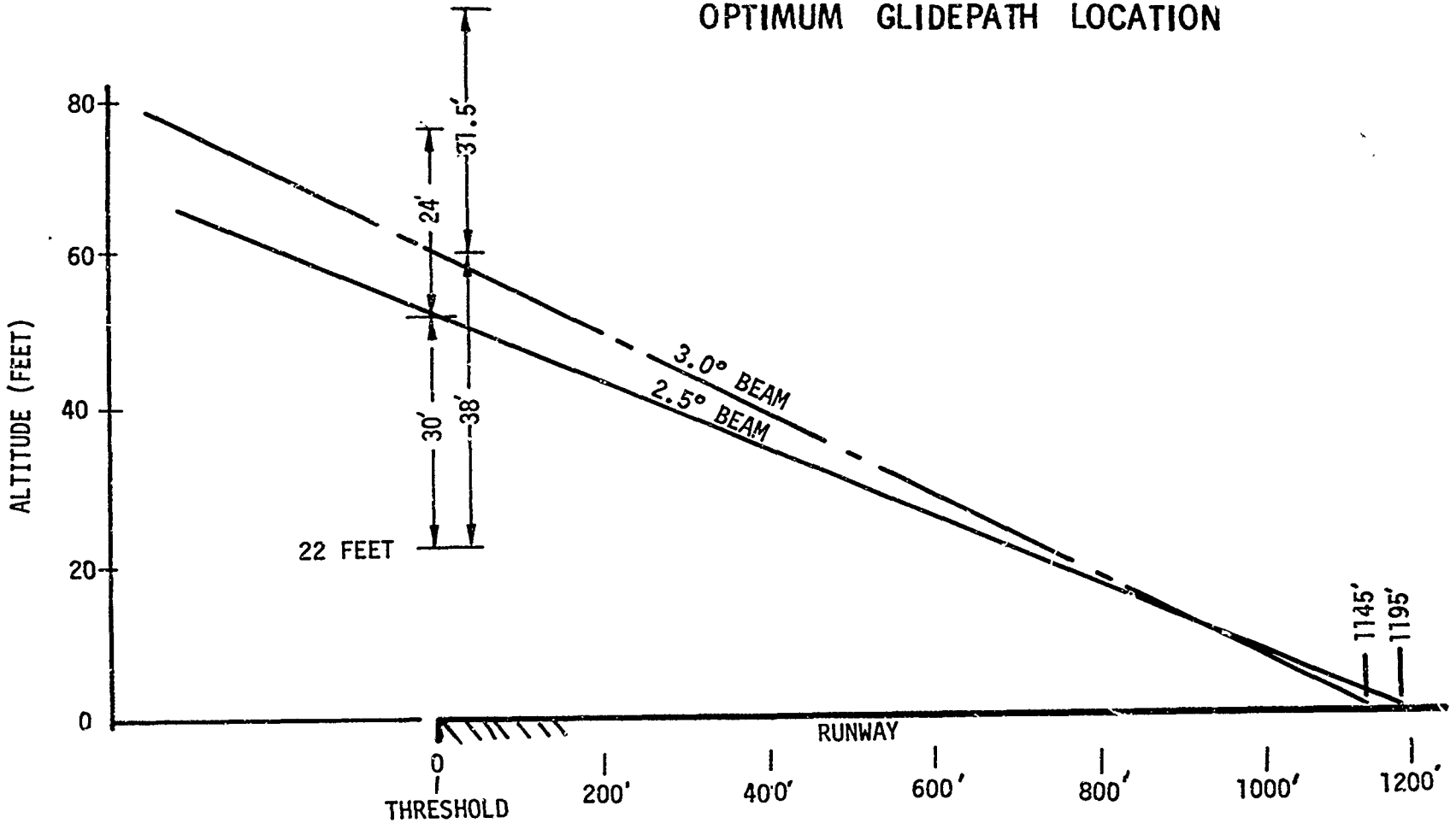

Figure 6.5.3
PITCH AXIS FOOTPRINT CRITERION
FOR "OPTIMALLY" LOCATED 3.0 DEGREE BEAM

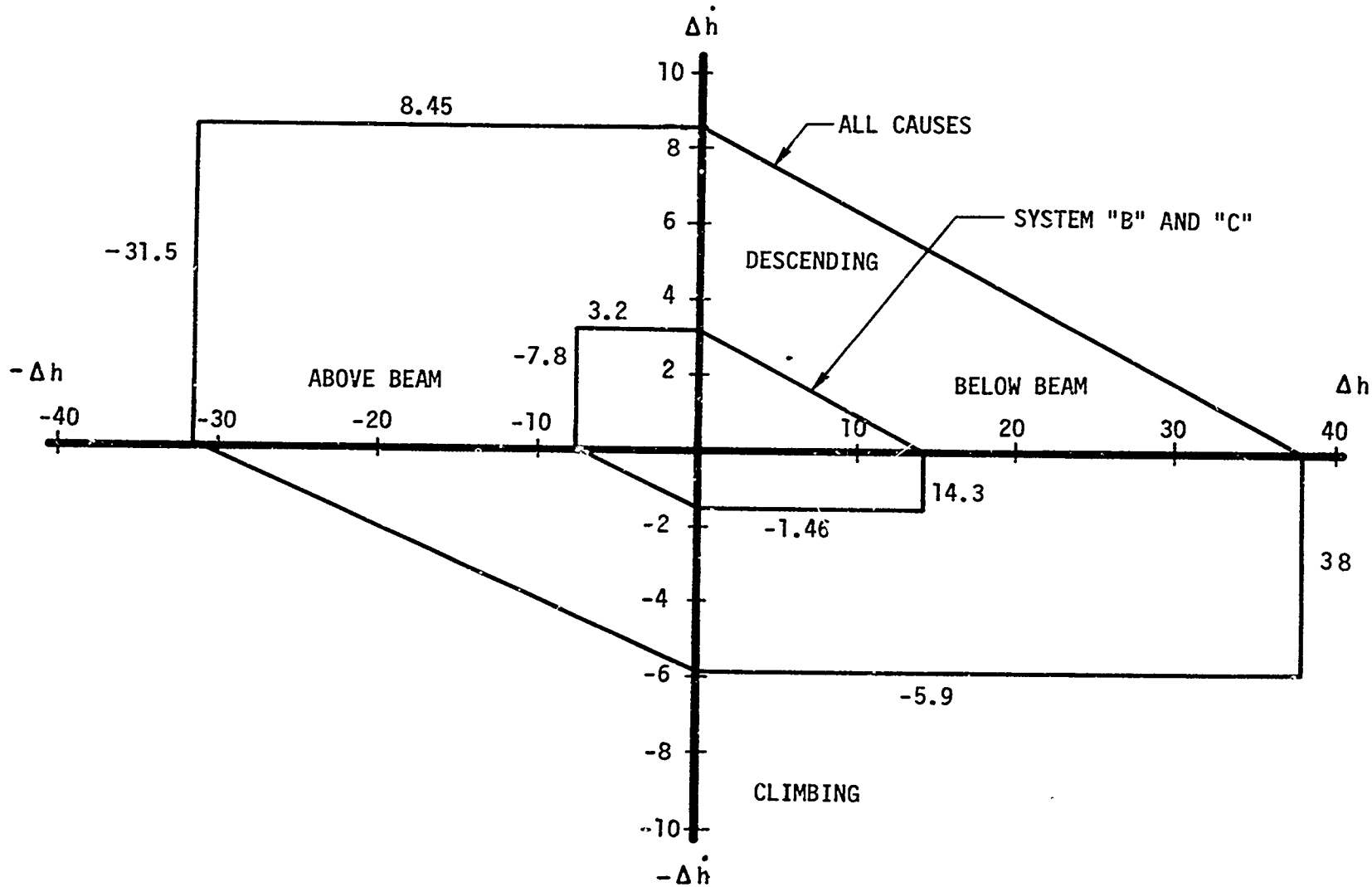

7.0 CONCLUSIONS

The System C autopilot was found to possess performance equal to or better than the other autopilots in all cases. The performance advantage was particularly noted for tracking problems resulting from imperfect ILS beam information. The attenuation of beam bend effects permits the path gain of System C to be increased over that of the non-inertially smoothed autopilots. This results in improved tracking performance in the face of wind (atmospheric) disturbances. Thus the complementary filtering technique that reduced the effect of beam anomalies also leads to a reduction in the effect of atmospheric disturbances.

7.1 Exploitation of Inertial Smoothing Advantages

Marked attenuation of the adverse effects of some unique characteristics of the ILS beams is made possible by use of the inertially smoothed control law. Localizer overflight interference and beam failure shutdown are two examples of ILS beam characteristics which are beyond the capability of non-inertially smoothed autopilots to satisfactorily cope with. The effect of localizer overflight on the performance of the conventional autopilot (System A) is so severe that unacceptable touchdown offset can result from overflights anywhere between outer marker and threshold. This unacceptable result does not, of course, happen every time as the residual effect at touchdown is proportional to the amplitude of the disturbance and its timing. The timing may result in the airplane being at a peak displacement at touchdown or at other times very nearly on center.

The claim has been made that the failure of non-inertially smoothed autopilots to satisfactorily cope with localizer overflight disturbances can be overcome by simply spacing airport approach/departure traffic to prevent an overflight situation. This operational solution has the direct consequence of reducing the arrival/departure rate per runway per hour to a level far below that for VFR conditions. Traffic delays in IFR conditions are almost assured. Furthermore, there is no guarantee that overflight effects are precluded by this operational procedure. Aircraft overflying the airport at two thousand feet or more can cause overflight transients. This phenomenon has been observed while approaching Boeing Field runway 13R as another aircraft passed over the airport at two thousand feet on an approach to Seattle Tacoma Airport. This is in spite of the fact the Boeing Field is equipped with a directional localizer system.

The ILS beams are single-thread in that there is no simultaneous redundancy employed to provide fail-passive or fail-operational characteristics. Rather, upon failure detection by the ground based monitors, a back-up transmitter is brought on line after some time delay. Should the cause have been the antenna system, the problem will persist and another time delay passed before complete shutdown. During this whole interval, the airplane may have been receiving hardover guidance information. The conventional autopilot equipped airplane, especially in

the pitch axis, maneuvers unacceptably within a half-second of an ILS hardover failure. The inertially smoothed autopilot control, by comparison, can withstand hardover failure for five seconds or more. Thus the delay times between ILS transmitter switchover and shutdown can be set to long enough periods to minimize nuisance (false) failure detections on the part of the ground based monitors and yet assure safety due to the tolerance of the inertially smoothed autopilots to limited period hardover guidance information.

In summary, with regard to these two particular ILS beam characteristics, the use of an inertially smoothed autopilot offers considerable relief to the compromise between system (combined ILS and airplane) utility and performance.

The advantages of the inertially-smoothed autopilot for operation on ILS beams are not limited to the alleviation of the two above mentioned unique characteristics of the ILS guidance system. As reviewed in Section 6.0, inertial smoothing provides significant attenuation of the effects of beam bends and noise which exist, to a significant extent, at many facilities.

The inertially smoothed autopilot has been flown on three Cat I ILS beams in the Seattle area. The Boeing Field ILS beam is the worst from the standpoint of low altitude localizer and glide slope bends. At this facility, both lateral and longitudinal control precision through to touchdown, are quite acceptable. The localizer back course at Boeing Field has many bends that far exceed the front course Cat I inspection limits and yet touchdown close to centerline has been achieved with the System C roll control law. The localizer guidance information was simply switched out just before overflying the antenna site and pure inertial guidance was then used for the last thirty seconds before touchdown. Limited actual flight experience with the inertially smoothed autopilot precludes justification for a claim that satisfactory approach and touchdown performance can be achieved at all ILS facilities. However, it does appear that if the average beam alignment is near centerline, satisfactory performance is achievable even in the presence of a continuous series of 30 ua bends, each up to ten seconds duration. Thus at facilities where the backcourse or the low altitude end of the frontcourse localizer is otherwise unusable due to large bends of ten seconds or less duration, the application of inertial smoothing may result in acceptable coupled approach performance. The same argument applies for low altitude glide path bends. That is, at those facilities where the minimum descent altitude in coupled approach is limited by consideration of excessive slope reversal, the inertially smoothed pitch autopilot may provide acceptable performance in spite of this problem.

7.2 ILS Siting to Maximize Approach Success Rate

The trades between ILS beam alignment and the tolerable levels of beam bends are explained in Section 6.5. It is apparent that there exists a great incentive to control both the localizer and glide slope

beam centers, at all facilities, to a common siting standard.

In the case of the localizer beam, the closer the beam alignment is maintained to runway centerline, the greater the tolerance that can be allowed for beam bends.

In the case of the glide slope beam, the allowable tolerance on bends is severely limited because the location of average beam center at commissioning is permitted a significant variation. The lack of a universal standard for glide path beam location with respect to the touchdown zone, results in a requirement to limit Cat II beam bends to values of approximately one-half of what might otherwise be tolerable. When concerned with providing a level of system performance that is consistent with Cat III operations, no allowance can be made for beam bends if the average beam location is permitted the same wide latitude as for Cat II beam specifications. Preliminary analysis leads to a choice of combination between beam angle and threshold crossing height as shown in Figure 6.5.2. However, in spite of this "optimal" placement of the 2.5 degree beam, only a small margin can be permitted as an allowance for beam bends. An "optimally" placed 3.0 degree beam can be permitted beam bends that are approximately one-half the size as are presently permitted by Cat II specifications.

8.0 REFERENCES

1. Boeing Document D6-24406, Performance Analysis of the 727-100 and 727-200 Autoland Systems, O'Toole, P. L.

2. United States Standard Flight Inspection Manual, 217 Instrument Landing System (ILS), OAP 8200.1 CHG 17, October 26, 1970.

3. Boeing Document D6-33220, 747/SPZ-1 Fail-Operational Autoland System Performance Analysis.

4. Analytical Study of ILS Beam Characteristics, The Bendix Corp., FAA Contract No. ARDS -451, August, 1962.

5. Todd M., Complementary Filter Scheme for Premixing INS and ILS Information, Service Technology Corp., Report 580, October, 1970.

6. Design, Development and Flight Evaluation of Inertially Augmented Automatic Landing Systems, Lear Siegler, Inc., Interim Report ADR-754, April, 1971.

7. Todd M., Second Order Complementary Filter for Premixing INS and ILS Information, Service Technology Corp., Report STC-DOT-TSC-43-71-755, May, 1971.

8. FAA Advisory Circular 20-57A, Automatic Landing Systems (ALS), January, 1971.

9. FAA Advisory Circular 120-29, Criteria for Approving Category I and Category II Landing Minima for FAR 121 Operators, September, 1970.

10. Boeing Document D6-22679-1, Instrumentation Camera System, Aircraft Noise Tests, C. J. Masreliez, April 1971.

11. Boeing Document D6-40198TN, Position Determination During Autoland Tests, J. W. Burrows, September 20, 1971.

12. Boeing Document D6-23937TN, Comparative Study of Automatic Landing Systems, M. El-Moslimany, June 6, 1969.

APPENDIX A

THEORY OF THE COMPLEMENTARY FILTER

This Appendix is included to provide mathematical background on complementary filtering for readers who may be unfamiliar with this control engineering technique. For this reason, the discussion may be somewhat pedestrian for the automatic control specialist. The discussion is particularly orientated to the use of a first order complementary filter to derive an improved estimate of lateral position.

Although the first order complementary filter is a classical device which is well known, it is informative to examine its characteristics from a particular point of view. The beam rate and inertially damped systems are briefly reviewed with the intent of establishing the point of view and a baseline for comparison.

A.1 THE ILS POSITION SIGNAL

The high frequency noise in the ILS beam signal has been removed (or attenuated) by a low pass filter. This may be expressed in block diagram form as in Figure A-1.

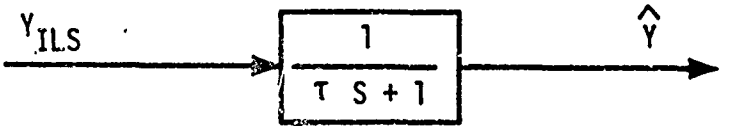

FIGURE A-1

In the block diagram Y_{ILS} is the lateral displacement from the runway centerline in cartesian coordinates derived from the ILS localizer, and $\hat{Y}$ is the estimated position. However, as previously mentioned, Y_{ILS} has errors, which may be represented as:

$$Y_{ILS} = Y + Y_e \qquad (A.1)$$

where Y is the true position and Y_e is the error in the measurement of position.

Now the block diagram of Figure A-1 may be expressed in equation form as:

$$\hat{Y} = \frac{1}{\tau s + 1} \quad Y_{ILS} = \frac{1}{\tau s + 1} \; Y + \frac{1}{\tau s + 1} \; Y_e \qquad (A.2)$$

It is seen from equation (A.2) that the true position signal has been dynamically modified in the process of modifying the position errors. In other words, the low pass filter removes high frequency information content from the position signal. This loss of information may be demonstrated graphically in Bode plot form as in Figure A-2.

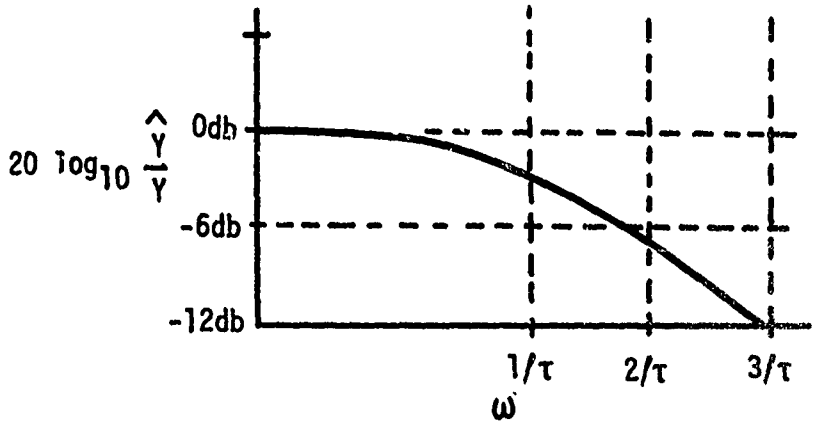

FIGURE A-2

Notice that the information loss is reflected by a decreasing ratio of estimated to actual position at frequencies above the breakpoint, $1/\tau$. However, this high frequency information may be necessary to preserve system stability (phase margin). As a consequence, the time constant, τ , is limited to some maximum value by stability considerations.

A.2 THE BEAM RATE SIGNAL

In the conventional system, the velocity signal, necessary for system damping, must be derived from the position signal. This has been done by a high pass or "washout" as shown in block diagram form in Figure A-3.

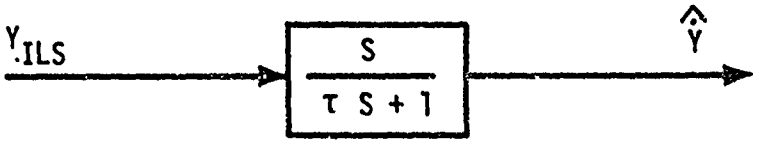

FIGURE A-3

However, since the position error is assumed to be mostly high frequency, the derived rate signal accentuates the noise problem by placing a higher gain on the high frequencies than the low frequencies. In order to help alleviate the problem, an additional low pass is added to the derived rate network as in Figure A-4.

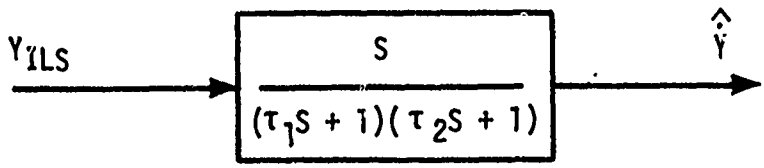

FIGURE A-4

In equation form the block diagram becomes:

$$\hat{\dot{Y}} = \frac{S}{(\tau_1 S+1)(\tau_2 S+1)} Y + \frac{S}{(\tau_1 S+1)(\tau_2 S+1)} Ye \qquad (A.3)$$

or replacing sY by $\dot{Y}$

$$\hat{\dot{Y}} = \frac{1}{(\tau_1 S+1)(\tau_2 S+1)} \dot{Y} + \frac{S}{(\tau_1 S+1)(\tau_2 S+1)} Ye \qquad (A.4)$$

Thus the velocity estimate is double low passed velocity corrupted by bandpassed noise. Both system stability and performance argue for high gains and small time constants in the velocity signal. However, the high frequency character of the noise forces a compromise between unnecessary activity resulting from noise and the desire to minimize path deviations in turbulence and windshear. In practice the optimal gains and time constants result in a system whose performance is less than desired.

A.3 THE INERTIAL VELOCITY SIGNAL

If a source of velocity information independent of the ILS beam signal is available, the problem of accentuating beam noise by differentiation to obtain velocity no longer exists as an impediment to system performance. Such an independent velocity signal may be obtained by processing the signals from an inertial navigation system.

The velocity signal, $v_{y_{INS}}$, from the inertial navigation system is good, but not perfect. There are errors in the signal which cause it to differ from the true velocity. That is:

$$v_{y_{INS}} = \dot{Y} + v_{y_e} \tag{A.5}$$

The inertial velocity errors, v_{Y_e}, are primarily low frequency errors. Therefore, a better estimate of the velocity is obtained by high passing the inertial velocity signal as in Figure A-5.

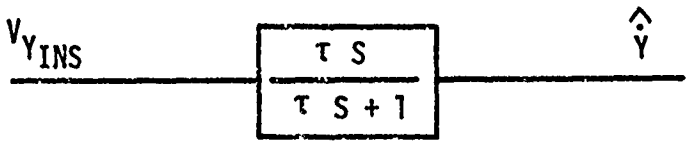

FIGURE A-5

Of course the true velocity as well as the new velocity errors are dynamically modified when using this velocity estimator:

$$\hat{\dot{Y}} = \frac{\tau S}{\tau S+1} \dot{Y} + \frac{\tau S}{\tau S+1} v_{y_e} \tag{A.6}$$

The effect of the high pass is to remove or attenuate the velocity damping signal at low frequencies, which may lead to undesirable, lightly damped, low frequency modes if system gains and time constants are not chosen with great care.

As a consequence of the removal of the low frequency velocity information, the best autoland system of the inertially damped class falls short of the design engineer's fond hopes. However, these autoland systems show a significant performance increment over those using velocity information derived from the ILS signal. These autoland systems exhibit less sensitivity to ILS beam noise, improved damping, and improved turbulence and windshear response. However, the time constant in the position estimator (Figure A-1) is still limited to a maximum value for which the estimator's response to low frequency beam disturbances or "beam bends" of ten seconds duration or longer is significant.

A.4 THE COMPLEMENTARY FILTER

The system sensitivity to localizer anomalies may be reduced by making further use of the inertial velocity signal. By properly combining velocity with position through the use of a complementary filter as the position estimator, system stability becomes independent

of the time constant of the low pass on position error. This allows the selection of the complementary filter time constant solely on the basis of ILS and inertial error characteristics with no need to consider system stability.

The first order complementary filter position estimator may be derived by first examining the low pass position estimator of equation (A.2):

$$\hat{Y} = \frac{1}{\tau S+1} \quad Y + \frac{1}{\tau S+1} \quad Ye \tag{A.7}$$

Notice that another term may be added to replace the high frequency information removed by the low pass on position. This may be written as:

$$\hat{Y} = \frac{1}{\tau S+1} \quad Y + \frac{1}{\tau S+1} \quad Ye + \frac{\tau S}{\tau S+1} \quad Y \tag{A.8}$$

By combining terms equation (A.8) may be reduced to:

$$\hat{Y} = Y + \frac{1}{\tau S+1} \quad Ye \tag{A.9}$$

This seemingly trivial result is important when a source of position and its derivatives with errors independent of the ILS errors is available. The inertial sensors will be shown to provide this required information.

Rewriting the expression for inertially determined velocity found in equation (A.5) gives:

$$v_{y_{INS}} = \dot{\hat{Y}} + v_{y_e} = SY + v_{y_e} \tag{A.10}$$

Clearly, the inertial navigator provides the velocity (sY) needed for the additional term in equation (A.8). Neglecting the INS error and making the substitution of (A.10) into (A.8) and making use of (A.1) to reduce $(Y + Y_e)$ yields

$$\hat{Y} = \frac{1}{\tau S+1} \quad Y_{ILS} + \frac{\tau}{\tau S+1} \quad v_{y_{INS}} \tag{A.11}$$

which is the equation for the first order complementary filter position estimator in the form which emphasizes its input signals. Figure A-6 illustrates equation (A.11) in block diagram form.

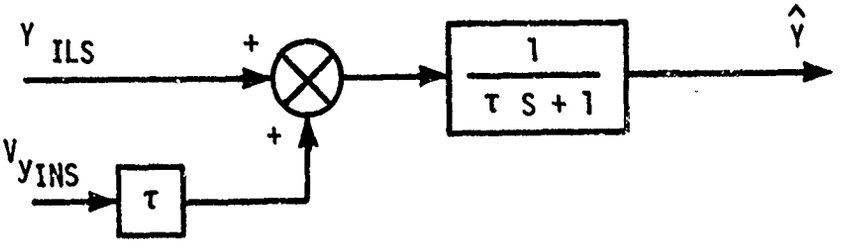

FIGURE A-6

In order to examine the errors in the estimated position, substitute (A.1) and (A.10) into (A.11) to obtain:

$$\hat{Y} = \frac{1}{\tau s+1} Y + \frac{1}{\tau s+1} Ye + \frac{\tau s}{\tau s+1} Y + \frac{\tau}{\tau s+1} v_{y_e} \qquad (A.12)$$

Then combine terms to obtain:

$$\hat{Y} = Y + \frac{1}{\tau s+1} Ye + \frac{\tau}{\tau s+1} v_{y_e} \qquad (A.13)$$

Notice that the position estimate produced by the complementary filter contains the signal or true position, Y, without dynamic modifications. This is why the complementary filter time constant has no influence on system stability. Only the errors are dynamically modified and it is solely by consideration of the response of the estimator to these errors that the complementary filter time constant is determined. The trade-off for optimization purposes is between attenuating ILS distortions above the break frequency and amplifying velocity errors below the break frequency of the complementary filter.

A.5 COMPLEMENTARY FILTER RESPONSE TO INERTIAL VELOCITY ERRORS

Recall that the errors in the velocity signal are primarily low frequency. These errors are essentially a bias error resulting from the long term integration of acceleration errors and a ramp error due to tilt.

The bias velocity error results in a bias error or standoff in the position estimate. These errors are related by a gain determined by the complementary filter time constant. This bias in the position estimate has the potential to cause the autoland system to track an offset course parallel to the runway centerline.

A.6 USE OF A WASHOUT TO REMOVE STANDOFF

The problem of the steady state estimation error by a first order complementary filter subjected to bias errors in the derivative signal has been frequently encountered and is a well known problem. The typical solution applied to the problem has been washing out the derivative signal before putting it into the complementary filter as in Figure A-7.

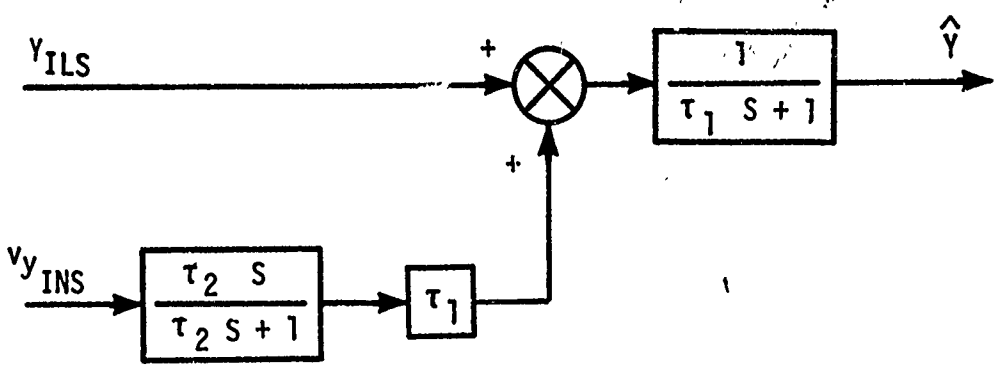

FIGURE A-7

In equation form, this becomes:

$$\hat{Y} = \frac{1}{\tau_1 S+1} \quad Y_{ILS} + \frac{\tau_1 \tau_2 \quad S}{(\tau_1 S+1)(\tau_2 S+1)} \quad v_{y_{INS}} \qquad (A.14)$$

Making the substitution from equations (A.1) and (A.10) yields:

$$\hat{Y} = \frac{1}{\tau_1 S+1} \quad Y + \frac{1}{\tau_1 S+1} \quad Ye + \frac{\tau_1 \tau_2 \quad S}{(\tau_1 S+1)(\tau_2 S+1)} \quad SY +$$

$$\frac{\tau_1 \tau_2 \quad S}{(\tau_1 S+1)(\tau_2 S+1)} \quad v_{y_e} \qquad (A.15)$$

And finally grouping terms yields:

$$\hat{Y} = \frac{\tau_1 \tau_2 s^2 + \tau_2 s + 1}{\tau_1 \tau_2 s^2 + (\tau_1 + \tau_2)s + 1} Y + \frac{1}{\tau_1 s + 1} Y_e + \frac{\tau_1 \tau_2 s}{(\tau_1 s + 1)(\tau_2 s + 1)} v_{y_e} \qquad (A.16)$$

This approach has indeed placed a free differentiation in the numerator of the transfer function multiplying v_{y_e}, thus there is no steady state estimation error resulting from the derivative bias error, v_{y_e}. But in the process the numerator and denominator of the transfer function on true position, Y, no longer cancel. The resulting dynamic modification of Y constrains the freedom of choice of time constants by the system designer. The constraints prevent obtaining the best possible system. However, to have the freedom to achieve the best possible system, the system designer may use a higher order complementary filter which removes the steady state estimation errors without dynamically modifying the true position information contained in the position estimate.

A.7 THE USE OF A PATH INTEGRATOR TO CANCEL STANDOFF

An alternate solution to the position estimation steady-state-offset problem is available using what is commonly called a "path integrator". The raw ILS signal is integrated and this integral summed with the position estimate for use in commanding aircraft maneuvering. This technique was investigated and successfully flight tested during Boeing sponsored work in 1969. The use of parallel integration was chosen because it allows more design freedom than the technique of Section A.6, and higher order complementary filters were not felt to be required where 561 quality INS systems were employed. If the aircraft is not following a path of zero ILS deviation, the deviation will be integrated to cause an appropriate maneuver to reduce the ILS deviation. Consequently, the stable autoland system with a path integrator will reach a steady state of zero ILS deviation. At this time, the output of the path integrator cancels the bias error in the position estimate. Thus the path integrator may be viewed as an estimator of the velocity error in the inertial velocity signal.

A.8 OTHER INERTIAL SMOOTHING PROBLEMS AND CURES

Use of the path integrator to cancel position estimation errors has inherent characteristics which prevent it from being the best possible system. These characteristics lead to the following problem

areas:

1) Initialization
2) Time required to reach steady state
3) Undesirable effects of changing the time constant while tracking the centerline
4) Undesirable response to INS tilt errors

The first problem is associated with turning on or starting the complementary filter. The position estimate, Y, at the time of turn-on must satisfy:

$$\hat{Y} = y_i + Y_{e_f} + \tau v_{y_{e_f}} \tag{A.17}$$

where Y_i is the instantaneous true position, Y_{e_f} is the steady state position error, and $v_{y_{e_f}}$ is the steady state inertial velocity error. Unfortunately, it is not possible to have sufficient information prior to starting the complementary filter to exactly establish the correct initial condition. The resulting initial condition error must propagate through the complementary filter to the steady state value. The propagation speed is strongly influenced by the time constant. For heavy filtering of the position errors, considerable time is required to reach the steady state.

This brings up the second problem, the time required to reach steady state. It was just shown that the complementary filter time constant is one factor contributing to the problem. The second contributing factor is the system dynamic response resulting from use of the path integrator.

The path integrator, in conjunction with other dynamics, introduces a low frequency response with a long settling time. The result is a system which requires about two and one-half minutes to settle out errors. This settling time places a constraint on system use in the form of a minimum tracking time or minimum intercept distance. For an aircraft with a velocity of 135 knots, the two and one-half minute settling time requires a minimum intercept distance of about five and one-half nautical miles from the runway threshold.

The third problem, undesirable effects of changing the time constant while tracking the centerline, results from the transfer function between inertial velocity error and the error in the position estimate. Subtract true position from the position estimate, equation A13, to obtain the error in the estimate.

$$Y_e = \hat{Y} - Y = \frac{1}{\tau S+1} Y_e + \frac{\tau}{\tau S+1} v_{y_e} \tag{A.18}$$

Notice that the inertial velocity error, v_{y_e}, is multiplied by the complementary filter time constant, τ. Thus, as the complementary filter time constant is changed, the aircraft is required to maneuver to change the path integrator output to the new value required to cancel the estimation error. This induced maneuver essentially prohibits changing the complementary filter time constant while tracking.

The fourth problem is the undesirable response to tilt errors. The tilt error results in an acceleration error induced by gravity. The acceleration error is integrated inside the inertial system to produce a ramp velocity error, which causes a ramp in the error in the estimated position. To cancel this ramp error in the steady state, the path integrator output must also ramp which requires that the aircraft fly an offset course parallel to the runway centerline in order to drive the path integrator. Thus the first order complementary filter system with path integral velocity error correction is vulnerable to standoff in the presence of tilt.

The configuration for System C resulted from a trade study to maximize the rejection of beam while minimizing the tracking errors resulting from these four problems. Although System C exhibited excellent performance, these problems may be further reduced by using the more complex technique of higher order complementary filtering. In addition, the higher order complementary filters allow achieving steady state estimation more rapidly than path integration, because the former case depends only on complementary filter dynamics while the latter is dependent on aircraft path following dynamics. Higher order filtering offers the potential of the use of INS systems of lower cost than the 561 types. This potential, however, can only be achieved through autoland system synthesis based on trades between the INS error characteristics and the ILS errors. Inadequate ILS data are available today to permit these trades to be properly accomplished.

APPENDIX B

ROLL AUTOPILOT STABILITY ANALYSIS

Several valid reasons can be stated to defend the autoland engineer's desire to include an inertial navigation platform in the flight controls hardware. Foremost among these reasons is the precise attitude control that can be attained using the high quality attitude feedback from the INS; the engineer does not have to concern himself with the long term washouts that result from vertical gyro erection systems. The availability of ground speed which can be utilized to generate precise γ commands constitutes another reason why the INS is a valuable asset. Also, stabilized accelerations, which are available in the INS, are highly desirable in autoland programs because of the excellent resistance to environmental upsets that can be obtained with good quality accelerometers.

In the lateral controls area, the INS system is invaluable in that it has the capability to compute and output ground track. For years, the lateral autoland controls designer has compromised between good system damping and excess control activity. Moreover, the adverse effect of crosswinds has continually hampered the engineer's effort to produce a highly accurate autoland system. Now, however, ground track from the INS has provided the means to reconcile the stability/wheel activity compromise and to resolve the wind problem. To illustrate, consider the following, simple analysis.

B.1 A SIMPLE ROOT-LOCUS ANALYSIS OF SYSTEM A

Figure B-1 (page 202) is an extremely simplified representation of the localizer controlled, lateral approach system. (Figure B-1 neglects actuator dynamics, beam filters, limits on command rate, and the block diagram is based on complete decoupling between the roll and directional axes). A root locus on K_η, the beam gain in Figure B-1, shows an unstable situation when the rate taker and lagged roll gains, $K_{\dot{\eta}}$ and K_{ϕ_L} respectively, are set to zero as seen in the sketch of Figure B-2.

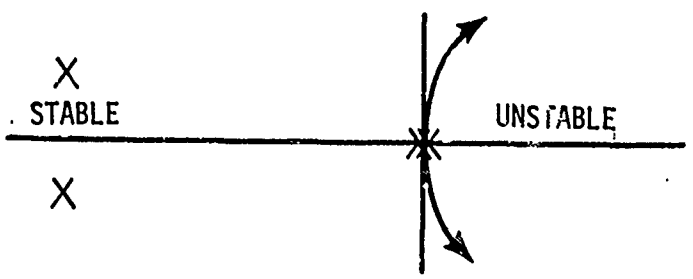

FIGURE B-2

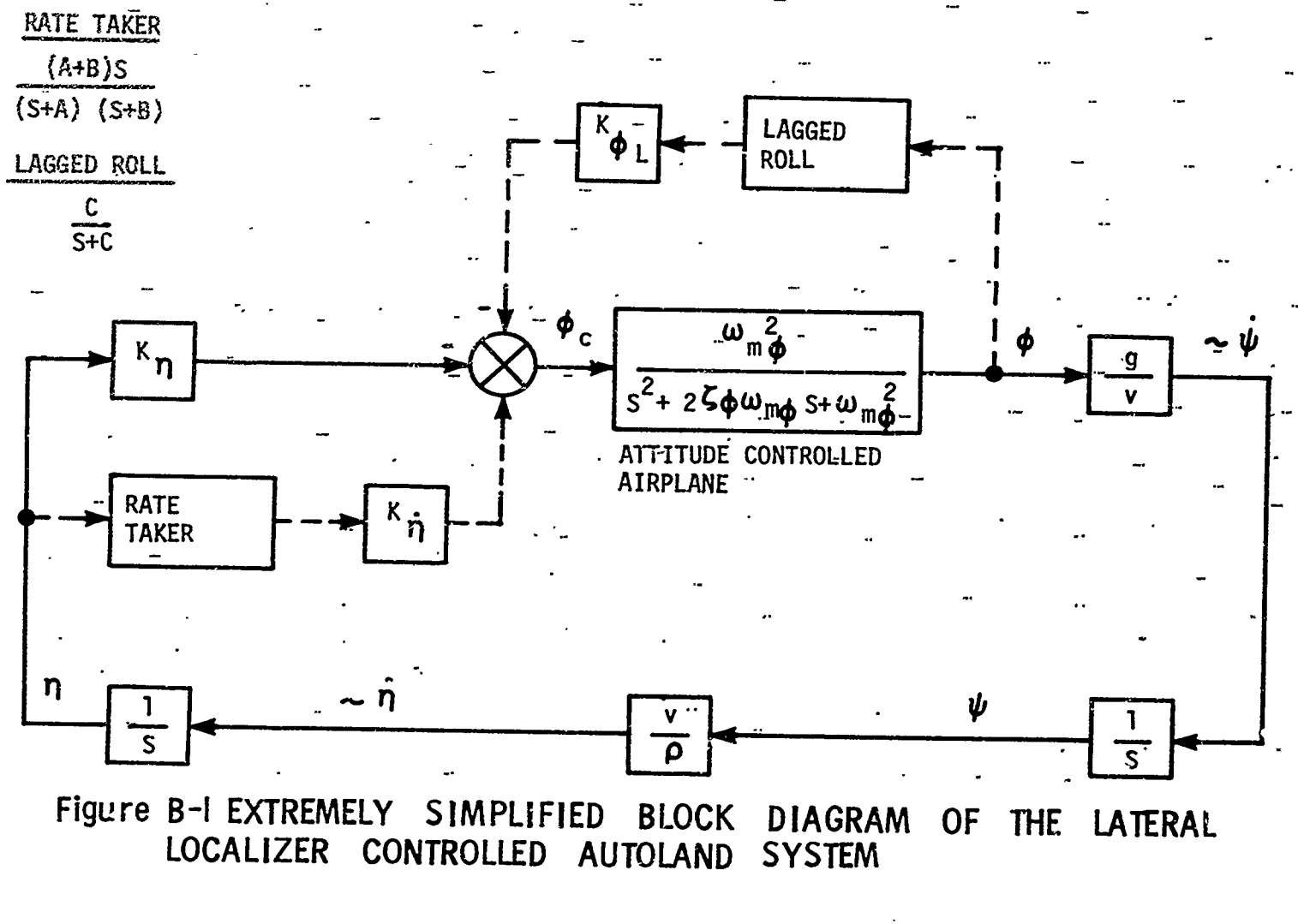

Figure B-I EXTREMELY SIMPLIFIED BLOCK DIAGRAM OF THE LATERAL LOCALIZER CONTROLLED AUTOLAND SYSTEM

The complex pair of poles (attitude loop) is approximately independent of K_η, but the pair of poles at the origin move off into the unstable region for any $K_\eta > 0$. To stabilize this outer loop, beam rate is required essentially to cancel one of the poles at the origin. Theoretically then, Figure B-3 shows the $K_{\dot{\eta}}$ root locus that would result if a nominal K_η were set and a perfect beam rate signal were fed back to the autopilot.

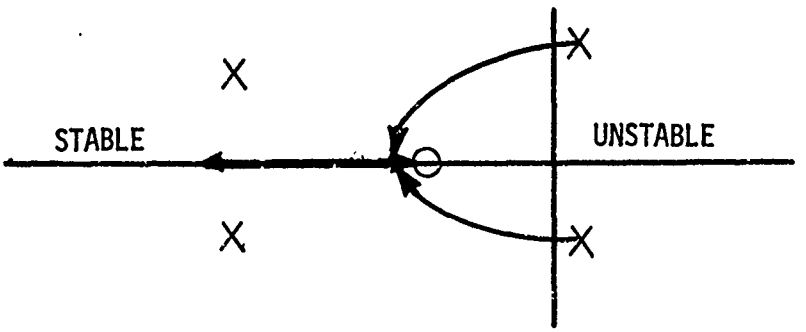

FIGURE B-3

However, perfect pole/zero cancellation is prohibited by the K_η gain and the imperfect beam rate taker; and, in actuality, owing to the two break frequencies of the rate taker, the root locus contains a pair of complex zeros as shown in Figure B-4. These loci are based on a fixed K_η gain and vary with $K_{\dot{\eta}}$ gain.

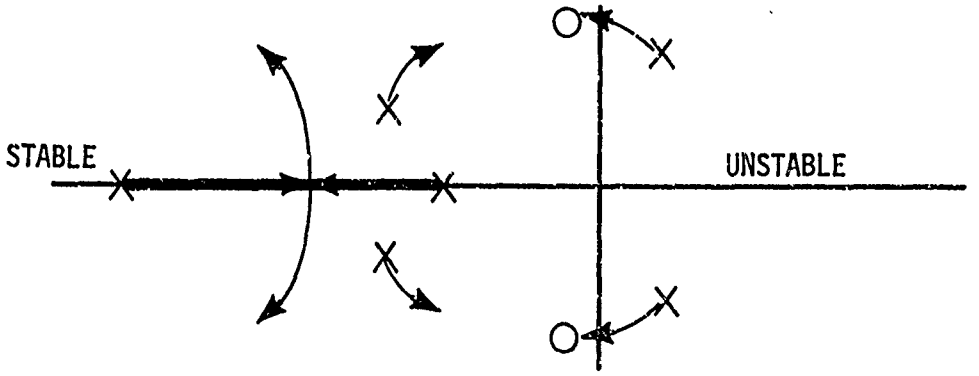

FIGURE B-4

Notice that the unstable poles in Figure B-4 move toward the complex zeros in the stable region as the $K\dot{\eta}$ gain is increased. Now, in order to effectively cancel the poles and zeros, the $K\dot{\eta}$ gain must be extremely large, so large in fact that the surface activity becomes prohibitive. An investigation of the crosswind induced lateral displacement also demands that the highest beam rate gain possible be incorporated into the system. But again, the wheel activity limits the value of the beam rate gain. (Directional stability is also affected). Since the extremely noisy beam (and other considerations) definitely limits the value of $K\dot{\eta}$, as well as $K\eta$, another source of damping must be sought.

Referring again to Figure B-1, for a constant speed, the beam rate is proportional to the product of true heading and distance to the localizer. (Actually this is not a true relationship as Figure B-1 ignores the side force contribution to beam rate, and consequently this block diagram can only be considered valid in a quiescent environment. This point is not to be taken lightly, because it is the side force contribution to $\dot{\eta}$ that establishes a great deal of the need for an INS). This proportional relationship raises the question - - why not feed back heading as a damping signal? This solution was used in many autopilots in the late '50's and early 1960's. However, there are problems with this solution also. To illustrate, when the airplane is subjected to a cross wind upset, the tendency of the airplane to weathercock produces a heading change which is not related to beam rate; i.e., the heading change during weathercocking commands a roll angle in the wrong direction. Further, low frequency heading changes required to track the beam in the presence of wind shears, required outputs from a path integrator, which due to stability limitation was slow in responding. The wind shear response of these systems was very poor. Therefore, heading cannot be relied upon to approximate beam rate because of the environmental disturbances.

In this analysis, airplane heading can be considered as being comprised of two distinct terms as follows:

$$\psi = \psi_{WIND} + \frac{g}{V} \int \phi \, dt \qquad \text{(B-1)}$$

where ψ_{WIND} is the initial heading transient that results from a wind upset. The second term in Eq. (B-1), as seen in Figure B-1, is the heading that results from bank angle-induced turns. It follows that since ψ is desired as a beam damping signal, and since ψ_{WIND} is always in the wrong direction, the next obvious step is to integrate

the bank angle and feed it back to the autopilot. However, pure integration cannot be used since the airplane may be mistrimmed; i.e., a steady roll angle may prevail throughout the approach. Consequently, prior to the innovation of the INS, the autoland engineer approximated this integral with a long time constant lag on the bank angle and used this signal to supplement the beam rate; hence, the term "lagged roll". The root locus of the lagged roll gain, K_{ϕ_L}, with K_η and $K_{\dot{\eta}}$ set to values which are generally being utilized in first generation autoland systems, resembles the sketch in Figure B-5.

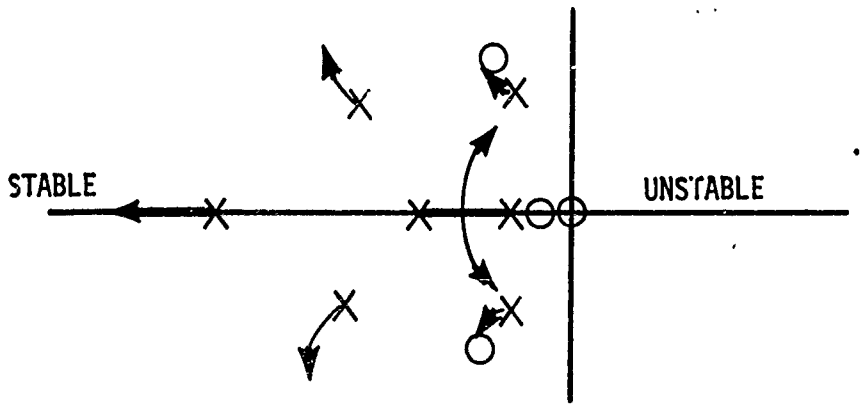

FIGURE B-5

Notice that while the "old" low-frequency oscillatory poles have migrated very close to the complex zero pair into a well-damped position, another low frequency, real pole (the lagged roll break frequency) has been created which moves toward the first low frequency pole, and the two form another complex pair. Higher K_{ϕ_L} gains will move these poles around a circle, return to the real axis between the two zeros, and move respectively toward each zero; i.e., good damping is difficult to achieve unless K_η and $K_{\dot{\eta}}$ can be increased to move the zeros further into the stable region. The lagged roll gain, unfortunately, also affects the Dutch Roll mode which, until now, has been assumed dormant. A more thorough analysis shows that a strong interaction exists between the lagged roll gain and the yaw damper gain. Consequently, a constraint is imposed on the lagged roll gain not only because of the low frequency damping but also because increasing K_{ϕ_L} tends to destabilize the Dutch Roll roots.

This simple root locus analysis has illustrated why a compromise always results when beam rate and lagged roll are used to stabilize the lateral system. The problem, though seemingly complex, boils down to one simple fact: a clean, complete representation of the beam rate is not available.

B.2 SIMPLE ANALYSIS OF SYSTEM B

The INS computes a track angle signal, ψ_{TA}, which can be expressed

$$\psi_{TA} = \psi + \beta_{DA} \tag{B-2}$$

In this expression, ψ is simply the true heading (including wind considerations) and β_{DA} is the drift angle across the ground. Thus, the combination of heading and drift avail a signal which is ideal for damping the beam; because a wind upset <u>always</u> induces a track error in the "correct" direction, and hence the resulting commanded bank angle is <u>into</u> the wind; i.e., a commanded return to beam center. While the block diagram of Figure B-1 shows that (inertial) heading leads the beam by 90-DEG and is, therefore, proportional to $\dot{\eta}$, the mathematical relationship between track angle and beam rate will now be derived.

The lateral velocity, in a two-dimensional axis system, can be expressed:

$$\dot{Y} = V_g \text{ SIN } (\Delta \psi_{TA})^* \tag{B-3}$$

Now, from simple trigonometry

$$\eta = \text{SIN}^{-1} \left(\frac{Y}{\rho}\right) \approx 57.3 \frac{Y}{\rho} \tag{B-4}$$

Differentiating Eq. (B-4)

$$\dot{\eta} = 57.3 \frac{(\dot{Y}\rho - \dot{\rho}Y)}{\rho^2}$$

$$= 57.3 \frac{\dot{Y}}{\rho} - \frac{\dot{\rho}(57.3 \frac{Y}{\rho})}{\rho} \tag{B-5}$$

* The $\Delta \psi_{TA}$ is the difference between commanded track and actual track.

But since $\dot{\rho} \approx - V_g$, multiplying by ρ and substituting EQ (B-4) into Eq (B-5) yields

$$\rho \dot{\eta} = 57.3 \dot{Y} + V_g \eta \qquad \text{(B-6)}$$

Now in the autopilot, the compensated beam error (the beam error that has been multiplied by a function of range),

η_p can be expressed

$$\eta_p = \frac{\rho}{K} \eta \qquad \text{(B-7)}$$

where k is a constant, usually about 40,000. Differentiating Eq. (B-7)

$$\dot{\eta}_p = \frac{1}{K} (\rho \dot{\eta} + \dot{\rho} \eta) = \frac{1}{K} (\rho \dot{\eta} - V_g \eta), \qquad \text{(B-8)}$$

since $\dot{\rho} = -V_g$ as noted before.

Substituting Eq. (B-6) into Eq. (B-8) and reducing yields

$$\dot{\eta}_p = \frac{1}{K} \quad 57.3 \dot{Y} \qquad \text{(B-9)}$$

But, from Eq. (B-3) and Eq. (B-9)

$$\dot{\eta}_p = \frac{57.3}{K} \; Vg \; SIN (\Delta \psi_{TA}) \qquad \text{(B-10)}$$

Thus, in the autopilot, the programmed beam rate, η_p , is proportional to the ground track angle, $\Delta \psi_{TA}$.

Now since it was assumed in Section B.1 that no wind upsets existed, Figure B-1 again applies and ψ can be regarded as ψ_{TA}, i.e., β_{DA} is always zero. Therefore, the damping signal for beam rate will be ψ , and the root locus for the track angle gain K_ψ is similar to the sketch in Figure B-6 (K_η is set to nominal and $K_{\dot{\eta}}$ and K_{ϕ_L} are set to zero).

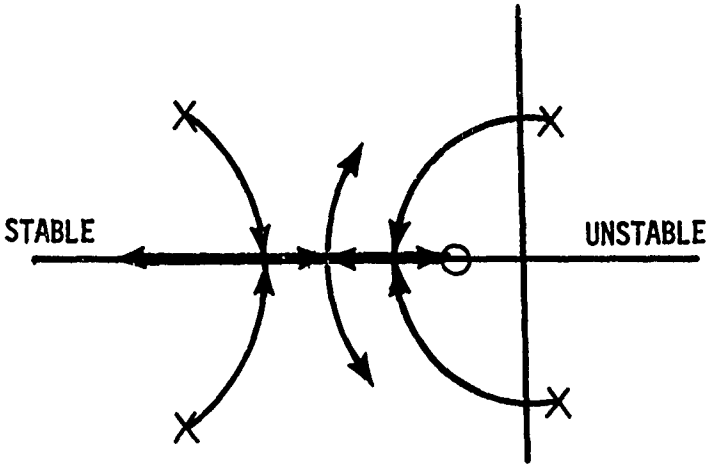

FIGURE B-6

It is important to note that the "unstable", low-frequency poles migrate toward the stable, real axis, and as K_ψ is increased further, one pole cancels the zero at the origin while the other forms a complex pair with one of the attitude loop poles. If the K_ψ gain is adjusted properly, the only remaining low frequency poles will be retained near the real axis and further from the origin than was possible with the lagged roll system. Hence, ψ_{TA} is by far the less complex and most straightforward damping signal with which the localizer coupler can be stabilized.

A more comprehensive analysis, which includes a 3-degree-of-freedom airplane, actuator dynamics, yaw damper, etc., draws the same conclusion as the above, simple analyses. There is no substitute for INS track angle in stabilizing the lateral approach coupler and, hence, "wind-proofing" the airplane during approaches.

B.3 OTHER FACTORS

The simple analyses in Sections B.1 and B.2 were presented to show that the INS offers the most desirable means of damping the ILS-localizer system. It was pointed out that beam rate was limited as a damping signal because of the poor quality beam error signal. It is interesting to see the relationship between the beam rate gain as used in conventional autoland system (System A), and the track angle gain used in System B and C. From Eq. (B-10),

$$\tilde{\eta}_p \approx \frac{V_g}{K} \Delta\psi_{TA} \approx .0055 \Delta\psi_{TA} \qquad \text{(B-11)}$$

Eq. (B-11) simply states that, during the approach, $\Delta\psi_{TA}$, in deg, is about 180 times greater than the programmed beam rate. This means that, if a synthesis of the track angle-damped system calls for a gain between 2.5 (System B) and 3.5 (System C) an equivalent gain in the beam rate-damped (A) system would be between 400 and 600, a virtual impossibility.[1] This comparison shows much more clearly why the INS-damped lateral autopilot is preferred to the beam rate-damped autopilot.

When the crosswind is taken under consideration, the argument for the INS is greatly enhanced. To illustrate, consider Figure B-7, a frequency response comparison between System A and System B. The subject response is lateral displacement, Y, to crosswind, V_y in ft/ft/sec, and while both systems show peak response near a .35 rad/sec, the lagged roll system peak response is twice that of the INS system.

Wind shear responses of these two couplers present even more convincing evidence that the INS-damped autopilot is preferred to a beam rate/lagged roll system. Responses to the classical 8 kt/100 ft wind shear show that peak lateral deviation of the INS-damped system is between 1/4 to 1/2 that of the beam rate system, depending upon the methods of implementation. Actually, this is not surprising when Eq. (B-2) is considered. Whenever the approaching airplane is subjected to a crosswind shear, the drift angle β_{DA} begins to develop according to the side force time constant (Cy_β) of the airplane. As the airplane weathercocks into the crosswind, heading changes adversely, but no adverse feedback ensues because the drift angle dominates the maneuver. Hence, if the airplane weathercocking time constant were zero, then $\Delta\psi$ would always be equal to the negative of $\Delta\beta_{DA}$ and no autopilot commands would be generated. However, $\Delta\beta_{DA}$ <u>leads</u> $\Delta\psi$ and a $\Delta\psi_{TA}$ begins to develop which commands the airplane to roll "into" the wind to null the $\Delta\psi_{TA}$. Meanwhile, the very small beam error which results is nulled by the beam error plus integral of beam error. All this takes place without concern for the roll angle, and it follows that the lead action afforded by the INS track angle will hold the lateral offset to the smallest possible value.

B.4 GAIN COMPARISONS

With respect to system gains, the track angle stabilized approach coupler exhibits gains which are considerably greater than the gains of a conventional coupler. Consider the following comparisons.

[1] System A rate gains are typically <u>75</u>.

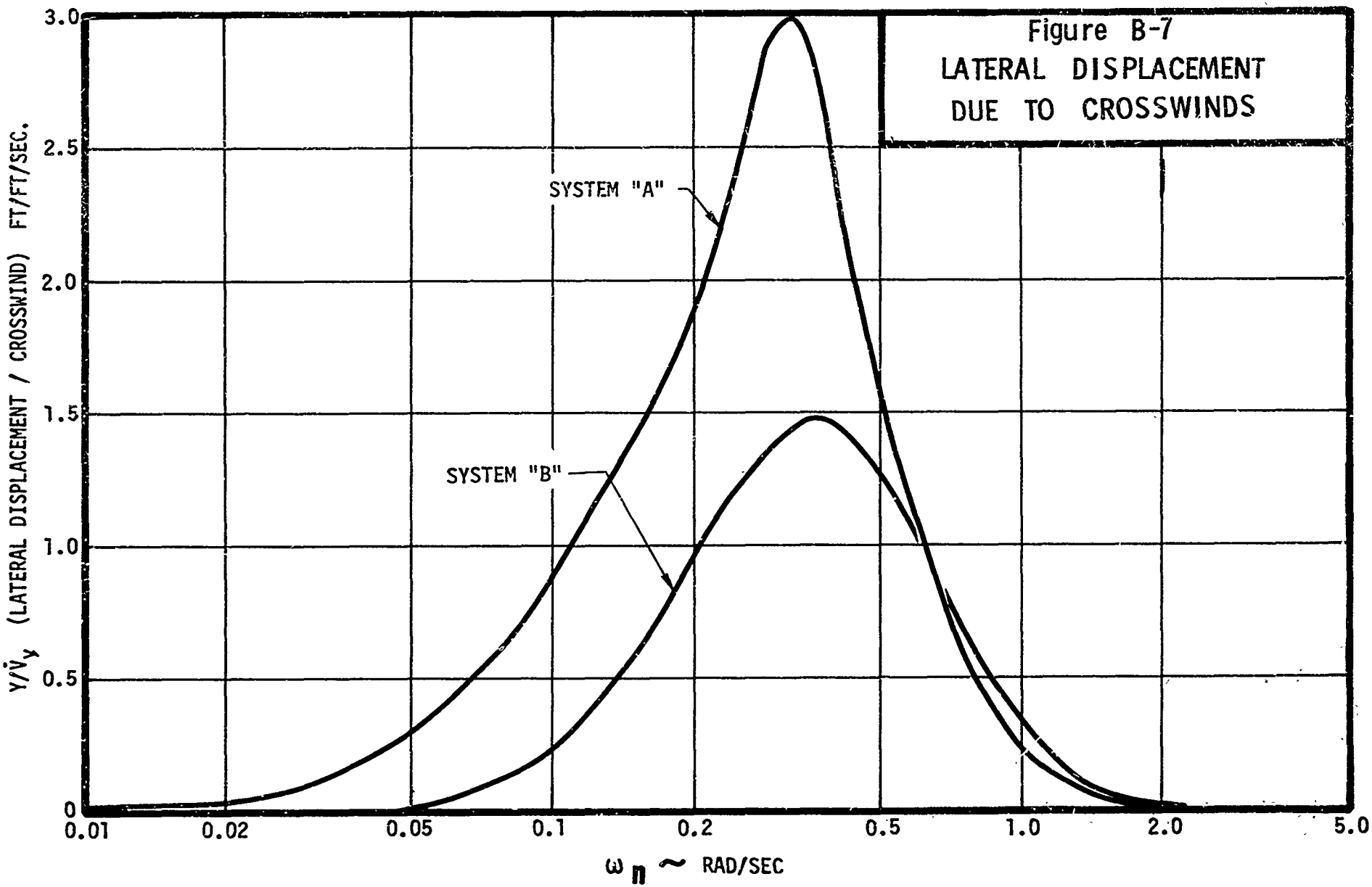
Figure B-7
LATERAL DISPLACEMENT
DUE TO CROSSWINDS
SYSTEM "A"
SYSTEM "B"
Y/V̇y (LATERAL DISPLACEMENT / CROSSWIND) FT/FT/SEC.
3.0
2.5
2.0
1.5
1.0
0.5
0
0.01
0.02
0.05
0.1
0.2
0.5
1.0
2.0
5.0
ωn ~ RAD/SEC

Gain	C Sys.	A Sys.
K_η	80	23
K_I	4	0.7
$K_{\dot{\eta}}$	600	75
K_{ϕ_L}	0	3.5

Intuitively, one would suppose that the wheel or surface activity would be prohibitive with the C system, but such is not the case. Figure B-8 shows the wheel/beam ($\delta\omega / \eta$) response for System B and System A. The improvement is obvious. To explain the reasons why the high gain, track angle-damped system exhibits less wheel activity than the beam rate-damped system would require a rather lengthy discussion. However, Reference 12 treats this subject in great detail and also contains many frequency response plots which compare several systems with respect to wheel activity, environmental performance, etc. It will be noted here that one may attain even greater reduction of wheel activity in System B by lowering the gains, but this will also cause degradation of crosswind performance, particularly wind shear.

B.5 SUMMARY OF ROLL AXIS STABILITY ANALYSIS

To summarize, the localizer tracking mode is more efficiently stabilized by the INS track angle signal rather than the combination of beam rate and lagged roll because:

1. A clean, localizer-independent signal, which is directly proportional to beam rate, is available in the INS. This signal requires no special shaping (except perhaps a simple granularity filter). Consequently, a straightforward approach toward properly tuning the system is available.
2. There is no noise induced limit on the damping gain.
3. The shifting of airplane heading in crosswinds does not affect the relationship between track angle and beam rate.
4. The crosswind-induced dispersion is considerably less in System B.

Ref. 12 Boeing Document D6-23937TN, Comparative Study of Automatic Landing Systems, M. El-Moslimany, June 6, 1969.

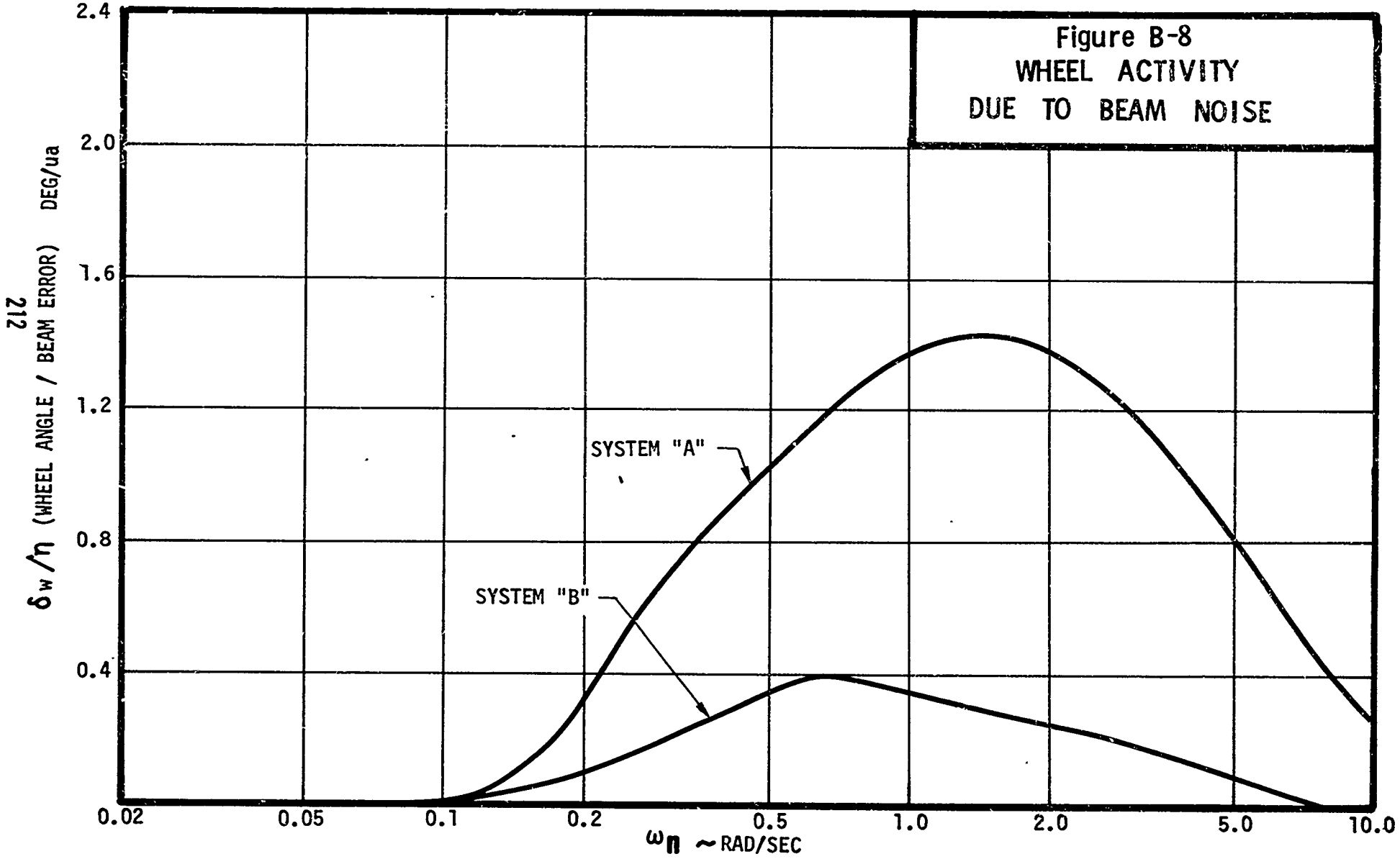
Figure B-8
WHEEL ACTIVITY
DUE TO BEAM NOISE
δ_w/η (WHEEL ANGLE / BEAM ERROR) DEG/ua
2.4
2.0
1.6
1.2
0.8
0.4
SYSTEM "A"
SYSTEM "B"
0.02
0.05
0.1
0.2
0.5
1.0
2.0
5.0
10.0
ω_η ~RAD/SEC

APPENDIX C

CAMERA TRACKING SYSTEM

Photographic data combined with on-board inertial navigation system data were utilized to measure the aircraft path from approximately 5,000 feet away from the runway threshold to touchdown. The camera system used was designed and built by The Boeing Company. Boeing document D6-22679-1, Instrumentation Camera System, Aircraft Noise Tests, describes this system in detail and gives an accuracy analysis. The inertial navigation system is the Carousel IV installed on-board the ILS Autoland test airplane. Boeing document D6-40198 TN, Position Determination During Autoland Tests, describes the method utilized to combine the photographic data and the INS data and the resulting expected accuracy.

C.1 CAMERAS INSTALLATION

The camera and target locations were surveyed utilizing Boeing document D6-19164, Grant County Runway Lights, for bench mark data. Figure C.1.1 shows the installation of Camera Number 1 and its surveyed reference points (targets). The same arrangement of targets was placed in front of the other three cameras. The field of view (azimuth) and approximate location of all four cameras is shown in Figure C.1.2. The elevation coverage of each camera was between horizon and ten degrees up. The airplane was in the field of view of the rear pair of cameras (#1 and #2) from 7000 feet before to 2000 feet after threshold. The forward pair of cameras provided redundant coverage as the airplane passed from 300 feet attitude down through 100 feet. This four camera coverage provided maximum accuracy in the last 4000 feet just ahead of threshold. Test pictures taken of a runway marker of known location confirmed that the cameras had an angular accuracy of better than one milliradian on a 1σ basis.

The cameras and their power supplies were remotely controlled by an interface installed in a van located immediately North of the glide slope trailer. All photographs were taken at two second intervals on the even integer second. The picture taking was started upon command from the test conductor aboard the aircraft. This command was verbally transmitted over the VHF transceiver as the airplane descended through 400 feet altitude. The photographs had BCD time code displayed in the lower right hand corner. Time code generators in the aircraft and on the ground were synchronized in the morning of the day of test prior to each day's testing. The aircraft time code generator was the master.

Figure C.1.1
CAMERA INSTALLATION

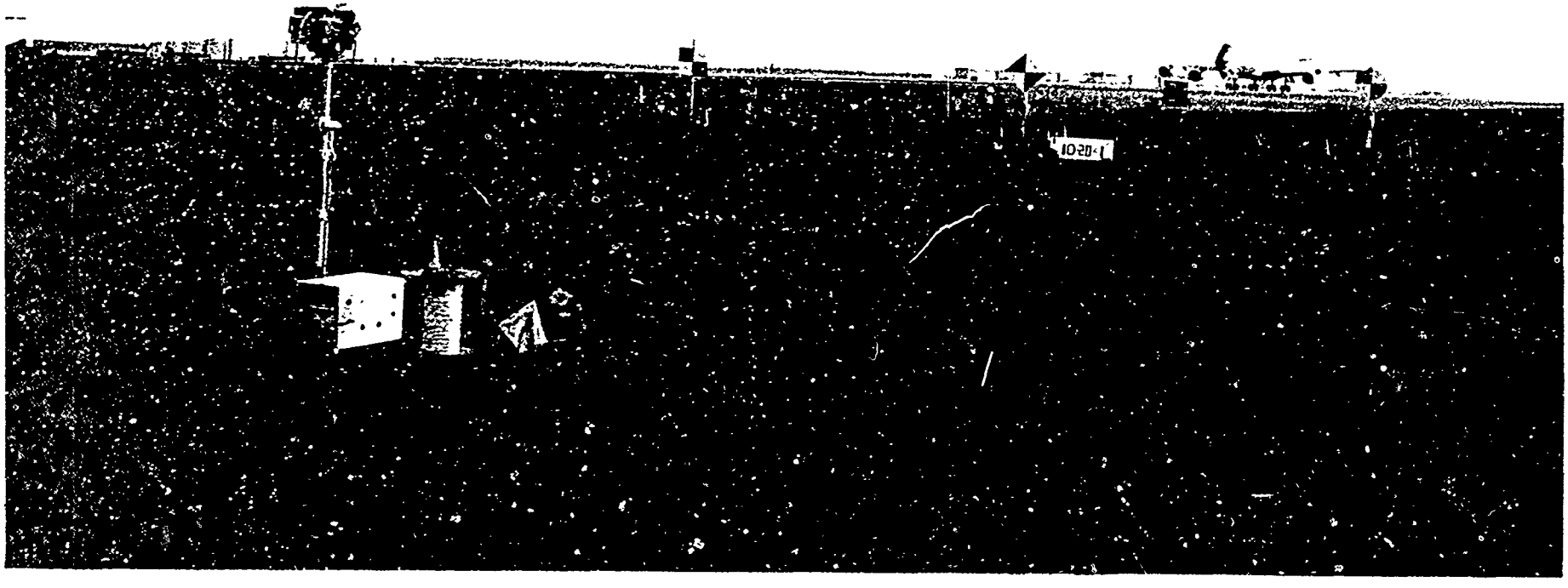

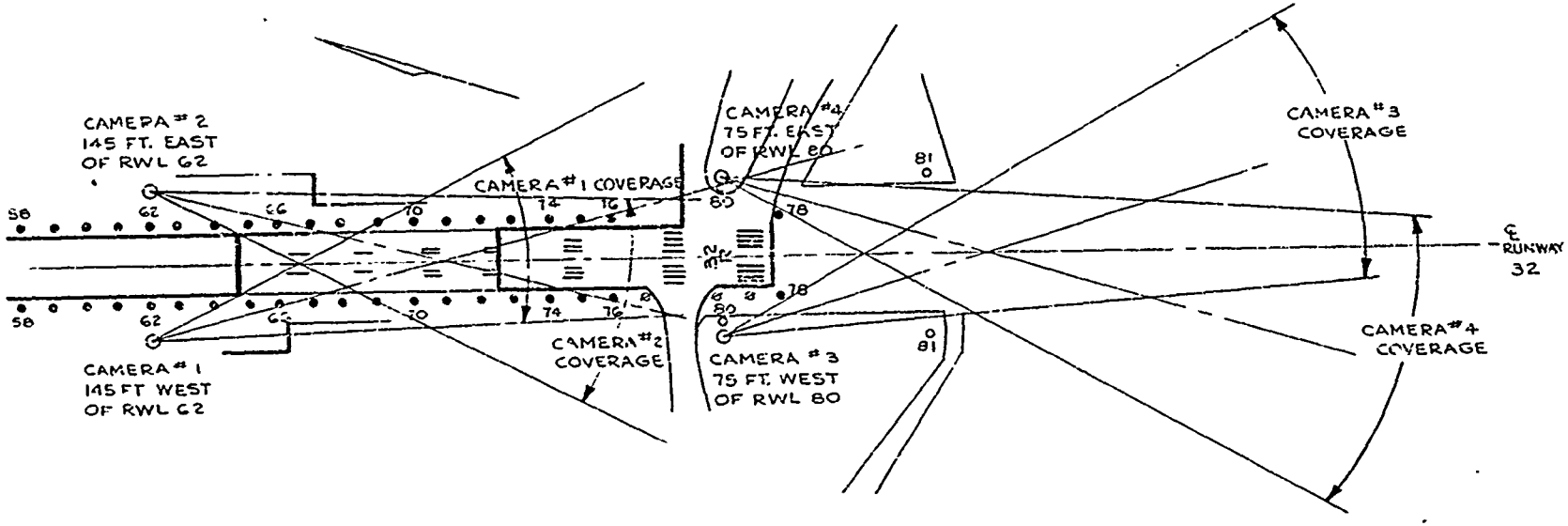

Figure C.1.2

GRANT COUNTY AIRPORT CAMERA PLACEMENT

C.2 POSITION DETERMINATION FROM CAMERA DATA

On each approach approximately twenty pictures were taken by each camera on 70 mm film. This film was "read" on a special projector with a moveable X-Y cursor. The azimuth and elevation angles between the airplane's right main landing gear and two of the targets were automatically recorded in digital format. These angles, in addition to known camera location and orientation, permitted computation of airplane position through triangulation. The resultant airplane position estimate was accurate to about three feet laterally and vertically, on a 1σ basis, over the last 6000 feet of the approach.

C.3 POSITION DETERMINATION FROM INS AND CAMERA DATA

Track angle, ground speed and vertical acceleration INS signal outputs were recorded in-flight. A filtering scheme using these pieces of information, a computer model of the INS Schuler loop, and the camera-generated estimate of airplane position, was mechanized to improve upon the camera-generated position estimate. Essentially, the INS model was initialized at the first space position that had been determined through triangulation of the camera data. The INS model was then caused to track the camera data at two second intervals until the end of the approach. Throughout the process, error estimates of recorded INS data were generated. This process was referred to as the forward pass. A backward pass was then made using INS data, corrected by the final error estimates.

C.4 PLOT ACCURACY ESTIMATES

The estimated accuracy of the photo-INS system is generated as part of the position estimation process, given initial INS error standard deviations and camera error standard deviations. The camera error was predicted to be 1 milliradian (2σ). The magnitudes, on a 2σ basis, of 13 inertial errors were selected to be as follows at the time of the first camera observation:

	X	Y	Z
Position, Ft	200	10	10
Velocity, Ft/Sec	10	10	5
Tilt, Milliradian	.5	.5	-
Accelerometer bias, 10^{-3} G	.2	.2	10
Azimuth, Milliradian		20	
Z Accelerometer scale factor %,			1

where: X - range from glide slope antenna - Ft.
Y - lateral displacement from centerline - Ft.
Z - altitude above runway elevation - Ft.

The resultant position accuracy estimates varied from approach to approach, due principally to varying times of camera turn-on. Figure C.1.3 shows representative accuracy estimates (specifically, those of the fourth flight, third approach). The discrete points plotted are the position estimates obtained during the forward pass through the camera data, i.e., the positions obtained are those at the instant a picture is taken, using only past and present inertial and camera data. The curves are generated by a backward pass using inertial data backwards from the last picture time, corrected by inertial error estimates at that time. In Figure C.1.3, the lateral displacement error probability for the backward pass is always better than two feet on a 2σ basis. The calculated accuracy of vertical position as a function of range is not as good.

Note that the forward pass vertical positions are estimated to be more accurate than the backward pass, due mainly to a vertical accelerometer scale factor and noise problem. On the second and subsequent flight, a poorly designed amplifier was placed between the vertical accelerometer outputs and the recorder inputs. And due to an unfortunate combination of circumstances, the post-flight position processing could not be carried out until the entire sequence of flights was completed, at which time it became apparent that considerable accelerometer scale factor, bias and random error had been introduced by the amplifier. Thus, the forward pass which is heavily weighted to camera information is the more accurate. Even so, the forward pass estimates are accurate to within two feet on a 2σ basis over the last five thousand feet of the approach. In the body of this report, for the vertical axis, the forward axis, the forward pass estimates are used.

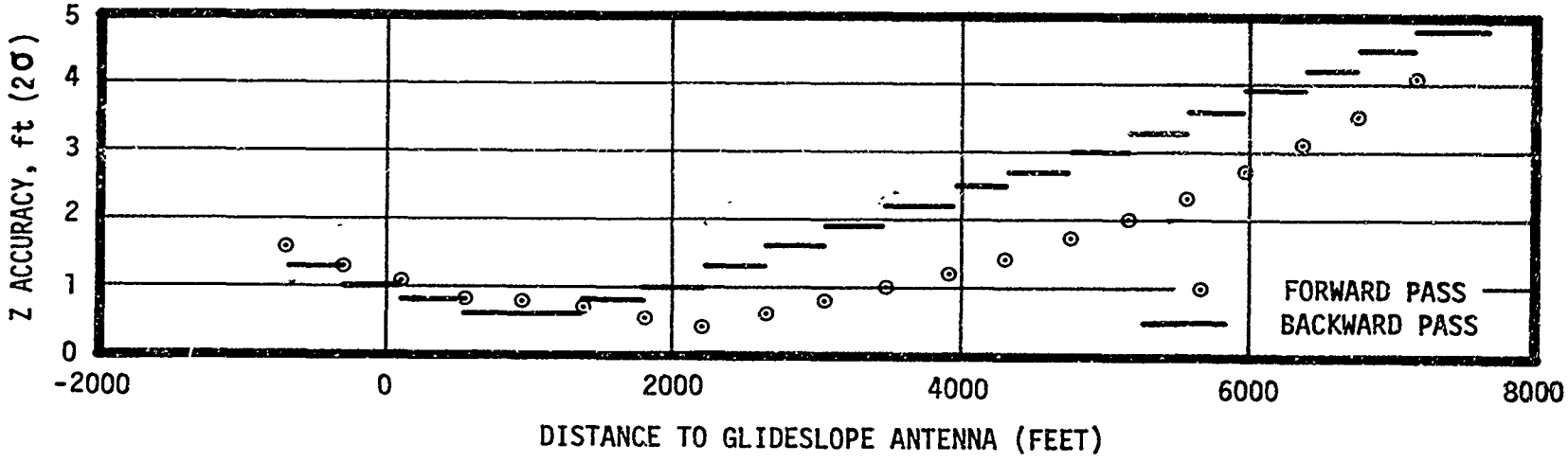

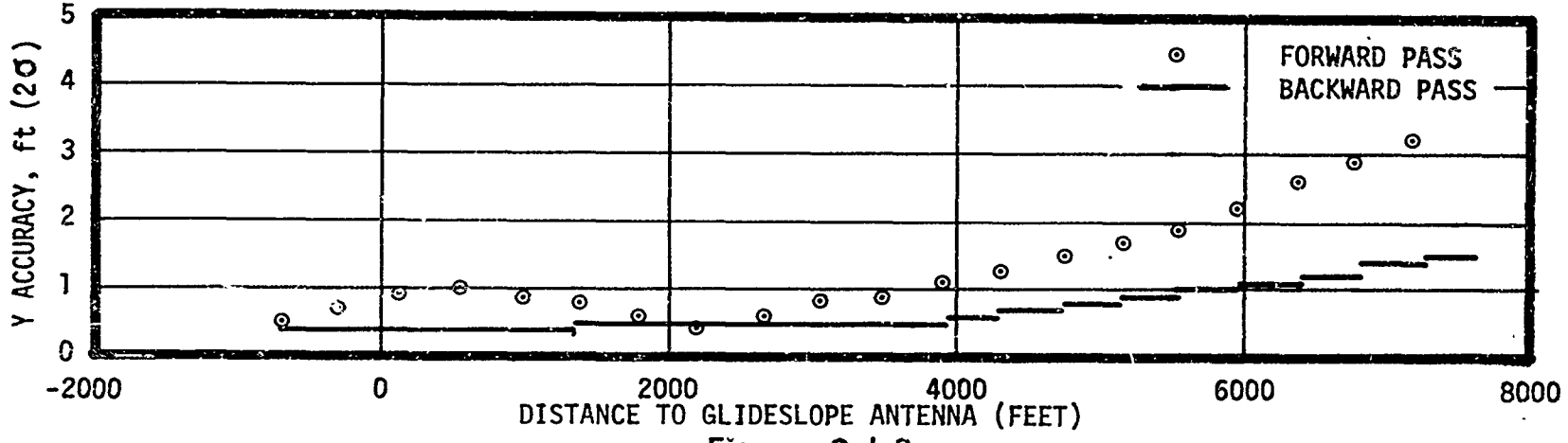

Figure C.1.3

ESTIMATED TRACKING ACCURACY

APPENDIX D

INERTIAL NAVIGATION SYSTEM (INS) MECHANIZATION

D.1 SUMMARY

A standard Delco Carousel IV ARINC 561 INS was used to support this program. The INS computer program was slightly modified to provide the outputs required by the G.E. Autoland autopilot computer at the correct rate, format and scaling. No hardware modifications were necessary.

The software modification involved approximately one man month of programming, integration and troubleshooting effort by one engineer.

D.2 INS REQUIREMENTS

Certain special INS requirements existed for operation with ILS Autoland equipment:

- Compute and output Track Angle (TK) and Ground Speed (GS) at a minimum rate of 5 times/sec. on the standard ARINC 561 binary digital output.
- Minimize the delay between computation and output.
- Provide additional digital outputs of Drift Angle (DA), True Heading (TH), Latitude (LT), and Longitude (LN) for test instrumentation purposes.
- Assign the following label codes to the ARINC 561 format digital outputs:

	MSB	8	7	6	5	4	3	2	1	LSB
TK		0	0	0	1	1	0	1	1	
GS		0	0	0	1	0	1	1	1	
DA		0	1	0	1	0	1	0	1	
TH		0	1	0	1	0	0	1	1	
LN		0	1	0	1	0	0	0	1	
LT		1	0	0	1	0	0	0	1	

- Scale all data as follows:

Data	Units	MSB (Bit 29)	Resolution
Velocity	Ft/Sec.	512	0.000488
Angular	Semi circles	90°	0.044

D.3 CAROUSEL IV SOFTWARE MODIFICATION

The baseline computer program was the 031J version currently used on the 747 airplane. This program has an identification number 4663-0010. Thirty nine (39) computer locations were modified (patched) and hand loaded into the Carousel IV computer to satisfy the requirements of the Inertially Augmented Autoland program. This modified computer program was identified as 4663-3333. The 'patches' and an explanation for each change are listed in Table D.1.

The 'patches' listed in Table D.1 represent the final version which was used on Flight test #4 and subsequent flights. For the first three flights, location 5576 was not patched to change the 75 Knot GS cutoff for TK and DA angle computation which is used in the 031J program. On Flight #3 under adverse head wind conditions, airplane groundspeed fluctuated between 70 and 80 knots during approach to Boeing Field. This caused 20° erroneous steps in the TK output from the INS because of the 75 knot cutout on the TK computation. Changing the GS limit to 38 knots eliminated the possibility of a recurrence. For the first two flights, different label codes were used for TH, DA, LT and LN, and a different output order was used. These were changed to correct an intermittent label recognition problem in the G.E. autopilot computer on Flights 1 and 2, and to decrease the staleness of TK data.

The basic 031J computer program has three computation loops of 50 msec, 200 msec and 600 msec. It also has automatic digital I/O which, after initiation by an OUT 35 instruction, transmits up to 64 memory locations - in sequence to the three digital outputs, the CDV, BCD, and binary outputs.

The modifications that were necessary for the inertially augmented autoland program were to change the computation loop in which the specified functions were calculated to the 200 msec loop, and to put them out on the binary bus immediately after computation.

Considering each computation loop, the following changes were made:

50 msec loop

- Delete the intersystem comparison automatic I/O because it would interfere with the output array and the 200 msec automatic I/O.
- Delete TK and DA computation.

200 msec loop

- o Add TK and DA computation
- o Compute GS
- o Load output array with TK, DA, GS and TH
- o Initiate automatic I/O to output 10 words, CDU Right, CDU Left, CDU Discretes, Spare, LT, LN, TK, TH, DA, GS.
- o Delete computation of Crosstrack, Track Angle error and Steering signal because these outputs were not required and the memory space saved was convenient for the above computation changes.

600 m sec loop

- o Change the Control Display Unit (CDU) output locations, CDU Right, CDU Left, and CDU Discrete, to include in the 200 m sec automatic I/O output.
- o Delete storage in automatic I/O memory array except for LN and LT.
- o Delete automatic I/O output of 30 words
- o Delete Intersystem comparison routine because not used and interfered with the automatic I/O memory array.

Miscellaneous

- o Changed the labels and allocations for the automatic I/O memory array.
- o Deleted setting of MALF code 31 because the changes resulted in MALF 31 being set in the Align mode causing a nuisance warning.
- o Changed the computer program identifier.
- o Changed the balances to validify the computer memory sum check.

The 031J computer program tape has six trailers, E, F, G, H, I, J, which are intended for laboratory use. Three of these trailers, H, I, and J, were loaded into the computer to give the capability of loading memory locations through the CDU. This was convenient since minor software changes can then be made without removing equipment from the airplane.

The final software changes used for the autoland test were functional rather than refined. A complete listing of the changes is given in Table D.1. Given more time, the specific requirements of the inertially augmented autoland program could have been met while retaining all the other features of the basic 031J program. Since Boeing does

not have the facilities to do a full reassembly of the Carousel IV computer program, the primary objective was to provide the specified outputs for the inertially augmented autoland program with a minimum of memory location changes. Boeing has a Carousel IV memory load and verify unit (LVDU) and system checkout installations at the Boeing Renton plant. These facilities were used to support this program. INS repairs and maintenance support were provided by Delco Electronics Seattle repair center.

Two basic weaknesses of the current 031J computer program were identified during this development. Firstly, the current practice of using the automatic I/O memory array locations for temporary storage of variables in addition to the output functions presented some difficulties and made some output array locations unuseable for the 200 m sec output mechanization. Secondly, the practice of cutting off the computation of TK and DA when GS is less than 75 Kt interfered with Flight test #3, and must be changed if the INS is used for autoland augmentation.

CAROUSEL IV COMPUTER PROGRAM MODIFICATION

TABLE D.1

LOCATION	MOD. CONTENTS	REMARKS
2370	70707645	Balancer number to correct memory sum check
2376	46633333	Modified computer program identification number
2420	16354337	Deletes normal intersystem comparison output
2700	21252027	Modified label codes for output functions
2702	20332123	
2704	22212121	
2706	40402111	
2710	42004100	
4260	00001213	Bypass autopilot interface test
4302	00005025	Bypass storage of TK in 50 m sec loop
4310	00005027	Bypass storage of DA in 50 m sec loop
5246	00003570	Bypass intersystem subroutine
5704	00000000	Bypass STANDBY mode JUMP instruction
5706	61503150	Compute GS in 200 m sec loop
5710	31662075	
5712	40756166	
5714	23101143	
5716	30242612	Store GS in output array
5720	20325025	Compute TK during 200 m sec loop
5722	26150102	Store, TK in output array
5724	01023027	Process TH during 200 m sec loop
5726	30322614	Store TH in output array
5730	20305027	Compute DA during 200 m sec loop
5732	26130102	Store DA in output array
5734	43623360	10 word array output during 200 m sec loop
5736	12240335	
6702	20623340	Relocate CNTRC
7034	33741204	Bypass MALF 31
7154	00006341	Bypass storage of Wind Speed in output array
7164	32550000	Bypass storage of Wind Angle in output array
7416	10360000	Bypass storage of GS during 600 m sec loop
10524	00000000	Bypass storage of TK during 600 m sec loop
10532	26213645	Relocate LEFT (CDU Display output)
10534	26223646	Relocate RIGHT (CDU Display output)
10536	26233647	Relocate OUTDIS (CDU Discrete output)
10542	32550000	Bypass output array during 600 m sec loop
12170	43773062	Relocate CNTRC
12172	01012062	
5576	14065356	Change GS Limit to 38 Knots

APPENDIX E

INSTRUMENTATION AND DATA REDUCTION

The data recording system components were mounted in a pallet consisting of a double-width AMCO rack 42 inches high. The AMCO frames (P/N F42-19-25) were bolted at their bases to a 1/4 inch thick aluminum plate which had four seat-track mounting brackets attached. Two 3/8 inch diameter steel cables with turnbuckles were attached to the aft side of the frames to provide a safety anchor for forward directed acceleration forces. Side panels for the pallet were fabricated with cut-outs to allow access to tape recorder electronics, see Figure E.1.

The data recording system functional diagram is shown in Figure E.2. Two Sangamo Model 3562 magnetic tape recorders with wideband FM record/reproduce electronics were used for data recording. IRIG B modulated time code was recorded with direct record electronics on Channel 1 of each recorder. Calico Model 7000 monitor oscilloscopes allowed continuous monitor of either the input signal to the record electronics or the reproduced recorded signal for each channel. The tape input panel (Drawing E2FAA 430.02) utilized 5,000 ohm trimpots to attenuate ±10 volt nominal signals from the autopilot pallet to ±1.4 volts compatible with the FM record electronics. Front panel switches provided for the insertion of a calibration voltage across the attenuator such that precise setting of attenuation was not necessary. The voltage calibration source (Drawing E2FAA 430.01) contained a regulated precision 10 volt power supply and switching necessary to provide +10 volts, zero and -10 volts calibration voltages. The calibration voltage was checked periodically with a digital voltmeter and found to be 10 ± .005 volts, with typical calibration current loading.

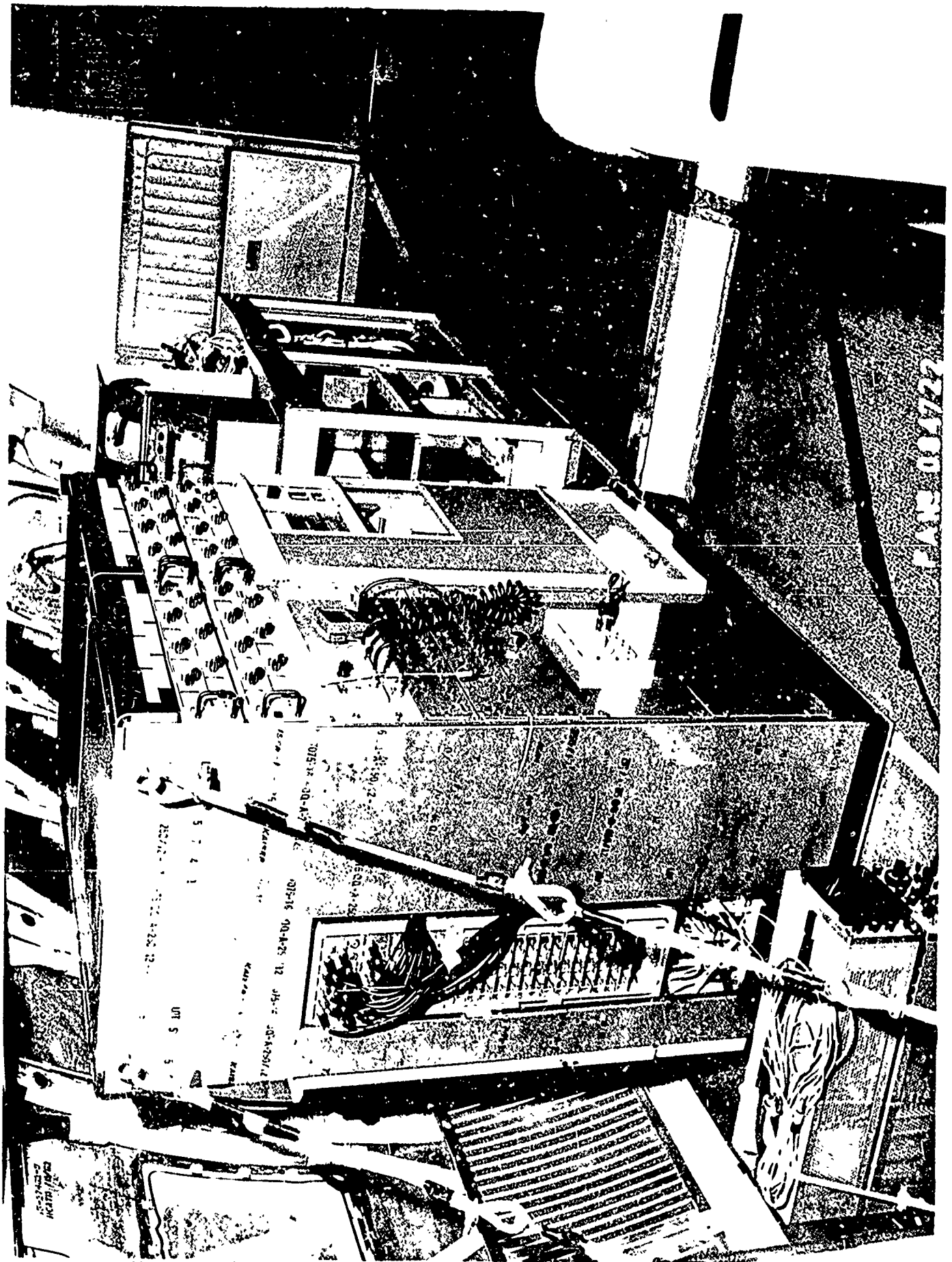

Figure E.1 INSTRUMENTATION PALLET - ILS AUTOLAND

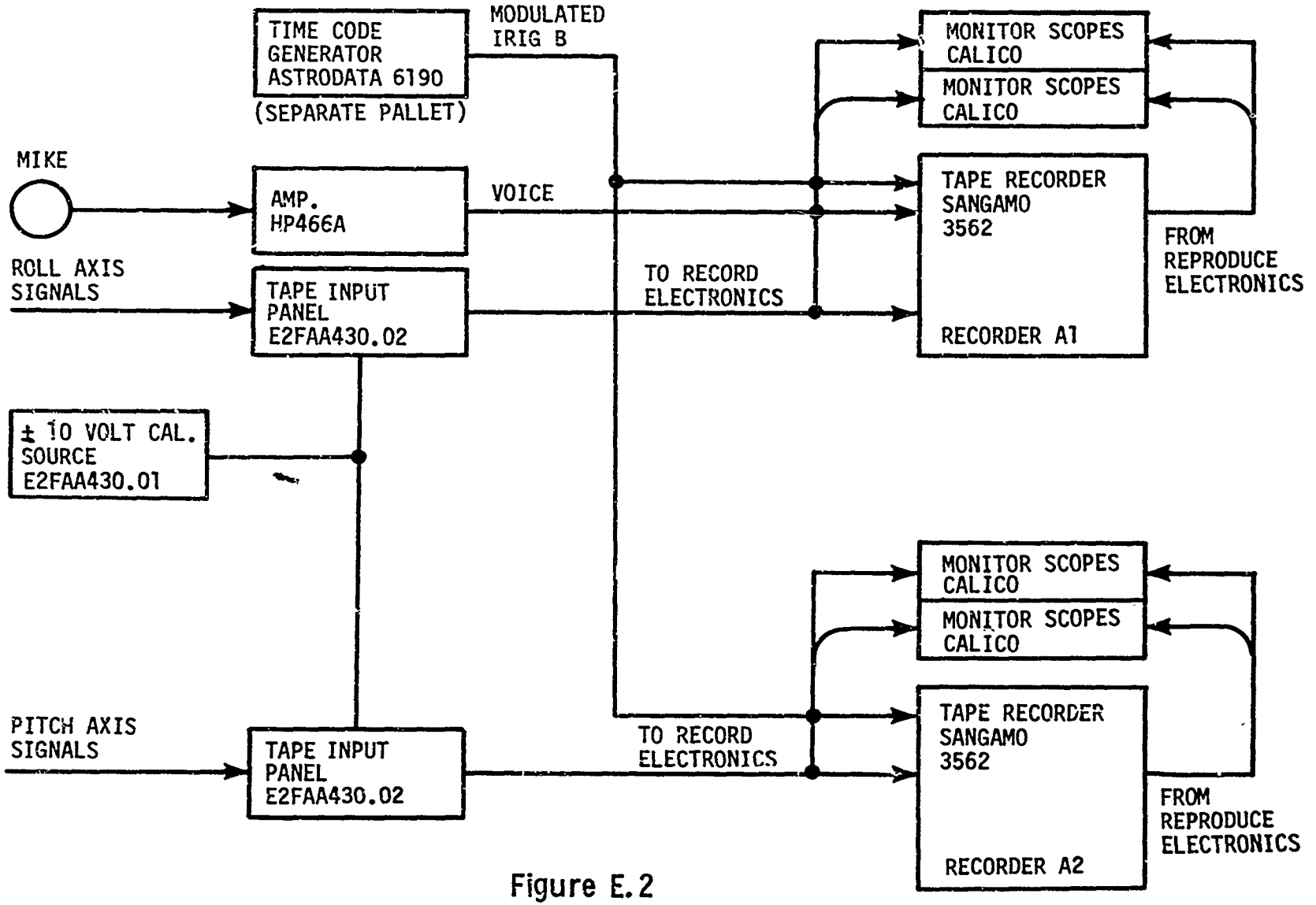

Figure E.2
INSTRUMENTATION PALLET FUNCTIONAL
BLOCK DIAGRAM ILS AUTOLAND

Recorded parameters were patched to the instrumentation pallet inputs at the Burndy-Block panel at the rear of the autopilot pallet. The channel assignments are shown below:

Pitch Axis	Roll Axis
IRIG B Time Code	IRIG B Time Code
Radio Altitude-Fine	Voice
Ground Speed	Radio Altitude-Coarse
Vertical Acceleration	Track Angle Deviation
Pitch Attitude	Roll Attitude
Pitch Rate	Roll Rate
Vertical Speed-Barometric	Roll Command
Vertical Speed-Derived	Aileron Command
Glide Slope Beam Error	Localizer Beam Error
Glide Slope Beam Disturbance	Localizer Beam Disturbance
Indicated Airspeed	Yaw Rate
Elevator Position	Course-Heading Error
Elevator Command	Track Select Error
Pitch Autopilot Mode	Roll Autopilot Mode

E.1 DATA REDUCTION

The recorded FM magnetic tapes were played back at the SIMCOM Facility shown in block diagram, Figure E.3. Quick-look analog strip-out of the data was accomplished on a direct-write oscillograph. Time intervals of data to be digitized were input via a teletype to the PDP-8 computer which controlled the FM magnetic tape transport, digitizing process, and digital data output format. This digital data, recorded on digital magnetic tape, was further processed and integrated with the photographic data by a CDC 6600 computer (See Appendix C).

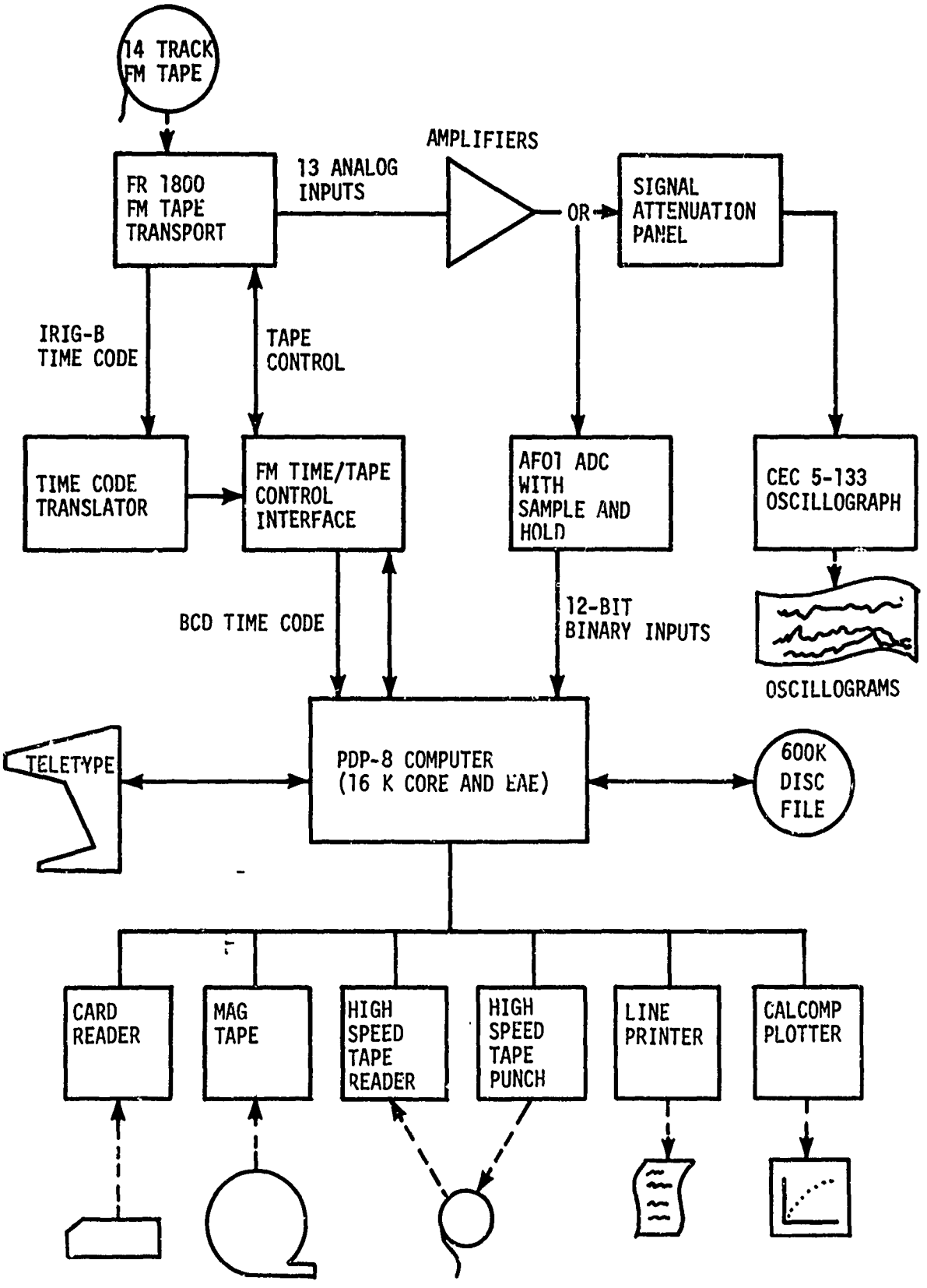

Figure E.3
SIMCOM FM TAPE DIGITIZING SYSTEM

*U.S. GOVERNMENT PRINTING OFFICE: 1972 721-587/69 1-3